Performance Assessment of iPVC Pipe and Couplings for Large Ground Movement

Submitted to:

David Katzev, East Bay Municipal Utility District

and

Katie Ross, Denver Water

Prepared by:

Nicholas W. Berty

Cory Ihnotic

Katherine O'Dell

Jessica Ramos

Brad Wham

Center for Infrastructure, Energy, and Space Testing
Civil, Environmental, and Architectural Engineering
University of Colorado Boulder
Boulder, CO 80309

March 2022

Table of Contents

List of Figures

List of Tables

1. Introduction

This report is submitted to East Bay Municipal Utility District (EBMUD) and Denver Water (DW). It presents results from a program to investigate the axial and transverse performance of nominal 6 in. (150mm) diameter iPVC pipe with hazard resilient connections. The work was undertaken in the Center for Infrastructure, Energy, and Space Testing (CIEST) which is affiliated with the Civil Environmental, and Architectural Engineering Department at the University of Colorado Boulder.

The purpose of this study is to evaluate and classify the response of segmented iPVC pipeline systems with reinforced couplings when subjected to substantial axial and transverse deformations. Deformations applied during testing are representative of significant ground deformations possible during an extreme seismic event, such as landslides, fault rupture, and liquefaction-induced lateral spreading. All tests were designed and performed in accordance with procedures and recommendations provided by Wham et al. (2018 & 2019).

The report is organized into six sections. Section 1 provides introductory remarks, including a discussion of the test specimens and experimental overview. Section 2 presents the general test setup and experimental protocols for axial and transverse loading. Section 3 discusses the experimental test results. Section 4 provides the analysis and results as it relates to the seismic classification for each pipeline system. Section 5 provides an overall summary of the report's findings and conclusions. Finally, Section 6 provides acknowledgments for the people and organizations that made this research and report possible.

1.1 State of Practice and Developing Seismic Design Standards

It is well known that underground pipeline distribution systems are susceptible to significant damages when exposed to large ground motions produced through earthquakes, fault ruptures, landslides, and other significant seismic events. For example, substantial damage was recorded during the Christchurch, New Zealand Earthquakes of 2011 in which an excess of 2,000 breaks and leaks to water distribution systems required repairs or replacements (O'Rourke et al., 2014). These disruptions in waterline systems not only leave populations without water services but can also severely impede firefighting efforts, as was the case in the 1906 and 1989 San Francisco earthquakes (O'Rourke et al., 2006). Since these events, significant advances have been made by manufacturers to improve pipeline systems' performances when subjected to seismic loading. However, current industry standards for the seismic design of pipeline systems remain lacking, with most industrial acceptance standards pertaining to hydrostatic loading produced by internal pressure and material testing such as ASTM D 1599 hydrostatic burst testing and ASTM D 638 tensile strength test (AWWA 2007). Experimental testing has shown that pipeline systems subjected to external

loading representative of earthquake-induced ground deformations can fail at axial stresses far less than those developed during hydrostatic burst testing (Ihnotic, 2019). As municipalities seek to renovate their aging utility systems, it is essential for designers to understand the ability of new and developing systems to accommodate ground motions imposed by seismic events.

The pipelines division of the Utility Engineering and Surveying Institute (UESI) is currently developing a Manual of Practice (MOP) designed to provide guidance to engineers when working in regions with varying levels of seismic risk. Current developing seismic design guidelines within the MOP consider three metrics for pipeline assessment: (1) axial strain demand, (2) transverse strain demand, and (3) connection force capacity. This study is intended to lay the groundwork for a procedure to assess and classify various pipeline systems for the first and third seismic demand metrics through full-scale testing and analytical modeling.

The only current industry design standard concerning the seismic design of buried pipeline systems is ISO16134: Earthquake- and subsidence-resistant design of ductile iron pipelines (ISO 2020). ISO16134 provides performance classes for the slip-out resistance, also more broadly referred to as the Connection Force Capacity (CFC), based on the nominal pipe diameter, D, (Table 1.1). While ISO provides recommended performance classes for pipelines of various diameters, the classification system only considers Earthquake Resilient Ductile Iron Pipe (ERDIP) systems and does not consider other materials, connection types, or geotechnical inputs such as burial depth or backfill conditions. Currently, there are two developing seismic guidelines known to the authors that have made efforts to expand on ISO's classification system and provide frameworks for classifying multiple pipeline systems with different material characteristics and connection types.

Table 1.1 ISO Performance Class Values (ERDIP)

Performance Class	**ISO 16134 (kN)**	**ISO 16134 (US units) (kips)**	**ISO DIP F_{CFC} for D = 6 in. (kips)**
Φ_A	less than 0.75D	less than 4.3D	< 25.7
Φ_B	0.75D to 1.5D	4.3D to 8.6D	25.7
Φ_C	1.5D to 3D	8.6D to 17.1D	51.4
Φ_D	greater than 3D	greater than 17.1D	102.8

The first classification system uses an analytical model proposed by Wham & Davis (2019) to define the Connection Force Capacity of various pipeline systems. The model quantifies the axial demand on a pipeline system, as a function of frictional resistance along the system, by considering various geometric combinations of ground movements (i.e., block length and ground displacement), pipeline geometry, and

various soil characteristics. A multiplication factor K is defined by comparing the calculated CFC of ERDIP systems that have performed well during past earthquakes to a system of interest (SOI) under the same ground movements and soil characteristics. The K factor is used to define the system's performance classes in relation to ISO standards ($3DK_C$, $1.5DK_B$, and $0.75DK_A$). Further discussion on the procedure is provided by Wham et al. (2019b).

Another effort to seismically classify pipeline systems was proposed by Davis et al. (2019). They define four classes of seismically-induced ground movement demands, quantified by ground strains that a pipeline must be able to accommodate in either the axial or transverse direction. The proposed values are provided in Table 1.2 and, when compared against a pipeline system's capacity under laboratory test conditions, can be used to assess expected field performance.

Table 1.2 Seismic Demand Levels Proposed by Davis et al. (2019)

Parameter (+ and -)	**Class**	**Seismic Strain Demand**	
Axial Strain (α)	α_A	0.01% up to 0.1%	
	α_B	0.1% up to 0.5%	
	α_C	0.5% up to 1%	
	α_D	1% or greater	
Radius of Curvature (R)/ Deflection Angle (ϕ)	ρ_A	$R_A > 344$m (1130 ft)	$\phi_A/L_g < 0.167$ deg./m (0.051 deg./ft)
	ρ_B	115 m (376 ft) $< R_B \leq 344$m (1130 ft)	$0.167 \leq \phi_B/L_g < 0.5$ deg./m (0.152 deg./ft)
	ρ_C	46 m (150 ft) $< R_C \leq 115$ m (376 ft)	$0.5 \leq \phi_C/L_g < 1.25$ deg./m (0.381 deg./ft)
	ρ_D	$R_D \leq 46$ m (150 ft)	$\phi_D/L_g \geq 1.25$ deg./m (0.381 deg./ft)

1.2 Test Specimens and Joint Restraints

Test specimens used in this study consisted of structurally enhanced PVC pipe (AWWA C900 iPVC) manufactured by PPI Pyungwha Co., Ltd. (PPI). All tests were performed on 6 in. (150 mm) nominal diameter pipe with a pressure class rating of 305 psi (2103 kPa). This paper reports on the response and seismic classification of five iPVC pipeline systems with different self-restraining connections designed to optimize the system's ability to accommodate large ground movements. An overview of all tests performed in this study is provided in Table 1.3.

Table 1.3 Overview of Performed Tests

Test # (CIEST)	Test Type	Pipe-Connection	Pipe-Material	Average Pressure	
				Psi	(kPa)
PT02	Axial-Tension	RCT	iPVC-DR14	59	(407)
PT27	Axial-Tension	TurnerLok	iPVC-DR14	61	(421)
PT30	Axial-Tension	EBAA C1900	iPVC-DR14	63	(434)
PT33	Axial-Tension	Lokx	iPVC-DR14	64	(441)
PT38	Axial-Tension	Hymax Grip	iPVC-DR14	64	(441)
PC37	Axial-Compression	RCT	iPVC-DR14	64	(441)
PC28	Axial-Compression	TurnerLok	iPVC-DR14	65	(448)
PC31	Axial-Compression	EBAA C1900	iPVC-DR14	67	(462)
PC35	Axial-Compression	Lokx	iPVC-DR14	64	(441)
PS12	Axial-Cyclic	RCT	iPVC-DR14	63	(434)
PS29	Axial-Cyclic	TurnerLok	iPVC-DR14	65	(448)
PS32	Axial-Cyclic	EBAA C1900	iPVC-DR14	66	(455)
PS36	Axial-Cyclic	Lokx	iPVC-DR14	65	(448)
PS39	Axial-Cyclic	Hymax Grip	iPVC-DR14	65	(448)
PB02	Bending	RCT	iPVC-DR14	53	(365)
PB11	Bending	TurnerLok	iPVC-DR14	65	(448)
PB12	Bending	EBAA C1900	iPVC-DR14	67	(462)
PB13	Bending	Continuous	iPVC-DR14	65	(448)
PB14	Bending	Lokx	iPVC-DR14	64	(441)
PB15	Bending	Hymax Grip	iPVC-DR14	63	(434)

The first set of tests was performed to investigate the response of an RCT Flex-Tite coupling. The connection consists of a self-restraining fitting with an integrated restraining gasket constructed primarily of ductile iron per ASTM A536. The fitting is pressure rated to 305 psi. The gasket is designed to grip the spigot under tensile loading, preventing slip-out at the connection. An example of an installed RCT connection is shown in Figure 1.1. This study focuses on the response of the straight coupling, and the results are intended to be representative of the pipe and gasket interaction. The second set of tests was performed on iPVC pipe with an internal TurnerLok gasket connection. The connection consists of a rubber gasket equipped with twelve toothed wedges designed to grip the spigot in tension. The gasket is designed to be manually inserted into a standard bell section of pipe, replacing the factory-installed gasket. An image of the restraining gasket is provided in Figure 1.2. The third set of tests investigated the response of an iPVC system restrained at the connection by EBBA C1900 Restraint Harnesses. The EBBA C1900 consists of two split ring restraints that are positioned on either side of the connection. The restraints are connected

with two 3/4 in. x 18 in. thrust bolts, as shown in Figure 1.3. The split ring restraints are constructed primarily of ductile iron conforming to ASTM A536 standards. The fourth set of tests was conducted on iPVC pipe segments connected by a Lokx coupling which is currently under development presented in Figure 1.4. The connection consists of a ductile iron fitting conforming to ASTM A536 standards, equipped with restraining gaskets. The final set of tests was performed on an iPVC system with a Hymax Grip coupling. The Hymax Grip coupling, presented in Figure 1.5, is a ductile iron coupling conforming to ASTM A536 standards. The coupling is equipped with a two-stage internal gasket system containing a rubber and gripper gasket designed to resist axial forces.

Figure 1.1. Typical RCT Connection

Figure 1.2. Typical TurnerLok Gasket

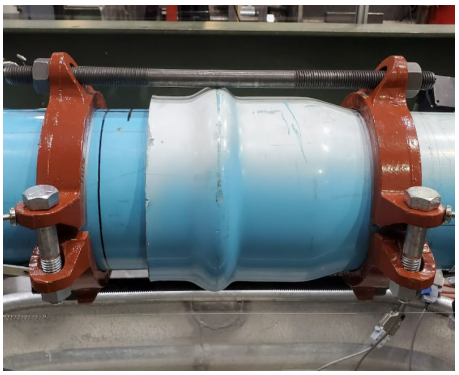

Figure 1.3. Typical EBBA C1900 Restraint

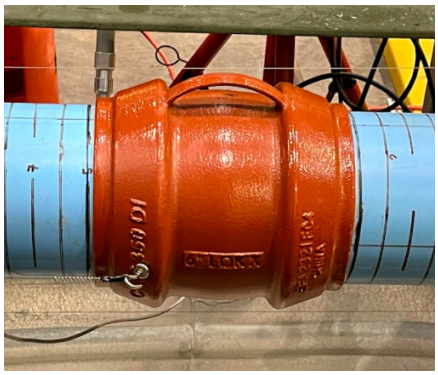

Figure 1.4. Typical Lokx Coupling Connection

Figure 1.5. Typical Hymax Grip Connection

2. Test Design and Instrumentation

This section provides detailed information about the setup and testing procedures associated with the application of axial and bending load to the pipeline system. The objective of testing is to determine the system's response and ultimate capacity when subjected to significant ground deformation. Three axial tests were performed on the pipeline system to achieve a preliminary understanding of the system's response to axial loading: a tension test, subjecting the pipeline to tensile loading, a compression test, subjecting the pipeline to compressive load, and a cyclic test, subjecting the pipeline to increasing cycles of tensile and compressive loading. One bending test was performed for each system. The bending test applies transverse loading to the specimen through a four-point bending setup. Lateral loading is applied through two load points on each side of the connection generating a constant moment across the tested connection. Supports and loading points consist of roller connections allowing the system to geometrically center throughout the test without applying unwanted excess axial loading to the system.

2.1 Axial Test Setup and Instrumentation

Figure 2.1 (a-b) provides a general overview of the axial test design and instrumentation. A 255.17 MTS actuator with a 110-kip (490-kN) load capacity and an 11 in. (279 mm) stroke is used to apply tensile and compressive load to the specimen within a self-contained axial loading frame. 2006PV Megalug external restraints are used at either end of the specimen to transfer the applied load to the pipeline system. The orientation and number of Megalug restraints vary for each loading procedure due to their engagement with the pipe in one primary direction [Figure 2.1 (c-e)]. Six high-strength steel threaded rods were used at either end of the setup to connect the pipe, pressurization end cap, and load frame.

Pipe specimens are cut to the required test length using standard field procedures outlined in Hughes et al. 2018. The specimen is prepared to 13 ft (4 m) for a tension test, 14 ft (4.25 m) for a compression test, and 13.5 ft (4.13 m) for a cyclic test. The pipe specimens consist of two pipe segments of equal length. For connections consisting of a bell and spigot connection, an additional 8 in. (203 mm) is added to the spigot section to account for the bell insertion length. The crown of the pipe is defined on the pipe by material designation written along the pipe. Using a half-moon leveling tool, as shown in Figure 2.2, the crown, invert, and spring lines are defined along the pipe specimen. Measurements are provided at every 1 in. (25 mm) along the spigot of the specimen, as shown in Figure 2.3. Once the crown, invert, and spring lines are marked along the specimen, each end restraint and the connection under investigation is installed following field installation guides. Nuts on the end restraints are tightened, using a star pattern, to 60 ft-lbs (81 N-m). Strain gauges are then fixed to the specimen. Once strain gauges are installed and end restraints are securely fixed to the pipe, the test specimen is lifted by crane into the loading frame.

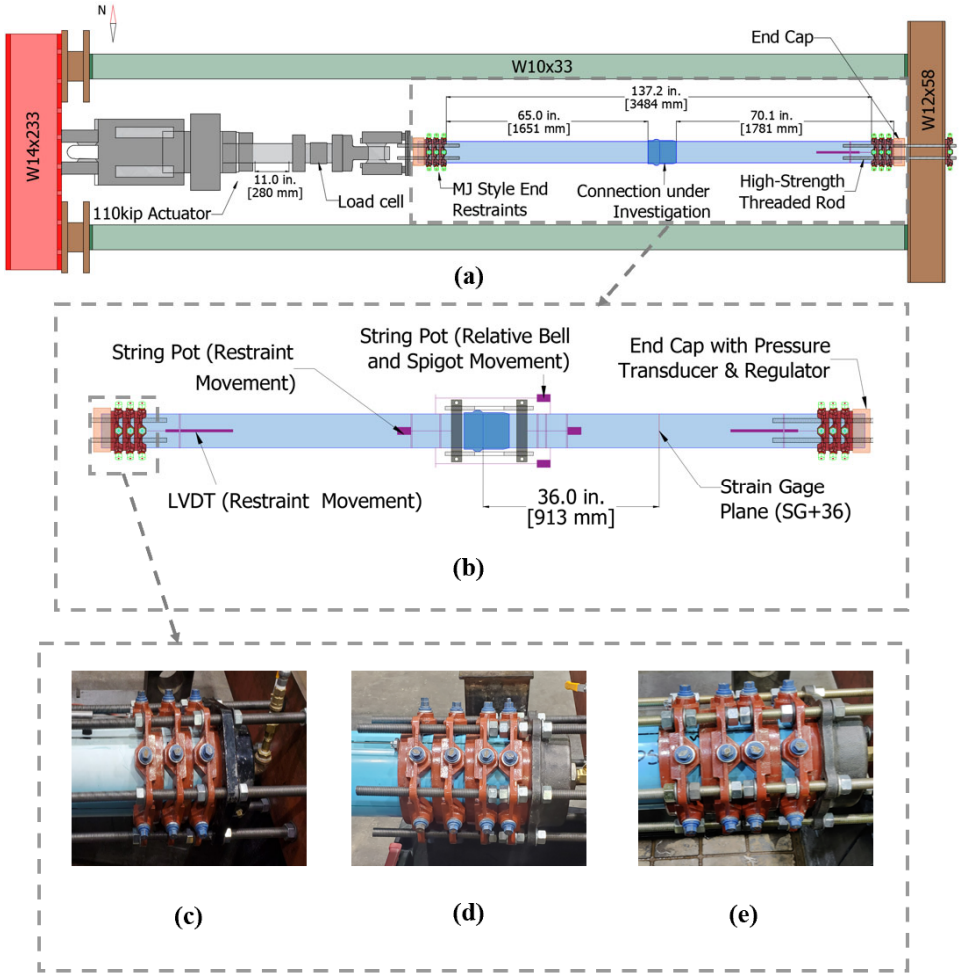

Figure 2.1. Axial Test Setup – (a) AutoCAD drawing, (b) Instumentation Location, (c) Tension Test End Restraint, (d) Compression Test End Restraint, (e) Cyclic Test End Restraint

Figure 2.2. Half Moon crowning tool (Identifying pipeline crown, invert, and spring lines)

Figure 2.3. Measurements along the pipe spigot

The actuator is positioned based on the test being performed: full stroke extended for a tension test, full stroke retracted for a compression test, and the actuator stroke placed at the halfway point for cyclic testing. Six 0.75-in (19 mm) diameter high-strength threaded rods are then installed at each end of the specimen to secure the pipe to the loading frame. During this procedure, the nuts threaded into place are oriented to engage the Megalug end restraints and resist axial load applied to the specimen.

A 110-kip (489 kN) load cell is attached to the actuator's hydraulic piston to measure the axial force applied to the specimen. A water supply hose running to an electronic pressure transducer is attached to the east end cap allowing for the application and measuring of internal pressure in the system throughout the test [Figure 2.5]. At each end of the specimen, an LVDT is used to measure the relative movement between the pipe segment and the end restraint [Figure 2.4]. Two to four string potentiometers are positioned at the center of the specimen to measure joint displacement or the local relative movement of the pipe sections to the connection, e.g., the bell and spigot or coupling [Figure 2.6]. Four X-Y strain gauge pairs, oriented in the axial and circumferential directions, are installed at the specimen's crown, invert, and spring lines and positioned approximately halfway between the connection and end restraints [36 in. (900 mm)] east of the specimen centerline to minimize the potential influence of end effects on the strain gauge measurements [Figure 2.1 (b)].

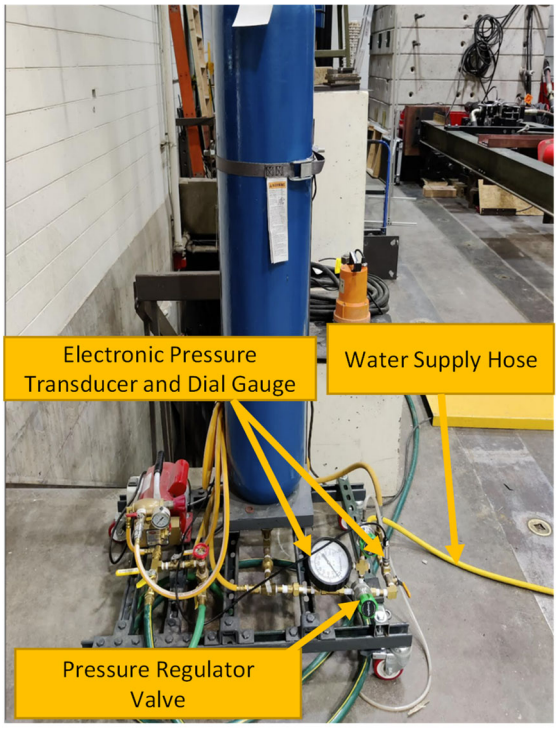

Figure 2.5. Electronic Pressure Transducer Setup

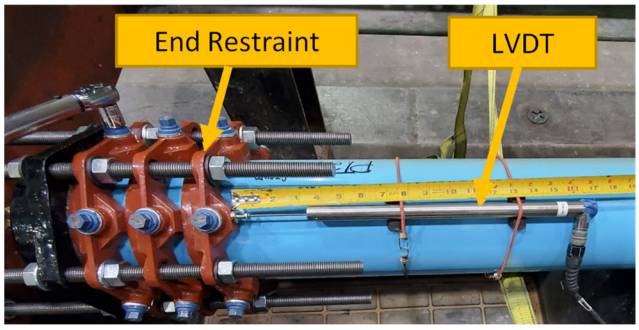

Figure 2.4. Typical LVDT Setup at End Restraints

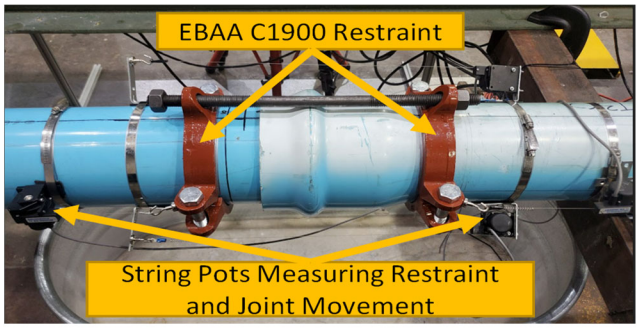

Figure 2.6. Typical String Pot Installation (PT30)

2.2 Axial Test Procedure

The following section provides details of the overall test sequence separated into three parts: pretest; tension and compression test sequence; and cyclic test sequence.

2.2.1 Pretest

Once the test specimen is instrumented and secured in the loading frame, an instrumentation check sequence, consisting of manually displacing string pots and LVDTs, is conducted to verify measurements are being recorded. The pipe system is then filled with water. As the system is being filled with water, the air bleeder valve at the west end restraint is left open, allowing air to be released from the specimen. After the system is filled with water, the air bleeder valve is closed, pressurizing the system to approximately 65 psi (450 kPa). The system is then checked for any signs of leaking. Pressure is then released from the system. A pressurization sequence is then performed to verify that load cell and strain gauge measurements are recording accurately. During the pressurization sequence, the system is pressurized to 65 psi (450 kPa) and back down to 0 psi (0 kPa) three times. Data is recorded throughout the sequence and analyzed to verify accurate measurement readings are being measured. Once all measuring systems are verified, the test frame and the surrounding area are cleaned. A pre-test meeting is conducted before the initiation of the test to discuss specimen instrumentation, testing procedures, test expectations, and safety concerns pertaining to the test.

2.2.2 Tension and Compression Test Sequence

Laboratory hydraulic systems are started to initiate the start of the test sequence. The data acquisition system is then started at a sampling rate of 4 Hz. The system is then pressurized to an internal pressure of around 65 psi (450 kPa). After pressurization, the axial load is ready to be applied to the specimen. Loading is performed under displacement control at a rate of 1 in. (25 mm) per minute. Displacement is applied to the specimen until the system is unable to hold internal pressure or until the full stroke of the actuator is reached. Once the test is completed, data acquisition is stopped, laboratory hydraulic systems are turned off, and data is backed up.

2.2.3 Cyclic Test Sequence

Laboratory hydraulic systems are started to initiate the start of the test sequence. The data acquisition system is then started at a sampling rate of 4 Hz. The system is then pressurized to an internal pressure of around 65 psi (450 kPa). After pressurization, cyclic loading is ready to be applied to the system. Cyclic loading is applied using FEMA 461 loading protocol, released in 2001 by the Applied Technology Council (ACT)

and funded by the Federal Emergency Management Agency (FEMA). The quasi-static protocol (Protocol I) has an intended use for members whose behavior is governed by seismic forces or displacements. Force control is used to apply fifteen compression/tension cycles to the specimen before switching to displacement control and pulling the specimen in tension to failure. While in force control, load is applied to the system at a constant rate of 2 kips (8.9 kN) per second. While in displacement control, load is applied to the system at a constant rate of 1 in. (25 mm) per second. Based on preliminary results from axial tension and compression tests, a maximum cycle of 20 kips (89 kN) was determined for all test specimens. Each step amplitude is increased by 40% from the previous step until the maximum cycle was reached. Once the test is completed, the data acquisition system is turned off, laboratory hydraulic systems are set to low pressure, and the data is backed up.

2.3 Four-point Bending Setup and Instrumentation

This section discusses the two test setups utilized to apply bending load to pipe specimens. The first test setup (Bending Setup 1) was used to test pipe specimens PB11, PB12, PB14, and PB15. The second test setup (Bending Setup 2) was used to test pipe specimen PB02.

2.3.1 Bending Setup 1 - Setup and Instrumentation

Figure 2.7 shows a profile view of a typical four-point bending setup for Bending Setup 1. A 255.17 MTS actuator with a 110-kip (490kN) load capacity and an 11 in. (279 mm) stroke is mounted vertically in a loading frame to apply transverse bending load to specimens. Two support chairs consisting of 6x6 HSS members located 49.5 in. (1257 mm) from the centerline of the specimen provide bearing for the system. The actuator is equipped with a spreader beam designed to distribute bending load to two load points located at 20 in. (508 mm) on either side of the specimen's centerline. Loading saddles equipped with rollers are used at loading and reaction points to transfer load throughout the system. The loading saddles allowed for free unrestrained lateral movement throughout the system, limiting the development of axial force applied to the system under transverse displacements. A dimensioned drawing of the test setup is presented in Figure 2.8.

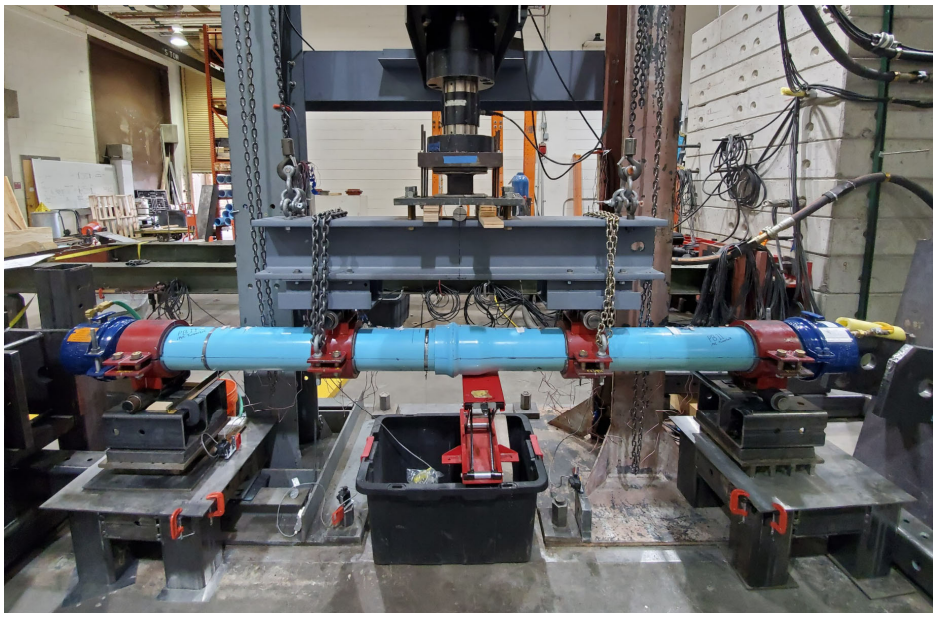

Figure 2.7. Four-Point Bending Test Setup 1 - Profile

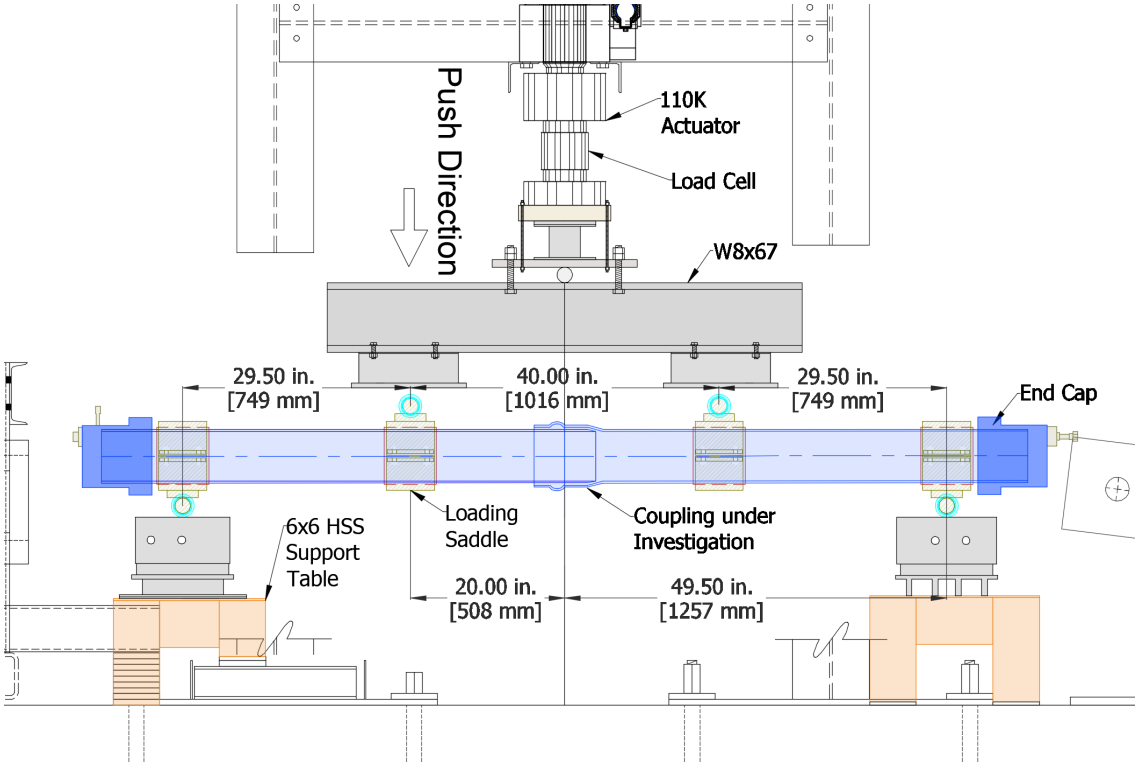

Figure 2.8. Dimensioned Drawing of Four-Point Bending Test Setup 1

Pipe specimens are cut to the required test length using standard field procedures outlined in Hughes et al. 2018. The specimen was prepared to 10 ft (3 m), consisting of two pipe segments of equal length, for a

typical bending test. The crown of the pipe is defined on the pipe by material designation written along the pipe. The crown, invert, and spring lines are defined along the pipe specimen using a half-moon leveling tool. Once the crown, invert, and spring lines are appropriately marked along the specimen, the connection under investigation is installed following field installation guidelines. End caps, shown in Figure 2.9, are then installed at each end of the specimen and tightened to 110 ft-lb (149 N-m). Load and support saddle locations, shown in Figure 2.10, are then defined from the centerline of the specimen and installed. Strain gauges are then fixed to the crown and invert of the specimen. Once strain gauges are installed, the actuator in the loading frame is fully retracted and the test specimen is placed inside the loading frame. The specimen is then centered in the frame and shims are placed at both supports, preventing lateral movement of the specimen.

Figure 2.9. Bending Test – End Cap

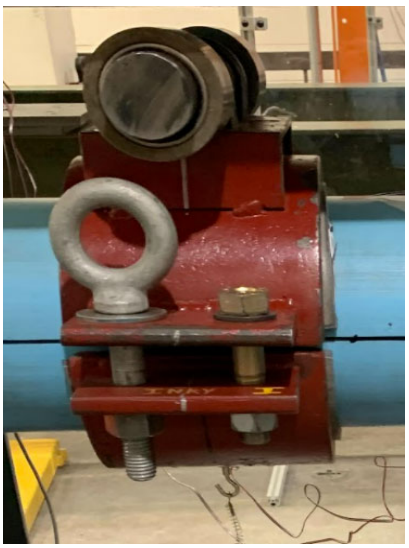

Figure 2.10. Bending Test – Loading Saddle

A list of all instruments used, naming conventions, and instrument location for each bending test performed on Bending Test Setup 1 is provided in Table 2.1. Applied force to the specimen is measured using a 110-kip (489 kN) load cell that is attached to the vertical actuator's hydraulic piston. Actuator displacements are a direct measurement of the actuator's hydraulic piston location, measured by an internal LVDT. A water supply hose running to an electronic pressure transducer is attached to the west endcap allowing for the application and measuring of internal pressure in the system throughout the test. Five vertical string potentiometers, secured to the lab floor and attached to the invert of the specimen, are used to measure various vertical displacements along the test specimen. Two X-Y strain gauge pairs are installed at four plane locations along the specimen to measure axial and circumferential strains at the crown and invert during the test. The planes were located at 10 in. (254 mm) and 35 in. (889 mm) on either side of the centerline. A schematic showing the typical instrument location for each test is presented in Figure 2.11.

Table 2.1. Four-Point Bending Test Setup 1 - Instrumentation

Instrument Description	Local Instrument Name	Location				
		PB11 - TurnerLok	**PB12 - EBBA C1900**	**PB14 - Lokx**	**PB15 - Hymax Gripper**	**PB13 - Continuous**
Crown, Axial Strain	SG35E-CA	35 in. East of CL	35.5 in. East of CL	35 in. East of CL	35 in. East of CL	35 in. East of CL
Invert, Axial Strain	SG35E-IA					
Crown, Circumferential Strain	SG35E-CC					
Invert, Circumferential Strain	SG35E-IC					
Crown, Axial Strain	SG10E-CA	10 in. East of CL	10.5 in. East of CL	10 in. East of CL	10 in. East of CL	10 in. East of CL
Invert, Axial Strain	SG10E-IA					
Crown, Circumferential Strain	SG10E-CC					
Invert, Circumferential Strain	SG10E-IC					
Crown, Axial Strain	SG10W-CA	10 in. West of CL	10.5 in. West of CL	10 in. West of CL	10 in. West of CL	10 in. West of CL
Invert, Axial Strain	SG10W-IA					
Crown, Circumferential Strain	SG10W-CC					
Invert, Circumferential Strain	SG10W-IC					
Crown, Axial Strain	SG35W-CA	35 in. West of CL	35.5 in. West of CL	35 in. West of CL	35 in. West of CL	35 in. West of CL
Invert, Axial Strain	SG35W-IA					
Crown, Circumferential Strain	SG35W-CC					
Invert, Circumferential Strain	SG35W-IC					
Vertical String Pot	VSP-40	40 in. East of CL	40.5 in. East of CL	40 in. East of CL	40 in. East of CL	40 in. East of CL
Vertical String Pot	VSP-20	20 in. East of CL	20.5 in. East of CL	20 in. East of CL	20 in. East of CL	20 in. East of CL
Vertical String Pot	VSP-6	6 in. East of CL	6.5 in. East of CL	6 in. East of CL	7 in. East of CL	6 in. East of CL
Vertical String Pot	VSP+6	N/A	6.5 in. West of CL	6 in. West of CL	7 in. West of CL	6 in. West of CL
Vertical String Pot	VSP+20	20 in. West of CL	20.5 in. West of CL	20 in. West of CL	20 in. West of CL	20 in. West of CL
MTS Actuator Piston Location	Actuator Displacement	Actuator (Above Specimen)	Actuator (Above Specimen)	Actuator (Above Specimen)	Actuator (Above Specimen)	Actuator (Above Specimen)
110-kip Load Cell	Applied Force	Actuator (Above Specimen)	Actuator (Above Specimen)	Actuator (Above Specimen)	Actuator (Above Specimen)	Actuator (Above Specimen)
Pressure Transducer	Internal Water Pressure	West Endcap	West Endcap	West Endcap	West Endcap	West Endcap

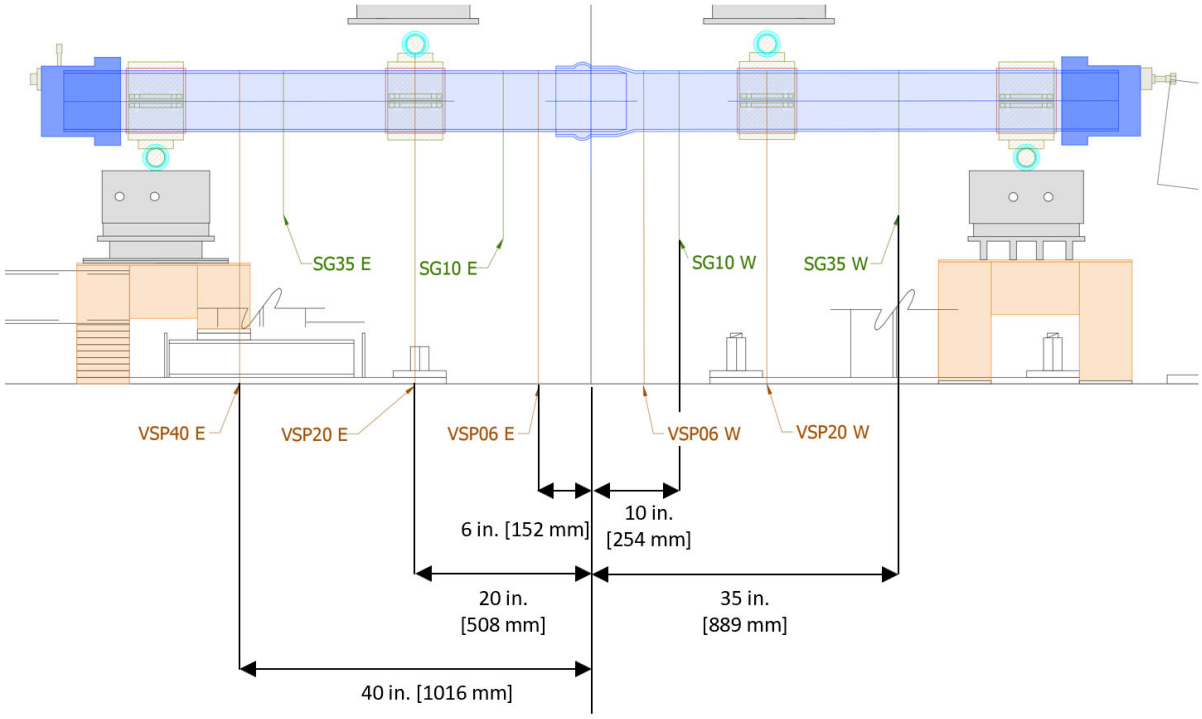

Figure 2.11. Four-Point Bending Setup 1 - Instrumentation Location

2.3.2 Bending Setup 2 - Setup and Instrumentation

Figure 2.12 shows a profile view of a typical four-point bending setup for Bending Setup 2. An MTS 661.32 Universal Testing Machine with a 1000-kip (4450-kN) capacity is used to apply transverse bending load to specimens. Two support columns consisting of HP10x57 members are located 84 in. (2134 mm) on either side of the specimen's centerline to provide bearing for the specimen. Support columns are fixed to a W12x53 beam attached to the base of the MTS testing machine. A W10x77 spreader beam is attached to the MTS Universal Testing Machines crosshead to transfer applied load to two loading saddles located 30 in. (762 mm) on either side of the specimen's centerline. All loading applied to the specimen is transferred through loading saddles equipped with rollers, allowing for free unrestrained lateral movement throughout the test, limiting the development of undesirable axial forces in the system. A dimensioned drawing of the test setup is presented in Figure 2.13.

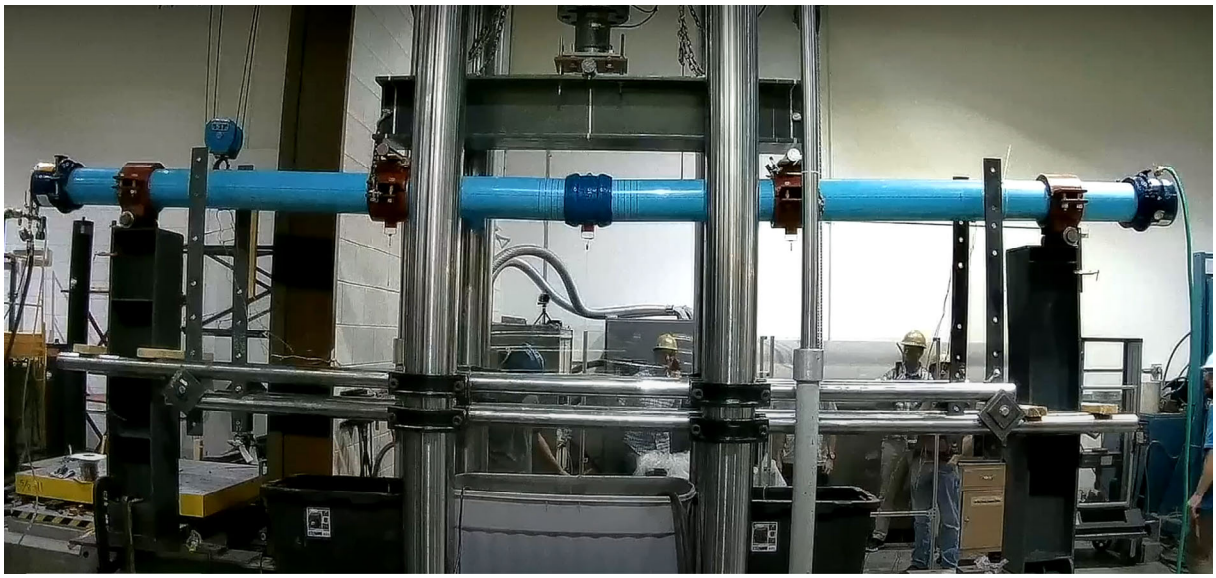

Figure 2.12. Four-Point Bending Test Setup 2 - Profile

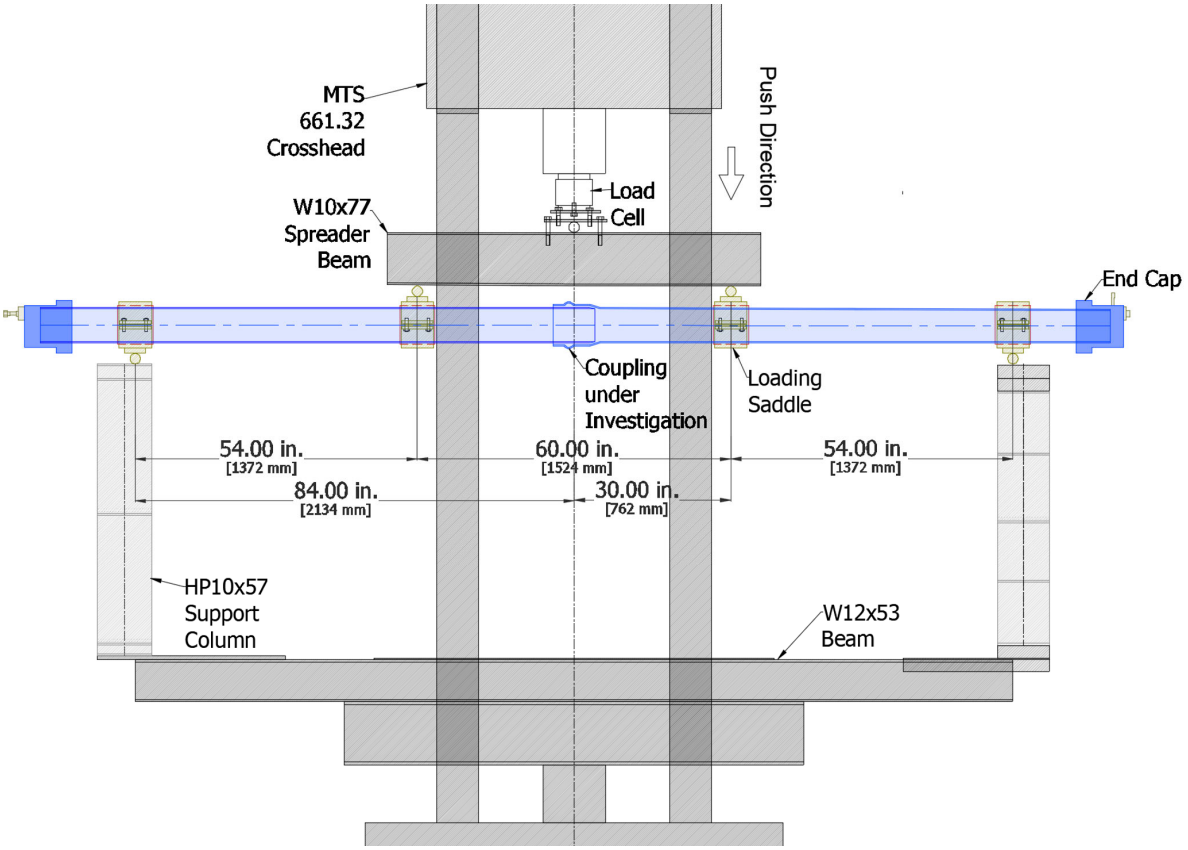

Figure 2.13. Dimensioned Drawing of Four-Point Bending Test Setup 2

Pipe specimens are cut to the required test length using standard field procedures outlined in Hughes et al. 2018. The specimen was prepared to 17 ft (5 m), consisting of two pipe segments of equal length, for a typical bending test. The crown of the pipe is defined on the pipe by material designation written along the pipe. Using a half-moon leveling tool a crown, invert, and spring lines are defined along the pipe specimen. Once the crown, invert, and spring lines are appropriately marked along the specimen, end restraints and the connection under investigation are installed following field installation guidelines. End caps are then installed at each end of the specimen and tightened to 110 ft-lb (149 N-m). Load and support saddle locations are then defined from the centerline of the specimen and installed. Strain gauges are then fixed to the crown and invert of the specimen. Once strain gauges are installed, the crosshead is raised to the maximum height, and the test specimen is placed inside the loading frame.

A list of all instruments used, naming conventions, and instrument location for each bending test performed on Bending Test Setup 2 is provided in Table 2.2. Applied force to the specimen is measured using a 32-kip (489 kN) load cell attached to the MTS testing system's crosshead. A water supply hose running to an electronic pressure transducer is attached to the east end cap allowing for the application and measuring of internal pressure in the system throughout the test. Five vertical string potentiometers, secured to the W12x53 support beam and attached to the invert of the specimen, are used to measure various vertical displacements along the test specimen. Two X-Y strain gauge pairs were installed at two plane locations along the specimen to measure axial and circumferential strains at the crown and invert during the test. The planes are located at approximately 10 in. (254 mm) west and 60 in. (1524 mm) east of the specimen's centerline. A schematic showing the typical instrument location for each test is presented in Figure 2.14.

Table 2.2. Four-Point Bending Test Setup 1 - Instrumentation

Instrument Description	Local Instrument Name	Location
		PB02 - RCT
Crown, Axial Strain	SG60E-CA	57 in. East of CL
Invert, Axial Strain	SG60E-IA	
Crown, Circumferential Strain	SG60E-CC	
Invert, Circumferential Strain	SG60E-IC	
Crown, Axial Strain	SG10W-CA	10 in. West of CL
Invert, Axial Strain	SG10W-IA	
Crown, Circumferential Strain	SG10W-CC	
Invert, Circumferential Strain	SG10W-IC	
Vertical String Pot	VSP-70	70 in. East of CL
Vertical String Pot	VSP-30	33 in. East of CL
Vertical String Pot	VSP-0	0 in. East of CL
Vertical String Pot	VSP+30	33 in. West of CL
Vertical String Pot	VSP+70	70 in. West of CL
35-kip Load Cell	Applied Force	MTS Crosshead (Above Specimen)
Pressure Transducer	Internal Water Pressure	East Endcap

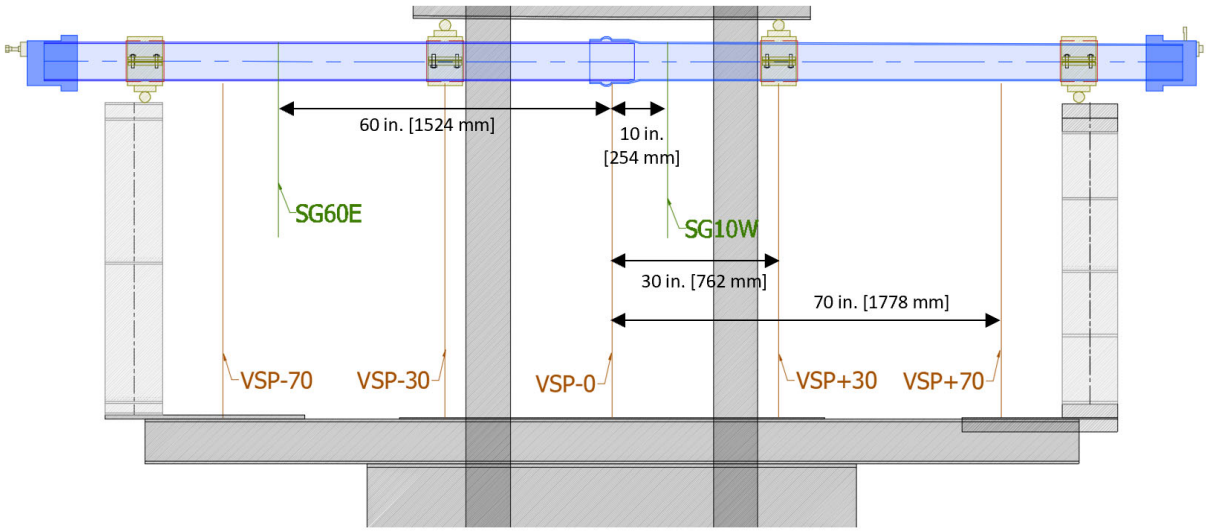

Figure 2.14. Four-Point Bending Setup 2 - Instrumentation Location

2.4 Four-Point Bending Test Procedure

The following section provides details of the overall test sequence for monotonic and cyclic four-point bending tests.

2.4.1 Pre-Test

Once the test specimen is instrumented and secured in the loading frame, an instrumentation check sequence, consisting of manually displacing string pots, is conducted to verify measurements are being recorded. The pipe system is then filled with water. As the system is being filled with water, the air bleeder valve at the west end restraint is left open, allowing air to be released from the specimen. After the system is filled with water the air bleeder valve is closed, pressurizing the system to approximately 65 psi (450 kPa). The system is then checked for any signs of leaking. Pressure is then released from the system. A pressurization sequence is then performed to verify that load cell and strain gauge measurements are recording accurately. Data is recorded throughout the sequence and analyzed to verify accurate measurement readings are being measured. Once all measuring systems are verified, the test frame and the surrounding area are cleaned. A pre-test meeting is conducted before the initiation of the test to discuss specimen instrumentation, testing procedures, test expectations, and safety concerns pertaining to the test.

2.4.2 Bending Test Setup 1 – Monotonic Test Sequence

The activation of hydraulics initiated the testing sequence to the vertical actuator in the load frame. Supporting chains, preventing the application of self-weight load from the spreader beam, are then loosened. Data acquisition is then started, and internal pressure of approximately 65 psi (448 kPa) is applied to the specimen. Data is recorded at a frequency of 4 Hz. After applying internal pressure, the supporting jack at the center of the specimen is removed, allowing the pipe to deflect under its self-weight. The actuator is then lowered until a preload of around 1 kip (4.45 kN) is applied to the system, ensuring the system is seated and centered properly in the frame. Shims at the supports are then removed, allowing the specimen to move laterally and geometrically center in the frame throughout loading. Vertical displacement is then applied to the specimen until the full stroke of the actuator [11 in. (279 mm)] is reached or the system experiences a complete loss of pressure due to leakage or fracture. Next, displacement is applied to the pipe at a loading rate of 1 in./min (25.4 mm/min). If no fracture or complete loss of pressure is observed, the specimen is unloaded, and the test is concluded. Once the test is completed, recorded data is backed up, spreader beam support chains are retightened, and hydraulics are turned off to the actuator.

2.4.3 Bending Test Setup 2 – Monotonic Test Sequence

The test starts with the activation of hydraulics to the MTS testing machine. The MTS crosshead is then lowered to approximately 1 in. (25 mm) above the specimen. Data acquisition is then initiated at 1 Hz and the pipe is pressurized to around 65 psi (448 kPa). Once the pipe maintained a consistent pressure, the center jack used to level the pipe at the connection is removed, allowing the specimen to deflect under self-weight. The crosshead is then lowered by releasing the crosshead locks and allowing the crosshead to displace downward at a consistent rate of 0.5 in./min (13 mm/min). The crosshead is lowered until the specimen experienced slippage or fracture at the connection resulting in significant loss of pressure or the maximum limits of the testing setup are reached. If no fracture or complete loss of pressure is observed, the specimen was unloaded, and the test was concluded. Once the test is completed, recorded data is backed up, spreader beam support chains are retightened, and hydraulics are turned off to the MTS testing machine.

2.4.4 Bending Test – Cyclic Test Sequence

Bending specimens that performed well and showed little or no signs of leaking during monotonic testing are subjected to several iterations of cyclic loading in the transverse direction. Laboratory hydraulic systems are started to initiate the start of the test sequence. The data acquisition system is then started at a sampling rate of 16 Hz. The system is then pressurized to an internal pressure of around 65 psi (450 kPa). After pressurization, load is applied to the specimen at 1 in./min (25.4 mm/min) until the specimen reaches a system rotation of double the allowable design standard proposed by Davis et al. 2019. The initial applied deformation is representative of a pipeline system significantly damaged/deformed in a significant seismic event. 100 cycles of cyclic loading are then applied to the specimen at a frequency of 1 Hz and a maximum amplitude of 0.25 in. (6.4 mm). If no failure is observed, the maximum amplitude is increased to 0.5 (12.8 mm) and another 100 cyclic cycles were applied. If no failure is observed, another 50 cycles of cyclic loading are applied to the specimen with a maximum amplitude of 1 in. (25.4 mm) at a frequency of 0.5 Hz. The actuator is then lowered an additional 4 in. (102 mm) and 50 more 1 in. (25.4 mm) cycles are administered to the specimen. Finally, the full stroke of the actuator is then applied to the specimen, followed by an additional 50 cycles at a 1 in. (25.4 mm) maximum amplitude. If no fracture or complete loss of pressure is observed, the specimen is unloaded, and the test was concluded. Once the test is completed, recorded data is backed up, spreader beam support chains are retightened, and hydraulics are turned off to the MTS testing system.

3. Experimental Test Results

3.1 Tension Test Results

The following sections provide results from axial tension tests performed on iPVC pipeline systems. A total of five tension tests were performed at the CIEST laboratory.

3.1.1 Tension Test PT02 Results – iPVC RCT Coupling

Pipe specimen PT02 consisted of an iPVC pipe with an RCT Flex-Tite coupling connection at the midpoint. The specimen was pulled in axial tension until failure occurred at the connection. Since this was one of the first pipe tests performed in this study, the test was paused at two locations for inspection to ensure the test setup was functioning properly. Figure 3.1 shows photos for the pre-test setup of specimen PT02 as well as the specimen just after failure at the connection.

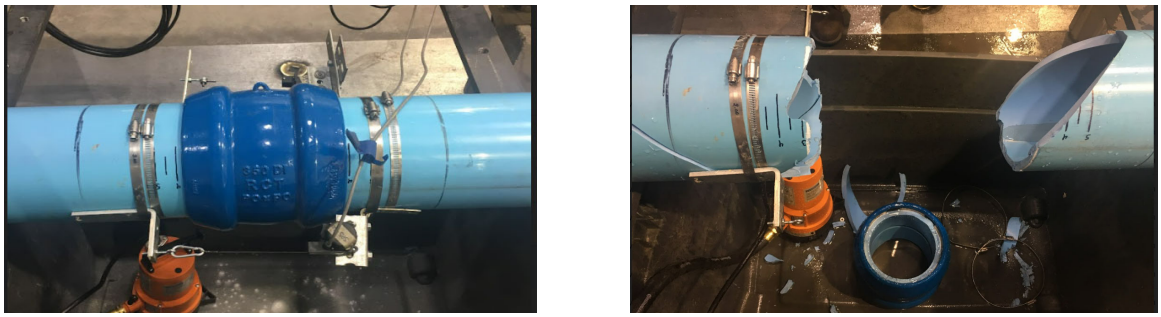

(a) Pre-Test Setup (b) Failure at Connection

Figure 3.1. Specimen PT02 (a) Setup and (b) after Failure

The progression of pressure, actuator force, and actuator displacement is presented in Figure 3.2. The specimen maintained an average pressure of 59 psi (407 kPa). The test was paused for inspection twice during the test, at approximately 250 seconds and 450 seconds. During each pause, the pressure in the system was manually released to around 50 psi (345 kPa) and then increased to its initial pressure of around 65 psi (448 kPa) to verify that the system's pressure transducer was functioning properly throughout the test. Figure 3.3 displays the actuator force versus displacement. Actuator displacement and actuator force are direct measurements of the actuator's hydraulic piston location and attached load cell, respectively. At the start of loading actuator force and actuator displacement increases at a relatively constant rate of around 15 kips/in. (2.6 kN/mm). At approximately 2.9 in. (74 mm) of actuator displacement and 44 kips (196 kN) of actuator force, the response begins to soften and become nonlinear. Two sharp drops in force are visible in the response at 1.1 in. (28 mm) and 2.3 in. (58 mm) of actuator displacement. These sharp drops can be attributed to the two pauses taken during the loading sequence, allowing the system to relax and load to

decrease. Figure 3.4 presents the actuator force versus joint displacement. Joint displacement was measured by two string pots at both the north and south spring lines of the specimen that spanned across the RCT connection. At approximately 0.53 in. (13 mm) of joint displacement, the string pot measuring the north spring line joint displacement started to slip, no longer providing accurate data. The joint displacement follows a similar response to the force versus actuator displacement, producing a maximum joint displacement of 0.92 in. (23 mm) at the south spring line before failure occurred at the connection.

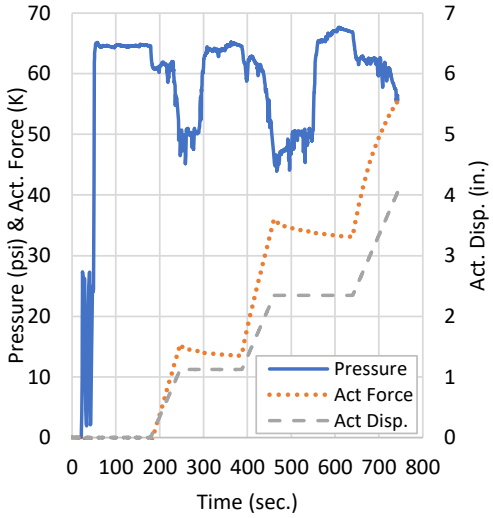

Figure 3.2. PT02-Pressure and Act. Disp. vs. Time

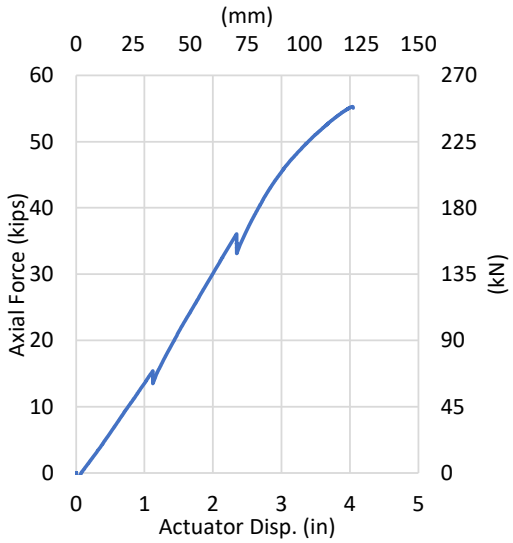

Figure 3.3. PT02-Force vs. Act. Disp.

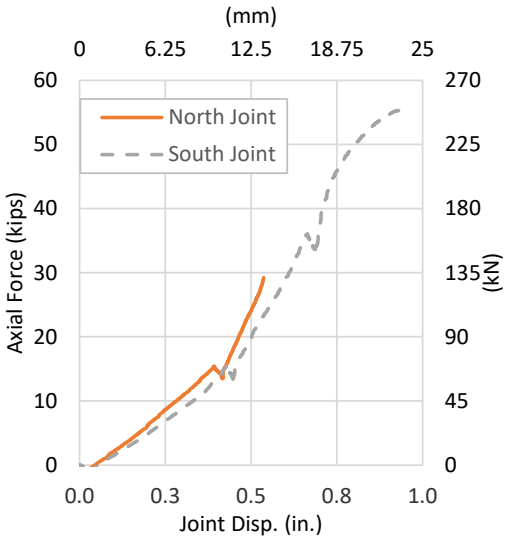

Figure 3.4. PT02-Force vs. Joint Displacement

Axial and circumferential strains were recorded at the crown, invert, and both spring lines of the bell section. Strain versus time and strain versus actuator displacement can be viewed in Figure 3.5 and Figure 3.6, respectively. During pressurization at the start of the test, an increase in circumferential strain is observed, accompanied by a slight decrease in axial strain. This slight decrease in axial strain can be attributed to the Poisson's effect as the pipe barrel expands circumferentially due to the load applied from internal pressure. Once loading is applied to the system, a sharp increase in axial strain and a decrease in circumferential strain is observed as the pipe barrel begins to elongate due to applied tensile force. The maximum axial strain peaked at 1.00 %, and the maximum circumferential strain peaked at -0.446 %. It is important to note that a measuring error occurred during the testing sequence, rendering the strain data inaccurate. Strain values used to assess the systems response in further analysis will be obtained from the subsequent cyclic test performed on the same system.

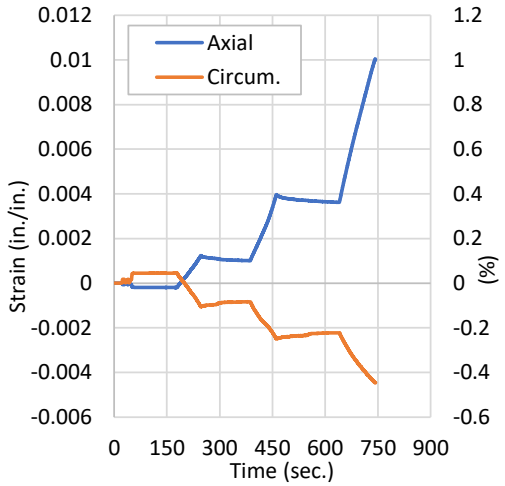

Figure 3.5. PT02-Strain vs. Time

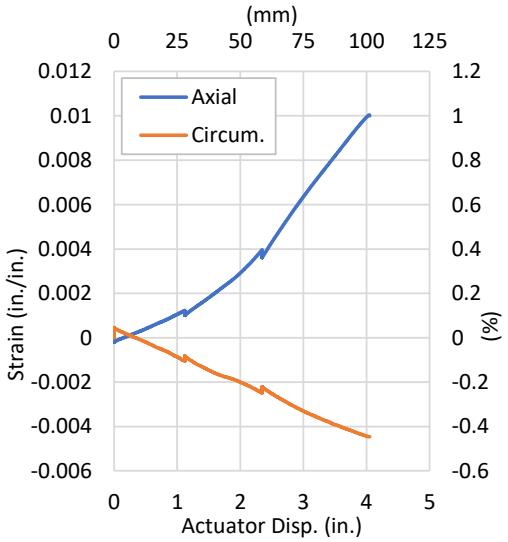

Figure 3.6. PT02-Strain vs. Act. Disp.

The test concluded with circumferential fractures occurring at both ends of the RCT coupling. At fracture, a maximum axial force of 55.3 kips (246 kN) and a maximum actuator displacement of 4.05 in. (103 mm) were recorded. The sudden fracture resulted in an abrupt loss of pressure in the system. The fracture propagated 4.5 in (114 mm) along the east pipe segment and 9.0 in. (229 mm) along the west pipe segment, as shown in Figure 3.7. Prior to fracture, there were no signs of leakage.

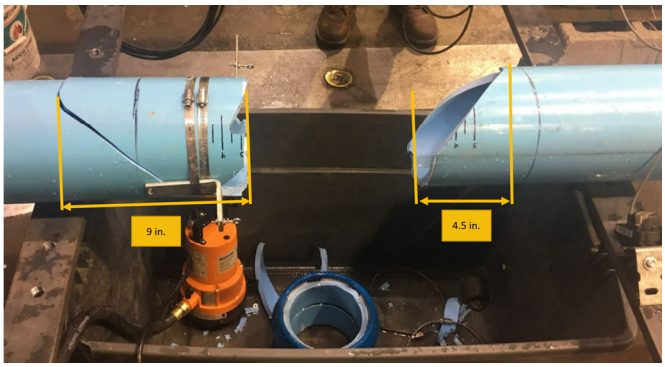

Figure 3.7. Specimen PT02 Fracture at Connection

3.1.2 Tension Test PT27 Results – iPVC TurnerLok Gasket

Pipe specimen PT27 consisted of an iPVC pipe with an internal TurnerLok gasket restraining the bell and spigot connection at the midpoint. The specimen was pulled in axial tension at a consistent rate until failure occurred at the bell and spigot connection. Figure 3.8 shows photos for the pre-test setup of specimen PT27 as well as the specimen just after failure at the connection.

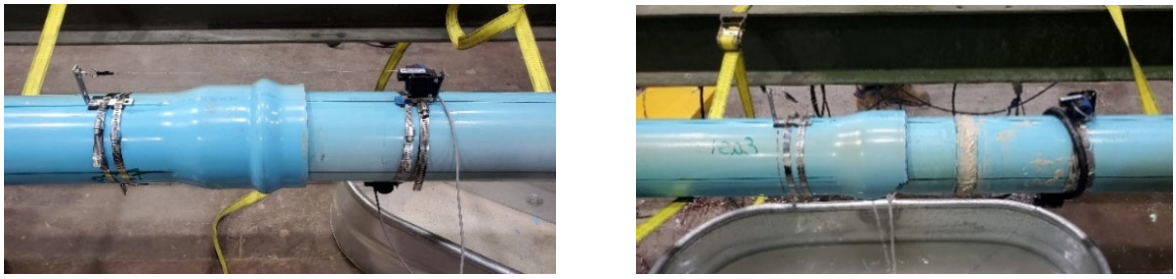

(a) Pre-Test Setup (b) Failure at Connection

Figure 3.8. Specimen PT27 (a) Setup and (b) after Failure

The progression of pressure, actuator force, and actuator displacement is presented in Figure 3.9. The specimen maintained an average pressure of 62 psi (430 kPa) throughout the test experiencing minor fluctuations during the loading sequence. Figure 3.10 displays the actuator force versus displacement. Actuator displacement and force are direct measurements of the actuator's hydraulic piston and attached load cell, respectively. At the start of loading, actuator force and actuator displacement increase at a relatively constant rate of around 17 kips/in. (3.0 kN/mm). There is a sharp drop in force at approximately 1.75 in (44 mm) of actuator displacement and 25 kips (111 kN) of actuator force. This drop in force can be attributed to the onset of yielding at the bell's gasket groove, allowing the gripper gasket to move into the end of the bell. At approximately 1.9 in (48 mm) of actuator displacement and a force of approximately 24 kips (107 kN), the gasket groove begins to harden, stopping the gasket from moving and stiffening the system's response.

Figure 3.11 presents the actuator force versus joint displacement. String pots measured joint displacement at both the crown and invert of the specimen that spanned from the spigot across the bell. The force reduction, due to yielding at the gasket groove, seen in Figure 3.10 is also present in Figure 3.11 at approximately 0.6 in. (15 mm) of joint displacement. A maximum joint displacement of 1.42 in. (36 mm) was recorded before failure occurred.

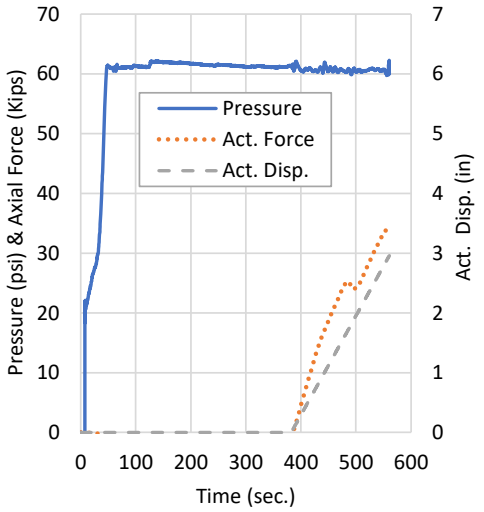

Figure 3.9. PT27-Pressure and Act. Disp. vs. Time

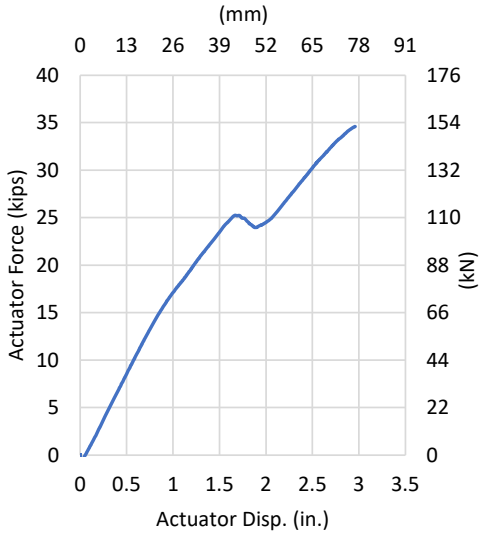

Figure 3.10. PT27-Force vs. Act. Disp.

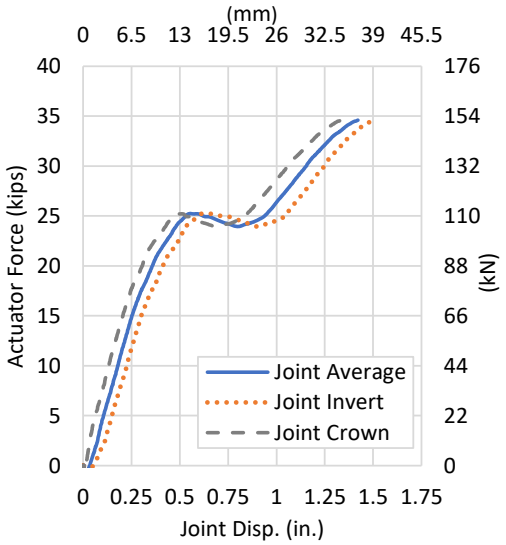

Figure 3.11. PT27-Force vs. Joint Displacement

Axial and circumferential strains were recorded at the crown, invert, and both spring lines of the bell section. Strain versus time and strain versus actuator displacement can be viewed in Figure 3.12 and Figure 3.13 respectively. During pressurization at the start of the test, an increase in circumferential strain is observed, accompanied by a slight decrease in axial strain. This slight decrease in axial strain can be attributed to Poisson's effect. Once loading is applied to the system, a sharp increase in axial strain and a decrease in circumferential strain are observed as the pipe barrel begins to elongate due to applied tensile force. The maximum axial strain peaked at 0.781 %, and the maximum circumferential strain peaked at -0.119 %.

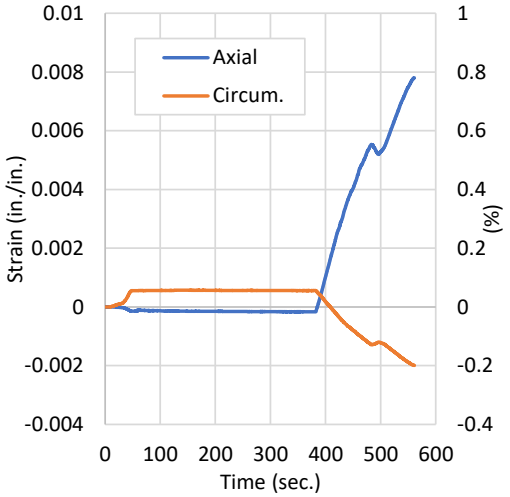

Figure 3.12. PT27-Strain vs. Time

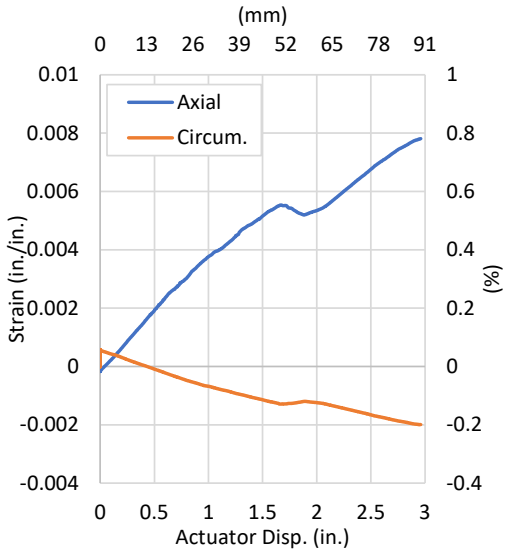

Figure 3.13. PT27-Strain vs. Act. Disp.

Just before fracture a maximum axial force of 34.6 kips (154 kN) and a maximum actuator displacement of 2.96 in. (75.2 mm). As shown in Figure 3.14 (a-d), yielding and circumferential cracking along the bell of the specimen was observed during failure. The sudden fracture of the bell resulted in an abrupt loss of pressure and ejection of the internal TurnerLok gasket, resulting in the conclusion of the test. Gouges from the gasket's toothed wedges were visible along the spigot of the specimen, shown in Figure 3.15. Prior to fracture, there were no signs of leakage.

(a) Start of PT27 Test

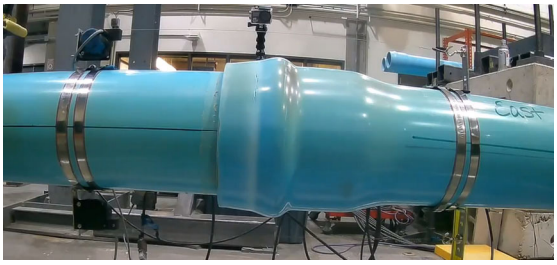

(b) Start of yielding and crack formation in the bell

(c) Yielding and cracking at the bell just before specimen failure

(d) Fracture of the bell resulting in loss of pressurization

Figure 3.14. Images of PT27 during the test progression

(a) Gouging in Spigot after Specimen Failure

(b) Gouging in Spigot after Specimen Failure

Figure 3.15. Spigot Gouging post PT27

3.1.3 Tension Test PT30 Results – iPVC EBAA C1900 Restraint Harness

Pipe specimen PT30 consisted of an iPVC pipe with an external EBAA C1900 Restraint Harness. Restraint nuts for this specimen were located to allow for 1 in. (25 mm) of joint opening before engaging and resisting axial deformation. The specimen was pulled in tension at a constant rate until failure occurred at the spigot at west restraint. Figure 3.16 shows photos for the pre-test setup of specimen PT30 as well as the specimen just after failure at the connection.

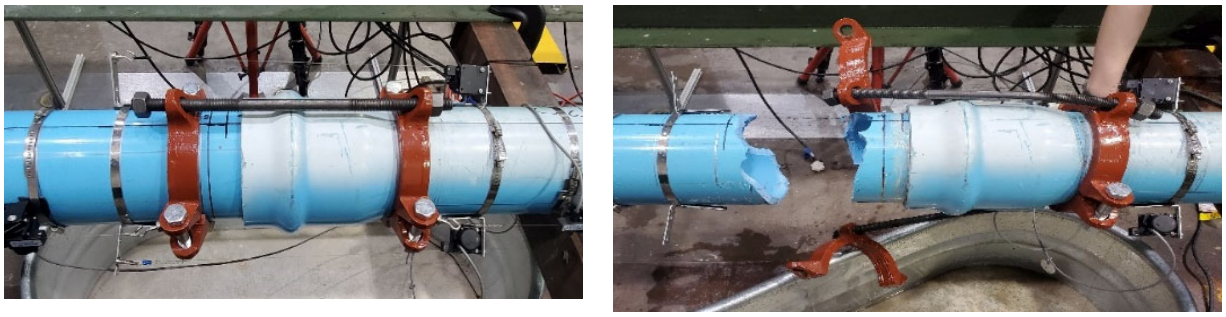

(a) Pre-Test Setup (b) Failure of Bell and Spigot

Figure 3.16. Specimen PT30 (a) Setup and (b) After Failure

The progression of pressure, actuator force, and actuator displacement is presented in Figure 3.17. The specimen maintained an average pressure of 63 psi (435 kPa) throughout the test with minor fluctuations. Figure 3.18 displays the actuator force versus displacement. A negative force is recorded at the start of the test from the force applied by internal pressure. Due to the allowable 1 in. (25 mm) of joint displacement, there is relatively little force increase for the first 1 in. (25 mm) of actuator displacement, and the joint is able to expand under the load from internal pressure. At approximately 2.9 in (74 mm) of actuator displacement and 20 kips (89 kN) of actuator force, the C1900 restraint bolts begin to yield and allow for rotation of the harnesses causing a slight slope softening in force versus displacement. At approximately 3.5 in (89 mm) of actuator displacement and a force of approximately 25 kips (111 kN), the top and bottom halves of the C1900 restraints make contact, stopping restraint rotation, and causing an increase in slope.

Figure 3.19 presents the actuator force versus joint displacement. Joint displacement was measured by a string pot at both the crown and invert of the specimen that spanned from the spigot across the bell. The reduction and increase in slope is also present in Figure 3.19 at a joint displacement of approximately 2 in. (51 mm) and 2.5 in. (64 mm) respectively. The joint allowed for a maximum displacement of 4.36 in. (111 mm) before failure occurred.

This particular test also provides an estimate of the force required to pull the spigot out of the bell for standard conditions without a restraining mechanism. Figure 3.20 provides the actuator force during the first 1 in. (25 mm) of pullout prior to restrain engagement. Also show in an estimate of the force imposed

on the actuator due to internal pressurization of the pipe. The difference of these two axial force quantities provides an estimate of the joint pullout force, shown in orange in the figure. Consistent with unpressurized conditions experienced by lab staff while assembling the specimens, approximately 150 to 200 pounds is required to displace an unrestrained joint. This value provides an estimate of the axial force required to displace an unrestrained bell and spigot joint during a ground movement event.

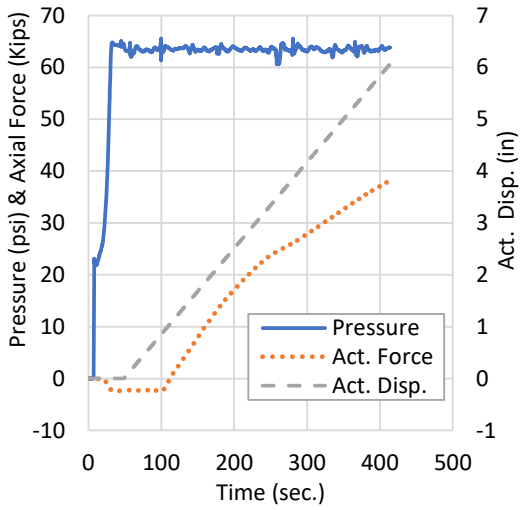

Figure 3.17. PT30-Pressure and Act. Disp. vs. Time

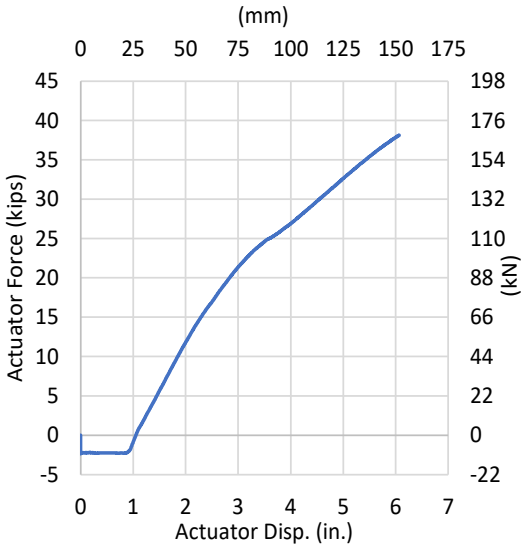

Figure 3.18. PT30-Force vs. Act. Disp.

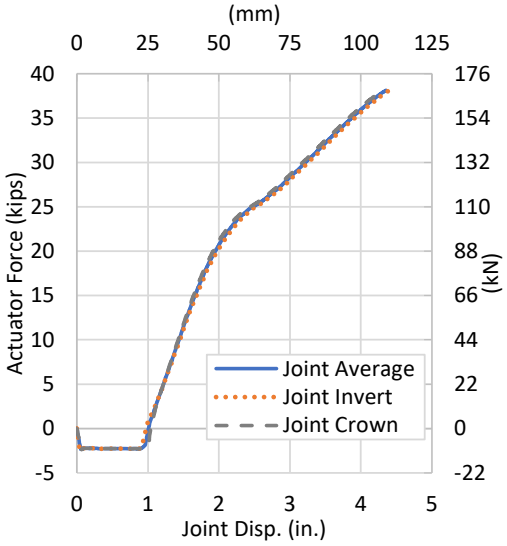

Figure 3.19. PT30-Force vs. Joint Displacement

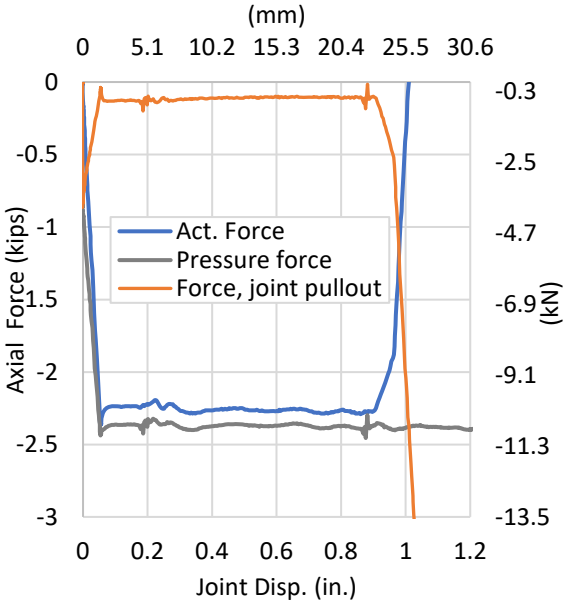

Figure 3.20. PT30-Axial force during initial joint pullout

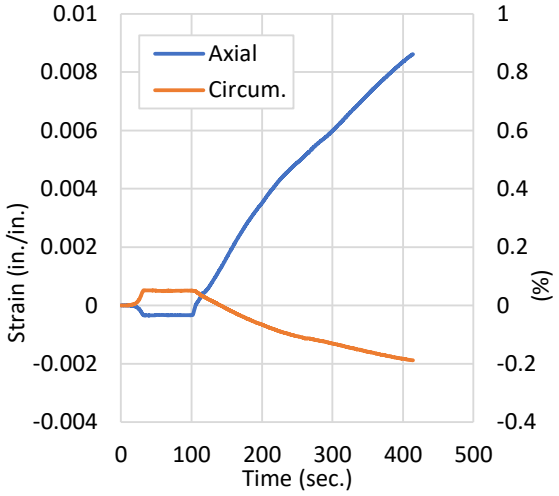

Figure 3.21. PT30-Strain vs. Time

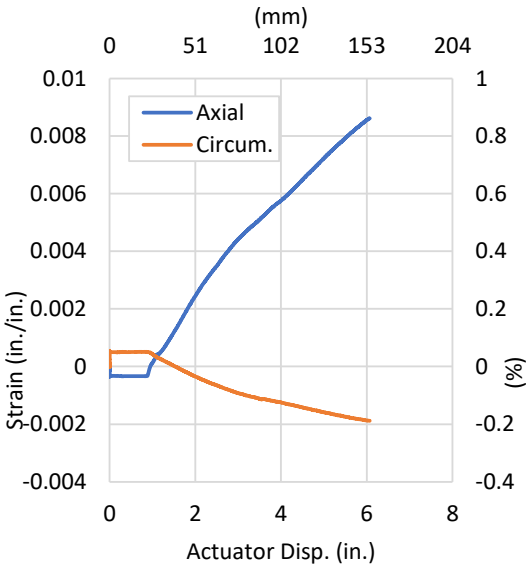

Figure 3.22. PT30-Strain vs. Act. Disp.

Axial and circumferential strains were recorded at the crown, invert, and both spring lines of the bell section. Strain versus time and strain versus actuator displacement can be viewed in Figure 3.21 and Figure 3.22, respectively. Due to pressurization, a negative axial and a positive circumferential strain are recorded at the test's start. At 1 in. (25 mm) of actuator displacement, the axial strain begins to increase as the restraint harnesses begin to engage and resist applied displacement. At this point, circumferential strains begin to decrease due to the Poison's effect on the material. The maximum axial strain peaked at 0.862 %, and the maximum circumferential strain peaked at -0.188 %.

At a maximum axial force of 38.1 kips (170 kN) and a maximum actuator displacement of 6.07 in. (154 mm), the spigot and west C1900 vertical bolt simultaneously fracture, causing a loss of pressurization in the system. Prior to this fracture, there were no signs of leakage. Images taken during the failure process are presented in Figure 3.23 (a-d).

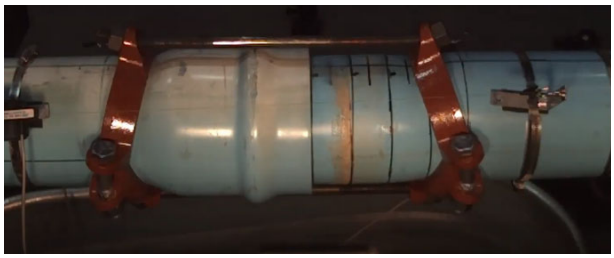

(a) Start of Failure

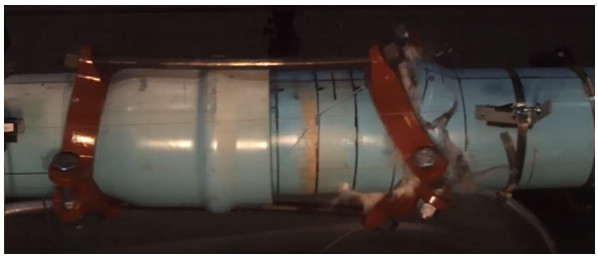

(b) Fracture of Spigot and Shearing of Restraint Bolts

(c) Immediately after Failure (d) After Failure

Figure 3.23. Images of PT30 failure progression

3.1.4 Tension Test PT33 Results – iPVC Lokx Coupling

Pipe specimen PT33 consisted of an iPVC pipe with a Lokx coupling located at the midpoint. Axial tension was applied to the specimen at 1 in./min (25.4 mm/min) until failure occurred at the coupling. Figure 3.24 shows photos for the pre-test setup of specimen PT33 as well as the specimen after failure at the connection.

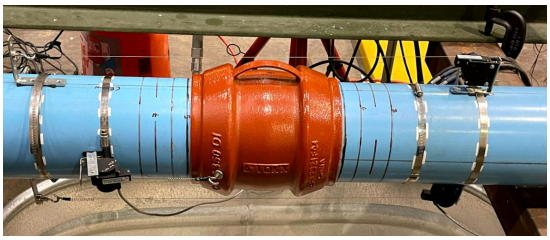

(a) Pre-Test Setup (b) Failure at Connection

Figure 3.24. Specimen PT33 (a) Setup and (b) Failure

The progression of pressure, actuator force, and actuator displacement is presented in Figure 3.25. The specimen maintained an average pressure of 64 psi (441 kPa) throughout the test experiencing minor fluctuations. Figure 3.26 displays the actuator force versus displacement. Actuator force and actuator displacement increase linearly at a relatively constant rate throughout the test of around 16 kips/in. (2.8 kN/mm). However, at approximately 4.15 in (105 mm) of actuator displacement and a maximum actuator force of 60 kips (267 kN), there is a sharp drop in force just before the sudden fracture of the Lokx connection. Figure 3.27 presents the actuator force versus joint displacement. Joint displacement was measured by a string pot at both the crown and invert of the specimen that spanned across the Lokx coupling to each pipe segment. Joint displacement shows a slightly different response to tensile load when compared to overall actuator displacement. For the first 0.38 in. (9.7 mm) of joint displacement, the system response increases at a rate of 40 kips/in. (7 kN/mm). The system response then increases to 90 kips/in. (15.8 kN/mm) until 1.13 in. (29 mm) of joint displacement, where the system response begins to soften just before failure. A maximum average joint displacement of 1.37 in. (35 mm) was recorded before failure occurred.

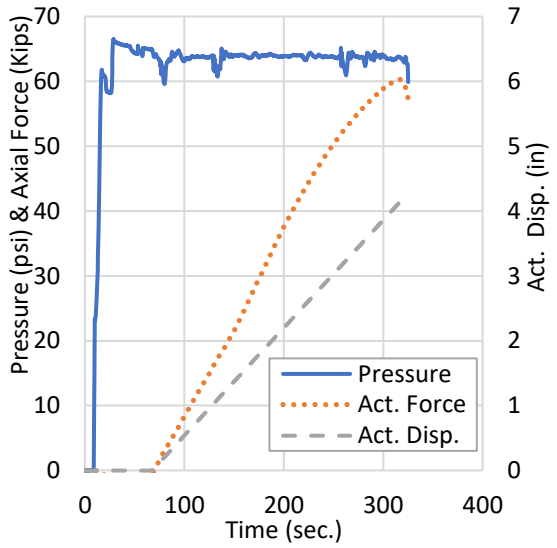

Figure 3.25. PT33-Pressure and Act. Disp. vs. Time

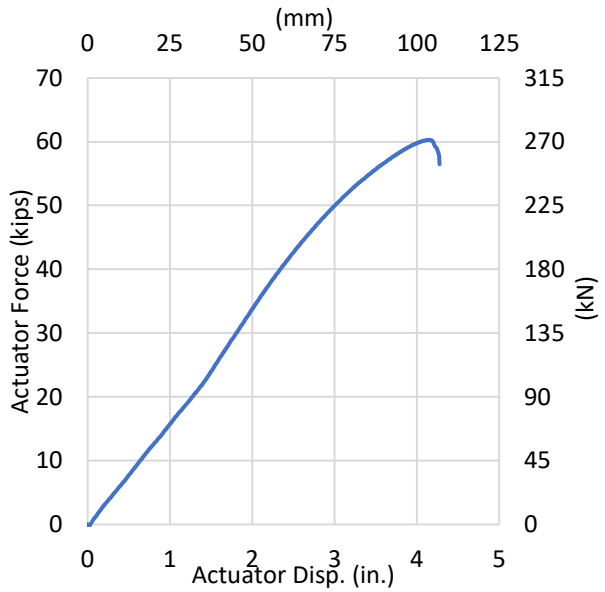

Figure 3.26. PT33-Force vs. Act. Disp.

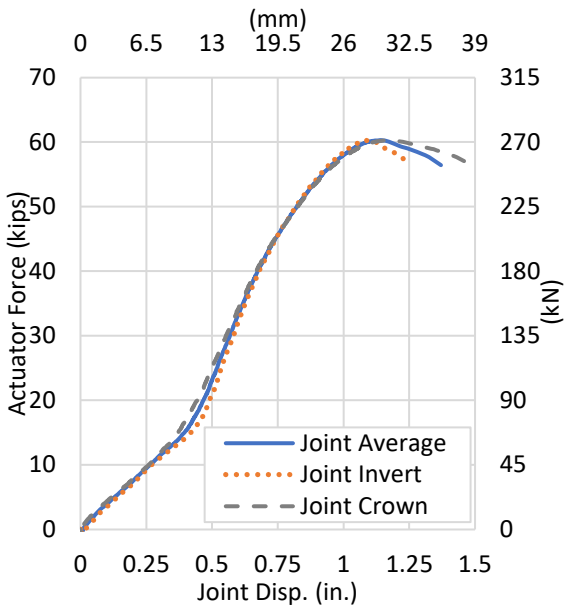

Figure 3.27. PT33-Force vs. Joint Displacement

Axial and circumferential strains were recorded at the east barrel's crown, invert, and both spring lines. Strain versus time and strain versus actuator displacement can be viewed in Figure 3.28 and Figure 3.29, respectively. During pressurization at the start of the test, an increase in circumferential strain is observed, accompanied by a slight decrease in axial strain. This slight decrease in axial strain can be attributed to

Poisson's effect. Once loading is applied to the system, a sharp increase in axial strain and a decrease in circumferential strain are observed as the pipe barrel begins to elongate due to applied tensile force. The maximum average axial strain peaked at 1.69%, and the maximum average circumferential strain peaked at -0.51 %.

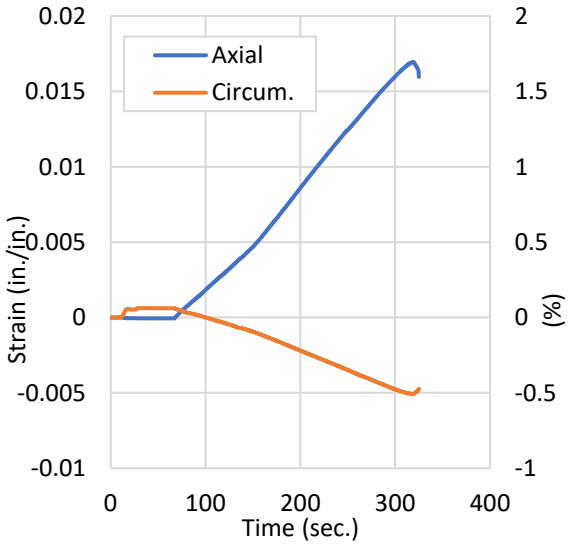

Figure 3.28. PT33-Strain vs. Time

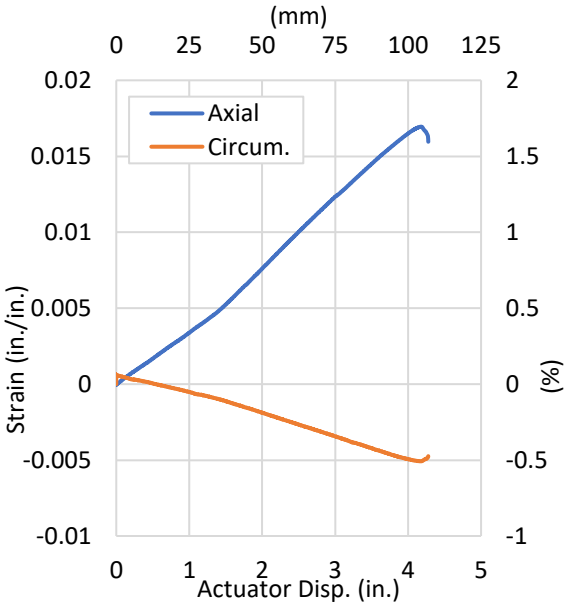

Figure 3.29. PT33-Strain vs. Act. Disp.

A maximum axial force of 60.3 kips (268 kN) and a maximum actuator displacement of 4.27 in. (108 mm) were recorded before the fracture of the connection. The sudden fracture of the coupling resulted in an abrupt loss of pressurization and ejection of the east Lokx gasket. Gouges from the gasket's toothed wedges were visible along the spigot of the specimen after failure. After the test, there were no signs of axial or circumferential cracking along the specimen. A series of photos taken during the specimen's failure can be viewed in Figure 3.30 (a-d). Gouges from the gasket's wedged teeth left on the spigot are visible in Figure 3.31. Prior to fracture, there were no signs of leakage.

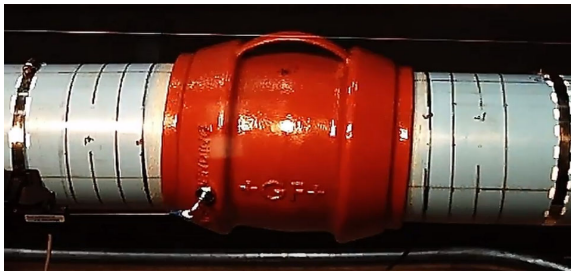

(a) Just before specimen failure

(b) Fracture of the lower east section of the coupling and ejection of the gasket

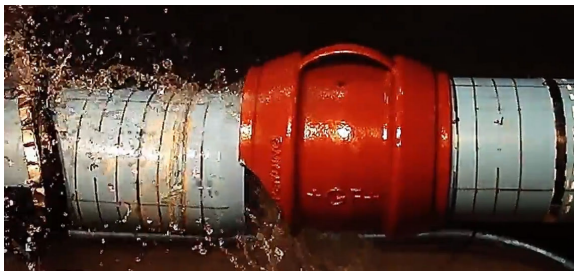

(c) Loss of pressure just after coupling fracture

(d) Specimen at rest after completion of the test

Figure 3.30. Images of PT33 during the test failure

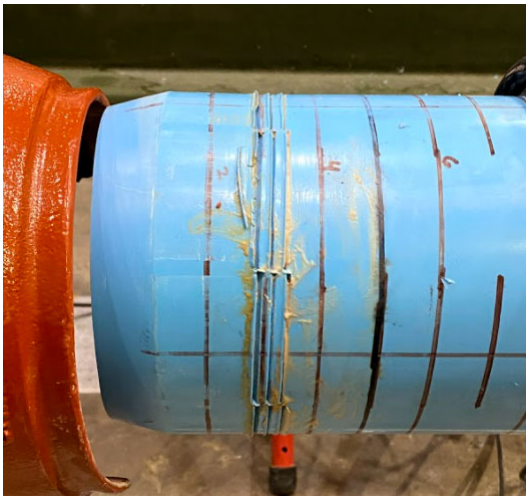

Figure 3.31. PT-33 Spigot Gouging

3.1.5 Tension Test PT38 Results – iPVC Hymax Grip Coupling

Pipe specimen PT38 consisted of an iPVC pipe with a Hymax Grip coupling located at the midpoint. Pipe segments were inserted 4 in. (102 mm) into each end of the Hymax coupling. Restraint bolts, located at the top of the coupling were tightened to the minimum required torque specifications for 6 in. (152 mm) nominal diameter pipes [110 lb.-ft (149 N-m)]. Tensile load was applied to the specimen at a constant rate of 1 in./min (25.4 mm/min) until slippage and ultimate failure occurred at the coupling. Just before failure, leaking was observed at the east end of the coupling. Figure 3.32 shows photos for the pre-test setup of specimen PT38 as well as the specimen after failure at the connection.

(a) Pre-Test Setup (b) Failure at Connection

Figure 3.32. Specimen PT38 (a) Setup and (b) Failure

The progression of pressure, actuator force, and actuator displacement is presented in Figure 3.33. The specimen maintained an average pressure of 64 psi (441 kPa) throughout the test experiencing minor fluctuations. Figure 3.34 displays the actuator force versus displacement. The initial response of the system increases linearly at a constant rate of around 20 kips/in. (3.5 kN/mm). However, at 5 kips (22.2 kN) and 0.25 in. (6.4 mm) the system response begins to soften to a constant rate of around 12.1 kips/in. (2.1 kN/mm). Just before failure at the connection, leaking was observed at the east end of the Hymax coupling at an applied force of 27.8 kips (124 kN) and an actuator displacement of 2.34 in. (59 mm). Figure 3.35 presents the actuator force versus joint displacement. Joint displacement was measured by a string pot at both the crown, invert, and both spring lines of the specimen that spanned across the Hymax coupling to each pipe segment. The joint displacement response has an initial increase of 2 kips (9 kN) under relatively no joint displacement. The joint response then increases at a relatively consistent rate of 32.9 kips/in. (5.8 kN/mm) until 0.55 in. (14 mm) of joint displacement, where slippage at the joint begins to occur. A maximum average joint displacement of 1.24 in. (31 mm) was recorded just before failure, with the onset of leaking occurring at 1.06 in. (27 mm) of average joint displacement.

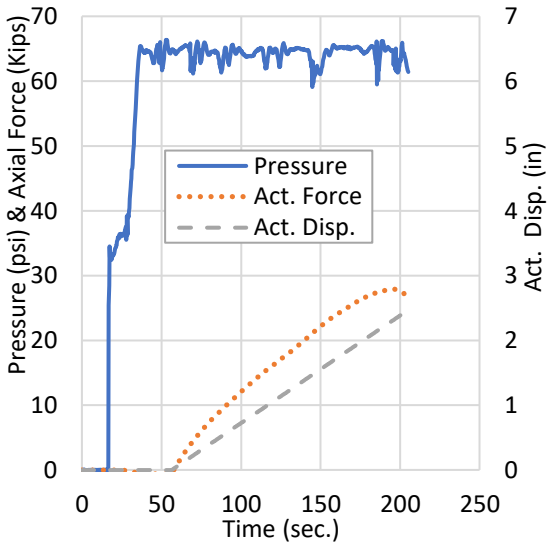

Figure 3.33. PT38-Pressure and Act. Disp. vs. Time

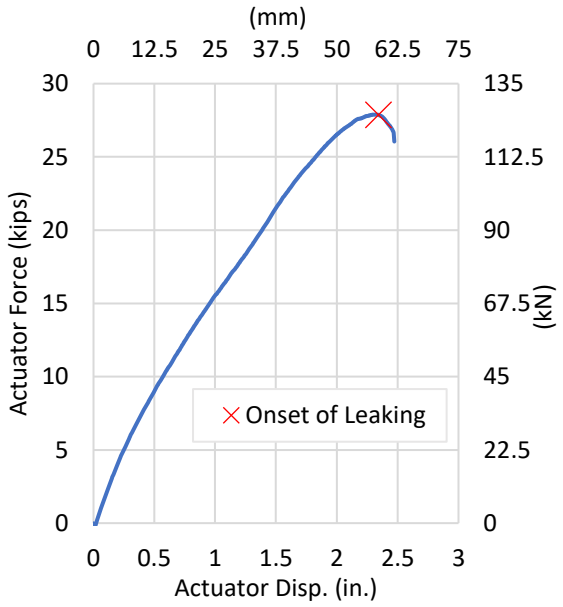

Figure 3.34. PT38-Force vs. Act. Disp.

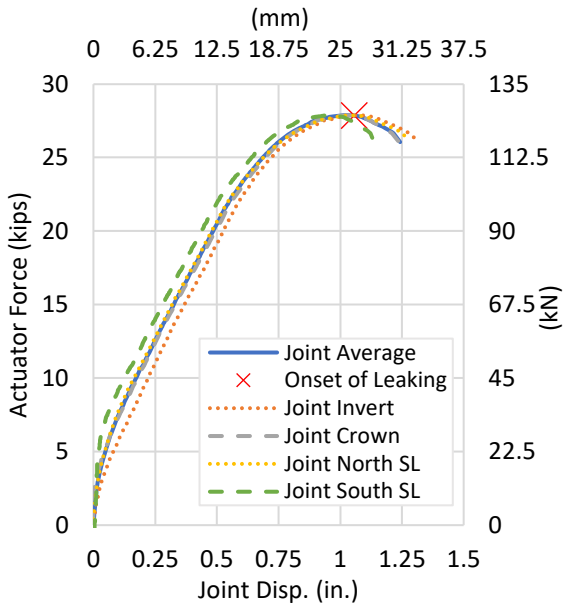

Figure 3.35. PT38-Force vs. Joint Displacement

Axial and circumferential strains were recorded at the east barrel's crown, invert, and both spring lines. Strain versus time and strain versus actuator displacement can be viewed in Figure 3.36 and Figure 3.37, respectively. During pressurization at the start of the test, an increase in circumferential strain is observed, accompanied by a slight decrease in axial strain. This slight decrease in axial strain can be attributed to

Poisson's effect. Once loading is applied to the system, a sharp increase in axial strain and a decrease in circumferential strain are observed as the pipe barrel begins to elongate due to applied tensile force. The maximum average axial strain peaked at 0.63%, and the maximum average circumferential strain peaked at -0.15 %.

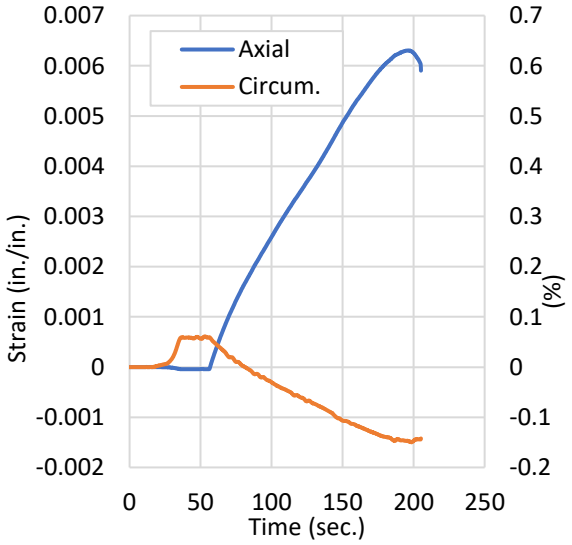

Figure 3.36. PT38-Strain vs. Time

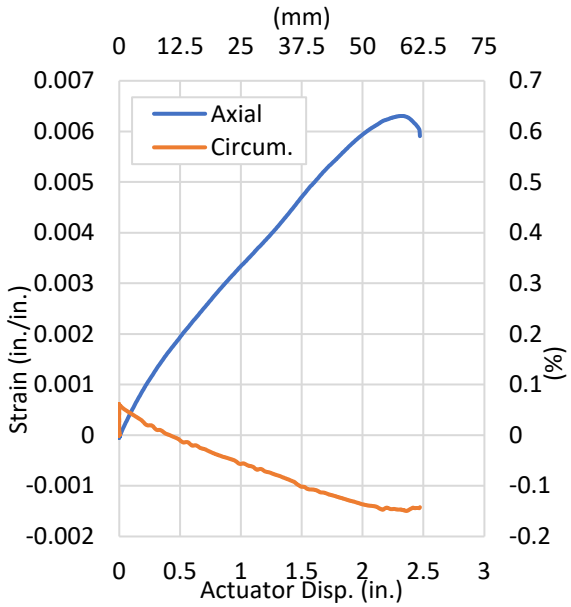

Figure 3.37. PT38-Strain vs. Act. Disp.

A maximum axial force of 27.9 kips (124 kN) and a maximum actuator displacement of 2.47 in. (63 mm) were recorded before fracture of the connection's internal grip gasket. The sudden fracture of the gasket resulted in an abrupt loss of pressure in the system. Gouges from the gasket's toothed wedges were visible along the spigot of the specimen after failure and are shown in Figure 3.39. The fractured gasket, responsible for the ultimate failure of the system is presented in Figure 3.40. After the test, there were no signs of axial or circumferential cracking along the specimen. A series of photos taken during the test can be viewed in Figure 3.38 (a-d).

(a) Specimen at the Start of the Test

(b) Specimen at the Onset of Leaking

(c) Just before Failure

(d) Just after Fracture of Internal Grip Gasket Resulting in Loss of Pressure

Figure 3.38. Images of PT38 during the test

Figure 3.39. PT38 – Gouges along the Spigot

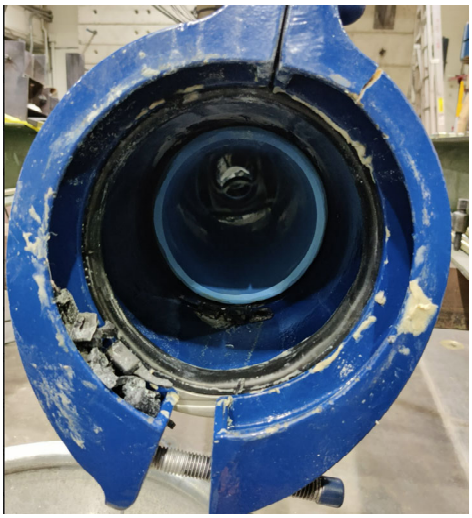

Figure 3.40. PT38 – Fractured Internal Grip Gasket

3.2 Axial Tension Test Summary and Comparison

This section provides a summary and comparison of the five axial tension tests performed on iPVC pipe with various restraining mechanisms. Table 3.1 shows an overview of the four tests and key factors recorded during testing. In addition, a comparison of applied axial load versus actuator displacement is provided in Figure 3.41, while Figure 3.42 shows the comparison of applied axial load versus joint displacement response for all tension tests performed in this study.

Table 3.1. Summary of Axial Tension Test Results

Test # (CIEST)	Pipe-Connection	Max. Axial Force		Max Axial Strain		Max Act. Disp.		Joint Disp.	
		kips	(kN)	in/in	%	in.	(mm)	in.	(mm)
PT02	RCT	55.3	(246)	-	-	4.10	(104)	0.93	(24)
PT27	TurnerLok	34.6	(154)	0.0078	0.78	2.96	(75)	1.42	(36)
PT30	EBAA C1900	38.1	(169)	0.0086	0.86	6.07	(154)	4.36	(111)
PT33	Lokx	60.3	(268)	0.0169	1.69	4.28	(109)	1.37	(35)
PT38	Hymax Grip	27.9	(124)	0.0063	0.63	2.47	(63)	1.24	(31)
PT38 at Leak	Hymax Grip	27.9	(124)	0.0063	0.63	2.34	(59)	1.06	(27)

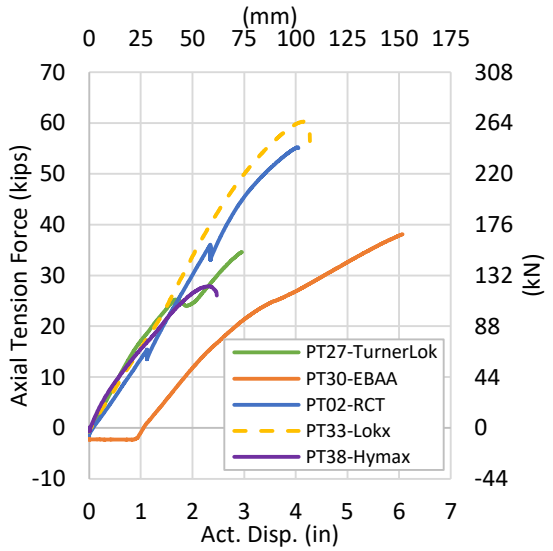

Figure 3.41. Tension Test Comparison – Axial Force vs. Act. Displacement

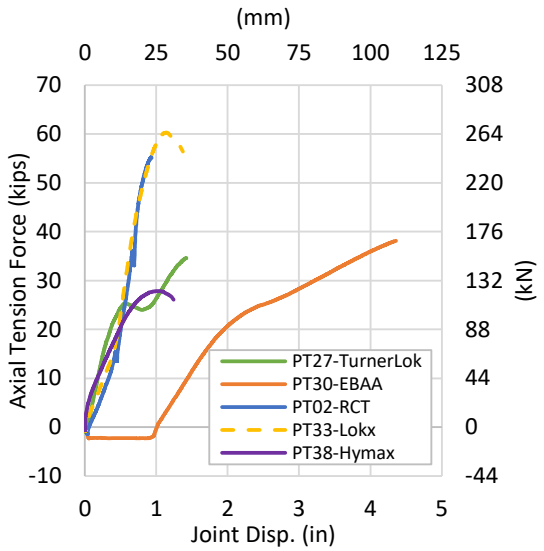

Figure 3.42. Tension Test Comparison – Axial Force vs. Joint Displacement

All tested restraining systems initially show a consistent linear actuator and joint response once tensile load is generated. However, at around 25 kips (111 kN), the systems' responses vary, with the Turnerlok, EBAA

C1900, and Hymax restraints beginning to show a nonlinear response. The RCT and Lokx connections recorded the stiffest responses, generating the highest axial loads [55.3 kips (246 kN), 60.3 kips (268 kN)] at actuator displacements of 4.10 in. (104 mm) and 4.27 in. (108 mm) and joint displacements of 0.93 in. (24 mm) and 1.37 in. (35 mm), respectively. While the RCT and Lokx connections generating the highest tensile force, the EBAA C1900 restraint reached the highest actuator and joint displacement [6.07 in. (154 mm) and 4.36 in. (111 mm), respectively] at a maximum axial load of 38.1 kips (169 kN).

Axial strain compared to axial force for all tested restraints is presented in Figure 3.43, while the stress and strain comparison is presented in Figure 3.44. The strain measurements recorded during PT02 (RCT) are omitted from the comparisons plots due to an instrumentation system error. The four restraining systems presented show an almost identical strain response to tensile load. The stress-strain response for each tension test was generally within the linear elastic region of the pipe material during the first 0.6% of measured strain, producing an average modulus of elasticity of 441 ksi (3041 MPa), as shown in Figure 3.44 . This compares well with the iPVC stress-strain data Appendix C, demonstrating the absence end fixture effects, repeatability of test setup and procedures, and validation of measurement systems and techniques. The Lokx coupling was able to produce the highest strain in the pipe barrel under the highest tensile load [1.69%].

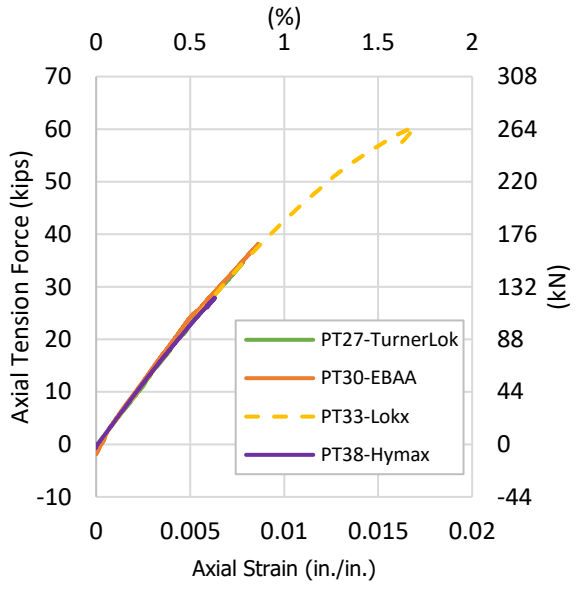

Figure 3.43. Tension Test Comparison – Axial Force vs. Axial Strain

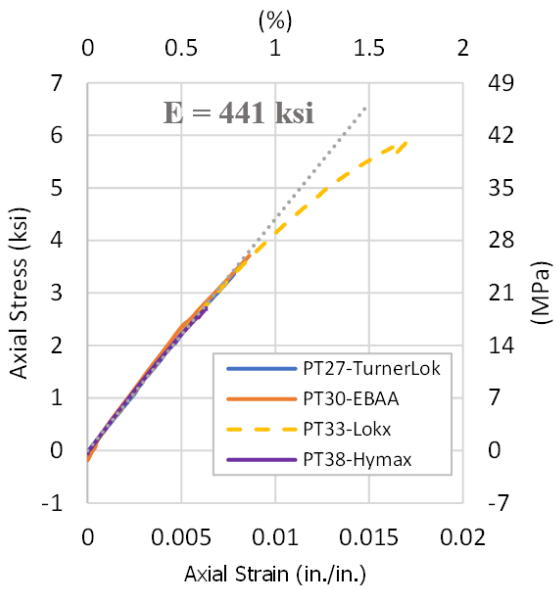

Figure 3.44. Tension Test Comparison – Axial Stress vs. Axial Strain including Elastic Modulus

3.3 Axial Compression Test Results

The following sections provide results from performed axial compression tests. A total of four compression tests were performed on iPVC pipe specimens with restrained connections. Lateral supports, consisting of steel angle members, were provided throughout the test to simulate partially restrained conditions due to soil confinement, limiting out-of-plane global buckling of the specimen. The compression test setup for PC28 is shown in Figure 3.45. Forces and displacements are reported as positive values for the typical compression test in this section.

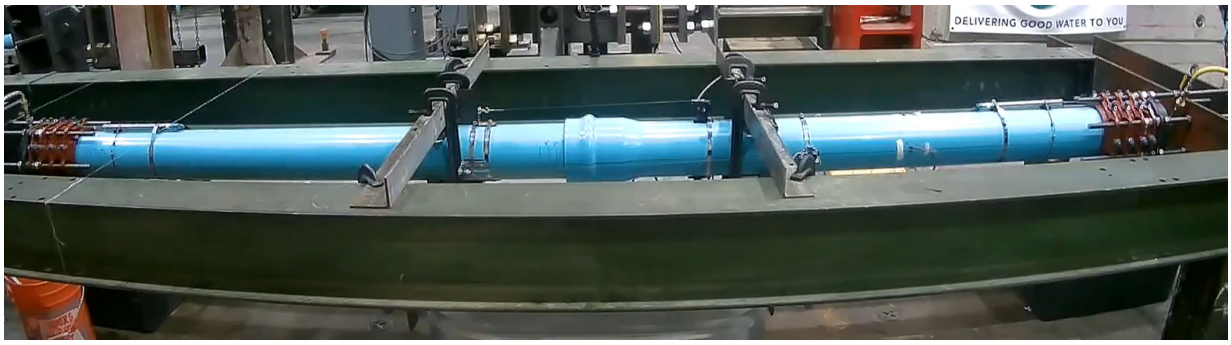

Figure 3.45. Compression Test Setup

3.3.1 Compression Test PC37 – iPVC RCT Coupling

Pipe specimen PC37 consisted of an iPVC pipe with an RCT coupling located at the midpoint. Compressive load was applied to the specimen at a constant rate until local buckling occurred at the connection warranted conclusion of the test. Figure 3.46 shows photos for the pre-test setup of specimen PC37 as well as the specimen just after completion of the test.

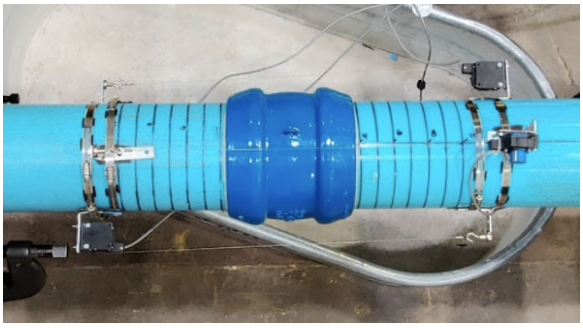

(a) Pre-Test Setup

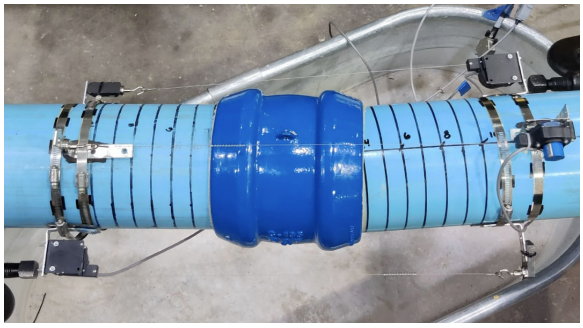

(b) End of Test, after unloading

Figure 3.46. Specimen PC37 (a) Setup and (b) End of Test

The progression of pressure, actuator force, and actuator displacement is presented in Figure 3.47. The specimen was initially pressurized to an internal pressure of 64 psi (441 kPa). At 190 seconds into data collection, the local bucking occurred at the connection causing a significant change in internal volume in the system. The sharp change in volume caused the system to experience an increase of internal pressure from 65 psi (448 kPa) to 127 psi (875 kPa). After buckling occurred at the connection, the system was unloaded until around 1 kip (4.45 kN) of compressive force remained in the system. Figure 3.48 displays the actuator force versus displacement. Actuator displacement and force are direct measurements of the actuator's hydraulic piston location and attached load cell, respectively. An initial actuator displacement of 0.22 in. (5.6 mm) is achieved before the specimen begins to contact the provided system bracing, causing the system's response to stiffen. After contacting the system bracing, the actuator displacement response increases at a constant rate of around 21.74 kips/in. (3.81 kN/mm) before the onset of buckling occurs.

Figure 3.49 presents the actuator force versus joint displacement. Due to the joint rotation and onset of buckling at the connection of the specimen, data recorded from string pots at the connection was inaccurate. Therefore, a global joint displacement was calculated to represent the system's joint response to compressive load. Global joint displacement was calculated by subtracting end restraint slippage and pipe strain from the total actuator displacement. Contact with the system bracing occurred at 0.11 in. (2.8 mm) of joint displacement before the joint response increased at a constant rate of 95.3 kips/in. (16.7 kN/mm). A joint displacement of 0.66 in. (17 mm) was recorded before buckling and a maximum joint displacement of 1.2 in. (30 mm) was recorded after buckling. Throughout the test there were no signs of leaking.

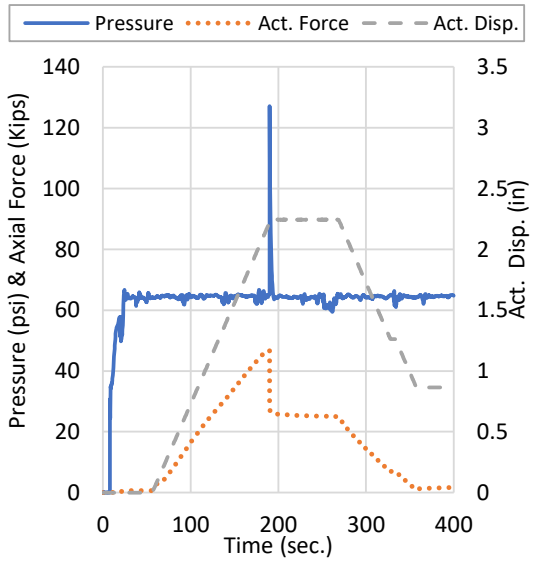

Figure 3.47. PC37-Pressure and Act. Disp. vs. Time

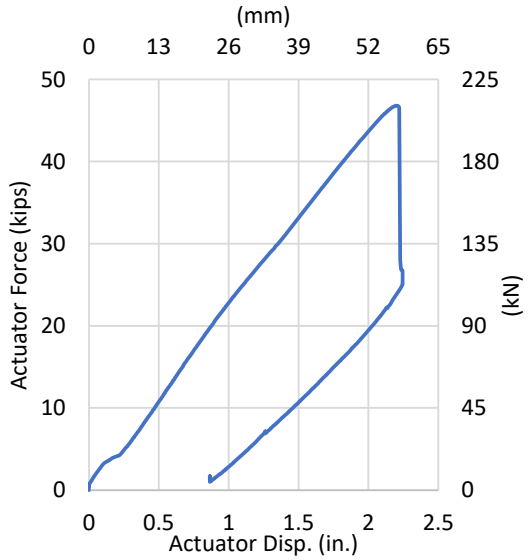

Figure 3.48. PC37-Force vs. Act. Disp.

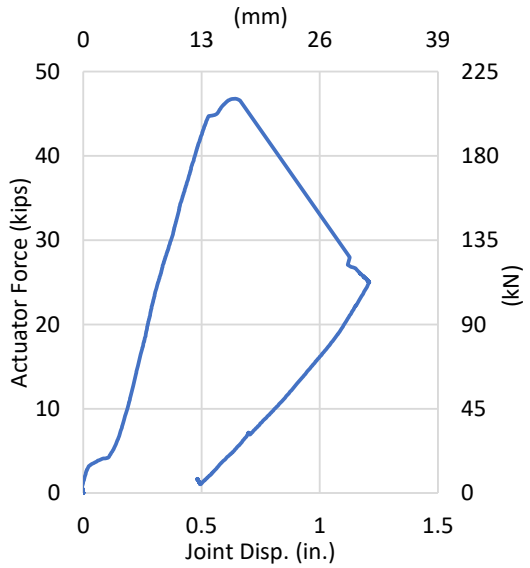

Figure 3.49. PC37-Force vs. Joint Displacement

Axial and circumferential strains were recorded at the crown, invert, and both spring lines of the bell section. Strain versus time and strain versus actuator displacement can be viewed in Figure 3.50 and Figure 3.51, respectively. During pressurization at the start of the test, an increase in circumferential strain is observed, accompanied by a slight decrease in axial strain. This slight decrease in axial strain can be attributed to Poisson's effect. Once loading is applied to the system, circumferential strains continue to increase as the pipe begins to be compressed, and a decrease in axial strain is observed as the pipe barrel begins to compress and expand circumferentially. The maximum axial strain peaked at -0.946%, and the maximum circumferential strain peaked at 0.242%.

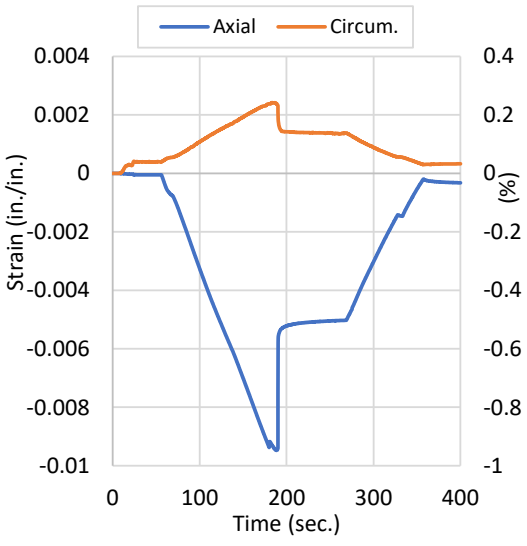

Figure 3.50. PC37-Strain vs. Time

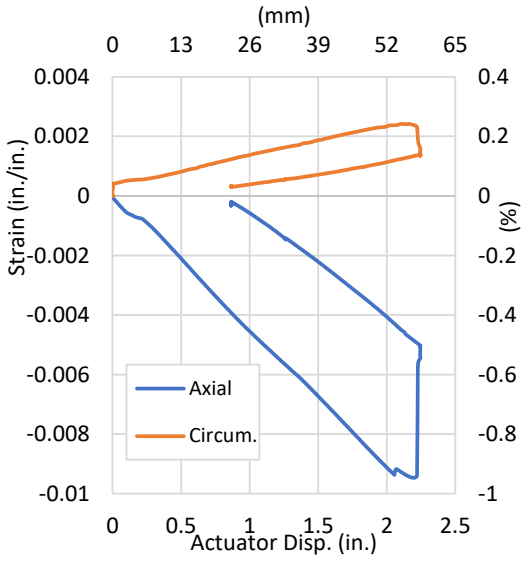

Figure 3.51. PC37-Strain vs. Act. Disp.

The test was concluded upon the onset of out-of-plane buckling at the connection, causing the system bracing to fail, shown in Figure 3.55. A maximum axial compressive force of 46.8 kips (208 kN) and a maximum actuator displacement of 2.25 in. (57 mm) were recorded during the test. After the compression test, the test specimen was pulled to failure under tensile loading (identified as PC37T). Figure 3.52 shows the progression plot of pressure, actuator force, and actuator displacement during both the compression and tension loading. The specimen reached a maximum tensile load and actuator displacement of 21.9 kips (97 kN) and 0.58 in. (15 mm) before circumferential fracture occurred at the coupling causing loss of pressure in the system, shown in Figure 3.56. Stain versus time for all the tension tests is shown in Figure 3.53. The maximum recorded axial and circumferential strain was 0.469% and -0.074%, respectively. A series of photos taken during the test is presented in Figure 3.54 (a-c).

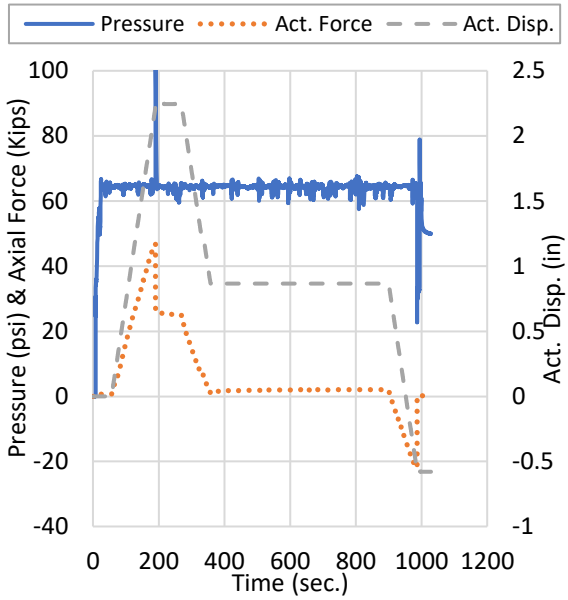

Figure 3.52. PC37T- Pressure and Act. Disp. vs. Time

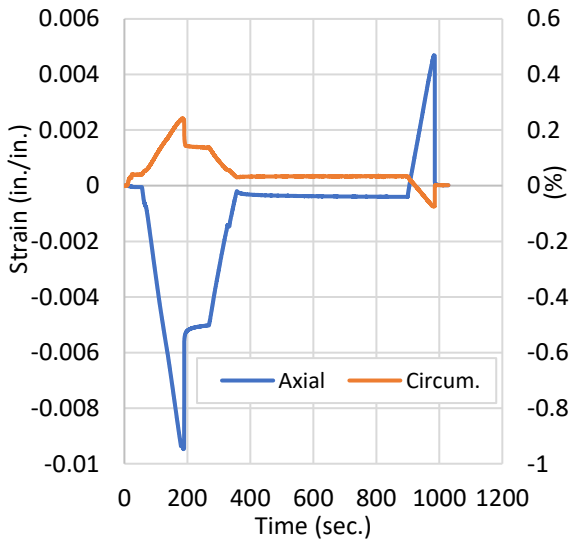

Figure 3.53. PC37T-Average Strains vs. Time

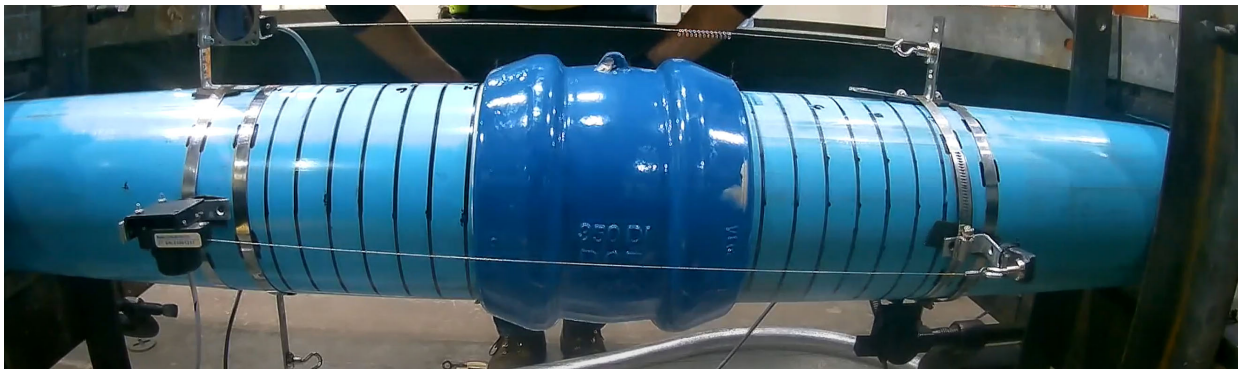

(a) Start of Test

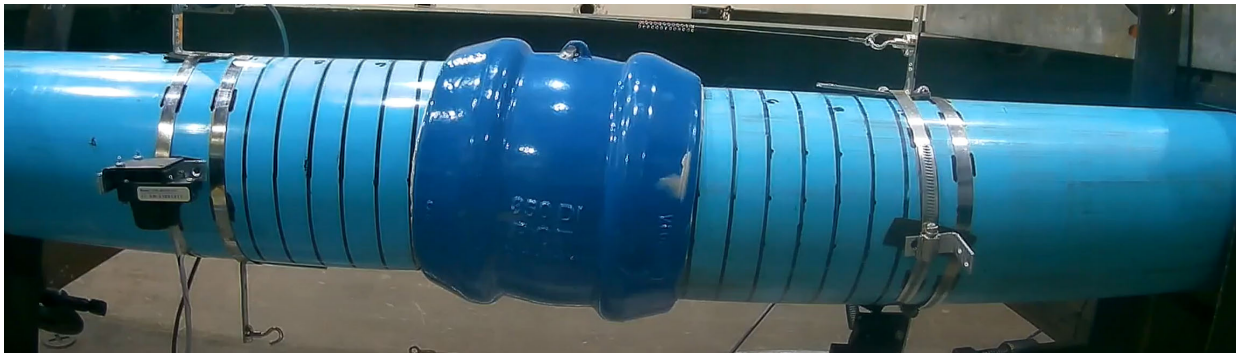

(b) Rotation and Local Buckling at Joint

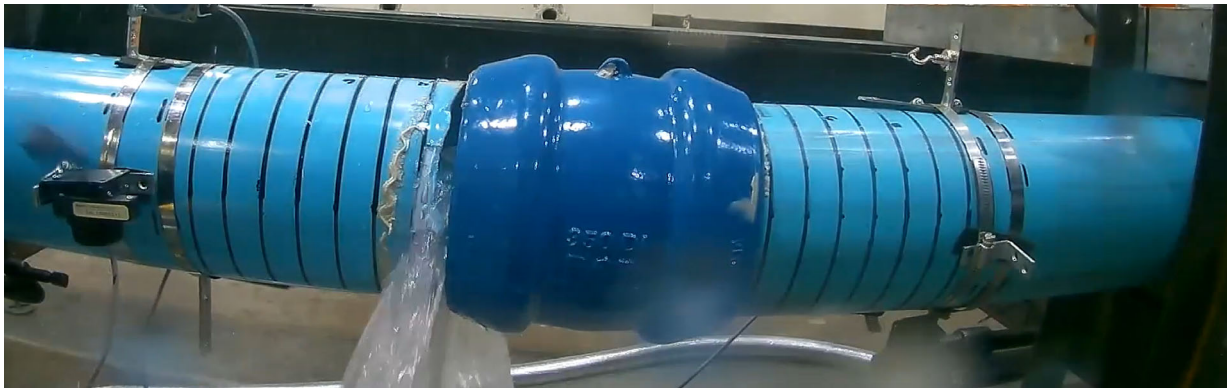

(c) Just After Circumferential Facture due to Tensile Loading

Figure 3.54. Images of PC37 During the Test Progression

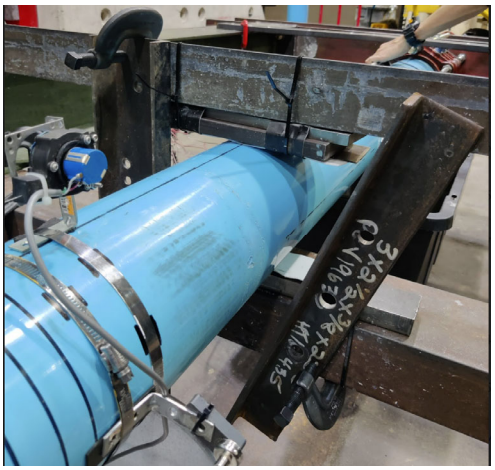

Figure 3.55. PC37-Lateral Bracing Failure caused by Local Joint Buckling

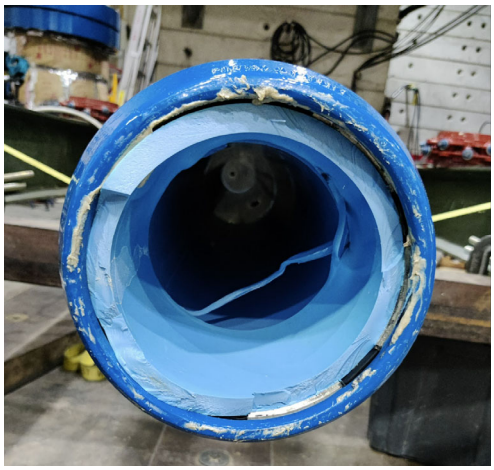

Figure 3.56. PC37-Circumferential Failure at RCT Couplings East End

3.3.2 Compression Test PC28 – iPVC TurnerLok Gasket

Pipe specimen PC28 consisted of an iPVC pipe with an internal TurnerLok gasket restraining the bell and spigot connection located at the midpoint. Compressive load was applied to the specimen until the maximum stroke limit of the actuator was reached. Figure 3.57 shows photos for the pre-test setup of specimen PC28 as well as the specimen just after completion of the test.

(a) Pre-Test Setup

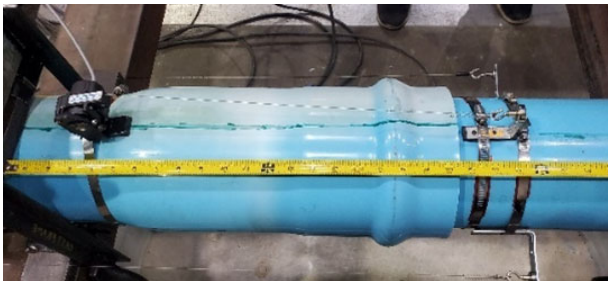

(b) End of Test

Figure 3.57. Specimen PC28 (a) Setup and (b) End of Test

The progression of pressure, actuator force, and actuator displacement are presented in Figure 3.58. The specimen maintained an average pressure of 65 psi (450 kPa) throughout the test, experiencing minor fluctuations during the loading sequence. Figure 3.59 displays the actuator force versus displacement. Actuator displacement and force are direct measurements of the actuator's hydraulic piston and attached load cell, respectively. At the start of the test, actuator force and actuator displacement increase at a relatively constant rate of 13.3 kips/in. (2.33 kN/mm). At approximately 2.5 in (64 mm) of actuator displacement and 21 kips (93 kN) of actuator force, there is a sharp drop in force as the back of the bell begins to yield, allowing the spigot to telescope through the specimen. At approximately 3.1 in (79 mm) of

actuator displacement and a force of approximately 18 kips (80 kN) force again begins to increase with actuator displacement. As force and displacement increase a ratcheting behavior is observed as the spigot continues to telescope through the bell. Figure 3.60 presents the actuator force versus joint displacement. Joint displacement was measured by string pots at the north spring line, south spring line, crown, and invert of the specimen that spanned from the spigot across the bell. The force reduction seen in Figure 3.59 is also present in Figure 3.60 at approximately 1.8 in. (46 mm) of joint displacement. A maximum joint displacement of 8.83 in. (224 mm) before the test was concluded.

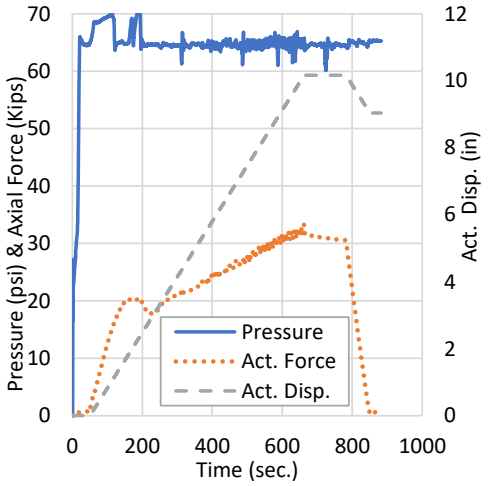

Figure 3.58. PC28-Pressure and Act. Disp. vs. Time (Compression +)

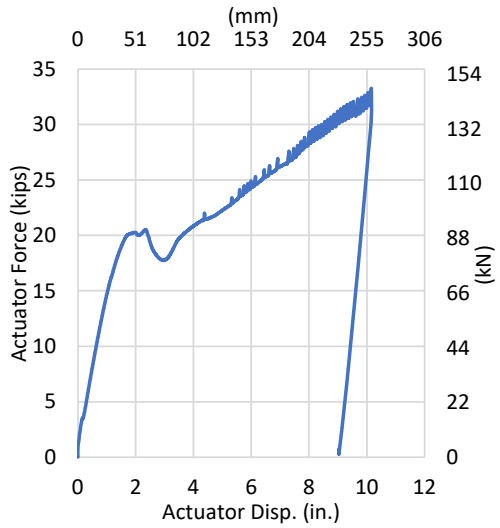

Figure 3.59. PC28-Force vs. Act. Disp. (Compression +)

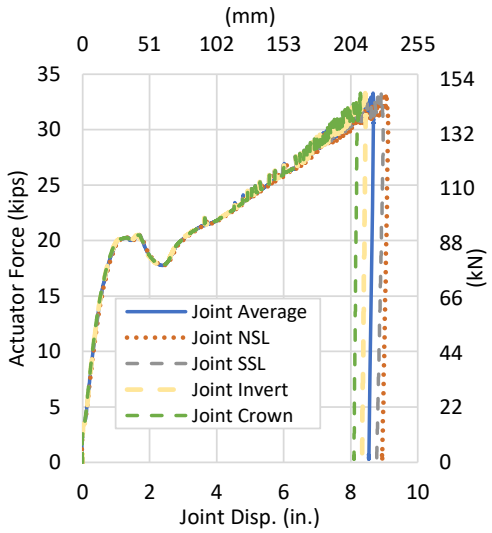

Figure 3.60. PC28-Force vs. Joint Displacement (Compression +)

Axial and circumferential strains were recorded at the crown, invert, and both spring lines of the bell section. Compressive strains are shown as negative values while tensile strains are shown as positive for the typical compression test performed in this section. Strain versus time and strain versus actuator displacement can be viewed in Figure 3.61 and Figure 3.62, respectively. During pressurization at the start of the test, an increase in circumferential strain is observed, accompanied by a slight decrease in axial strain. This slight decrease in axial strain can be attributed to Poisson's effect. Once loading is applied to the system, a sharp increase in circumferential strain and a decrease in axial strain are observed as the pipe barrel begins to compress and expand circumferentially. The maximum axial strain peaked at -0.666%, and the maximum circumferential strain peaked at 0.305%.

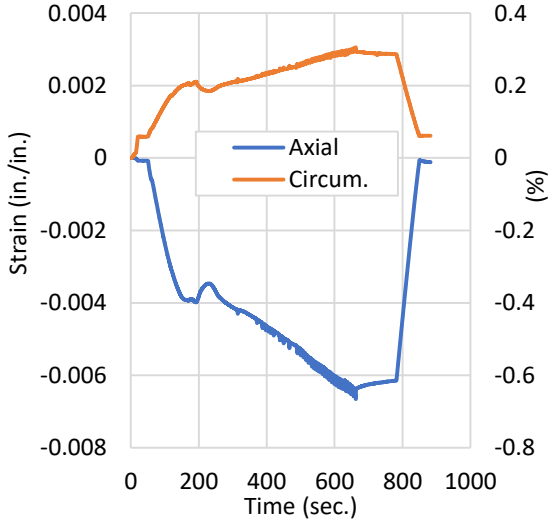

Figure 3.61. PC28-Strain vs. Time

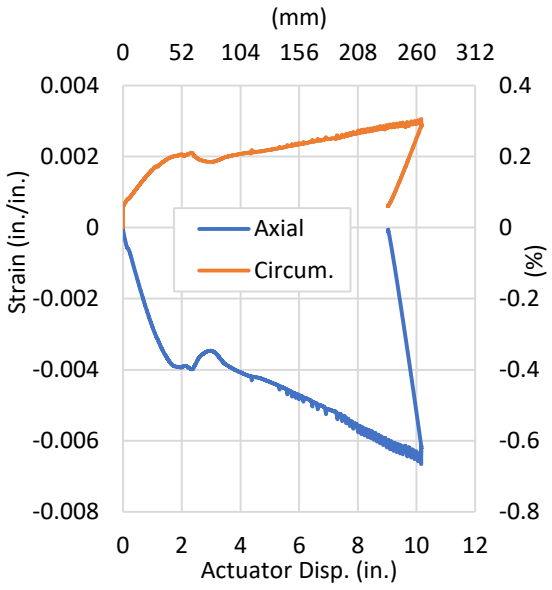

Figure 3.62. PC28-Strain vs. Act. Disp.

After the compression test, a total of three subsequent tension tests were performed on the specimen. The first tension test (PC28T1) ended in slippage of the east end restraints at a maximum tension force of 43.7 kips (194 kN). This response was expected due to the end restraint assembly previously used to resist compressive forces during the axial compression test. Therefore, the East end restraints were changed to the standard tension test assembly before starting the second tension test (PC28T2). Subsequent tension tests were not pressurized. A maximum tensile force of 48.7 kips (217 kN) was recorded during the second tension test before circumferential splitting of the pipe at the western restraint. Despite minor discoloration observed at the bell gasket groove during the first tension test, leaks or cracking were observed at the

connection for the first two tension tests. Restraint slippage and circumferential failure occurring in PC28T1 and PC28T2 can be viewed in Figure 3.63 and Figure 3.64, respectively.

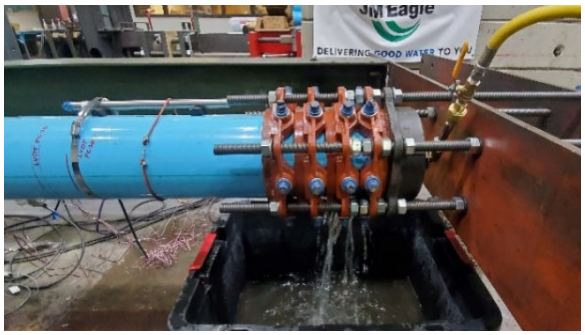

Figure 3.63. PC28T1 Slippage of East End Restraint

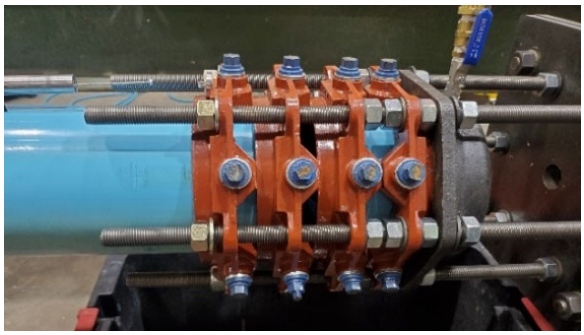

Figure 3.64. PT28T2 Failure of West End Restraint

The West end restraints were then changed to the standard tension test assembly before starting the third tension test (PC28T3). A maximum axial tension force of 52.5 kips (234 kN) was applied before the sudden fracture of the bell and spigot. This increase in tensile capacity can likely be attributed to lower stress concentrations formed at the gasket as friction force from the telescoped spigot partially resists tensile force applied to the system. A series of photos taken during the final tension test can be viewed in Figure 3.65 (a-d). The progression plot of pressure, actuator force, and actuator displacement for all three subsequent tension tests is presented in Figure 3.66. Stain versus time for all three tension tests is shown in Figure 3.67. Tension forces, displacements, and axial strains for all subsequent tension tests are presented as positive values.

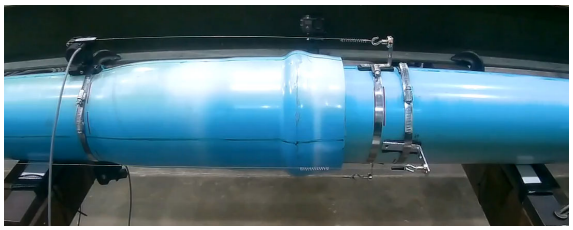

(a) Start of PT27 Test

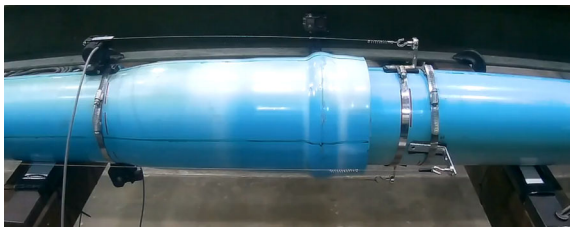

(b) Just before Fracture

(c) Fracture of Bell and Spigot

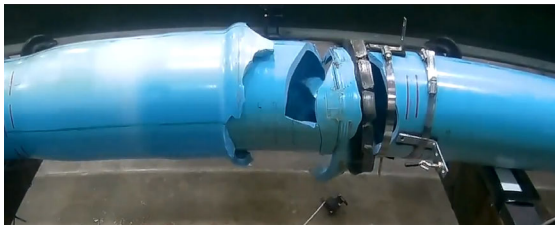

(d) Just after Fracture of Bell and Spigot

Figure 3.65. Images of PC28T3 Fracture of Bell and Spigot

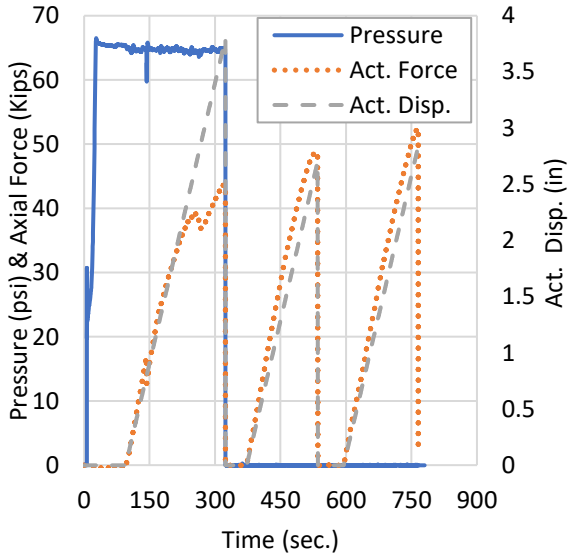

Figure 3.66. PC28-All Tension Tests-Pressure and Act. Disp. vs. Time (Tension +)

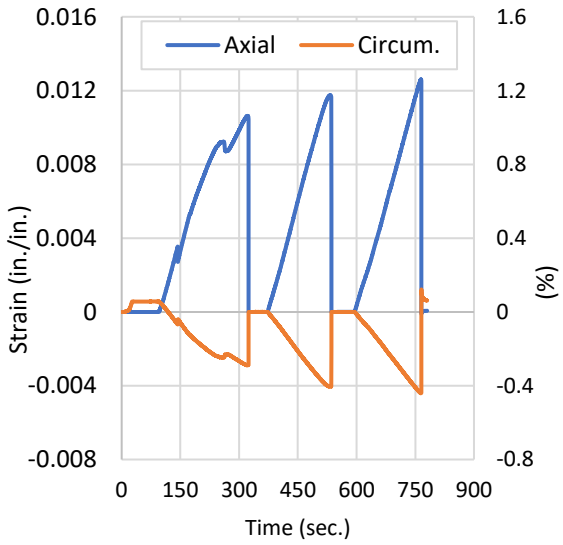

Figure 3.67. PC28-All Tension Tests- Strain vs. Time (Tension +)

3.3.3 Compression Test PC31 – iPVC EBAA C1900 Restraint Harness

Pipe specimen PC31 consisted of an iPVC pipe with an external EBAA C1900 restraint. Restraint nuts for this specimen were located to allow for 1 in. (25 mm) of joint opening before engaging and resisting axial deformation. The test concluded in failure of the east end restraint bolts. Figure 3.68 shows photos for the pre-test setup of specimen PC31 as well as the failure of the east end restraint that resulted in the completion of the test.

(a) Pre-Test Setup (b) Buckling at East End Restraint

Figure 3.68. Specimen PC31 (a) Setup and (b) Failure at East End Restraint

The progression of pressure, actuator force, and actuator displacement is presented in Figure 3.69. The specimen maintained an average pressure of 67 psi (462 kPa), increasing slightly as the compressive load was applied and the internal volume of the system decreased. During the test, the spigot telescoped through

the bell until contact was made with the western C1900 restraint. The spigot then continued to telescope, ratcheting through both the bell and C1900 external restraint. Figure 3.70 shows the actuator force versus displacement. At approximately 2.9 in (74 mm) of actuator displacement and 26 kips (116 kN) of actuator force, the bell contacts the western C1900 restraint causing a sharp increase in force. A ratcheting response is visible at approximately 5 in. (127 mm) of actuator displacement as the spigot continues to telescope through the bell and the C1900 restraint.

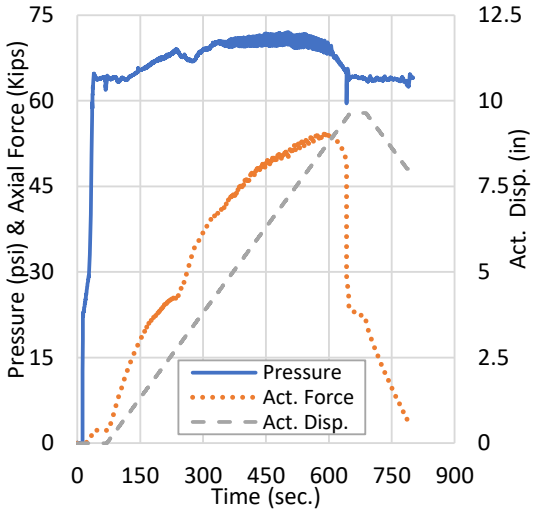

Figure 3.69. PC31-Pressure and Act. Disp. vs. Time

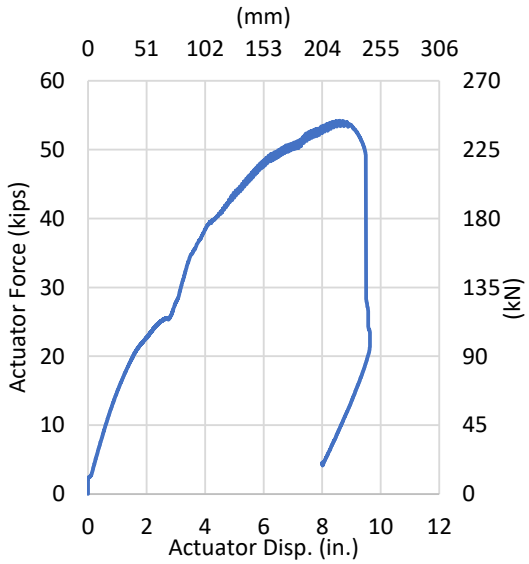

Figure 3.70. PC31-Force vs. Displacement

Figure 3.71 presents the actuator force versus joint displacement, while Figure 3.72 shows actuator force versus restraint displacement. The joint displacement was measured by a string pot at both the crown and invert of the specimen that spanned from the spigot across the bell. Restraint displacement is representative of the location of the restraint relative to the original restraint location on the specimen. The increase in force is also present at 2 in. (51 mm) of joint displacement in Figure 3.71. A maximum joint displacement of 6.52 in. (166 mm) was recorded before the conclusion of the test.

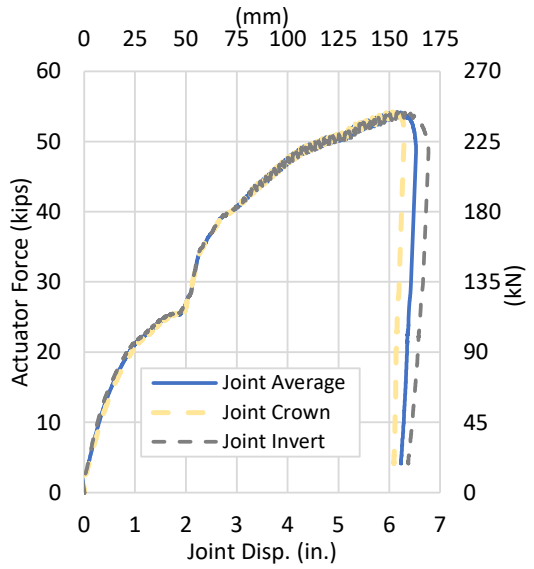

Figure 3.71. PC31-Force vs. Joint Displacement

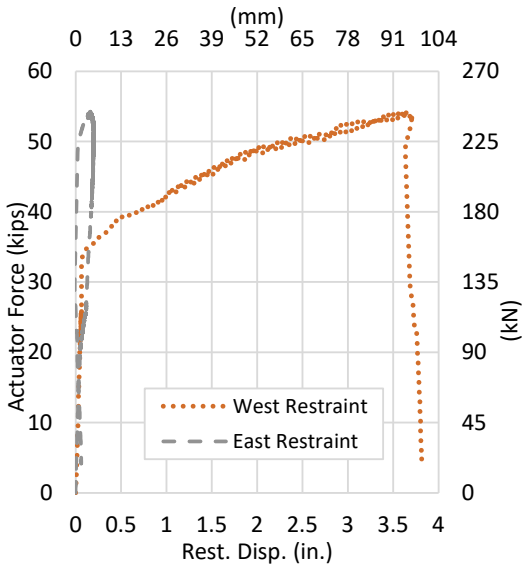

Figure 3.72. PC31-Force vs. Restraint Displacement

Axial and circumferential strains were recorded at the crown, invert, and both spring lines of the bell section. Strain versus time and strain versus actuator displacement can be viewed in Figure 3.73 and Figure 3.74, respectively. As a compressive load is applied to the specimen, the pipe barrel begins to compress and expand circumferentially increasing the circumferential strain in the specimen. Axial strain begins to decrease during loading due to the Poisson's effect. The maximum axial strain peaked at -0.816 % and the maximum circumferential strain peaked at 0.312 %.

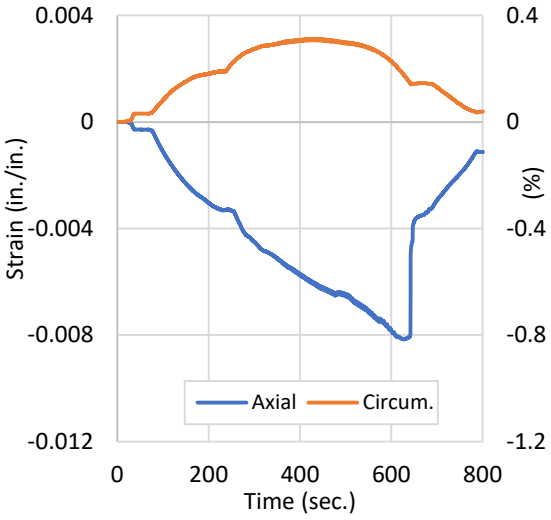

Figure 3.73. PC31-Strain vs. Time

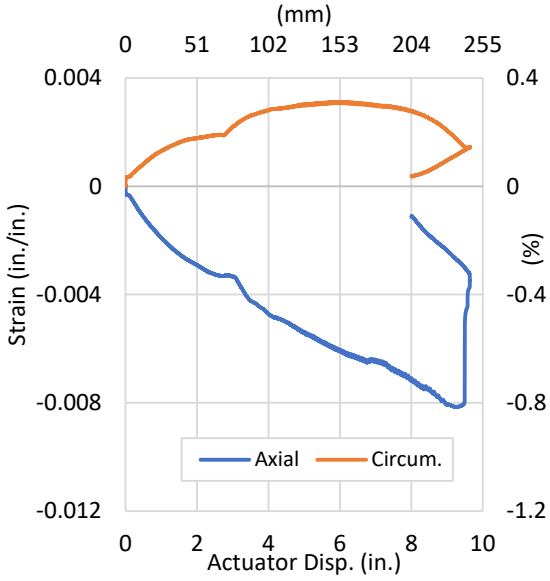

Figure 3.74. PC31-Strain vs. Displacement

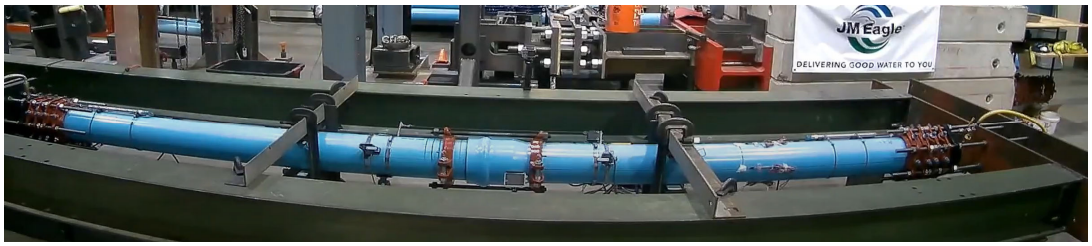

(a) Start of Test

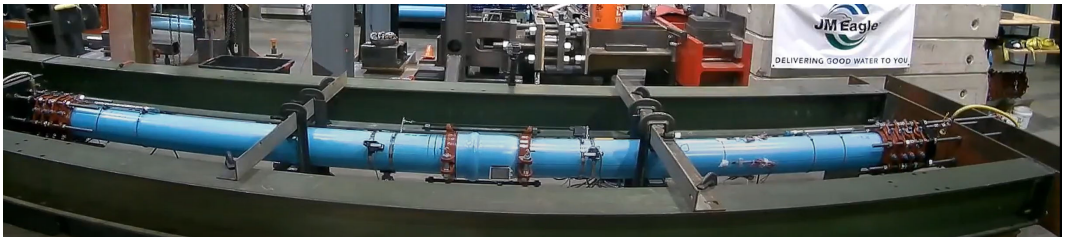

(b) Bell in Contact with West Restraint

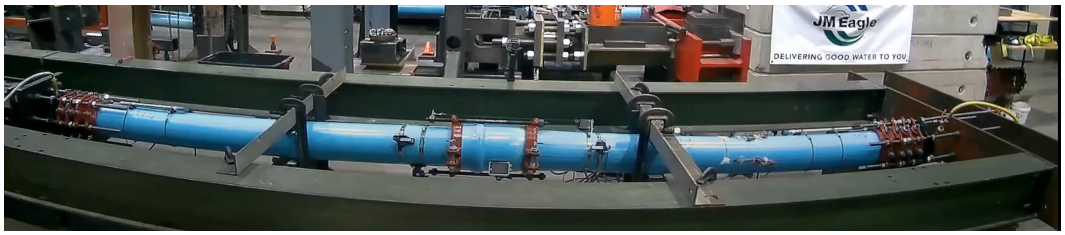

(c) Onset of Out of Plane Bending

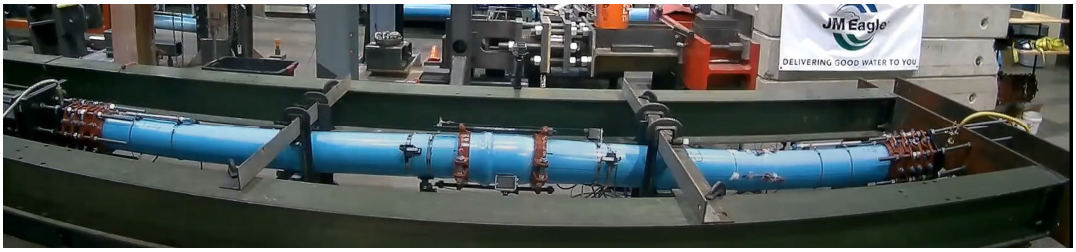

(d) Maximum Bending before Setup Failure

Figure 3.75. Images of PC31 During the Test Progression

Buckling of the east end restraint bolts concluded the test. Just before bolt failure a maximum axial force of 54.2 kips (241 kN) and a maximum actuator displacement of 9.64 in. (245 mm) was recorded in the system. There were no signs of leakage during or after the conclusion of the test. A series of photos taken during the test are presented in Figure 3.75 (a-d).

3.3.4 Compression Test PC35 – iPVC Lokx Coupling

Pipe specimen PC35 consisted of an iPVC pipe with Lokx coupling located at the midpoint. Compressive load was applied to the specimen at a constant rate until significant leakage and local buckling at the connection warranted the conclusion of the test. Figure 3.76 shows photos for the pre-test setup of specimen PC35 as well as the specimen just after completion of the test.

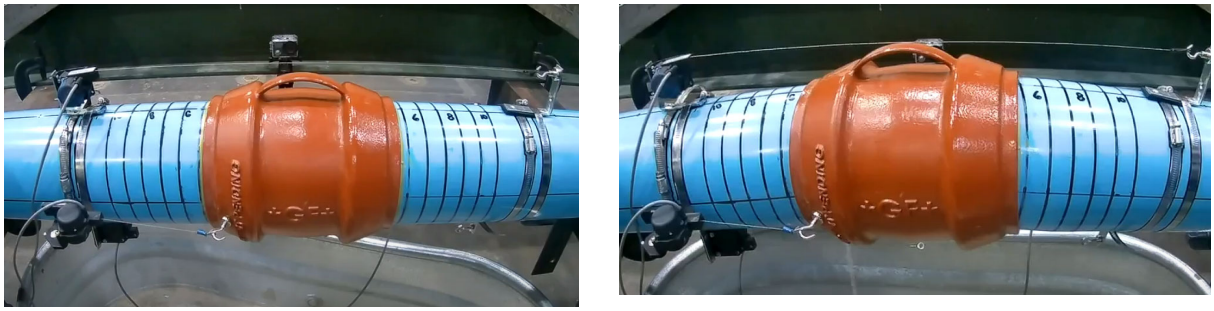

(a) Pre-Test Setup (b) End of Test

Figure 3.76. Specimen PC35 (a) Setup and (b) End of Test

The progression of pressure, actuator force, and actuator displacement is presented in Figure 3.77. The specimen was initially pressurized to an internal pressure of 65 psi (450 kPa). As the test progressed, the coupling began to rotate horizontally, allowing the gasket seal to break and leaking to occur at the connection. The first onset of leaking occurred 202.75 seconds into the test, where a steady stream of water was seen leaking from the eastern end of the coupling. As loading continued leaking began to increase in rate. At 221 seconds into the test, the loading sequence was paused, the specimen was unloaded to around 5 kips (22 kN), and internal pressure was manually released from the system. The specimen was then inspected for damage. Loading was then continued, and internal pressure was again applied to the specimen. Leaking continued throughout the rest of the test sequence. Figure 3.78 displays the actuator force versus displacement. Actuator displacement and force are direct measurements of the actuator's hydraulic piston location and attached load cell, respectively. Throughout the test, the system maintains a linear response with some softening occurring near the end of the test due to out-of-plane buckling at the connection. The onset of leaking occurred at approximately 35.3 kips (157 kN) of applied force and 2.3 in. (58 mm) of applied actuator displacement. Figure 3.79 presents the actuator force versus joint displacement. Due to the joint rotation and onset of buckling at the connection of the specimen, data recorded from string pots at the connection were inaccurate. Therefore, a global joint displacement was calculated to represent the system's joint response to compressive load. Global joint displacement was calculated by subtracting end restraint slippage and pipe strain from the total actuator displacement. The onset of leaking occurred at 1.04 in. (26

mm) of joint displacement. A maximum joint displacement of 1.8 in. (46 mm) was recorded before the test was concluded.

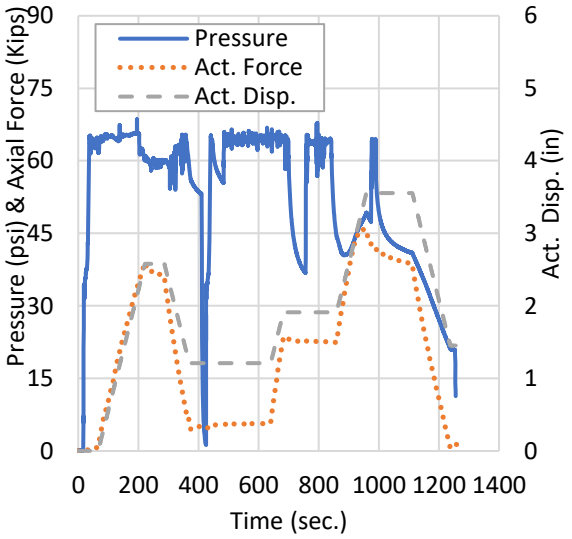

Figure 3.77. PC35-Pressure and Act. Disp. vs. Time

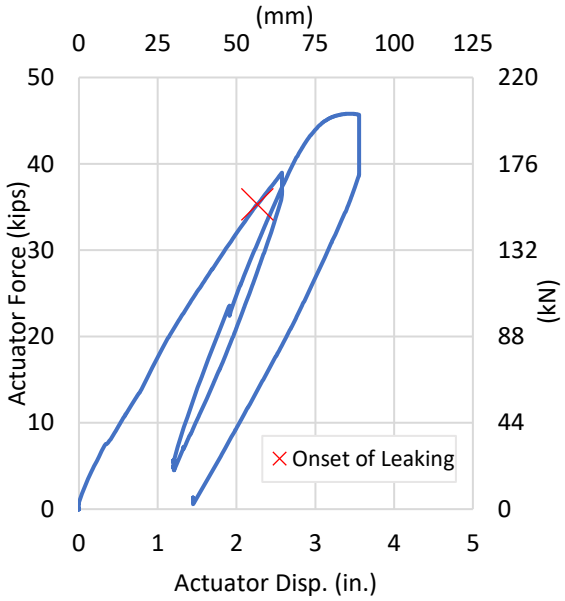

Figure 3.78. PC35-Force vs. Act. Disp.

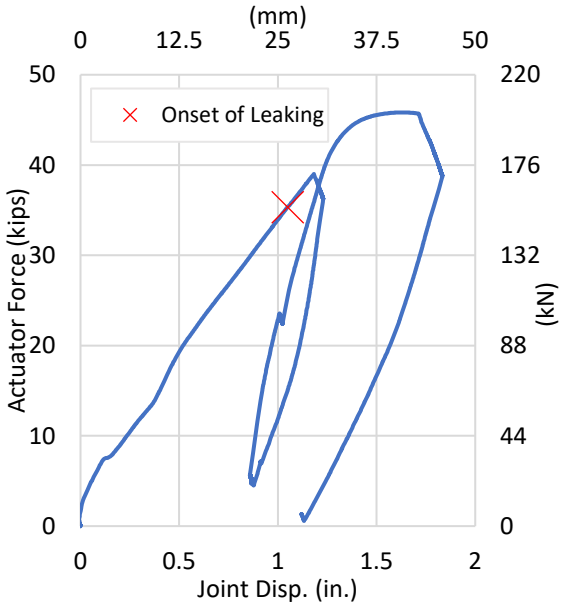

Figure 3.79. PC35-Force vs. Joint Displacement

Axial and circumferential strains were recorded at the crown, invert, and both spring lines of the bell section. Strain versus time and strain versus actuator displacement can be viewed in Figure 3.80 and Figure 3.81, respectively. During pressurization at the start of the test, an increase in circumferential strain is observed, accompanied by a slight decrease in axial strain. This slight decrease in axial strain can be attributed to Poisson's effect. Once loading is applied to the system, circumferential strains continue to increase as the pipe begins to be compressed, and a decrease in axial strain is observed as the pipe barrel begins to compress and expand circumferentially. The maximum axial strain peaked at -1.08 %, and the maximum circumferential strain peaked at 0.568%.

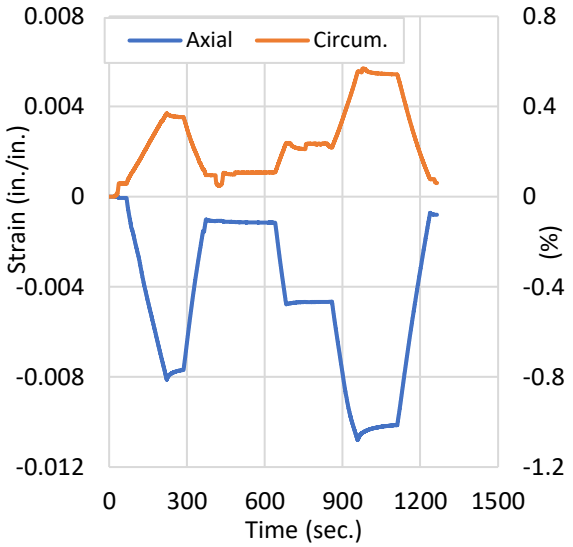

Figure 3.80. PC35-Strain vs. Time

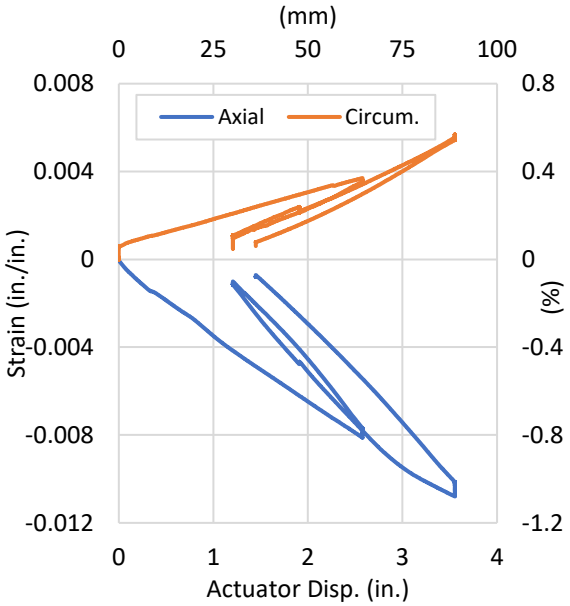

Figure 3.81. PC35-Strain vs. Act. Disp.

The test was concluded upon the onset of out-of-plane buckling at the connection. Significant leaking was observed at the coupling as the test was concluded. The maximum axial force of 45.8 kips (204 kN) and a maximum actuator displacement of 3.6 in. (91 mm) were recorded during the test. A series of photos taken during the test is presented in Figure 3.82 (a-d).

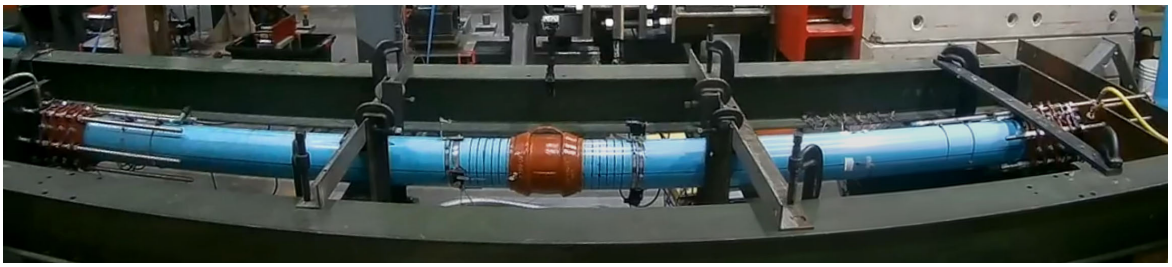

(a) Start of Test

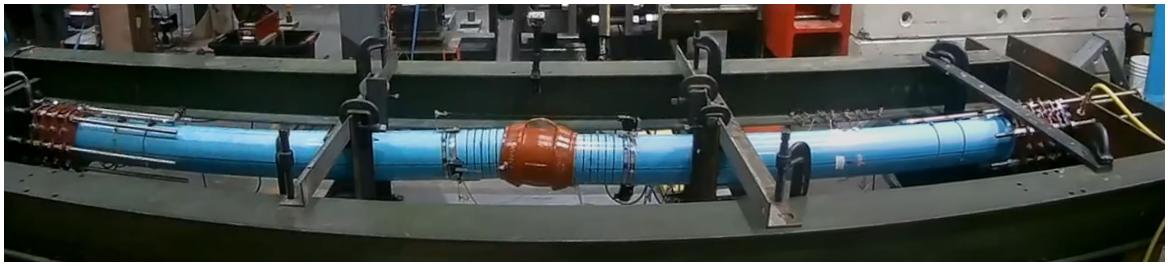

(b) Onset of Leaking

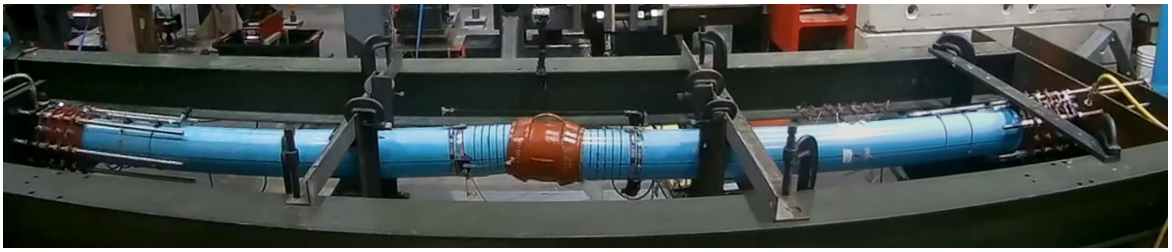

(c) Just Before Unloading and Inspection of the Specimen

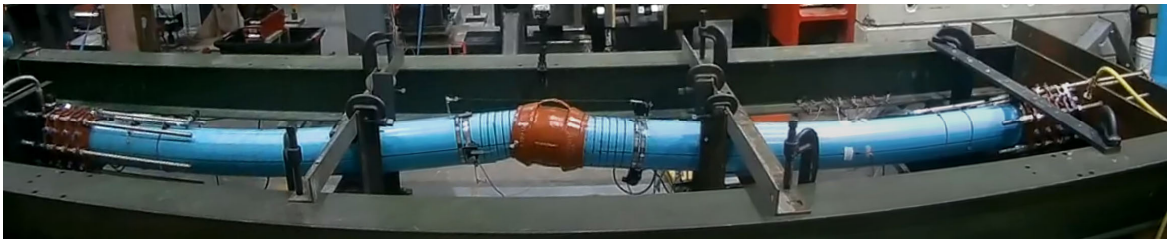

(d) Maximum Applied Load/Displacement

Figure 3.82. Images of PC35 During the Test Progression

3.4 Axial Compression Test Summary and Comparison

This section provides a summary and comparison of the four compression tension tests performed on 6 in. (150mm)-diameter iPVC pipe. Table 3.2 provides an overview of the four tests and key measures recorded during testing. In addition, a comparison of applied axial load versus actuator displacement is provided in

Figure 3.83, while Figure 3.84 shows the comparison of applied axial load versus joint displacement response for all compression tests performed in this study.

Table 3.2. Summary of Axial Compression Test Results

Test # (CIEST)	Pipe-Connection	Max. Axial Force		Max Axial Strain		Max Act. Disp.		Joint Disp.	
		kips	(kN)	in/in	%	in.	(mm)	in.	(mm)
PC37	RCT	46.8	(208)	0.0095	0.95	2.25	(57)	1.23	(31)
PC28	TurnerLok	33.3	(148)	0.0067	0.67	10.2	(259)	8.38	(213)
PC31	EBAA C1900	54.2	(241)	0.0082	0.82	9.64	(245)	6.52	(166)
PC35	Lokx	45.8	(204)	0.0108	1.08	3.56	(90)	1.83	(46)
PC35 at Leak	Lokx	35.3	(157)	0.0072	0.72	2.26	(57)	1.05	(27)

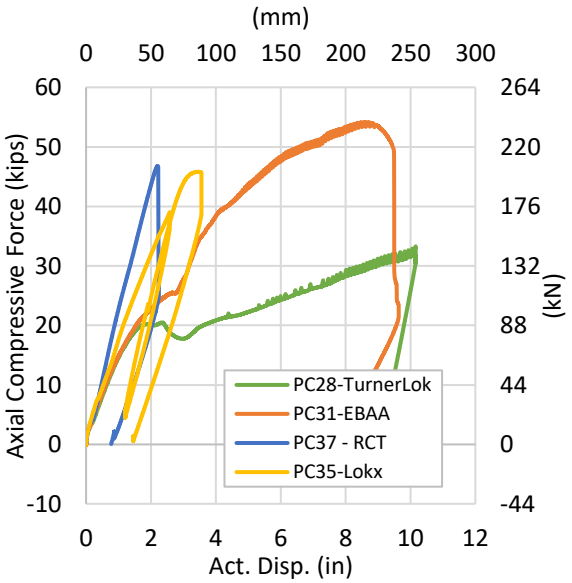

Figure 3.83. Compression Test Comparison – Axial Force vs. Act. Displacement

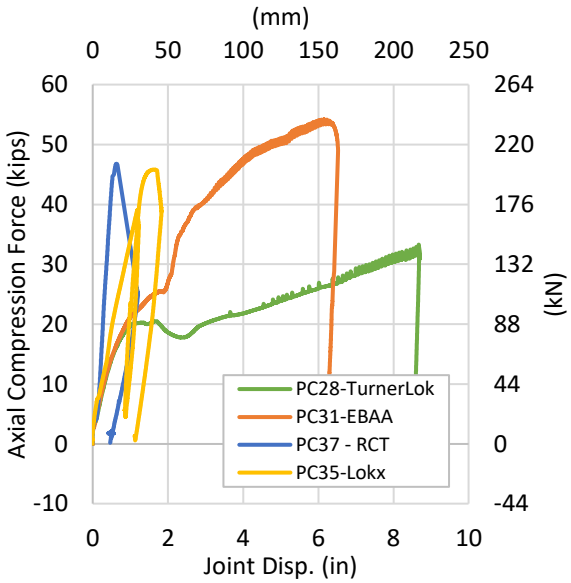

Figure 3.84. Compression Test Comparison – Axial Force vs. Joint Displacement

It is important to note that the TurnerLok, EBAA C1900, and RCT restraints showed no signs of failure during testing, reaching the limitations of the test setup or actuator stroke before failure occurred. The four systems showed two distinct responses to compressive loading. Due to the back stopper inside the RCT and Lokx coupling, both systems generate a significant force [46.8 kips (208 kN) and 45.8 kips (204 kN), respectively] under a relatively low actuator [2.25 in. (57 mm), 3.56 in. (90 mm)] and joint displacement [1.2 in. (31 mm), 1.8 in. (46 mm)], causing the onset of local buckling in the system. Despite significant

local bucking of PC37 (RCT), as shown previously in Figure 3.54, no leakage was observed during compressive loading. The TurnerLok and EBAA C1900 restraints demonstrated the iPVC pipe system's ability to accommodate significant deformations [Actuator displacement: 10.2 in. (259 mm) and 9.64 in. (245 mm)] under compressive loading [33.3 kips (148 kN) and 54.2 kips (241 kN)] by allowing the spigot of the pipe to telescope through the bell while maintaining the system's ability to hold internal pressure.

Axial strain compared to axial force for all compression tests is presented in Figure 3.85, while the stress and strain comparison is presented in Figure 3.86. The TurnerLok, RCT, and Lokx restraints show an almost identical strain response to compressive load, generating an average elastic modulus at a 0.6% strain of 496 ksi (3234 MPa). The EBAA C1900 restraint shows a slightly stiffer strain response to compressive load generating an elastic modulus of 782 ksi (5392 MPa) at 0.6% strain. The strains recorded ranged from 0.67% to 1.08% with the maximum strain being recorded during the Lokx test. However, The Lokx connection recorded a lower axial strain at the onset of leaking [0.72%].

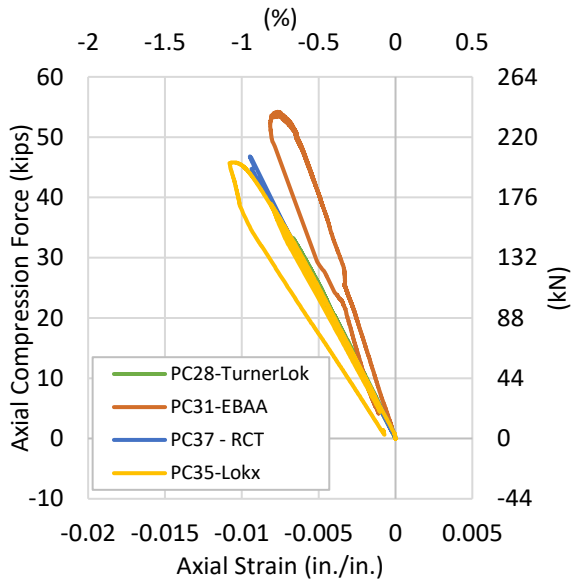

Figure 3.85. Compression Test Comparison – Axial Force vs. Axial Strain

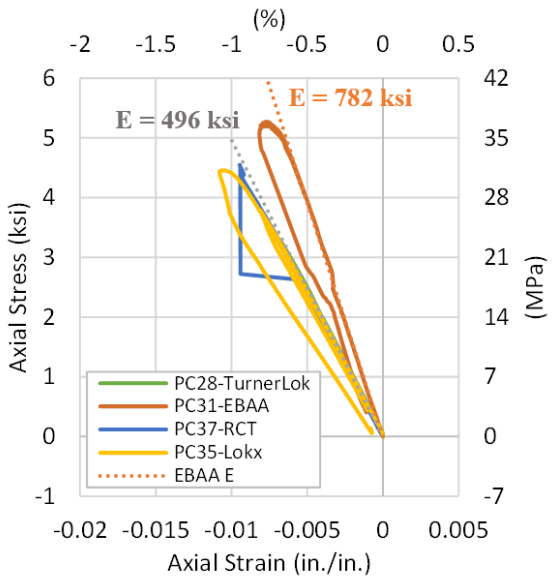

Figure 3.86. Compression Test Comparison – Axial Stress vs. Axial Strain

3.5 Axial Cyclic Test Results

The following sections provide results from axial cyclic tests performed on iPVC pipeline systems. A total of five cyclic tests were performed at the CIEST laboratory. In this section, tensile loads and deformations are recorded as positive values and compressive loads and deformations are recorded as negative values.

3.5.1 Cyclic Test PS12 Results – iPVC RCT Coupling

Pipe specimen PS12 consisted of an iPVC pipe with an RCT Flex-Tite Coupling connection located at the midpoint. The specimen was subjected to cyclic loading following Quasi-Static Cyclic Testing protocols outlined in FEMA-461. During the test, fifteen tensile and compressive loading cycles were applied to the specimen using force control. Loading cycles were increased by 40% until a cycle of 20 kips (89 kN) was reached. After the 20-kip cycle was completed, actuator force control was switched to displacement control and the specimen was pulled in tension to failure. Figure 3.87 shows photos for the pre-test setup of specimen PS12 as well as the specimen just after failure at the connection.

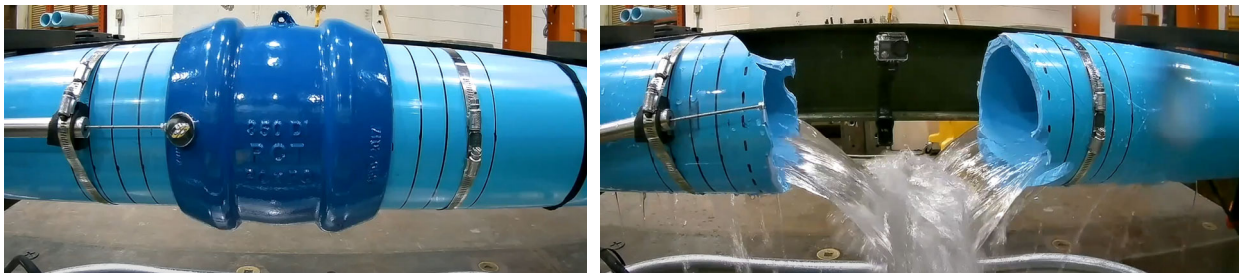

(a) Pre-Test Setup (b) Circumferential Failure at RCT Coupling

Figure 3.87. Specimen PS12 (a) Setup and (b) After Failure

The progression of pressure, actuator force, and actuator displacement is presented in Figure 3.88. The specimen maintained an average pressure of 63 psi (434 kPa) throughout the test with several spikes in pressure ranging from 53 psi (365 kPa) to 77 psi (531 kPa) due to the changing of internal volume in the system as tensile and compressive load is applied. Figure 3.89 displays the actuator force versus actuator displacement. Actuator displacement and force are direct measurements of the actuator's hydraulic piston and attached load cell, respectively. A maximum force of 52.5 kips (224 kN) at an actuator displacement of 3.59 in. (91 mm). Figure 3.90 presents the actuator force versus joint displacement. Joint displacement was measured by LVDTs located at each end of the coupling. A maximum joint displacement of 0.82 in. (21 mm) was recorded before failure occurred.

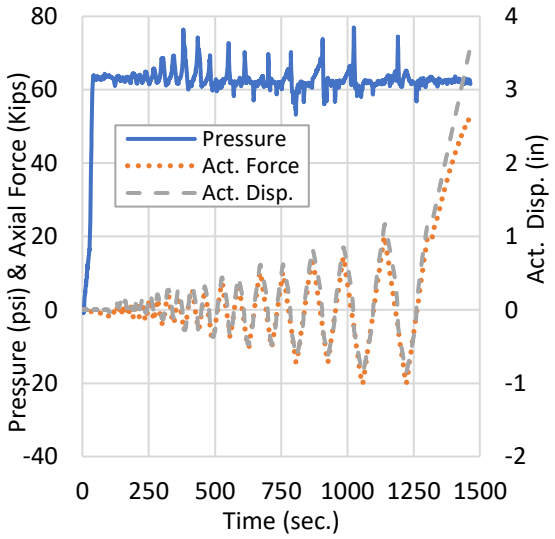

Figure 3.88. PS12-Pressure and Act. Disp. vs. Time

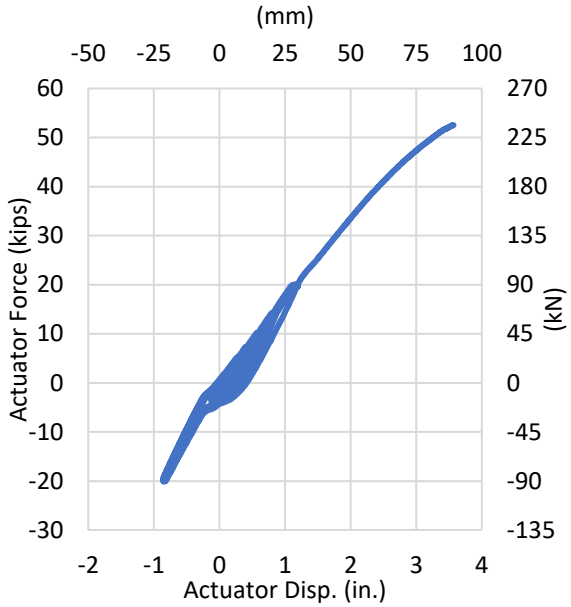

Figure 3.89. PS12-Force vs. Act. Disp.

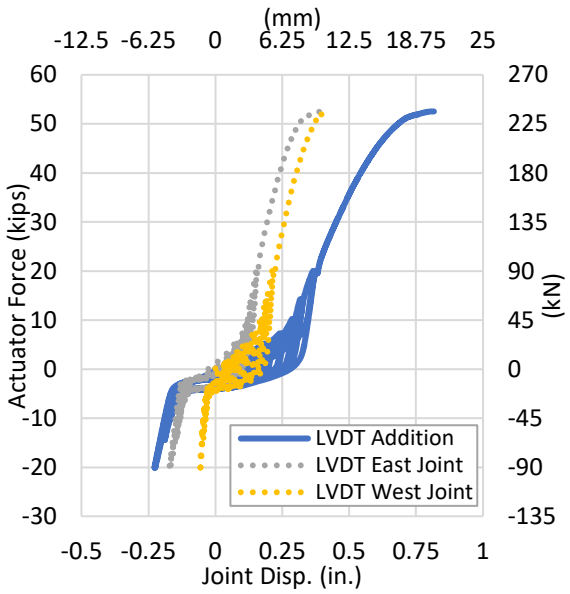

Figure 3.90. PS12- Force vs. Joint Displacement

Axial and circumferential strains were recorded at the eastern pipe section's crown, invert, and both spring lines. Strain versus time and strain versus actuator displacement can be viewed in Figure 3.91 and Figure 3.92, respectively. As cyclic load is applied to the specimen, axial strains increase as tensile load is applied and decrease as compressive load is applied. Due to the Poisson's effect, the circumferential strains show an opposite response, increasing as compressive load is applied and decreasing when subjected to tensile loading. The maximum axial strain peaked at 1.60 % and, the maximum circumferential strain peaked at -0.405%.

At a maximum axial force of 52.5 kips (224 kN) and a maximum actuator displacement of 3.59 in. (91 mm), the pipe specimen circumferentially fractured at both ends of the RCT coupling caused a total loss of pressure and the conclusion of the test.

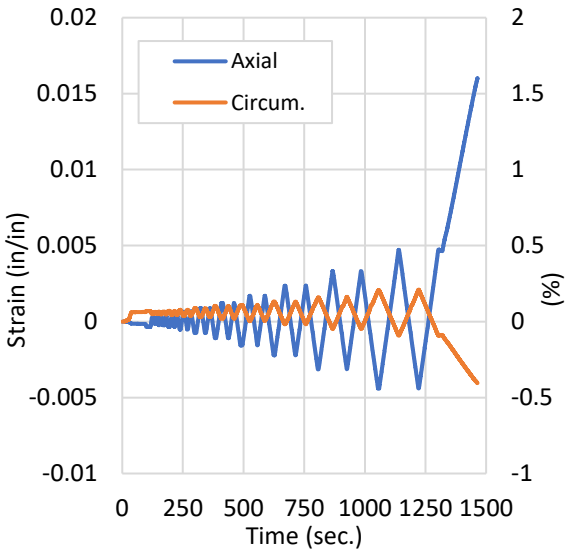

Figure 3.91. PS12-Strain vs. Time

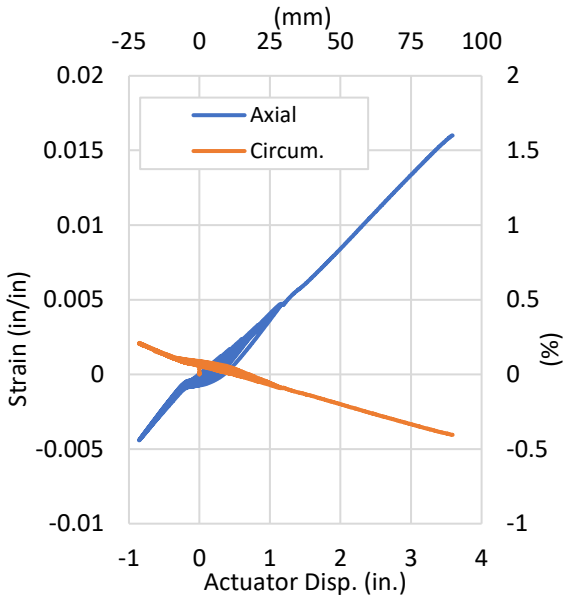

Figure 3.92. PS12-Strain vs. Act. Disp.

3.5.2 Cyclic Test PS29 Results – iPVC TurnerLok Gasket

Pipe specimen PS29 consisted of an iPVC pipe with an internal TurnerLok gasket restraining the bell and spigot connection located at the midpoint. The specimen was subjected to cyclic loading following Quasi-Static Cyclic Testing protocols outlined in FEMA-461. During the test, fifteen tensile and compressive loading cycles were applied to the specimen using force control. Loading cycles were increased by 40% until a cycle of 20 kips (89 kN) was reached. After the 20-kip cycle was completed, actuator force control was switched to displacement control and the specimen was pulled in tension to failure. Figure 3.93 shows photos for the pre-test setup of specimen PS29 as well as the specimen just after failure at the connection.

(a) Pre-Test Setup (b) Failure of Bell and Spigot

Figure 3.93. Specimen PS29 (a) Setup and (b) After Failure

The progression of pressure, actuator force, and actuator displacement is presented in Figure 3.94. The specimen maintained an average pressure of 65 psi (450 kPa) throughout the test with minor fluctuations. Figure 3.95 displays the actuator force versus actuator displacement. Actuator displacement and force are direct measurements of the actuator's hydraulic piston and attached load cell, respectively. Figure 3.96 presents the actuator force versus joint displacement. Joint displacement was measured by a string pot at both the crown, invert, and both spring lines of the specimen that spanned from the spigot across the bell. During the final compressive cycle, significant actuator and joint displacement was observed with the actuator reaching 1.39 in. (35 mm) and the joint reaching 0.74 in. (19 mm) of compressive displacement. During the final pull to failure of the specimen, a slight reduction in force occurs at 25 kips (111 kN) as the gasket groove begins to yield allowing additional joint and actuator movement. A maximum joint displacement of 0.96 in. (24 mm) was recorded before failure occurred.

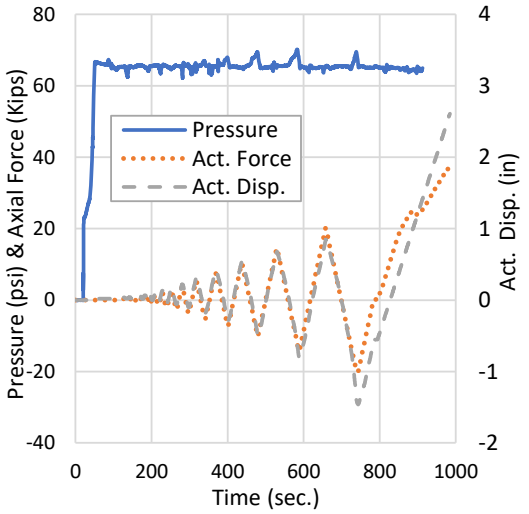

Figure 3.94. PS29-Pressure and Act. Disp. vs. Time

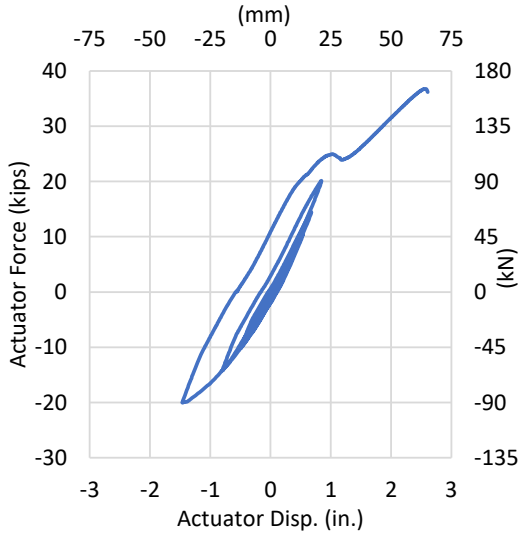

Figure 3.95. PS29-Force vs. Act. Disp.

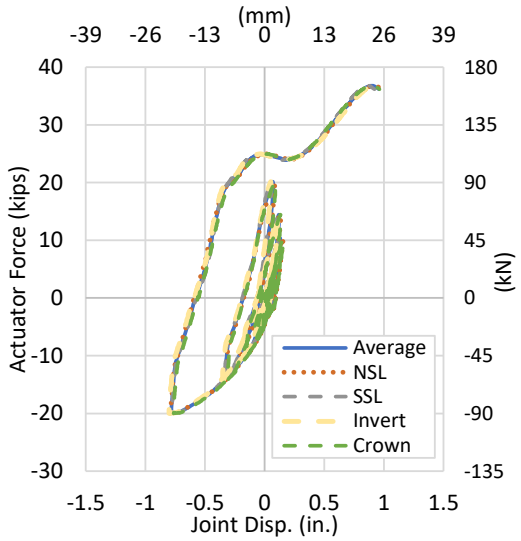

Figure 3.96. PS29- Force vs. Joint Displacement

Axial and circumferential strains were recorded at the crown, invert, and both spring lines of the bell section. Strain versus time and strain versus actuator displacement can be viewed in Figure 3.97 and Figure 3.98, respectively. As cyclic load is applied to the specimen, axial strains increase as tensile load is applied and decrease as compressive load is applied. Due to the Poisson's effect, the circumferential strains show an opposite response, increasing as compressive load is applied and decreasing when subjected to tensile loading. The maximum axial strain peaked at 0.829 % and the maximum circumferential strain peaked at -0.212%.

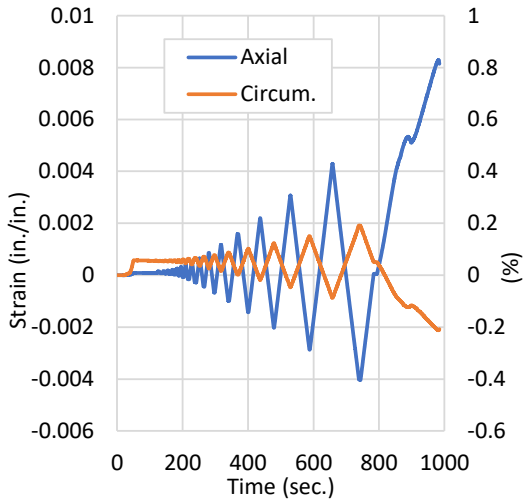

Figure 3.97. PS29-Strain vs. Time

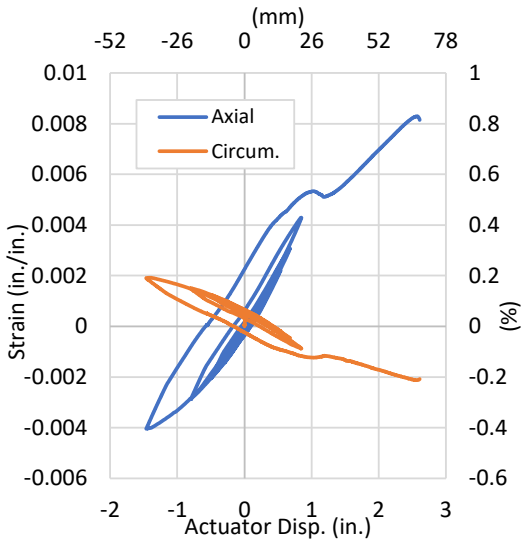

Figure 3.98. PS29-Strain vs. Act. Disp.

At a maximum axial force of 36.8 kips (164 kN) and a maximum actuator displacement of 2.61 in. (66.3 mm), the bell suddenly shatters causing a loss of pressurization and the ejection of the internal TurnerLok gasket. Just before failure, yielding and discoloration of the bell was observed. Circumferential cracking was visible along the spigot after the failure of the specimen. There were no signs of leaking before failure. A series of photos taken during the test are presented in Figure 3.99 (a-d).

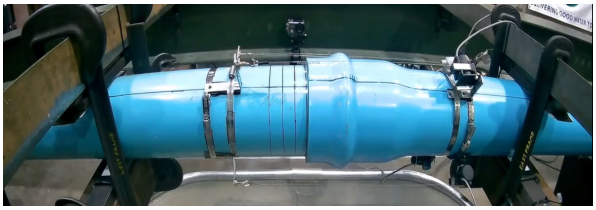

(a) Maximum Tension Cycle

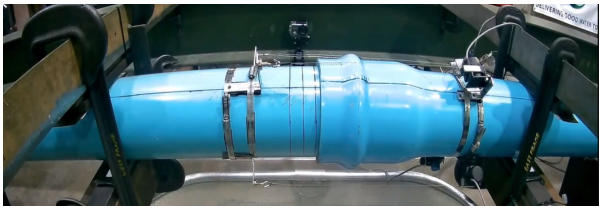

(b) Maximum Compression Cycle

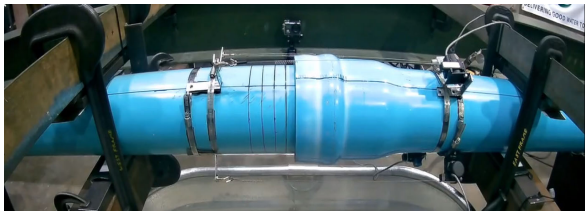

(c) Just Before Fracture

(d) Fracture of Bell and Cracking of Spigot

Figure 3.99. Images of PS29 during the test progression

3.5.3 Cyclic Test PS32 Results – iPVC EBAA C1900 Restraint Harness

Pipe specimen PS32 consisted of an iPVC pipe with an external EBAA C1900 restraint harness. Restraint nuts for this specimen were located to allow for 1 in. (25 mm) of joint opening before engaging and resisting axial deformation. The specimen was subjected to cyclic loading following Quasi-Static Cyclic Testing protocols outlined in FEMA-461. During the test, fifteen tensile and compressive loading cycles were applied to the specimen using force control. Loading cycles were increased by 40% until a cycle of 20 kips (89 kN) was reached. After the 20-kip cycle was completed, actuator force control was switched to displacement control and the specimen was pulled in tension to failure. Figure 3.100 shows photos for the pre-test setup of specimen PS32 as well as the specimen just after failure at the connection.

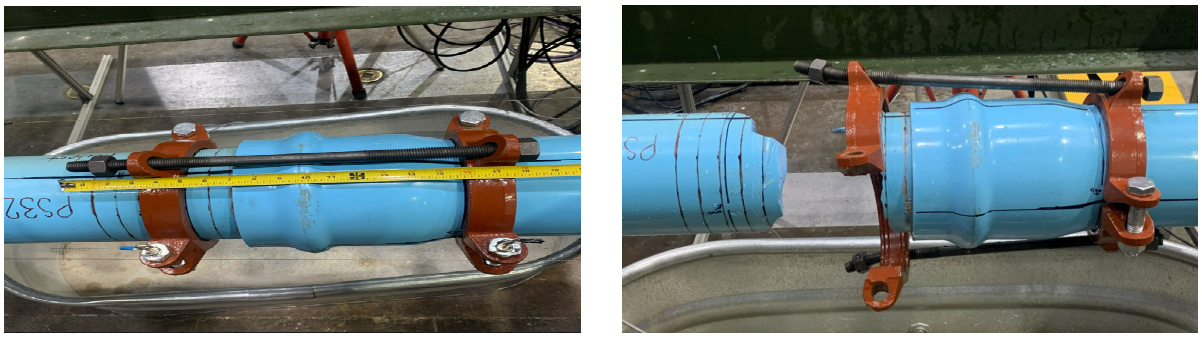

(a) Pre-Test Setup (b) Failure of the Bell and Spigot

Figure 3.100. Specimen PS32 (a) Setup and (b) Failure of the Bell and Spigot

The progression of pressure, actuator force, and actuator displacement is presented in Figure 3.101. Due to the significant change in the internal area during compression cycles, large spikes in pressure can be observed with the largest spike reaching 139 psi (958 kPa) at 909.5 sec into the test. Figure 3.102 shows the actuator force versus displacement, while Figure 3.103 presents the actuator force versus joint displacement. Actuator displacement and force are direct measurements of the actuator's hydraulic piston and attached load cell, respectively. Joint displacement was measured by a string pot at both the crown and invert of the specimen that spanned from the spigot across the bell. Actuator force versus actuator displacement shows a flat response between -0.5 in. (-13 mm) and 1 in. (25 mm), which can be attributed to the 1 in. (25mm) of axial displacement allowed by the C1900 restraint. The system experienced an average load of -3 kips (13 kN) throughout the flat response due to internal pressure. During the final pull to failure in the specimen, the system reached a maximum actuator and joint displacement of 5.08 in. (129 mm) and 3.68 in. (93 mm) before failure.

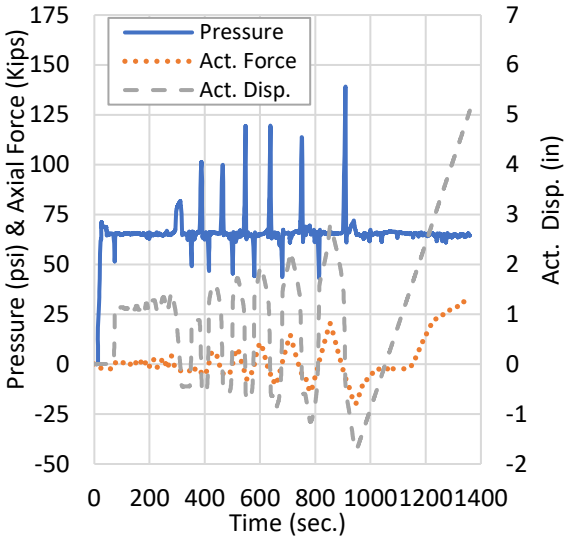

Figure 3.101. PS32-Pressure and Act. Disp. vs. Time

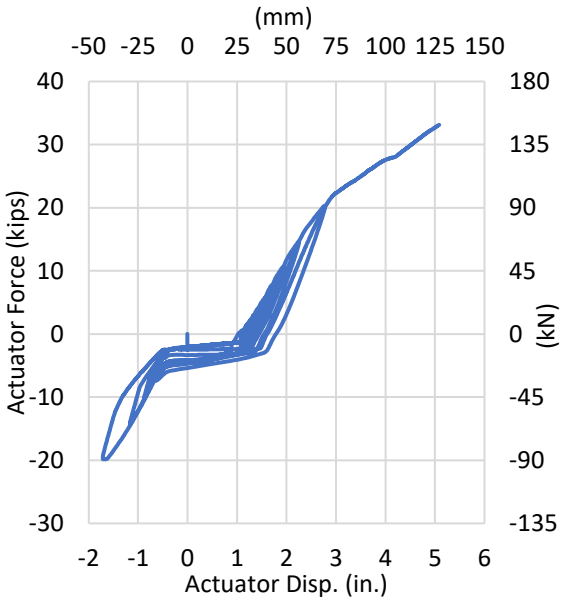

Figure 3.102. PS32-Force vs. Displacement

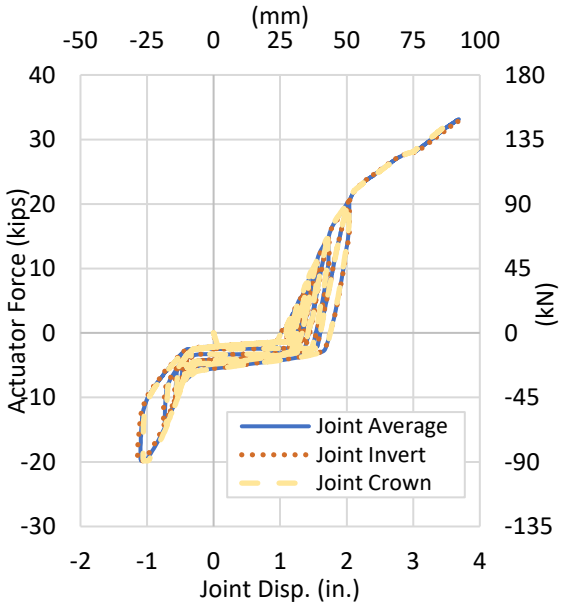

Figure 3.103. PS32-Force vs. Joint Displacement

Axial and circumferential strains were recorded at the crown, invert, and both spring lines of the bell section. Similar to previous cyclic test specimens, as cyclic load is applied to the specimen, axial strains increase as tensile load is applied and decrease as compressive load is applied. Due to the Poisson's effect, the circumferential strains show an opposite response, increasing as compressive load is applied and decreasing

when subjected to tensile loading. Strain versus time and strain versus actuator displacement can be viewed in Figure 3.104 and Figure 3.105, respectively. The maximum axial strain peaked at 0.779% and the maximum circumferential strain peaked at -0.185 %.

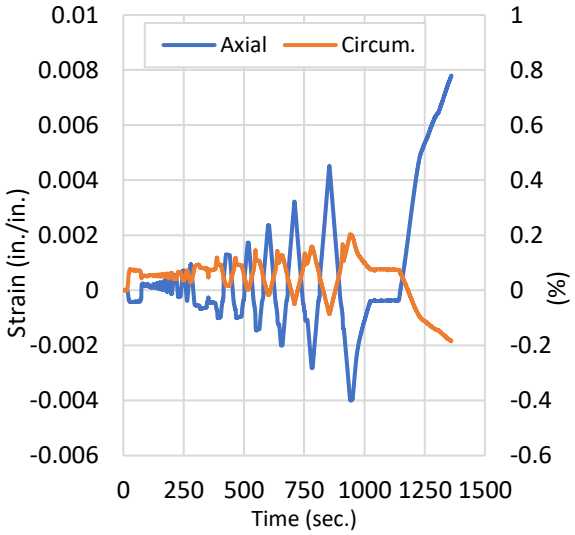

Figure 3.104. PS32-Strain vs. Time

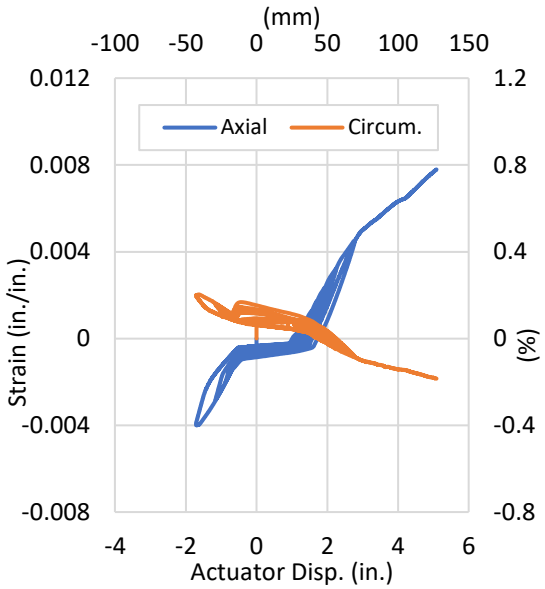

Figure 3.105. PS32-Strain vs. Displacement

At a maximum axial force of 33.1 kips (147 kN) and a maximum actuator displacement of 5.09 in. (129 mm), the spigot suddenly fractured, causing a loss of pressurization. As the spigot fractured, shearing was observed in the C1900 restraint vertical bolts. A hairline crack traveling approximately 8.5 in. (216 mm) from the spigot fracture is visible in Figure 3.106. A series of photos taken during the test are presented in Figure 3.107 (a-d). Prior to this fracture, there were no signs of leakage.

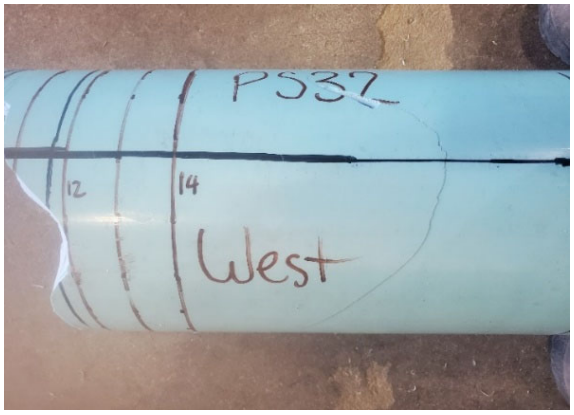

Figure 3.106. PS32 - Hairline Cracking along Spigot

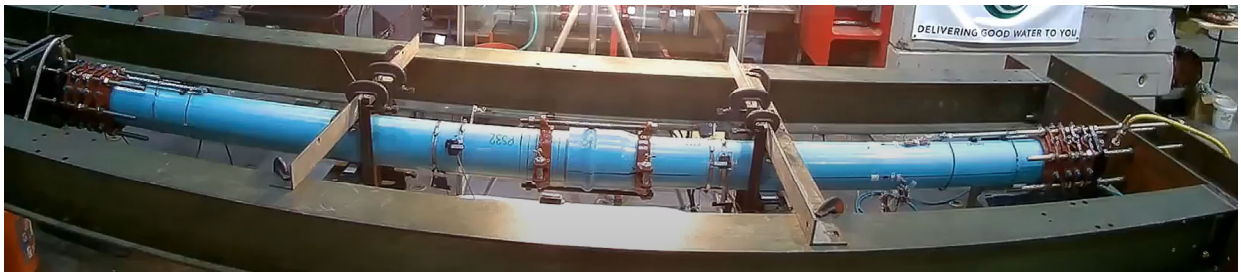

(a) Start of Test

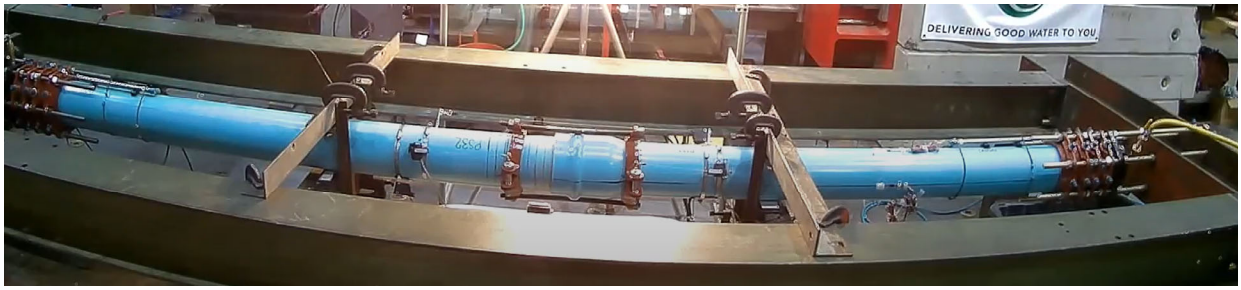

(b) Maximum Tension Cycle

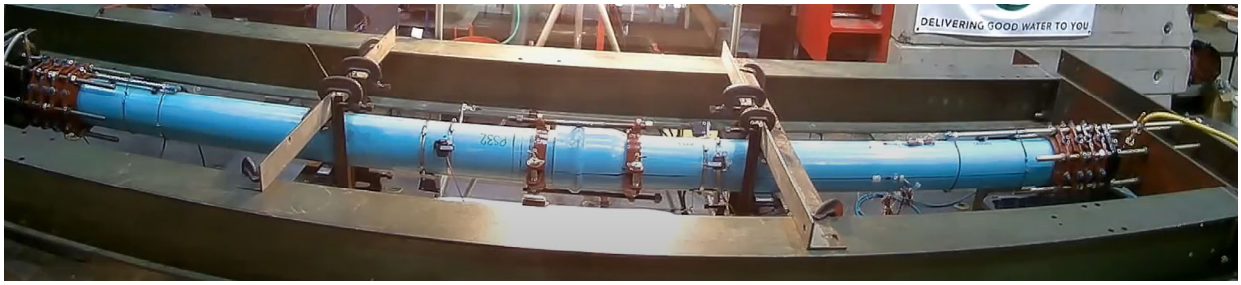

(c) Maximum Compression Cycle

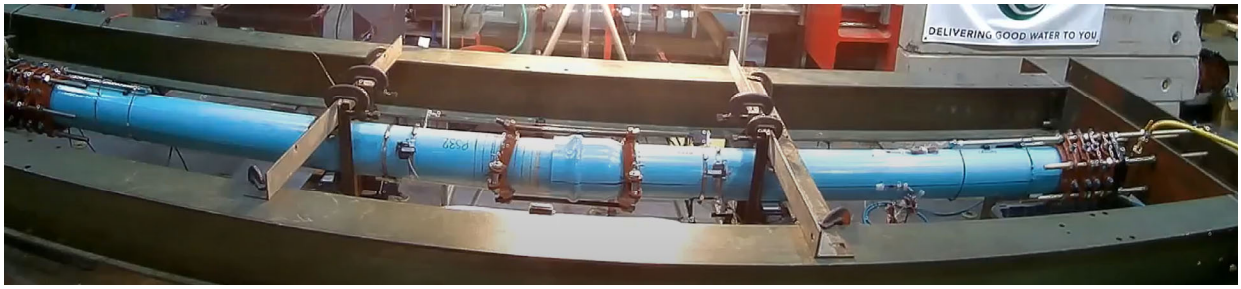

(d) Just Before Fracture

Figure 3.107. Images of PS32 during the test progression

3.5.4 Cyclic Test PS36 Results – iPVC Lokx Coupling

Pipe specimen PS36 consisted of an iPVC pipe with a Lokx coupling connection at the midpoint. The specimen was subjected to cyclic loading following Quasi-Static Cyclic Testing protocols outlined in FEMA-461. During the test, fifteen tensile and compressive loading cycles were applied to the specimen using force control. Loading cycles were increased by 40% until a cycle of 20 kips (89 kN) was reached. After the 20-kip cycle was completed, actuator force control was switched to displacement control and the specimen was pulled in tension to failure. Figure 3.108 shows photos for the pre-test setup of specimen PS36 as well as the specimen just after failure at the connection.

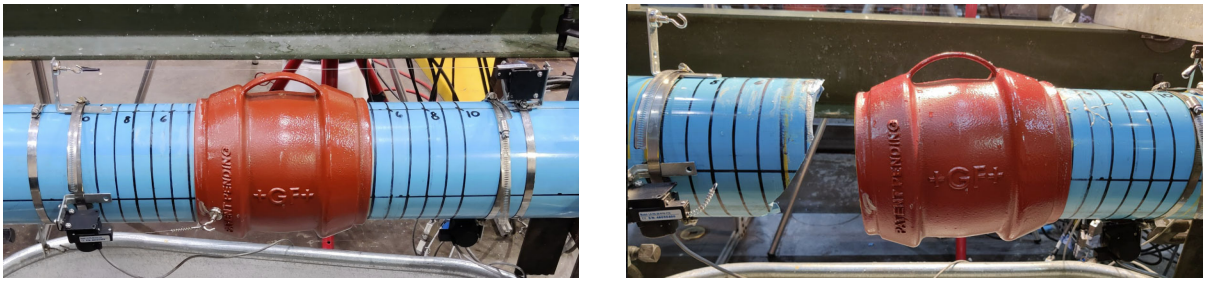

(a) Pre-Test Setup (b) Circumferential Failure at Coupling

Figure 3.108. Specimen PS36 (a) Setup and (b) After Failure

The progression of pressure, actuator force, and actuator displacement is presented in Figure 3.109. The specimen maintained an average pressure of 65 psi (450 kPa) throughout the test. During the test, moderate pressure fluctuations were seen, with pressure peaking at 78 psi (538 kPa). Figure 3.110 displays the actuator force versus actuator displacement. Actuator displacement is a direct measurement of the movement of the actuator's hydraulic piston. Figure 3.111 presents the actuator force versus joint displacement. Due to the joint rotation at the connection of the specimen, data recorded from string pots at the connection were inaccurate. Therefore, a global joint displacement was calculated to represent the system's joint response to compressive load. Global joint displacement was calculated by subtracting end restraint slippage and pipe strain from the total actuator displacement. Leaking occurred at several locations throughout the test, quickly halting as tensile load was applied to the system. The first onset of leaking occurred at 3.8 kips (16.9 kN) into the second to last tension cycle [14.3 kips (63.6 kN)] with leaking quickly stopping at 13.7 kips (60.9 kN) within the same cycle. The second start of leaking occurs at a similar force of 5.4 kips into the next tension cycle [20.0 kips (89.0 kN)] with leaking quickly stopping as further tensile load is applied. The final start and stop of leaking at the connection occurred during the final pull to failure of the specimen with leaking occurring at -15.4 kips (-68.5 kN) of compressive load. The final leak eventually stopped at 25.8 kips (115 kN) of tension into the final pull of the specimen. A large jump in joint displacement [0.2 in. (5mm)] is observed during the -10.2-kip (45 kN) compression cycle as the west spigot

penetrates through the back stopper of the Lokx connection. A maximum joint displacement of 0.26 in. (7 mm) was recorded before circumferential failure at the connection occurred.

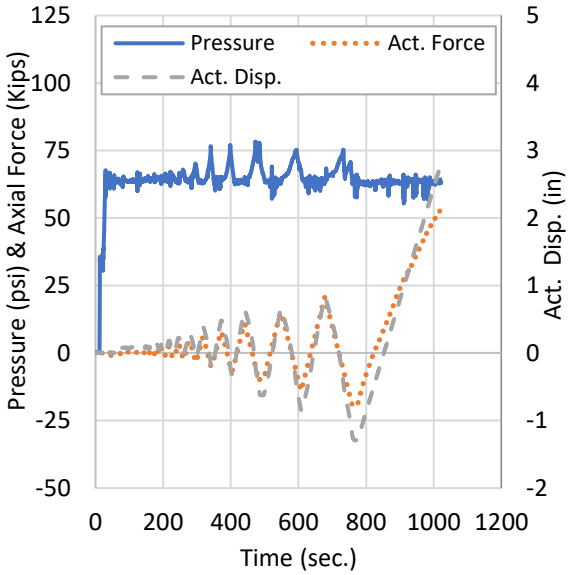

Figure 3.109. PS36-Pressure and Act. Disp. vs. Time

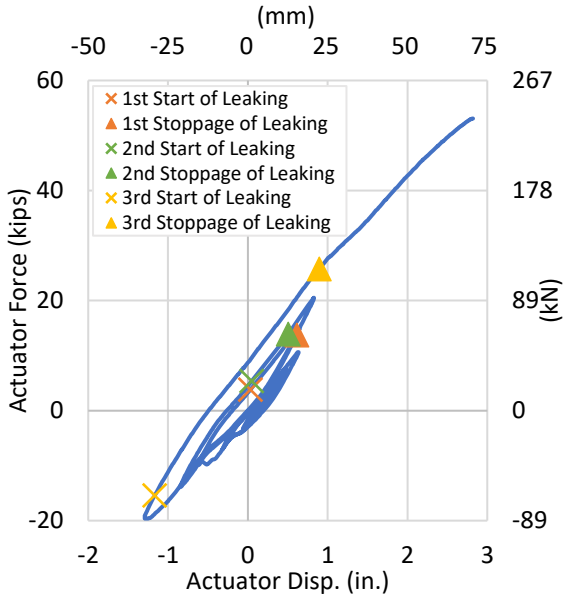

Figure 3.110. PS36-Force vs. Act. Disp.

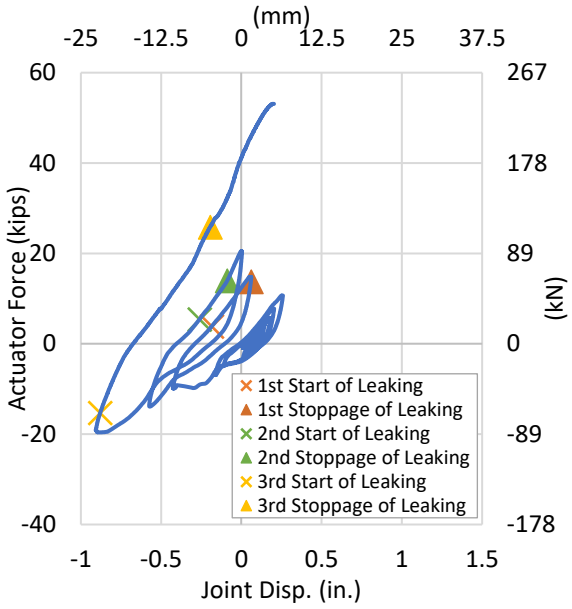

Figure 3.111. PS36- Force vs. Joint Displacement

Axial and circumferential strains were recorded at the crown, invert, and both spring lines of the bell section. Strain versus time and strain versus actuator displacement can be viewed in Figure 3.112 and Figure 3.113, respectively. The maximum axial strain peaked at 1.36 % and the maximum circumferential strain peaked at -0.263%.

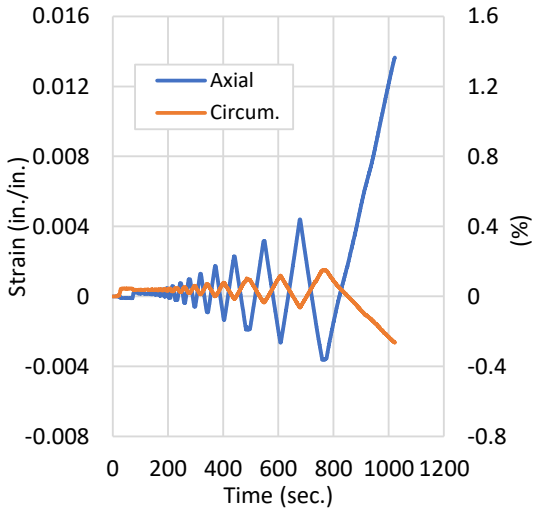

Figure 3.112. PS36-Strain vs. Time

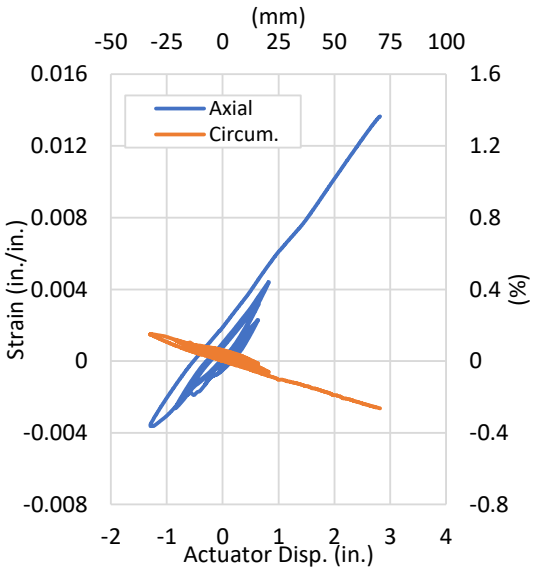

Figure 3.113. PS36-Strain vs. Act. Disp.

The test concluded as the western pipe segment circumferentially fractured at the face of the Lokx coupling connection. A maximum axial force of 53.1 kips (236 kN) and a maximum actuator displacement of 2.82 in. (72 mm) were recorded just before the specimen fractured. Figure 3.114 presents the interior of the Lokx connection after failure.

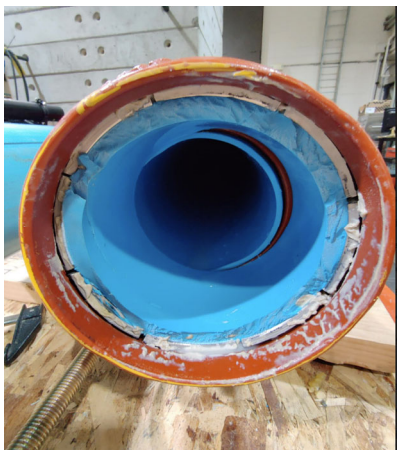

Figure 3.114. PS36-Fracture at Lokx Connection

3.5.5 Cyclic Test PS39 Results – iPVC Hymax Coupling

Pipe specimen PS39 consisted of an iPVC pipe with a Hymax Grip Coupling located at the specimen's midpoint. Pipe segments were inserted 4 in. (102 mm) into each end of the Hymax coupling. Restraint bolts, located at the top of the coupling were tightened to the minimum required torque specifications for 6 in. (152 mm) nominal diameter pipes [110 lb.-ft (149 N-m)]. The specimen was subjected to cyclic loading following Quasi-Static Cyclic Testing protocols outlined in FEMA-461. During the test, fifteen tensile and compressive loading cycles were applied to the specimen using force control. Loading cycles were increased by 40% until a cycle of 20 kips (89 kN) was reached. After the 20-kip cycle was completed, actuator force control was switched to displacement control and the specimen was pulled in tension to failure. Figure 3.115 shows photos for the pre-test setup of specimen PS39 as well as the specimen just after the conclusion of the test.

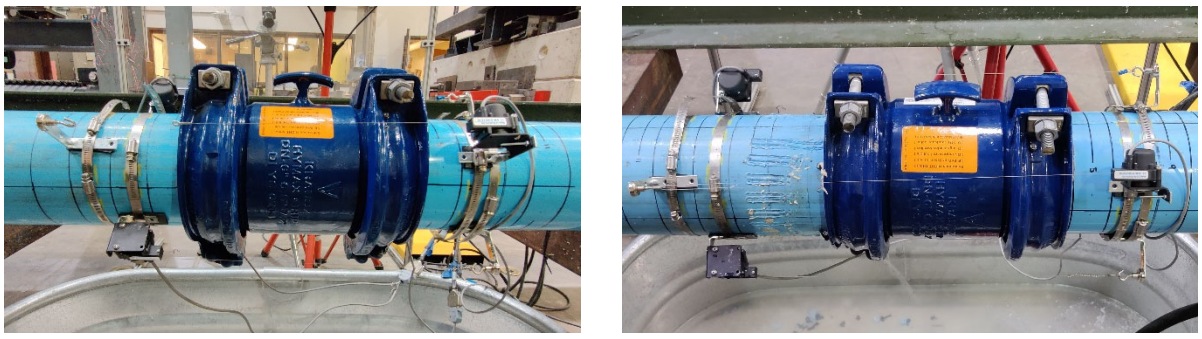

(a) Pre-Test Setup (b) Failure of the Bell and Spigot

Figure 3.115. Specimen PS39 (a) Setup and (b) Failure of the Bell and Spigot

The progression of pressure, actuator force, and actuator displacement is presented in Figure 3.116. The specimen was pressurized to an average internal pressure of 65 psi (448 ksi). During the final compressive load, cycle buckling began to occur at the connection, causing a force error limit to be reached. Reaching the force error limit initiated hydraulic shutoff to the actuator, causing a steep decline in force and displacement. Hydraulics were then reintroduced to the system, and the final compressive cycle was completed under displacement control before the specimen was pulled in tension to failure.

Figure 3.117 shows the actuator force versus displacement, while Figure 3.118 presents the actuator force versus joint displacement. Actuator displacement and force are direct measurements of the actuator's hydraulic piston and attached load cell, respectively. Due to the joint rotation at the connection of the specimen, data recorded from string pots at the connection were inaccurate. Therefore, a global joint displacement was calculated to represent the system's joint response to compressive load. Global joint displacement was calculated by subtracting end restraint slippage and pipe strain from the total actuator displacement. A maximum compressive force of 18.0 kips (80.1 kN) was reached before the onset of

buckling at the connection caused a reduction of force under further compressive displacement. Leaking occurred during the final tension pull to failure, at a tensile force of 20.9 kips (93.0 kN), an actuator displacement of 1.50 in. (38 mm), and a joint displacement of 0.93 in. (24 mm). Just after leaking started after the connection slippage occurred at the connection causing significant loss of pressure in the system. The slip occurred at a tensile force of 21.8 kips (97.0 kN) an actuator displacement of 1.94 in. (49 mm), and a joint displacement of 1.34 in. (34 mm). The slip location was determined to be the ultimate capacity of the system, despite the system's ability to generate minor axial forces as the spigot continued to be pulled out of the Hymax coupling.

Axial and circumferential strains were recorded at the crown, invert, and both spring lines of the bell section. Similar to previous cyclic test specimens, as cyclic load is applied to the specimen, axial strains increase as tensile load is applied and decrease as compressive load is applied. Due to the Poisson's effect, the circumferential strains show an opposite response, increasing as compressive load is applied and decreasing when subjected to tensile loading. Strain versus time and strain versus actuator displacement can be viewed in Figure 3.119 and Figure 3.120, respectively. The maximum axial strain peaked at 0.476% and the maximum circumferential strain peaked at 0.180 %.

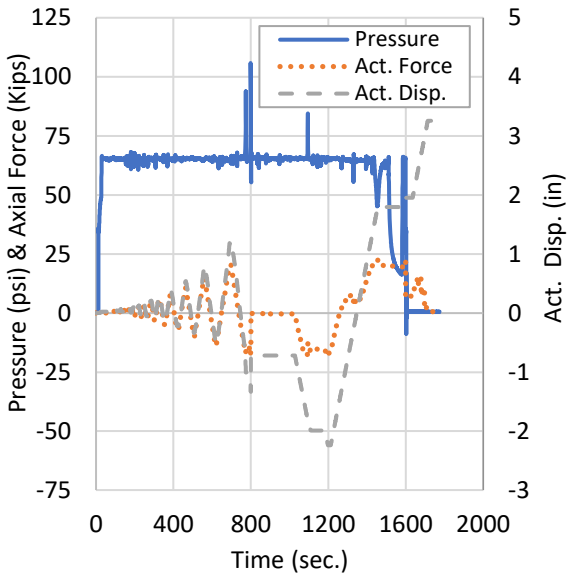

Figure 3.116. PS39-Pressure and Act. Disp. vs. Time

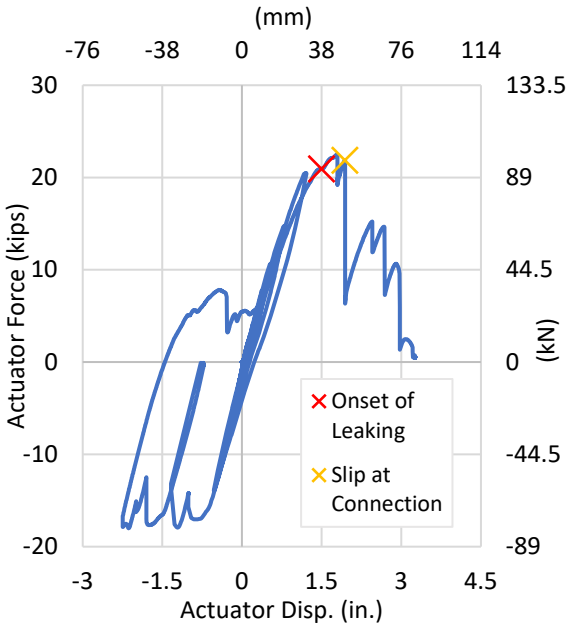

Figure 3.117. PS39-Force vs. Displacement

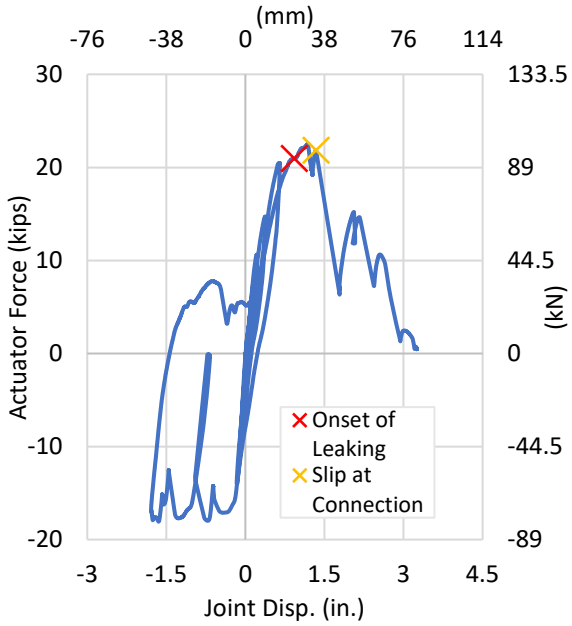

Figure 3.118. PS39-Force vs. Joint Displacement

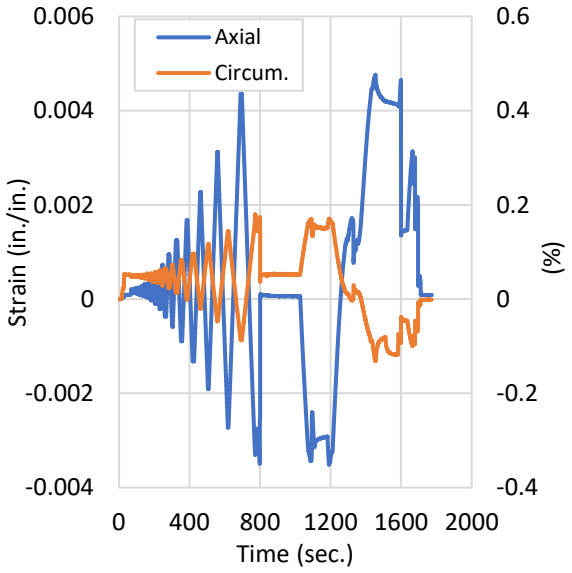

Figure 3.119. PS39-Strain vs. Time

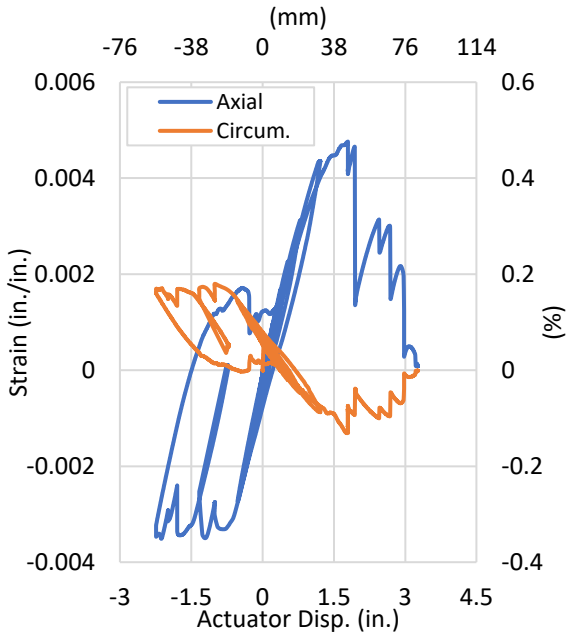

Figure 3.120. PS39-Strain vs. Displacement

At the conclusion of the test, a maximum axial tension force of 22.5 kips (100 kN) and a maximum actuator displacement of 3.26 in. (83 mm) was reached. As shown in Figure 3.122, gouges from the gripper gaskets teeth were visible along the spigot of the specimen. A series of photos taken during the test are presented in Figure 3.121 (a-d).

(a) Start of Test

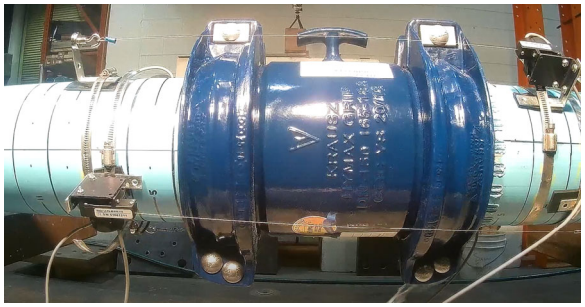

(b) Onset of Leaking

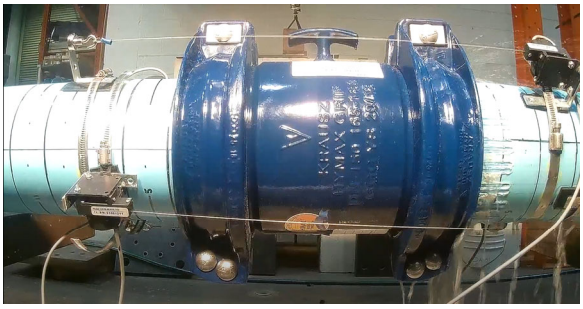

(c) Just after Slippage at the Connection Resulting in Significant Pressure Loss

(d) End of Test

Figure 3.121. Images of PS39 during the test progression

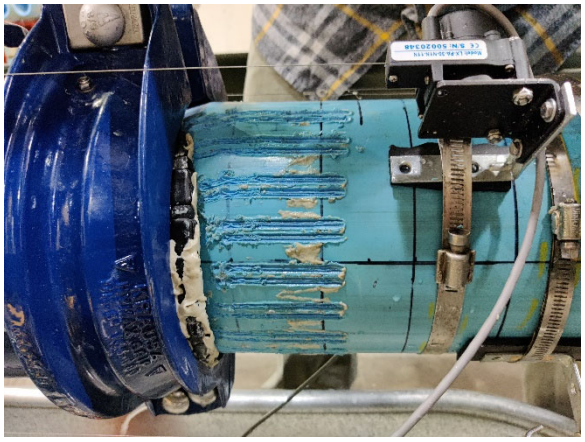

Figure 3.122. PS39 – Gouges in Spigot/Bulging of Grip Gasket

3.6 Axial Cyclic Test Summary and Comparison

This section provides a summary and comparison of the five axial cyclic tests performed on iPVC pipe along with results from corresponding tension tests previously reported in Section 3.1. Table 3.3 shows an overview of the tests and key factors recorded during testing. Figures 3.123 to 3.131 show comparisons of various metrics between tensile and cyclic tests performed on the same restraint type.

Table 3.3. Summary of Axial Cyclic and Tension Test Results

Test # (CIEST)	Pipe-Connection	Max. Axial Force		Max Axial Strain		Max Act. Disp.		Joint Disp.	
		Kips	(kN)	in/in	%	in	(mm)	in	(mm)
PT02	RCT	55.3	(246)	-	-	4.10	(104)	0.93	(24)
PS12	RCT	52.5	(234)	0.0160	1.60	3.59	(91)	0.82	(21)
PT27	TurnerLok	34.6	(154)	0.0078	0.78	2.96	(75)	1.42	(36)
PS29	TurnerLok	36.8	(164)	0.0083	0.83	2.61	(66)	0.96	(24)
PT30	EBAA C1900	38.1	(169)	0.0086	0.86	6.07	(154)	4.36	(111)
PS32	EBAA C1900	33.1	(147)	0.0078	0.78	5.09	(129)	3.68	(93)
PT33	Lokx	60.3	(268)	0.0169	1.69	4.28	(109)	1.37	(35)
PS36	Lokx	53.1	(236)	0.0136	1.36	2.82	(72)	0.26	(7)
PS36 at Leak	Lokx	3.84	(17)	0.0012	0.12	0.03	(1)	-0.26	-(7)
PT38	Hymax Grip	27.9	(124)	0.0063	0.63	2.47	(63)	1.24	(31)
PT38 at Leak	Hymax Grip	27.9	(129)	0.0063	0.63	2.34	(88)	1.06	(57)
PS39	Hymax Grip	22.5	(100)	0.0048	0.48	1.94	(49)	1.34	(34)
PS39 at Leak	Hymax Grip	20.9	(93)	0.0045	0.45	1.50	(38)	0.93	(24)

Note: “PT” denotes Pipe Tension test and “PS” denotes Pipe Cyclic test

Figure 3.123 shows that the RCT connection performed well under cyclic loading (PS12), generating a similar joint displacement response to the monotonic tension test (PT02). The cyclic test showed a slight reduction in ultimate axial force and joint displacement before failure, recording a 5.1% reduction in axial tension force and a 12% reduction in joint displacement. While the cyclic response slightly varied from the monotonic test, the maximum recorded values suggest that cyclic loading does not significantly impact the ultimate capacity and performance of the iPVC-RCT coupling system.

Figure 3.124 and Figure 3.125 present axial force versus joint displacement and axial force versus axial strain response for both TurnerLok monotonic (PT27) and cyclic (PS29) tests, respectively. As shown in Figure 3.124, the TurnerLok connection shows moderate reduction in tensile joint displacement at failure (32%) when subjected to cyclic loading. This response is likely due to the iPVC-TurnerLok system’s ability to allow for telescoping of the spigot through the joint bell under compression load, causing the gripper gaskets teeth to engage further down the spigot. Moreover, the cyclic test outperformed the monotonic test in ultimate axial force and strain capacity, generating an increase in ultimate axial tensile force and strain capacity of 6.4%. This response, along with results from tension tests performed on compression test PC28,

suggests that cyclic and compressive loading does have a significant impact on the iPVC-TurnerLok system's tensile performance.

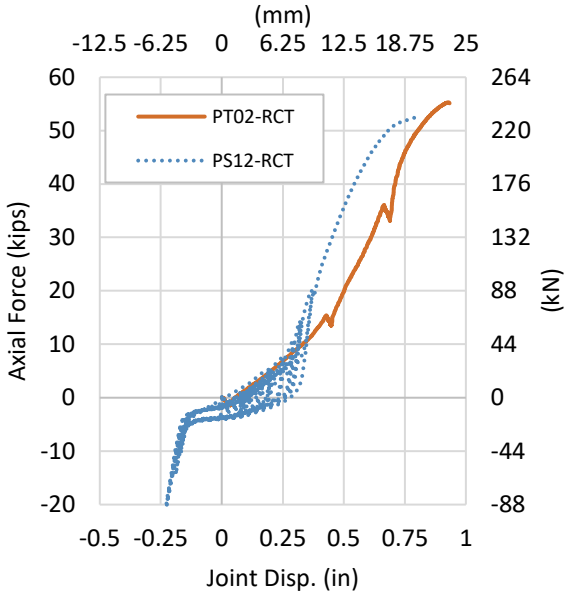

Figure 3.123. Cyclic Comparison – RCT – Axial Force vs. Joint Disp.

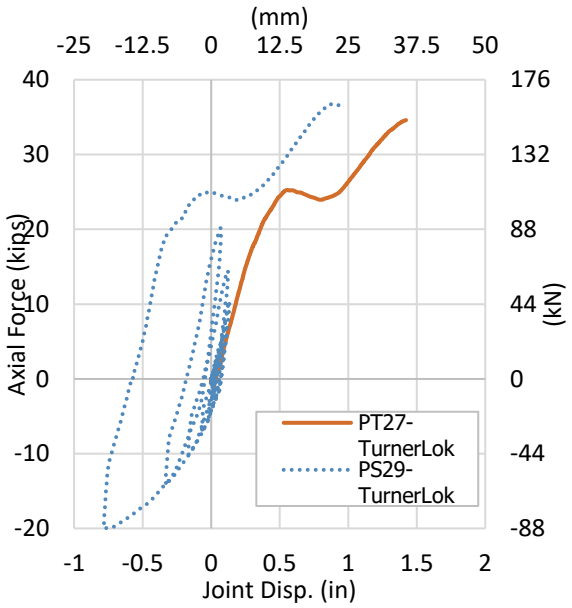

Figure 3.124. Cyclic Comparison – TurnerLok – Axial Force vs. Joint Disp.

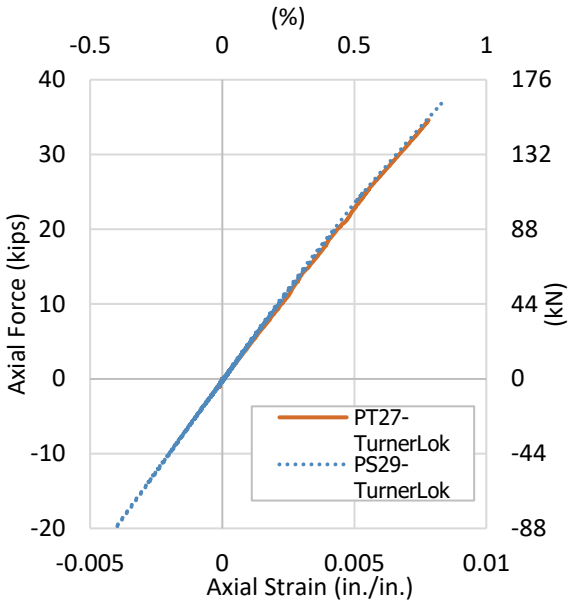

Figure 3.125. Cyclic Comparison – TurnerLok – Axial Force vs. Axial Stain

Figure 3.126 and Figure 3.127 present axial force versus joint displacement and axial force versus axial strain response for both EBAA C1900 monotonic tension (PT30) and cyclic (PS32) tests, respectively. As

shown in Figure 3.126 and Figure 3.127, the cyclic response of the iPVC-EBAA system matches the monotonic test in both shape and slope when pulled in tension to failure. The cyclic test showed a 16% reduction in maximum joint displacement. The system also showed a decrease in ultimate axial tension force and strain of 13% and 9.3%, respectively. Without further testing, the cyclic response of the iPVC-EBAA system suggests that minor variation occurs in the system's response when subjected to cyclic loading but does not significantly impact the overall capacity or performance of the system.

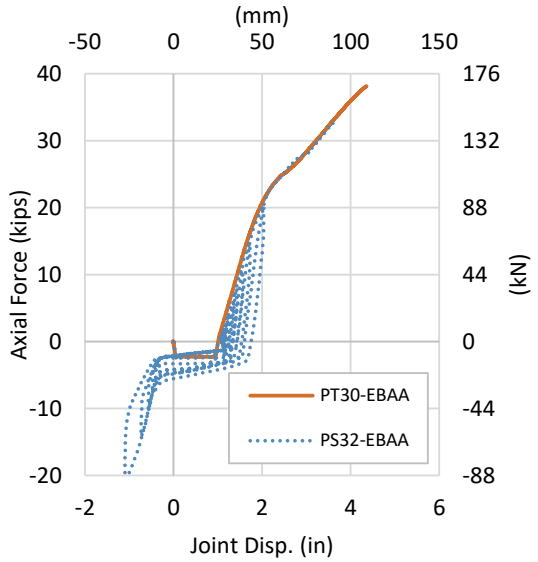

Figure 3.126. Cyclic Comparison – EBAA – Axial Force vs. Joint Disp.

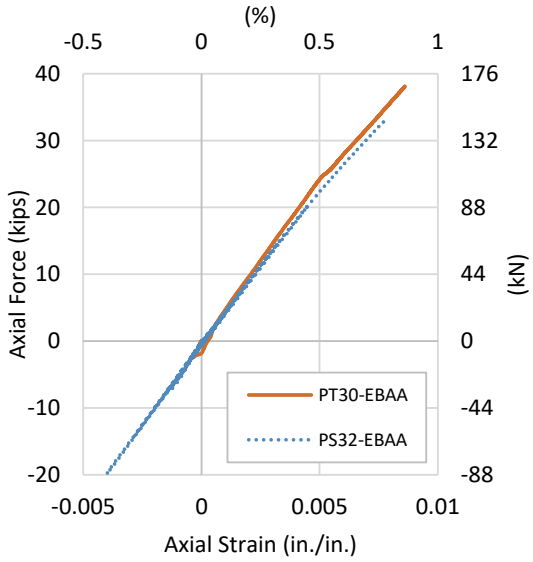

Figure 3.127. Cyclic Comparison – EBAA – Axial Force vs. Axial Stain

Figure 3.128 and Figure 3.129 present axial force versus joint displacement and axial force versus axial strain response for both Lokx monotonic tension (PT33) and cyclic (PS36) tests, respectively. The Lokx connection showed a significant reduction in ultimate joint tensile displacement at failure (81%). As Figure 3.128 shows, this reduction in displacement is in part due to the reengagement of the restraint teeth following each successive compression stroke, similar to the response of PS29. A 12% reduction in ultimate tensile force capacity and a 20% difference in ultimate strain capacity were recorded during the cyclic test. The cyclic test also showed signs of leaking during several compression and tension cycles throughout the test, likely caused by internal movement of the Lokx gasket. The Lokx cyclic response suggest that compressive and cyclic loading have an influence on the systems overall response and ultimate capacity.

Figure 3.130 and Figure 3.131 present axial force versus joint displacement and axial force versus axial strain response for both Hymax Grip monotonic tension (PT38) and cyclic (PS39) tests, respectively. Despite buckling occurring at the connection and significant compressive joint displacement during cyclic

testing, the cyclic test showed an 8.1% increase in total joint displacement at failure. However, the cyclic test also recorded a lower ultimate tensile force and strain, showing a 19% and 29% reduction, respectively. Both cyclic and monotonic tests showed signs of leaking just before ultimate failure in the system. It is also important to note that the primary failure mode in the monotonic test was fracture of the grip gasket while the primary failure mode in the cyclic test was slippage and pullout of the spigot, suggesting that cyclic and or compressive loading plays a significant role in the iPVC-Hymax system tensile response.

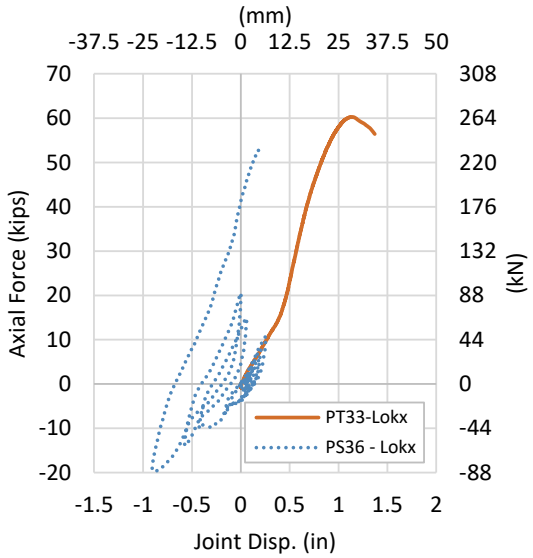

Figure 3.128. Cyclic Comparison – Lokx – Axial Force vs. Joint Disp.

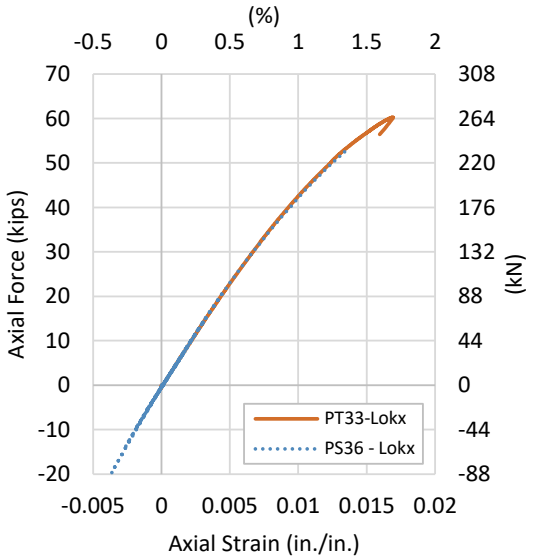

Figure 3.129. Cyclic Comparison – Lokx – Axial Force vs. Axial Stain

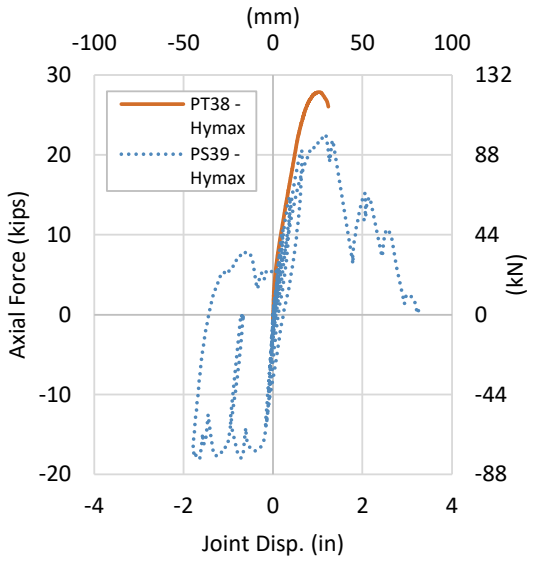

Figure 3.130. Cyclic Comparison – Hymax – Axial Force vs. Joint Disp.

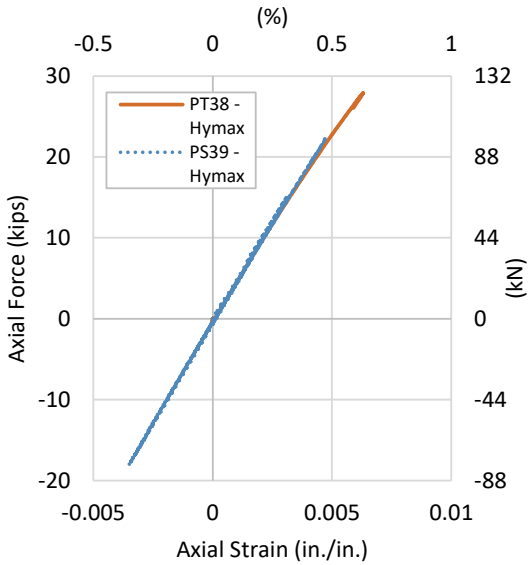

Figure 3.131. Cyclic Comparison – Hymax – Axial Force vs. Axial Stain

3.7 Four-Point Bending Test Results

The following sections provide results from performed four-point bending tests. A total of five bending tests were performed at the CIEST laboratory.

3.7.1 Bending Test PB11 Results – iPVC TurnerLok Gasket

Pipe specimen PB11 consisted of an iPVC pipe with a bell and spigot connection equipped with a TurnerLok gasket located at the midpoint and was performed using Bending Test Setup 1. During the test, the specimen was pressurized to around 65 psi (448 kPa) with minor fluctuations. Transverse displacement was then applied to the system at the two interior loading saddles until the full stroke of the actuator was applied to the specimen. The applied force generated by the transverse loading was captured and recorded by the vertical actuator equipped with a 110-kip load cell. Applied displacement is the average measurement of two string pots (VSP-20 and VSP+20) located directly under each loading saddles. Figure 3.132 presents the progression of pressure, applied displacement, and actuator force through the test.

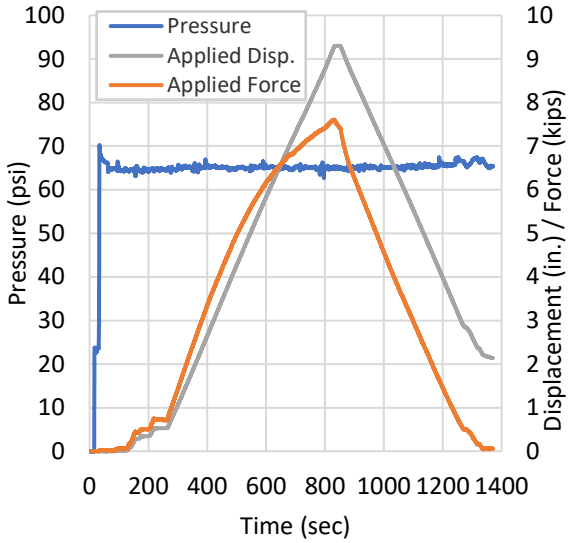

Figure 3.132. PB11-Progression of Pressure, Applied Displacement, and Force.

Force and applied displacement generated in the first 264 seconds can be attributed to the preloading of the specimen. A maximum force of 7.61 kips (33.8 kN) was recorded at the maximum stroke of the actuator, 9.3 in. (236 mm) of applied displacement. Load was applied to the specimen at a constant rate of 1 in. (25.4 mm) per minute. A moment generated over the connection was calculated for the system by considering the pipe system as a continuous beam subjected to two equal concentrated loads. The moment generated over the connection as displacement is applied to the system is presented in Figure 3.133. Self-weight and

the weight of water are included when calculating the moment of the system. Calculations for moment are provided in Appendix A.

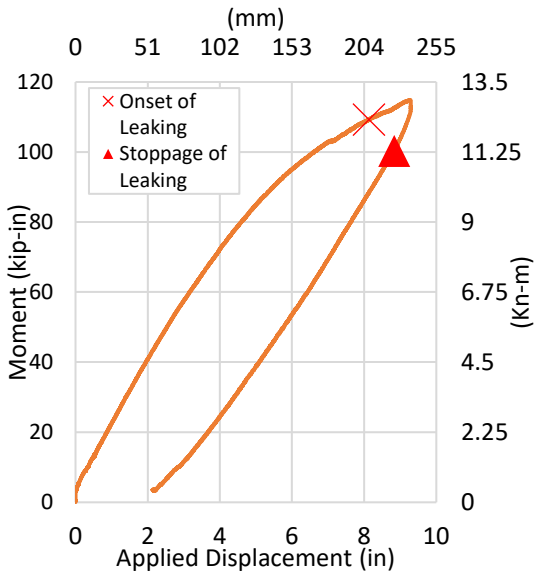

Figure 3.133. PB11-Moment vs. Applied Displacement

An initial moment of 2.95 kip-in (0.33 kN-m) under no applied displacement was generated by the self-weight of the specimen. As displacement is applied to the system, the moment increases at a relatively constant rate. At approximately 80 kip-in (9.04 kN-m) and 5.17 in. (131 mm) of applied displacement, the system's response begins to soften, reaching the system's elastic limits. During the test, leaking at the joint was recorded at around 8.13 in. (207 mm) of applied displacement and 109 kip-in (12.3 kN-m) of generated moment. Leaking quickly halted during unloading of the system, at approximately 8.83 in. (224 mm) of applied displacement and 100 kip-in (11.3 kN-m) of generated moment. A maximum moment of 115 kip-in (13.0 kN-m) was generated during the test at an applied displacement of 9.3 in. (236 mm).

Vertical displacements of the specimen were recorded at four locations, 40 in. (1016 mm) east, 20 in. (508 mm) east, 6 in. (152 mm) east, and 20 in. (508 mm) west of the centerline. Figure 3.134 presents vertical string pot measurements recorded throughout the test at corresponding applied displacements. String pot displacements show a relatively symmetric response in the system when subjected to lateral loading suggesting that the system is centered in the test frame throughout the test.

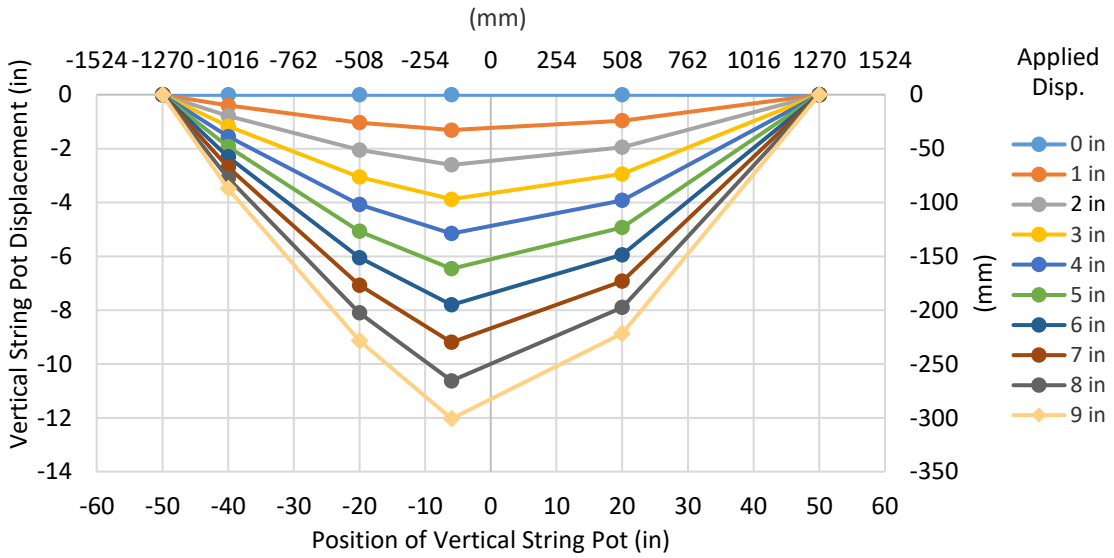

Figure 3.134. PB11-Vertical String Pot Measurements

A radius of curvature was calculated using vertical string pot measurements along the invert of the specimen. A circumcenter for the system's deformation was able to be calculated using the known locations and vertical displacements of three string pots located along the specimen. Calculating the distance from the circumcenter to the location of the vertical string pots allowed a radius of curvature to be defined. By taking the inverse of this radius, a curvature of the system was able to be defined. Calculations for the radius of curvature and curvature are presented in Appendix B. To capture the maximum curvature experienced by the system, a local curvature was calculated using string pots located between the two load saddles (VSP-20, VSP-6, and VSP+20). Local curvature of the system versus applied displacement and moment versus curvature is shown in Figure 3.135 and Figure 3.136, respectively.

Curvature shows a linear response with respect to applied displacement throughout the test. Moment versus curvature increases at a constant rate until around 80 kip-in (9.04 kN-m) and a curvature of 0.0071 in^{-1} (0.281 m^{-1}) where the system begins to reach its elastic range, and the system response begins to soften. The system reached a curvature of 0.0142 in^{-1} (0.559 m^{-1}) before leakage was observed. At the maximum applied displacement and moment, a radius of curvature of 59.1 in. (1501 mm) and a curvature of 0.0169 in^{-1} (0.666 m^{-1}) was generated.

Axial and circumferential strains were recorded at the crown and invert of four locations along the specimen. Strain planes were located at 10 in. (254 mm) and 35 in. (889 mm) on either side of the centerline. Recorded strains were intended to provide a secondary measurement of force applied to the system. Figure 3.137 and Figure 3.138 present axial and circumferential strains with respect to applied displacement throughout the test.

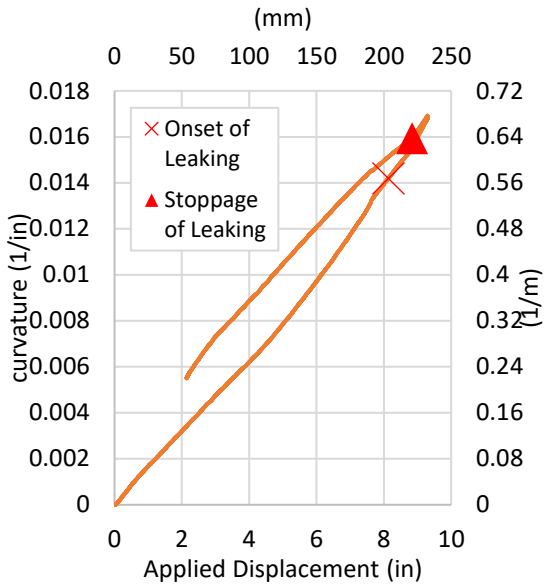

Figure 3.135. PB11 - Curvature vs. App. Disp.

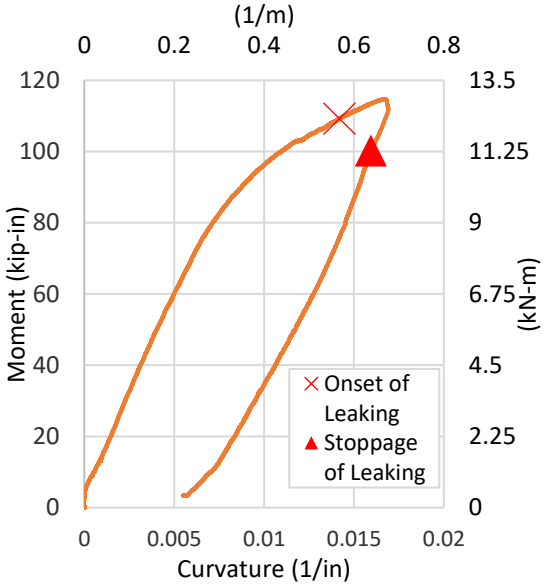

Figure 3.136. PB11 - Moment vs. Curvature

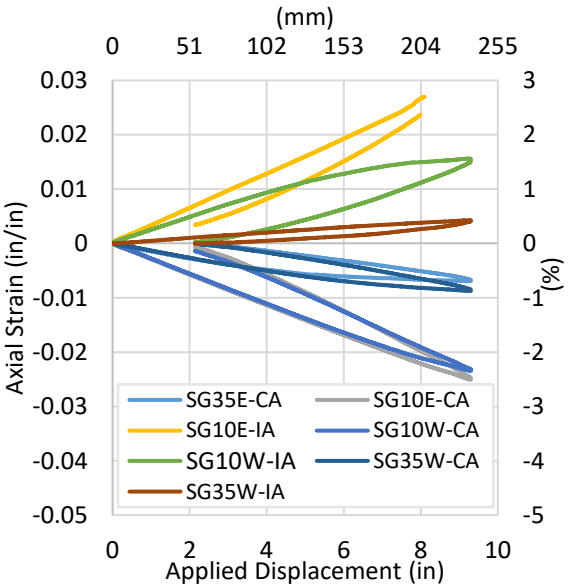

Figure 3.137. PB11 - Axial Strain vs. App. Disp.

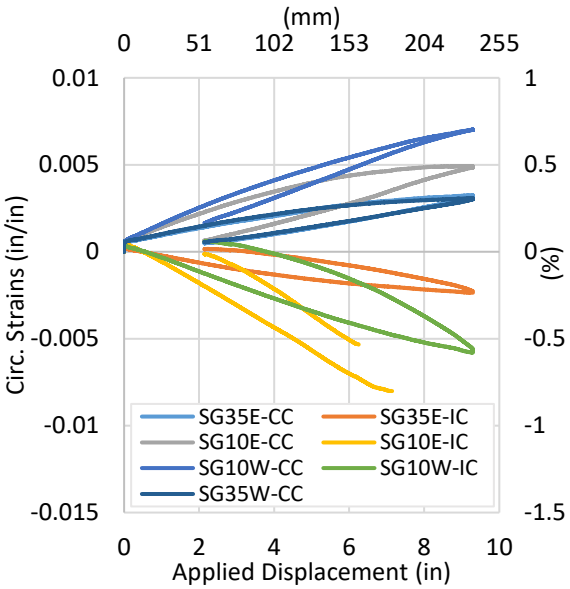

Figure 3.138. PB11 - Circumferential Strain vs. App. Disp.

The strain gauge located at the invert 35 in. west of the centerline overheated during the test; data for SG35W-IA and SG35W-IC is not presented. SG10E-IA disconnected from the data acquisition system at 8.1 in. (206 mm) of applied displacement, the gauge reconnected at 8.0 in. (203 mm) of applied

displacement during unloading. SG10E-IC also disconnected from the data acquisition system at 7.1 in. (180 mm) of applied displacement, the gauge reconnected at 6.3 in. (160 mm) of applied displacement during unloading. Both figures show consistent and relatively symmetric responses due to applied displacement. SG10-IA recorded a maximum axial strain of 2.7% before the gauge disconnected from the system. A maximum circumferential strain of -0.8% was recorded by SG10E-IC before the gauge disconnected from the system.

Despite minor leakage during the test, the system maintained constant pressure throughout loading and unloading. After the test concluded, 2.1 in. (53 mm) of residual deformation remained in the system. Figure 3.152 (a-e) presents pictures taken during significant moments during the test.

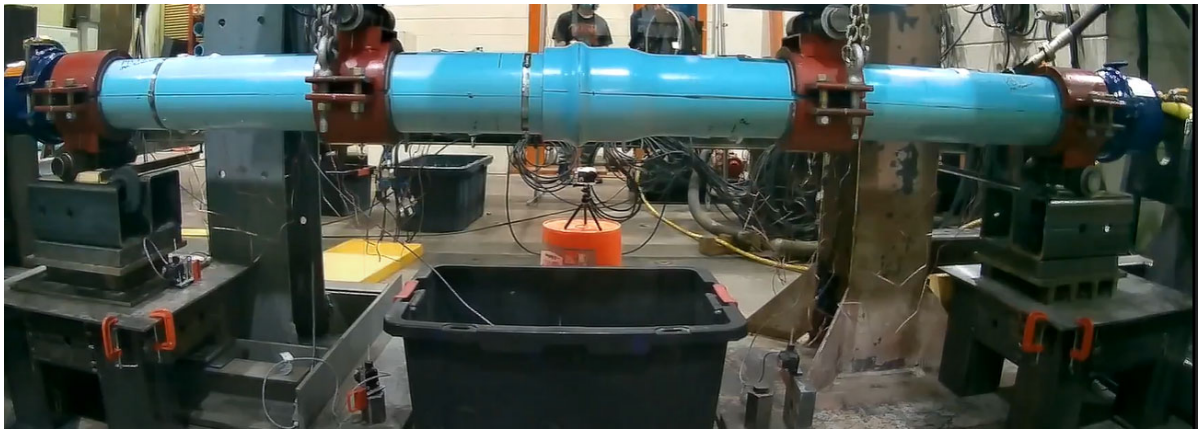

(a) Start of the Test

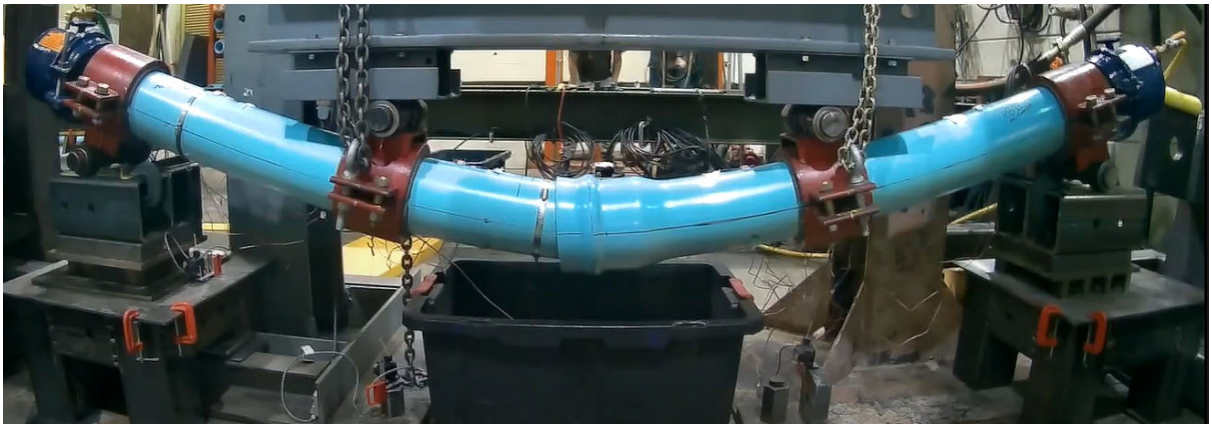

(b) Onset of Leaking at the Joint

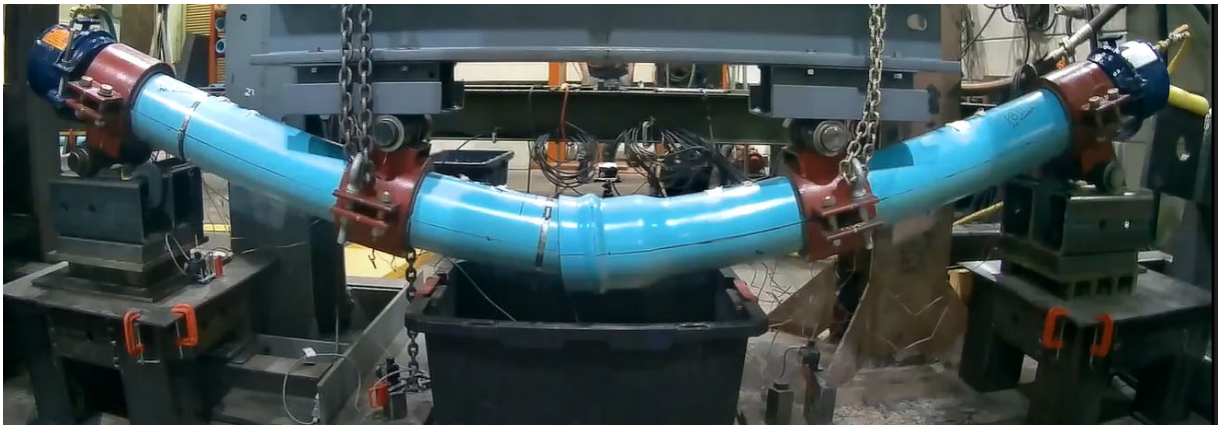

(c) Application of full Actuator Stroke

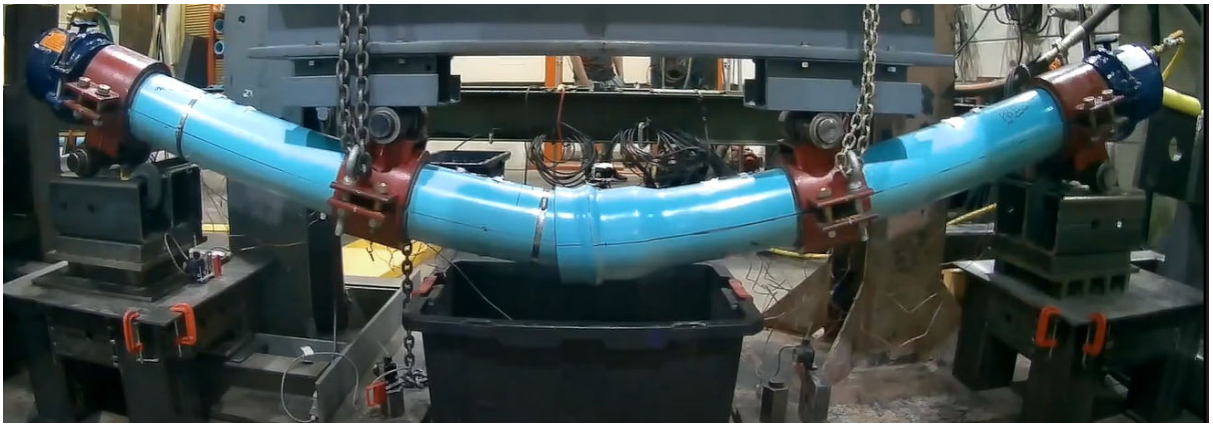

(d) Stoppage of Leaking

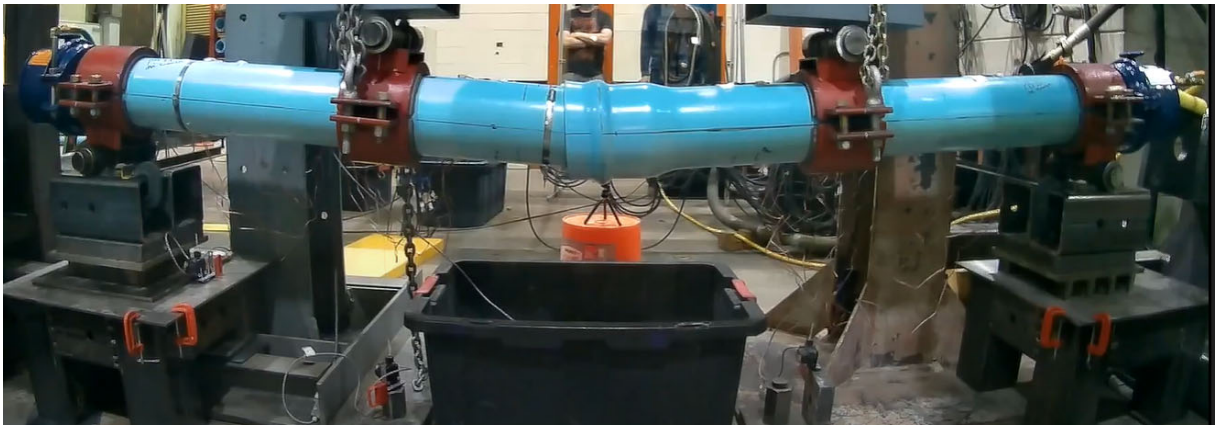

(e) 2.1 in. of Residual Deflection at the End of the Test

Figure 3.139. PB-11 Pictures during Test Progression

Since pipe specimen PB11 performed well under monotonic loading, the specimen was subjected to cyclic loading protocols outlined in Section 2.4.4. Instrumentation and measurements taken during the test were identical to PB11's monotonic test. The specimen was pressurized to an average pressure of 62 psi (427 kPa) throughout the test, experiencing moderate fluctuations. During the test, VSP-20 disconnected

between 1327 and 1807 seconds into the data acquisition. During this timeframe, applied displacement was reported as direct measurements from VSP+20. Figure 3.140 presents the progression of pressure, applied displacement, and actuator force through the test.

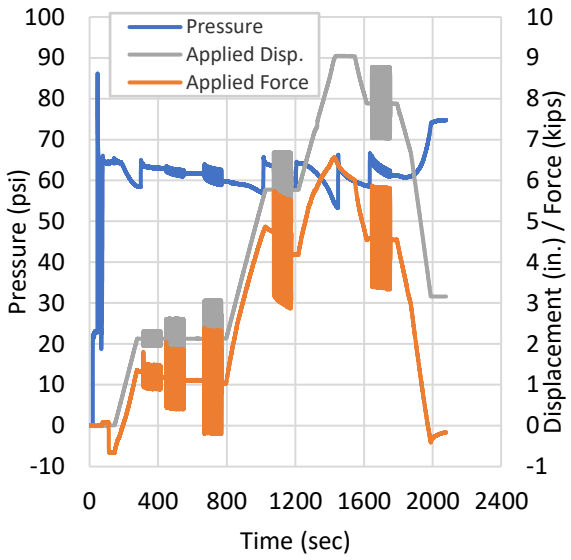

Figure 3.140. PB11-Cyclic - Progression of Pressure, Applied Displacement, and Force.

A maximum force of 6.57 kips (29.2 kN) was recorded at the maximum stroke of the actuator, 9.0 in. (229 mm) of applied displacement. Applied displacement locations at the start of each cycle and recorded applied force ranges are as follows for each cycle location:

- First Cycle:
  - Starting Applied Displacement: 2.13 in. (54.1 mm)
  - Applied Force Range: 0.88-1.81 kips (3.91-8.05 kN)
- Second Cycle:
  - Starting Applied Displacement: 2.13 in. (54.1 mm)
  - Applied Force Range: 1.64-2.61 kips (7.30-11.6 kN)
- Third Cycle:
  - Starting Applied Displacement: 2.13 in. (54.1 mm)
  - Applied Force Range: -0.21-3.06 kips (-0.93-13.6 kN)
- Fourth Cycle:
  - Starting Applied Displacement: 5.77 in. (147 mm)
  - Applied Force Range: 4.85-6.68 kips (21.6-29.7 kN)
- Final Cycle:
  - Starting Applied Displacement: 7.88 in. (200 mm)

- Applied Force Range: 7.03-8.78 kips (31.3-39.1 kN)

A moment generated over the connection as well as curvature were calculated following the same procedure used in monotonic testing. The moment generated over the connection as displacement is applied to the system is presented in Figure 3.141. Moment generated over the connection versus local curvature is shown in Figure 3.142.

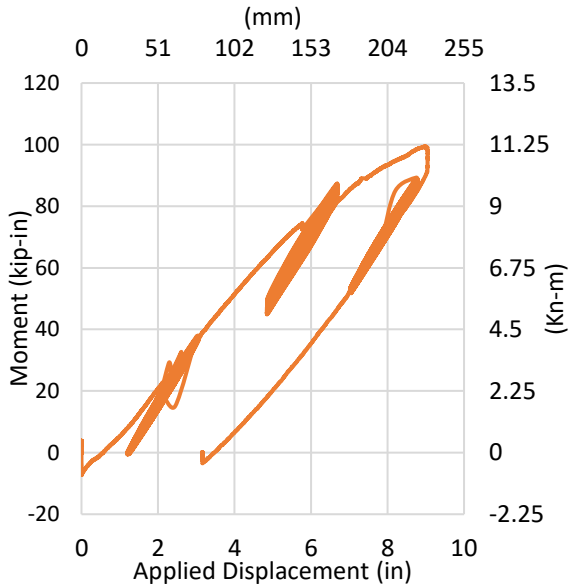

Figure 3.141. PB11-Cyclic - Moment vs. Applied Displacement

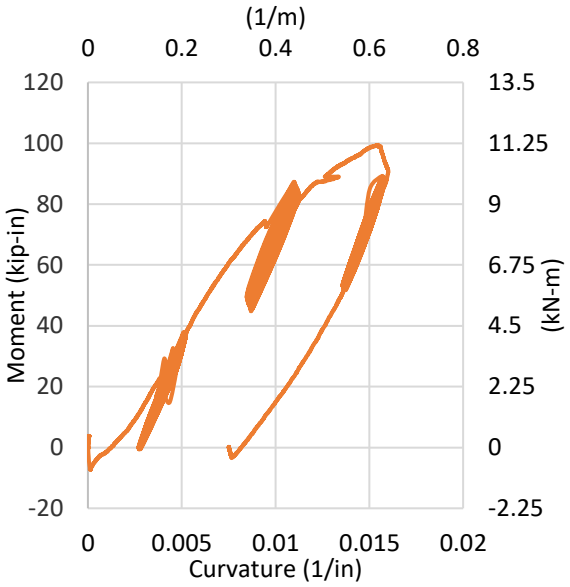

Figure 3.142. PB11-Cyclic - Moment vs. Curvature

A maximum moment of 99.5 kip-in. (11.2 kN-m) and a minimum radius of curvature of 62.5 in. (1.59 m), corresponding to a maximum curvature of 0.0160 in.$^{-1}$ (0.630 m^{-1}), was generated during the test. Ranges of generated moment and curvature produced during at each cycle location are as follows:

- First Cycle:
  - Moment Range: 15.6-29.3 kip-in. (1.76-3.31 kN-m)
  - Curvature Range: 0.0037-0.0041 in.$^{-1}$ (0.144-0.163 m^{-1})
- Second Cycle:
  - Moment Range: 8.46-32.7 kip-in. (0.96-3.69 kN-m)
  - Curvature Range: 0.0033-0.0046 in.$^{-1}$ (0.130-0.180 m^{-1})
- Third Cycle:
  - Moment Range: -0.45-38.0 kip-in. (-0.05-4.29 kN-m)
  - Curvature Range: 0.0027-0.0052 in.$^{-1}$ (0.106-0.206 m^{-1})
- Fourth Cycle:
  - Moment Range: 44.9-87.4 kip-in. (5.07-9.87 kN-m)

- Curvature Range: 0.0085-0.0112 in.$^{-1}$ (0.333-0.441 m^{-1})

- Final Cycle:
  - Moment Range: 51.8-89.3 kip-in. (5.85-10.1 kN-m)
  - Curvature Range: 0.0136-0.0158 in.$^{-1}$ (0.534-0.623 m^{-1})

Axial and circumferential strains were recorded at the crown and invert of four locations along the specimen. Figure 3.143 and Figure 3.144 present axial and circumferential strains with respect to applied displacement throughout the test. SG10E-IA, SG10W-CA, SG10E-IC, SG35W-IC were damaged after monotonic testing and are not included in the axial and circumferential strain data. SG10E-CA recorded a maximum axial strain of -2.1%. A maximum circumferential strain of -0.65% was recorded by SG10W-C.

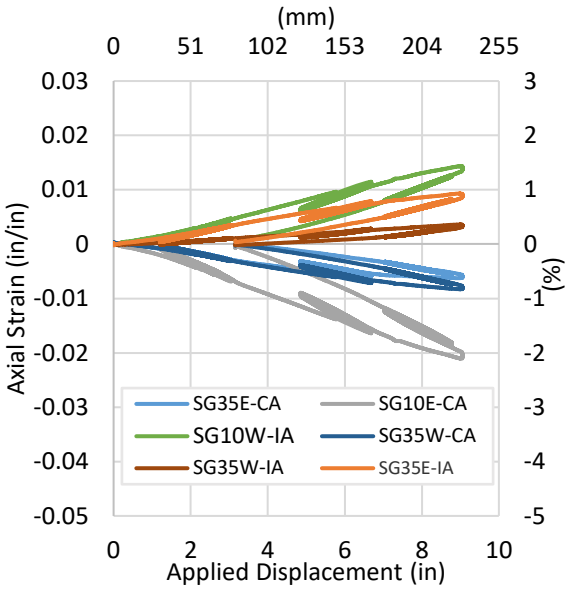

Figure 3.143. PB11-Cyclic - Axial Strain vs. App. Disp.

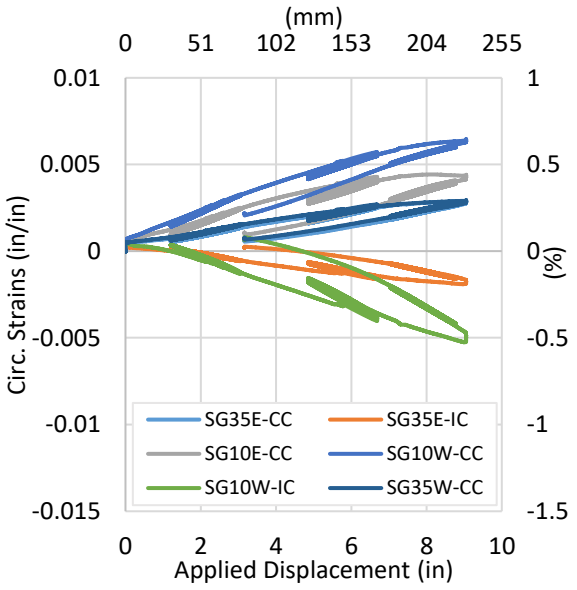

Figure 3.144. PB11-Cyclic - Circumferential Strain vs. App. Disp.

Despite minor leakage occurring during the monotonic test, the system showed no signs of leaking throughout cyclic loading. After the test concluded, 3.2 in. (53 mm) of residual deformation remained in the system.

3.7.2 Bending Test PB12 Results – iPVC EBAA C1900 Restraint Harness

Pipe specimen PB12 consisted of an iPVC pipe with a bell and spigot connection equipped with an EBAA C1900 Restraint Harness spanning the connection at the midpoint and was performed using Bending Test Setup 1. The EBAA C1900 Restraint nuts were positioned to allow for 1 in. (25 mm) of displacement before engaging. The restraint was tested under the worst-case scenario, allowing the joint to displace the 1 in. (25

mm) as the specimen is pressurized. During the test the specimen was pressurized to around 67 psi (462 kPa) with minor fluctuations. Transverse displacement was then applied to the system at the two interior loading saddles until the full stroke of the actuator was applied to the specimen. The applied force generated by the transverse loading was captured and recorded by the vertical actuator equipped with a 110-kip load cell. Applied displacement is the average measurement of two string pots (VSP-20 and VSP+20) located directly under each loading saddle. Figure 3.145 presents the progression of pressure, applied displacement, and actuator force through the test.

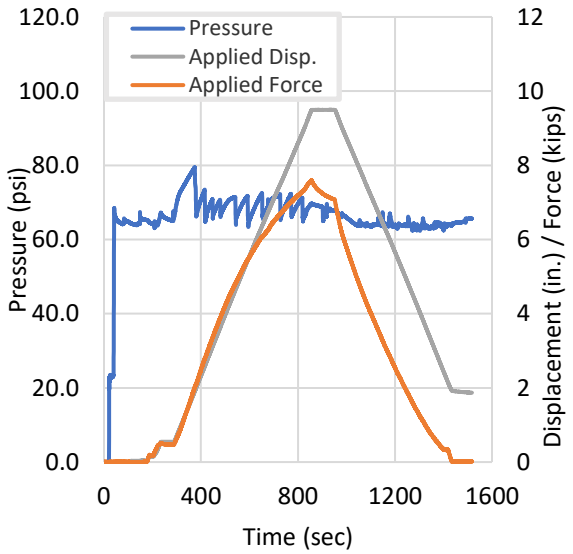

Figure 3.145. PB12-Progression of Pressure, Applied Displacement, and Force.

Force and applied displacement generated in the first 290 seconds can be attributed to the preloading of the specimen. A maximum force of 7.60 kips (33.8 kN) was recorded at the maximum stroke of the actuator, 9.5 in. (241 mm) of applied displacement. Load was applied to the specimen at a constant rate of 1 in (25.4 mm) per minute. A moment generated over the connection was calculated for the system by considering the pipe system as a continuous beam subjected to two equal concentrated loads. The moment generated over the connection as displacement is applied to the system is presented in Figure 3.146. Self-weight and the weight of water are included when calculating the moment of the system. Calculations for moment are provided in Appendix A.

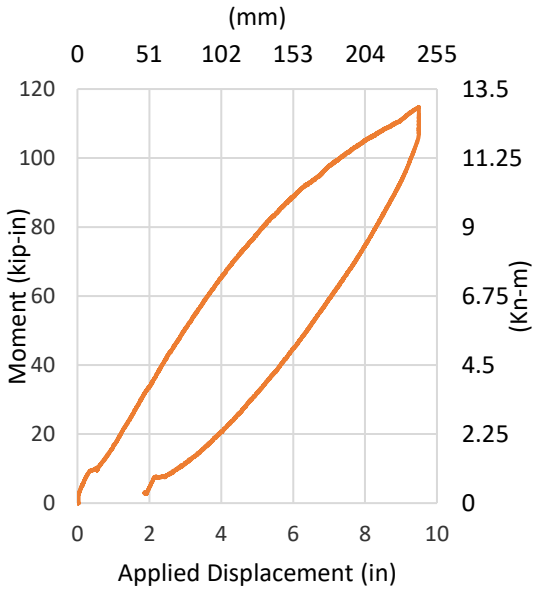

Figure 3.146. PB12-Moment vs. Applied Displacement

An initial moment of 2.95 kip-in (0.33 kN-m) under no applied displacement was generated as the supporting jacks were removed and self-weight was applied to the specimen. At approximately 0.54 in. (14 mm) the bottom threaded rod of the EBAA C1900 restraint harness engages causing a sharp increase in moment as displacement is applied. Once the restraint engages, moment in the system increases at a relatively constant rate. However, at approximately 80 kip-in (9.04 kN-m) and 5.2 in. (132 mm) of applied displacement, the system begins to reach its elastic limits and the response begins to soften. A maximum moment of 115 kip-in (13.0 kN-m) was generated during the test at an applied displacement of 9.5 in. (241 mm).

Vertical displacements of the specimen were recorded at five locations, 40.5 in. (1029 mm) east, 20.5 in. (521 mm) east, 6.5 in. (165 mm) east, 6.5 in. (165 mm) west, and 20.5 in. (521 mm) west of centerline. Figure 3.147 presents vertical string pot measurements recorded throughout the test at corresponding applied displacements. String pot displacements show a relatively symmetric response in the system when subjected to lateral loading, suggesting that the system is centered in the test frame throughout the test.

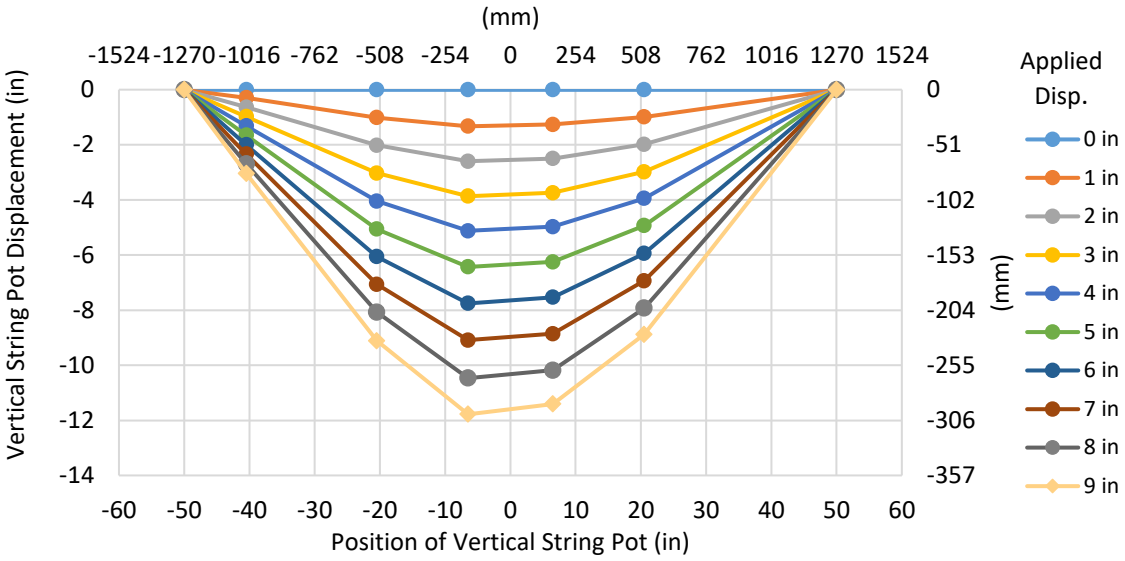

Figure 3.147. PB12 -Vertical String Pot Measurements

A radius of curvature was calculated using vertical string pot measurements along the invert of the specimen. A circumcenter for the system was able to be calculated using the location and vertical displacement of three string pots. Calculating the distance from the circumcenter to the location of the vertical string pots allowed a radius of curvature to be defined. By taking the inverse of this radius, a curvature of the system was able to be defined. Calculations for the radius of curvature and curvature are presented in Appendix B. To capture the maximum curvature experienced by the system, a local curvature was calculated using string pots located between the two load saddles (VSP-20, VSP-6, and VSP+20). Local curvature of the system versus applied displacement and moment versus curvature is shown in Figure 3.148 and Figure 3.149, respectively.

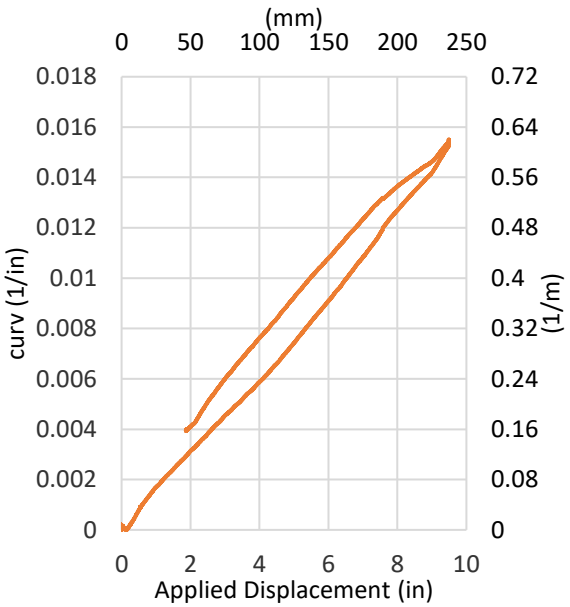

Figure 3.148. PB12 - Curvature vs. App. Disp.

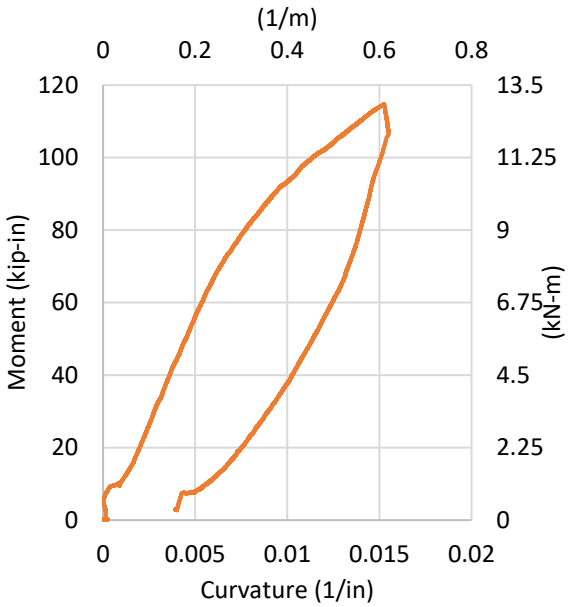

Figure 3.149. PB12 - Moment vs. Curvature

Curvature shows a linear response with respect to applied displacement throughout the test. Moment versus curvature increases at a constant rate until around 80 kip-in (9.04 kN-m) and a curvature of 0.0071 in^{-1} (0.281 m^{-1}) where the system begins to reach its elastic range, and the system response begins to soften. At a curvature of 0.0009 in^{-1} (0.0354 m^{-1}), there is a sharp increase in moment as the bottom bolt of the EBAA restraint engages. The system produced a minimum radius of curvature of 64.5 in (1638 mm) at the full stroke of the actuator, corresponding to a maximum curvature of 0.0155 in^{-1} (0.610 m^{-1}).

Axial and circumferential strains were recorded at the crown and invert of four locations along the specimen. Strain planes were located at 10.5 in. (267 mm) and 35.5 in. (902 mm) on either side of the centerline. Recorded strains were intended to provide a secondary measurement of force applied to the system. Figure 3.150 and Figure 3.151 present axial and circumferential strains with respect to applied displacement throughout the test.

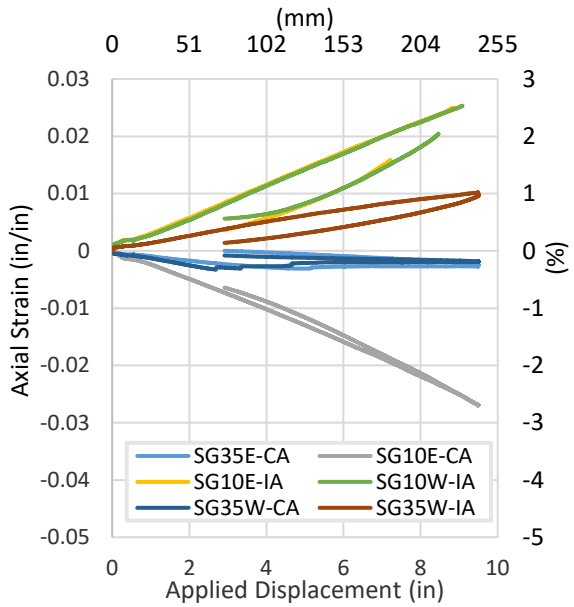

Figure 3.150. PB12 - Axial Strain vs. App. Disp.

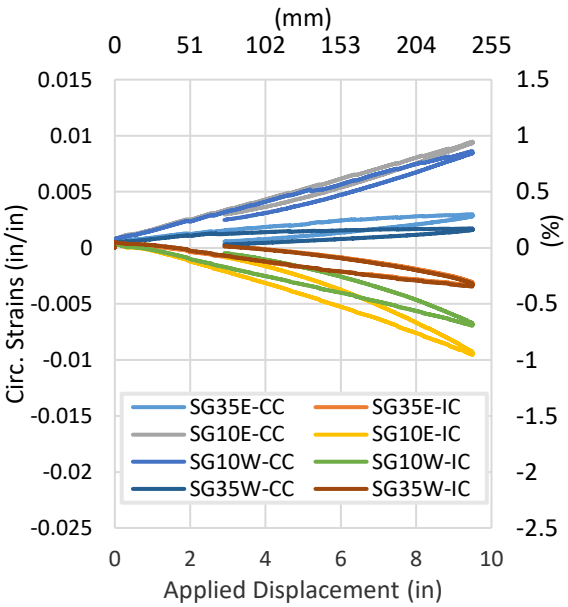

Figure 3.151. PB12 - Circumferential Strain vs. App. Disp.

The axial strain gauges located at the invert 35.5 in. east and 10.5 in. west of the centerline recorded inaccurate data during the test sequence and are not presented in Figure 3.150. SG10E-IA and SG10W-IA disconnected from the data acquisition system at around 9 in. (229 mm) of applied displacement, the gauges reconnected as the specimen was unloaded at around 8.5 in. (216 mm) and 7.4 in. (188 mm) of applied displacement, respectively. SG10W-IA recorded a maximum axial strain of 2.5% before the gauge disconnected from the system. A maximum circumferential strain of 0.95% was recorded by SG10E-CC at the maximum applied displacement during the test.

Figure 3.152 (a-e) presents pictures taken during significant moments during the test. During the test, there were no signs of leakage at the connection. After the test, there was 1.9 in. (48 mm) of residual deflection in the system at both loading saddle locations.

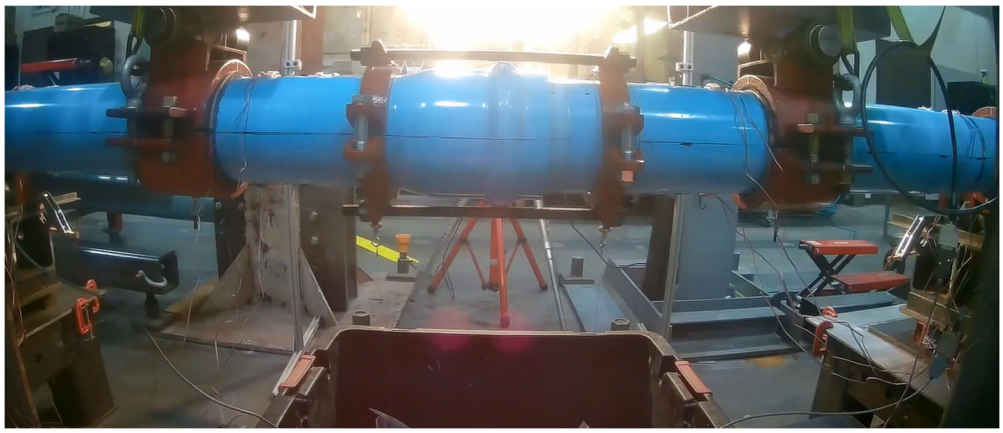

(a) Start of the Test

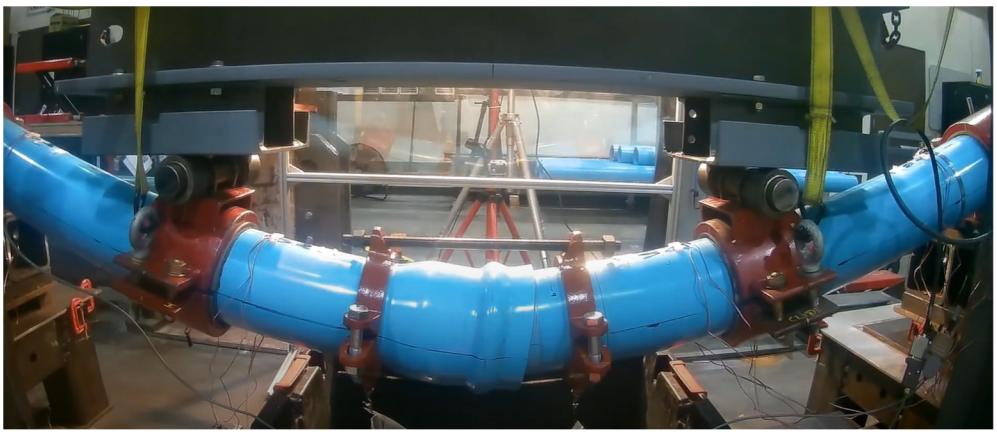

(b) Application of Full Actuator Stroke

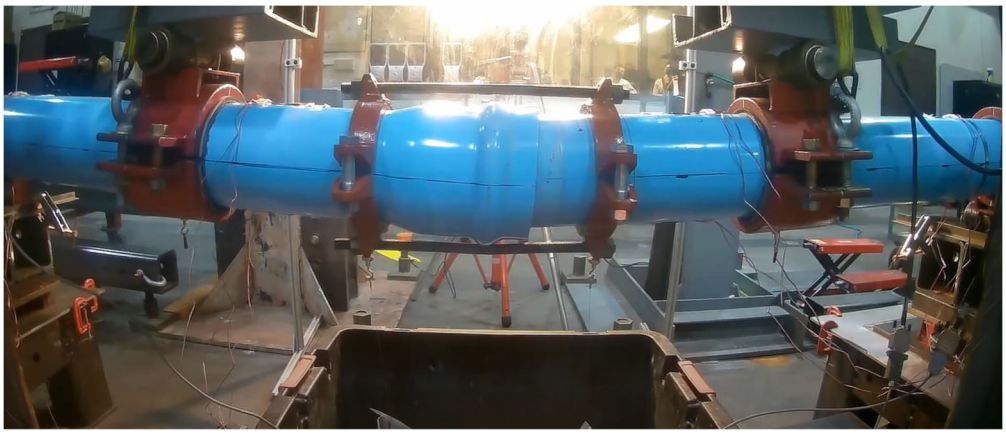

(c) 1.9 in. of Residual Deflection at the End of the Test

Figure 3.152. PB-12 Pictures during Test Progression

Since pipe specimen PB12 performed well under monotonic loading, the specimen was subjected to cyclic loading protocols outlined in section 2.4.4. Instrumentation and measurements taken during the test were identical to PB12's monotonic test. The specimen was pressurized to an initial pressure of 68 psi (469 kPa)

throughout the test, experiencing moderate fluctuations at the locations of cyclic loading. During the test, VSP-20 disconnected between 1062 and 1489 seconds into the data acquisition. During this timeframe, applied displacement was reported as direct measurements from VSP+20. Figure 3.153 presents the progression of pressure, applied displacement, and actuator force through the test. No signs of leaking throughout cyclic loading.

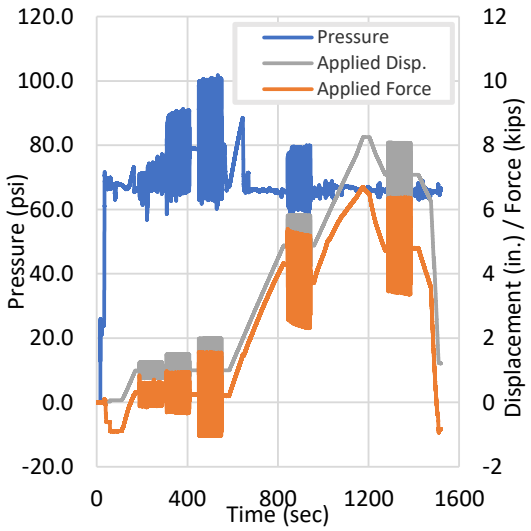

Figure 3.153. PB12-Cyclic - Progression of Pressure, Applied Displacement, and Force.

A maximum force of 6.70 kips (29.8 kN) was recorded at the maximum stroke of the actuator, 8.25 in. (210 mm) of applied displacement. Applied displacement locations at the start of each cycle and recorded applied force ranges are as follows for each cycle location:

- First Cycle:
  - Starting Applied Displacement: 1.00 in. (25.4 mm)
  - Applied Force Range: -0.12-0.71 kips (-0.53-3.16 kN)
- Second Cycle:
  - Starting Applied Displacement: 1.00 in. (25.4 mm)
  - Applied Force Range: -0.35-0.97 kips (1.56-4.31 kN)
- Third Cycle:
  - Starting Applied Displacement: 1.00 in. (25.4 mm)
  - Applied Force Range: -1.05-1.57 kips (-4.67-6.98 kN)
- Fourth Cycle:
  - Starting Applied Displacement: 4.88 in. (124 mm)
  - Applied Force Range: 2.31-5.40 kips (10.3-24.0 kN)

- Final Cycle:
    - Starting Applied Displacement: 7.10 in. (180 mm)
    - Applied Force Range: 3.35-6.37 kips (14.9-28.3 kN)

A moment generated over the connection as well as curvature were calculated following the same procedure used in monotonic testing. The moment generated over the connection as displacement is applied to the system is presented in Figure 3.154. Moment generated over the connection versus local curvature is shown in Figure 3.155.

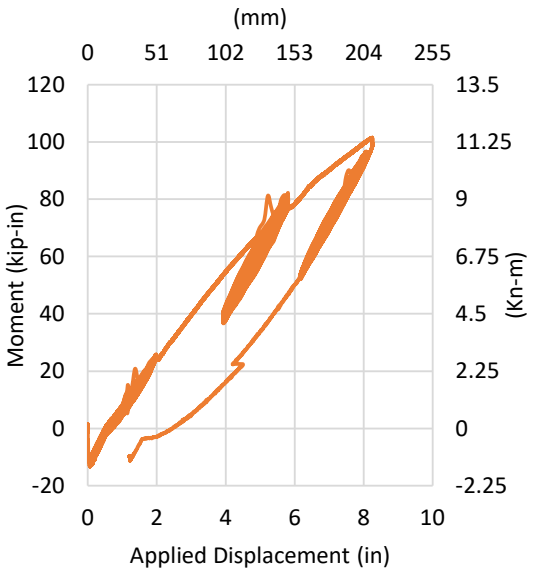

Figure 3.154. PB12-Cyclic - Moment vs. Applied Displacement

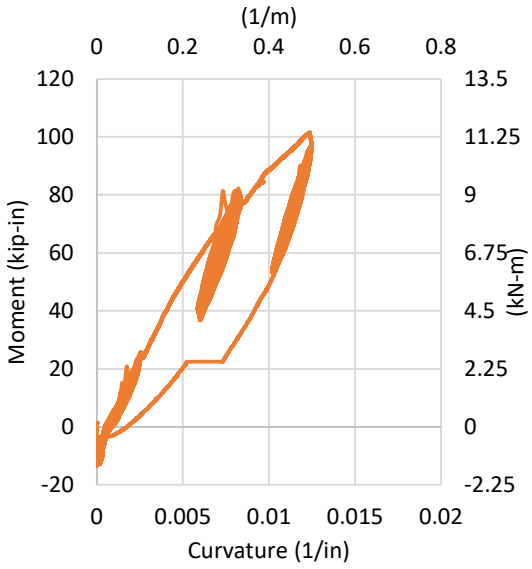

Figure 3.155. PB12-Cyclic - Moment vs. Curvature

A maximum moment of 101 kip-in. (11.4 kN-m) and a minimum radius of curvature of 80.1 in. (2.03 m), corresponding to a maximum curvature of 0.0125 $in.^{-1}$ (0.492 m^{-1}), was generated during the test. Ranges of generated moment and curvature produced during at each cycle location are as follows:

- First Cycle:
    - Moment Range: 0.81-13.1 kip-in. (0.09-1.48 kN-m)
    - Curvature Range: 0.0008-0.0016 $in.^{-1}$ (0.035-0.062 m^{-1})
- Second Cycle:
    - Moment Range: -2.47-17.0 kip-in. (-0.28-1.92 kN-m)
    - Curvature Range: 0.0005-0.0019 $in.^{-1}$ (0.020-0.075 m^{-1})
- Third Cycle:
    - Moment Range: -12.8-25.8 kip-in. (-1.45-2.92 kN-m)
    - Curvature Range: 0.0002-0.0026 $in.^{-1}$ (0.006-0.102 m^{-1})

- Fourth Cycle:
    - Moment Range: 36.7-82.2 kip-in. (4.15-9.29 kN-m)
    - Curvature Range: 0.0058-0.0084 $in.^{-1}$ (0.230-0.330 m^{-1})
- Final Cycle:
    - Moment Range: 52.1-96.7 kip-in. (5.89-10.9 kN-m)
    - Curvature Range: 0.0102-0.0125 $in.^{-1}$ (0.400-0.492 m^{-1})

Axial and circumferential strains were recorded at the crown and invert of four locations along the specimen. Figure 3.156 and Figure 3.157 present axial and circumferential strains with respect to applied displacement throughout the test. SG10E-IA, SG10W-CA, SG10W-IA, SG35E-CA were damaged after monotonic testing and are not included in the axial strain data. SG10E-CA recorded a maximum axial strain of -2.3%. A maximum circumferential strain of -0.88% was recorded by SG10E-IC.

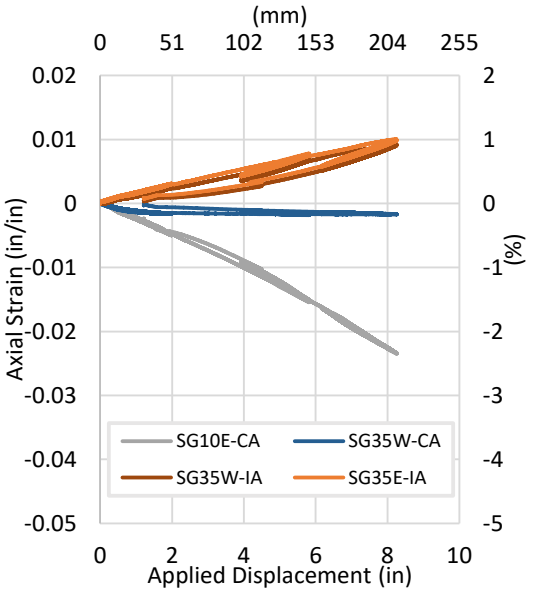

Figure 3.156. PB12-Cyclic - Axial Strain vs. App. Disp.

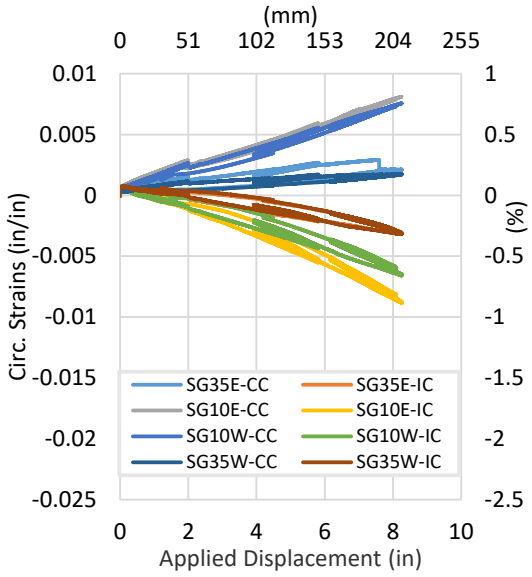

Figure 3.157. PB12-Cyclic - Circumferential Strain vs. App. Disp.

3.7.3 Bending Test PB13 Results – iPVC Continuous Segment

Pipe specimen PB13 consisted of a continuous iPVC pipe segment without a connection and was performed using Bending Test Setup 1. During the test, the specimen was pressurized to around 65 psi (448 kPa) with minor fluctuations. Transverse displacement was then applied to the system at the two interior loading saddles until the full stroke of the actuator was applied to the specimen. The applied force generated by the transverse loading was captured and recorded by the vertical actuator equipped with a 110-kip load cell.

Applied displacement is the average measurement of two string pots (VSP-20 and VSP+20) located directly under each loading saddles. Figure 3.158 presents the progression of pressure, applied displacement, and actuator force through the test.

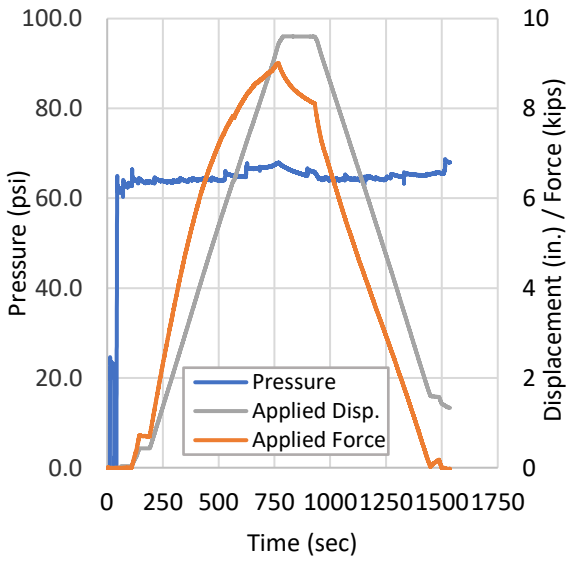

Figure 3.158. PB13-Progression of Pressure, Applied Displacement, and Force.

Force and applied displacement generated in the first 230 seconds can be attributed to the preloading of the specimen. A maximum force of 9.01 kips (40.1 kN) was recorded at the maximum stroke of the actuator, 9.6 in. (244 mm) of applied displacement. Load was applied to the specimen at a constant rate of 1 in. (25.4 mm) per minute. A moment generated over the connection was calculated for the system by considering the pipe system as a continuous beam subjected to two equal concentrated loads. The moment generated over the connection as displacement is applied to the system is presented in Figure 3.159. Self-weight and the weight of water are included when calculating the moment of the system. Calculations for moment are provided in Appendix A.

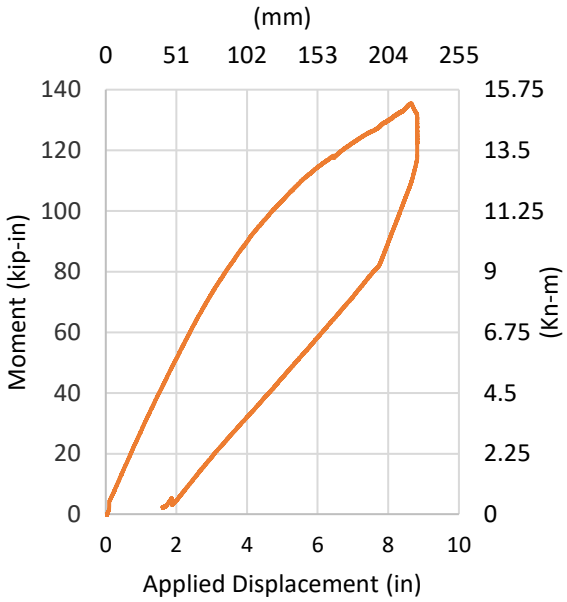

Figure 3.159. PB13-Moment vs. Applied Displacement

As displacement is applied to the system, the moment increases at a relatively constant rate. At approximately 80 kip-in (9.04 kN-m) and 3.37 in. (85.6 mm) of applied displacement, the system's response begins to soften, reaching the system's elastic limits. A maximum moment of 135 kip-in (15.3 kN-m) was generated during the test at an applied displacement of 9.4 in. (239 mm). Vertical displacements of the specimen were recorded at five locations, 40 in. (1016 mm) east, 20 in. (508 mm) east, 6 in. (152 mm) east, 6 in. (152 mm) west, and 20 in. (508 mm) west of the centerline. Figure 3.160 presents vertical string pot measurements recorded throughout the test at corresponding applied displacements. String pot displacements show a relatively symmetric response in the system when subjected to lateral loading suggesting that the system is centered in the test frame throughout the test. A maximum displacement of 11.9 in. (292 mm) was recorded by the string pot located at 6 in. (152 mm) east of centerline.

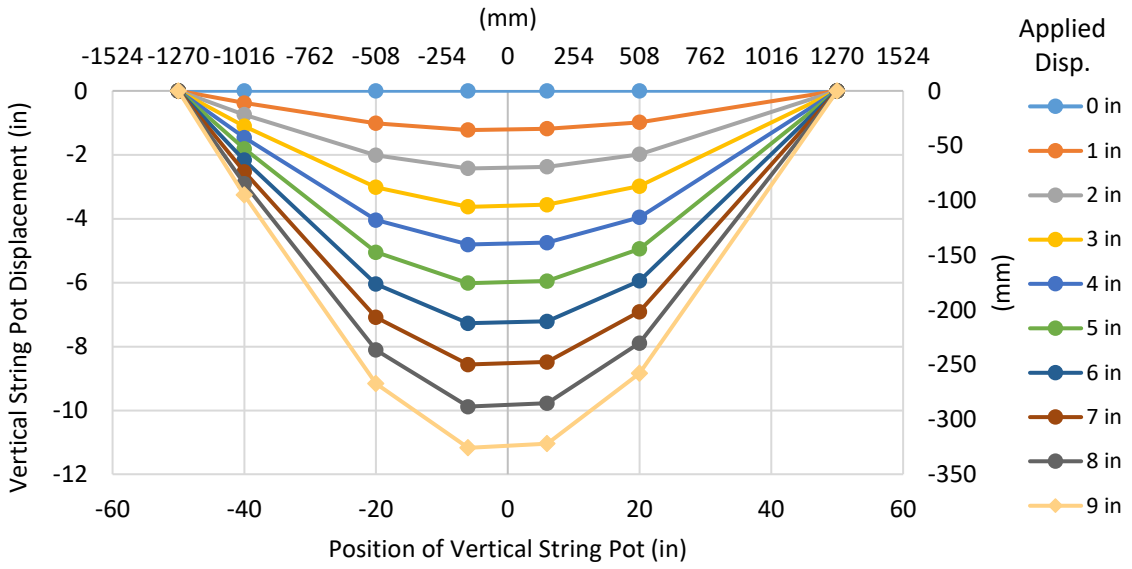

Figure 3.160. PB13-Vertical String Pot Measurements

A radius of curvature was calculated using vertical string pot measurements along the invert of the specimen. A circumcenter for the system's deformation was able to be calculated using the known locations and vertical displacements of three string pots located along the specimen. Calculating the distance from the circumcenter to the location of the vertical string pots allowed a radius of curvature to be defined. By taking the inverse of this radius, a curvature of the system was able to be defined. Calculations for the radius of curvature and curvature are presented in Appendix B. To capture the maximum curvature experienced by the system, a local curvature was calculated using string pots located between the two load saddles (VSP-20, VSP-6, and VSP+20). Local curvature of the system versus applied displacement and moment versus curvature is shown in Figure 3.161 and Figure 3.162, respectively.

Curvature shows a linear response with respect to applied displacement throughout the test. Moment versus curvature increases at a constant rate until around 80 kip-in (9.04 kN-m) and a curvature of 0.0038 in^{-1} (0.150 m^{-1}) where the system begins to reach its elastic range, and the system response begins to soften. At the maximum applied displacement and moment, a radius of curvature of 80.2 in. (2037 mm) and a curvature of 0.0125 in^{-1} (0.491 m^{-1}) was generated.

Axial and circumferential strains were recorded at the crown and invert of four locations along the specimen. Strain planes were located at 10 in. (254 mm) and 35 in. (889 mm) on either side of the centerline. Recorded strains were intended to provide a secondary measurement of force applied to the system. Figure 3.163 and Figure 3.164 present axial and circumferential strains with respect to applied displacement throughout the test.

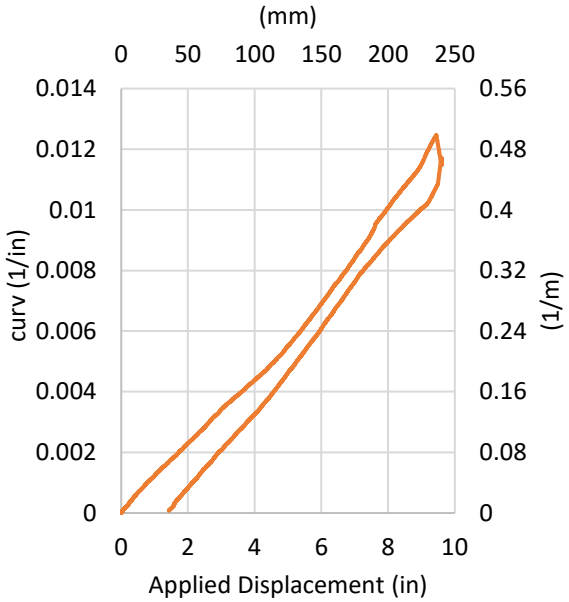

Figure 3.161. PB13 - Curvature vs. App. Disp.

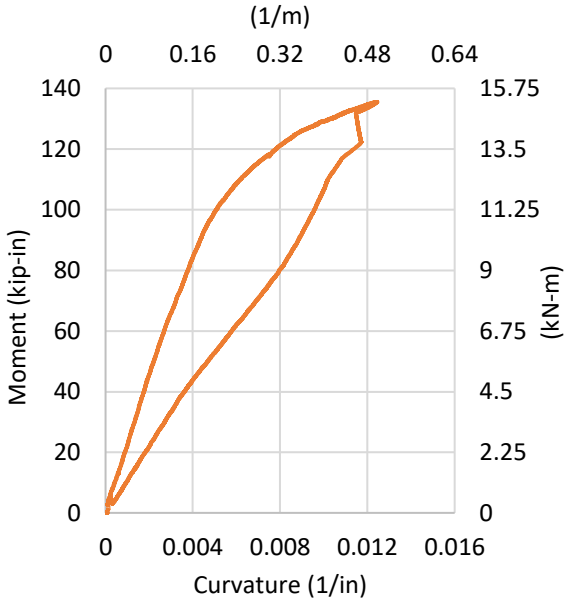

Figure 3.162. PB13 - Moment vs. Curvature

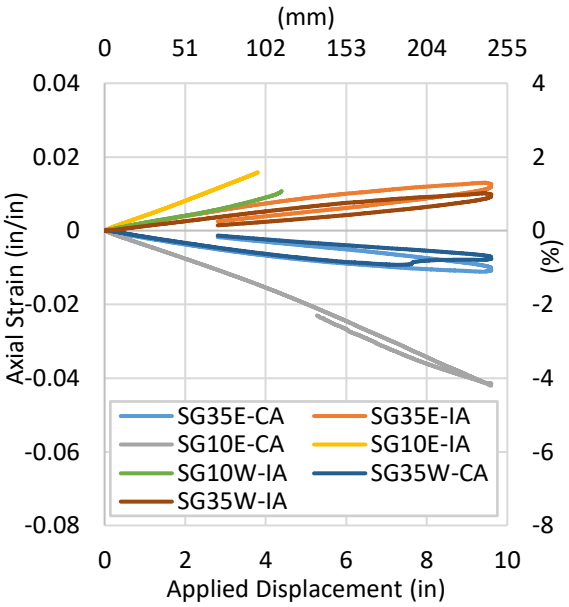

Figure 3.163. PB13 - Axial Strain vs. App. Disp.

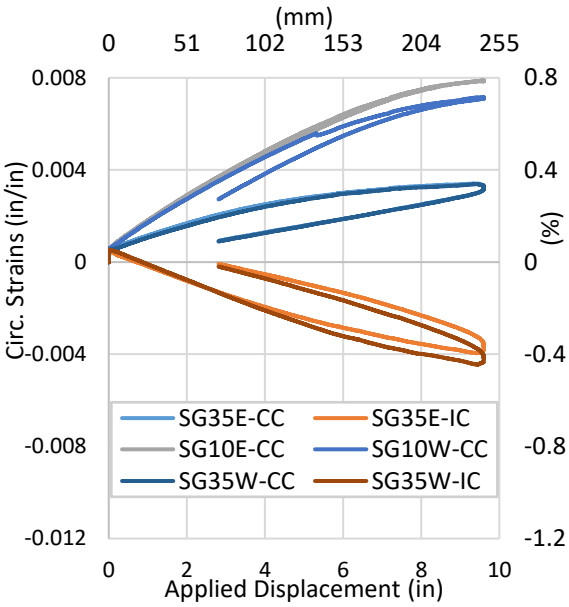

Figure 3.164. PB13 - Circumferential Strain vs. App. Disp.

SG10E-CA, SG10E-IA, and SG10W-IA disconnected from the data acquisition system at 5.27 in. (134 mm), 3.81 in. (96.8 mm), and 4.40 in. (112 mm), respectively. SG10E-CA recorded a maximum axial strain

of -4.2% before the gauge disconnected from the system. A maximum circumferential strain of 0.79% was recorded by SG10E-CC.

After the test concluded, 1.4 in. (36 mm) of residual deformation remained in the system. Figure 3.165 (a-c) presents pictures taken during significant moments during the test.

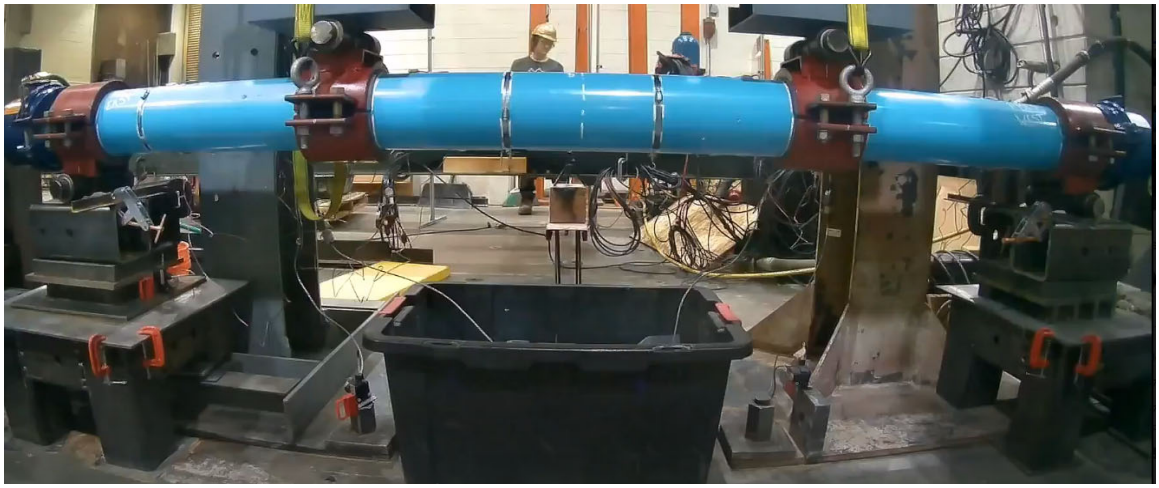

(a) Start of the Test

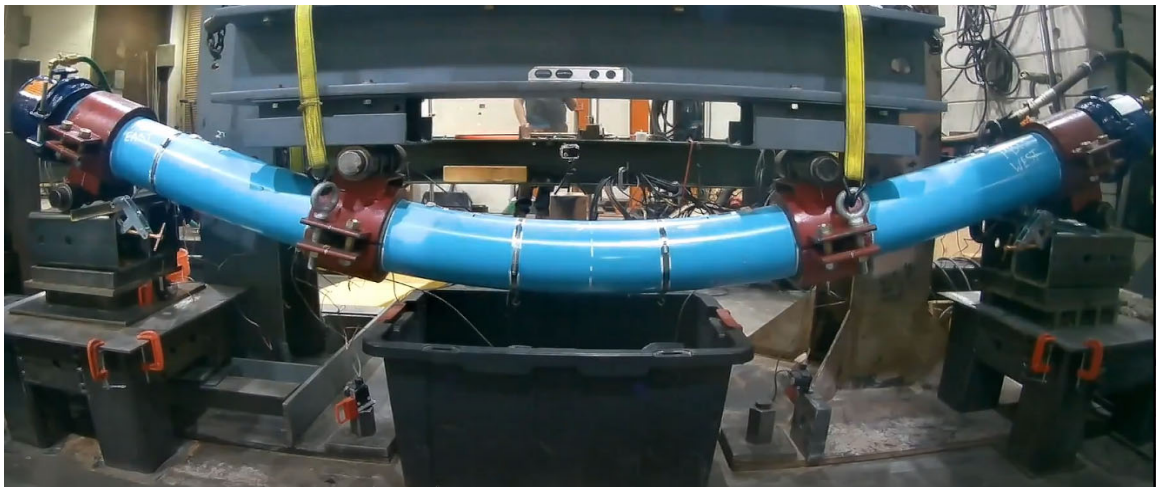

(b) Application of full Actuator Stroke

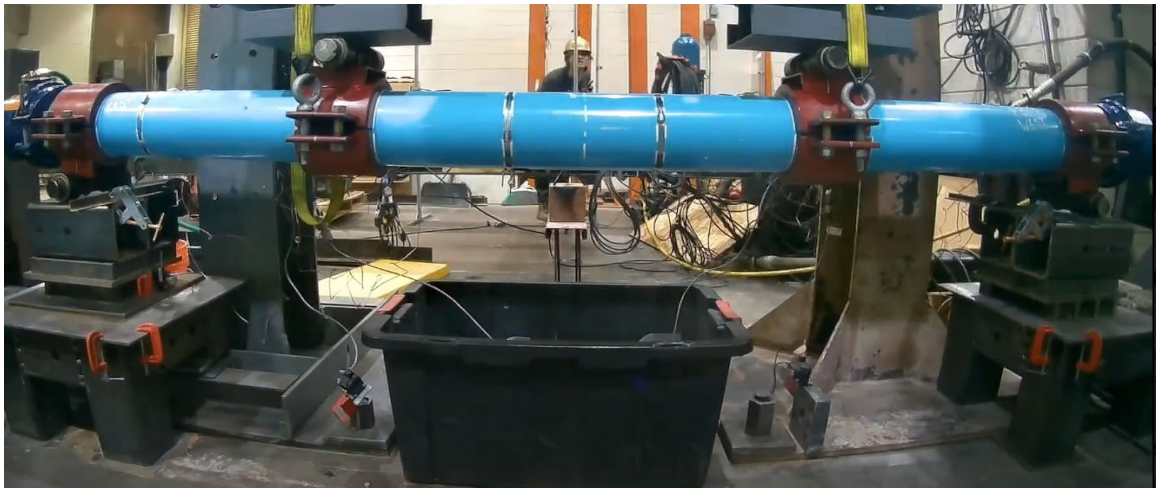

(c) Unload Specimen at the End of the Test

Figure 3.165. PB-13 Pictures during Test Progression

3.7.4 Bending Test PB14 Results – iPVC Lokx Coupling

Pipe specimen PB14 consisted of an iPVC pipe with a Lokx coupling connection at the midpoint and was performed using Bending Test Setup 1. During the test, the specimen was pressurized to around 64 psi (441 kPa) at the beginning of the test. Transverse displacement was then applied to the system at the two interior loading saddles until the full stroke of the actuator was applied to the specimen. The applied force generated by the transverse loading was captured and recorded by the vertical actuator equipped with a 110-kip load cell. Applied displacement is the average measurement of two string pots (VSP-20 and VSP+20) located directly under each loading saddle. Figure 3.166 presents the progression of pressure, applied displacement, and actuator force through the test.

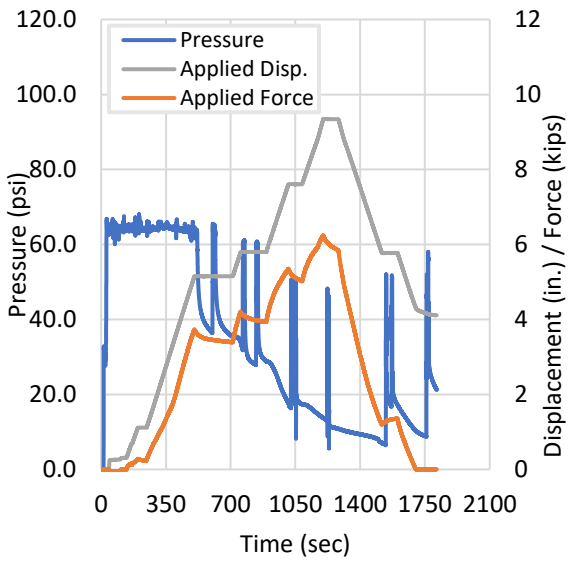

Figure 3.166. PB14-Progression of Pressure, Applied Displacement, and Force.

Force and applied displacement generated in the first 250 seconds can be attributed to the preloading of the specimen. Loading of the specimen was paused at several locations throughout the test due to leaking at the Lokx coupling. Water was shut off to the specimen at each pause, allowing the system to lose pressure as the coupling leaked. Water was then reintroduced to the specimen allowing the system to repressurize. The first pause occurred 505 seconds into the test at an applied displacement of 3.7 in (94 mm). Despite significant leaking at the connection, the system was able to maintain an average pressure of 63 psi (434 kPa). The second pause occurred 762 seconds into the test at an applied displacement of 4.1 in (104 mm). At the second pause, the system saw a decrease in the ability to maintain internal water pressure, with the system recording a maximum pressure of 60 psi (414 kPa). The third pause occurred 1013 seconds into the test sequence at an applied displacement of 8.5 in (216 mm). Major leaking was observed at this pause with the system holding only holding a maximum pressure of 49 psi (kPa). The fourth pause occurred 1201 seconds into the test at the maximum applied displacement [9.3 in (236 mm)]. Leaking was most severe at this actuator location, with the system only being able to maintain an internal pressure of 46 psi (317 kPa). The test was paused for a fifth time during unloading of the specimen at 1518 seconds into the test and an applied displacement of 5.8 in. (147 mm). At this location, the specimen was able to maintain an internal pressure of 50 psi (345 kPa). This response by the system suggests that the Lokx connection's ability to maintain internal pressure is a function of the radius of curvature experienced by the system or rotation experienced at the coupling. A maximum force of 6.24 kips (28 kN) was recorded at the maximum stroke of the actuator, 9.3 in. (236 mm) of applied displacement. Moment generated over the connection was calculated for the system by considering the pipe system as a continuous beam subjected to two equal

concentrated loads. The moment generated over the connection as displacement is applied to the system is presented in Figure 3.167. Self-weight and the weight of water are included when calculating the moment of the system. Calculations for moment are provided in Appendix A.

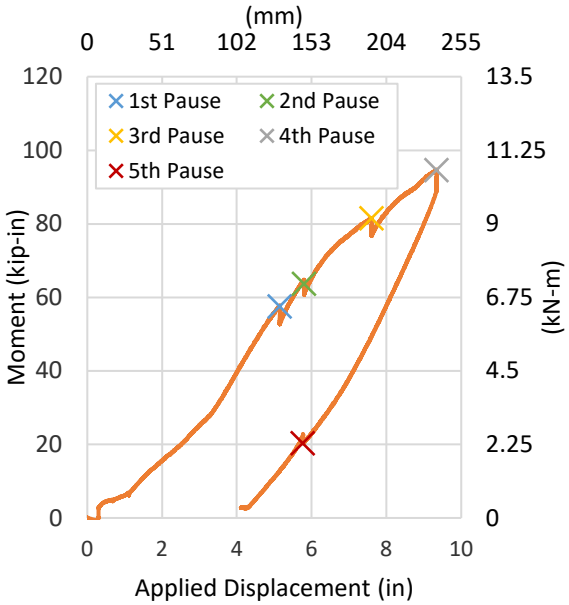

Figure 3.167. PB14-Moment vs. Applied Displacement

As supporting jacks were removed at the center of the specimen, an initial displacement of 0.3 in. (7.6 mm) was recorded at the loading saddles as the connection deflected under the self-weight of the system [2.95 kip-in (0.33 kN-m)]. The system initially shows a softer response to applied displacement as the connection allows for approximately 5 degrees of rotation at each end of the coupling. At approximately 3.4 in. (86 mm) of applied displacement and an applied moment of 29 kip-in (3.3 kN-m), the system reaches the allowable rotation at the connection and the moment response of the system shows a sharp increase as displacement is applied. At the onset of leaking and the first pause of the test, a moment of 58 kip-in. (6.6 kN-m) was generated at the connection. A maximum moment of 95 kip-in. (10.7 kN-m) was generated during the test, corresponding to the fourth pause of the test and the application of the full actuator stroke to the system.

Vertical displacements of the specimen were recorded at five locations, 40 in. (1016 mm) east, 20 in. (508 mm) east, 6 in. (152 mm) east, 6 in. (152 mm) west, and 20 in. (508 mm) west of centerline. Figure 3.168 presents vertical string pot measurements recorded throughout the test at corresponding applied displacements. String pot displacements show a relatively symmetric response in the system when subjected

to lateral loading suggesting that the system is centered in the test frame throughout the test. A maximum vertical displacement of 12.9 in. (328 mm) was recorded during the test by VSP-06.

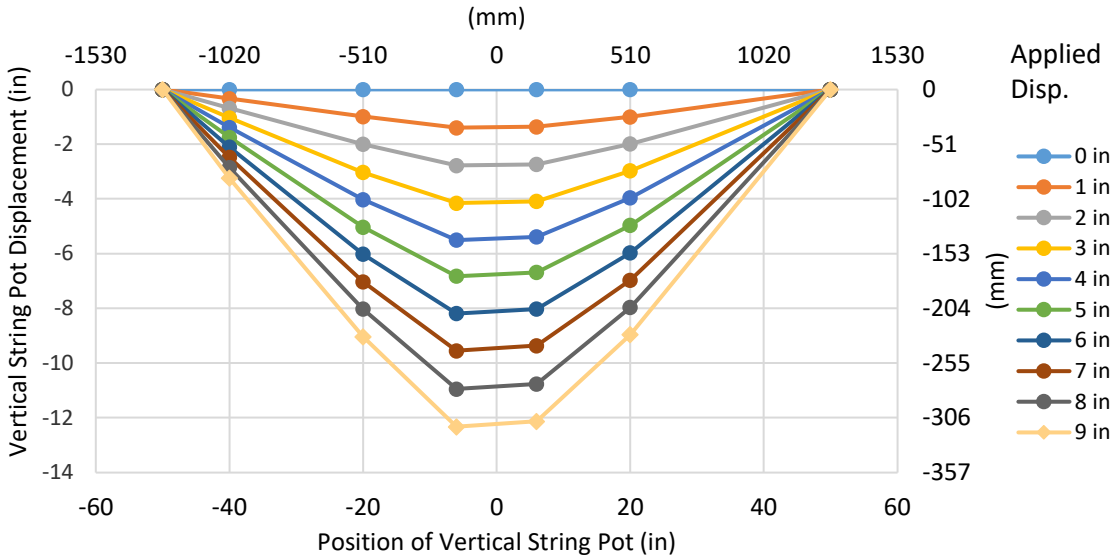

Figure 3.168. PB14 -Vertical String Pot Measurements

A radius of curvature was calculated using vertical string pot measurements along the invert of the specimen. A circumcenter for the system was able to be calculated using the location and vertical displacement of three string pots. Calculating the distance from the circumcenter to the location of the vertical string pots allowed a radius of curvature to be defined. By taking the inverse of this radius, a curvature of the system was able to be defined. Calculations for the radius of curvature and curvature are presented in Appendix B. To capture the maximum curvature experienced by the system, a local curvature was calculated using string pots located between the two load saddles (VSP-20, VSP-6, and VSP+20). Local curvature of the system versus applied displacement and moment versus curvature is shown in Figure 3.169 and Figure 3.170, respectively.

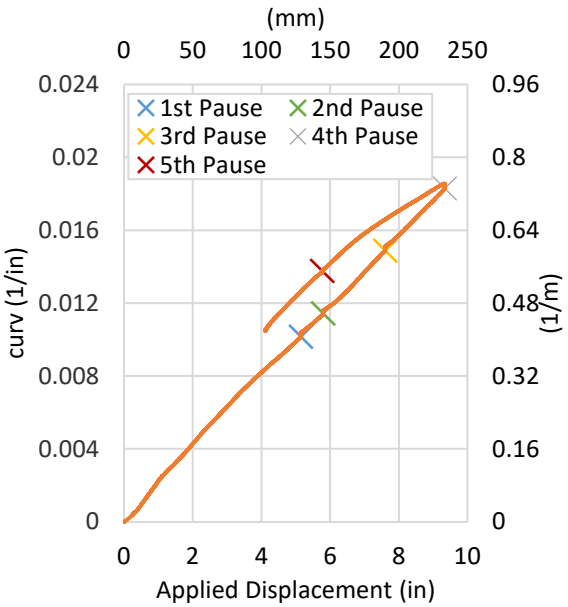

Figure 3.169. PB14 - Curvature vs. App. Disp.

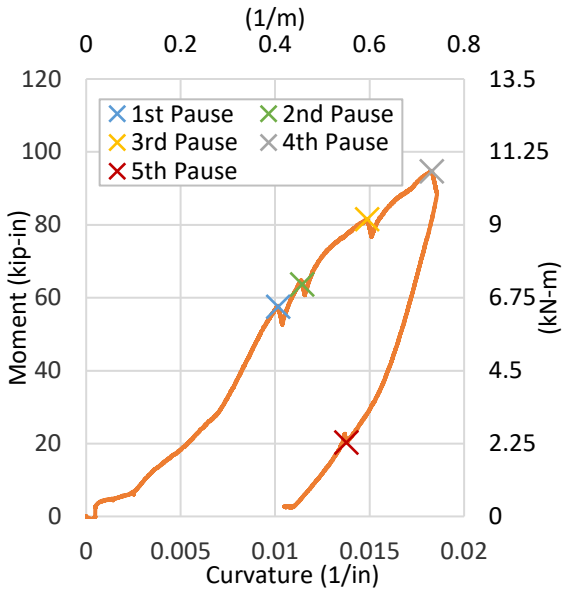

Figure 3.170. PB14 - Moment vs. Curvature

Curvature shows a linear response with respect to applied displacement throughout the test. Moment versus curvature shows a relatively soft response until the system reaches a curvature of 0.007 in^{-1} (0.275 m^{-1}) where the coupling reaches its allowable rotation. The system reached a curvature of 0.0102 in^{-1} (0.402 m^{-1}) at the onset of leaking and the first pause of the test. A maximum curvature of 0.0186 in^{-1} (0.732 m^{-1}) was generated during the test, corresponding to the fourth pause location.

Axial and circumferential strains were recorded at the crown and invert of four locations along the specimen. Strain planes were located at 10 in. (254 mm) and 35 in. (889 mm) on either side of the centerline. Recorded strains were intended to provide a secondary measurement of force applied to the system. Figure 3.171 and Figure 3.172 present axial and circumferential strains with respect to applied displacement throughout the test.

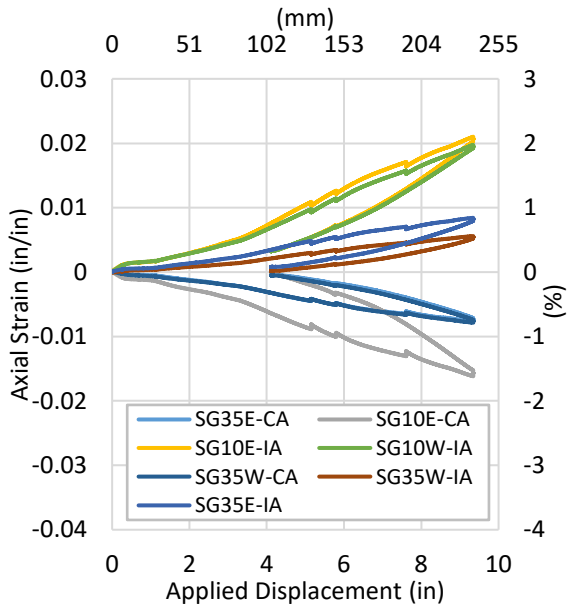

Figure 3.171. PB14 - Axial Strain vs. App. Disp.

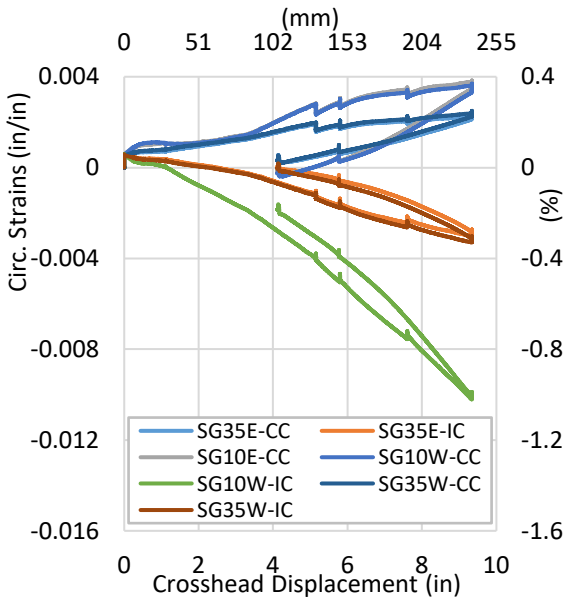

Figure 3.172. PB14 - Circumferential Strain vs. App. Disp.

The axial strain gauge located at the crown 10 in. (254 mm) west of centerline and the circumferential strain gauge located at the invert 10 in. (254 mm) east of centerline recorded inaccurate data during the test sequence and are not presented in Figure 3.171 or Figure 3.172. SG10E-IA recorded a maximum axial strain of 2.1% at the maximum applied displacement during the test. A maximum circumferential strain of 3.7% was recorded by SG10W-IC at the maximum applied displacement during the test.

Figure 3.173 (a-g) presents pictures taken during significant moments during the test. After the test, there was 4.1 in. (104 mm) of residual deflection in the system at both loading saddle locations.

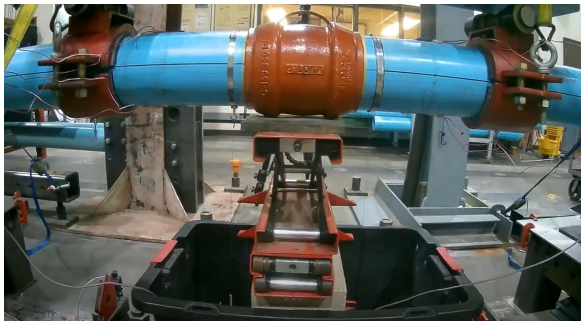

(a) Start of the Test

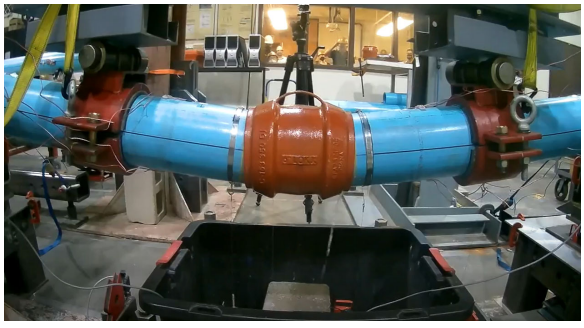

(b) 1st Pause (Leaking at Coupling's East End)

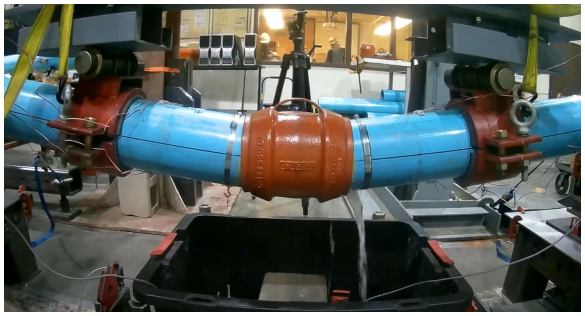

(c) 2nd Pause (Leaking at Coupling's East End)

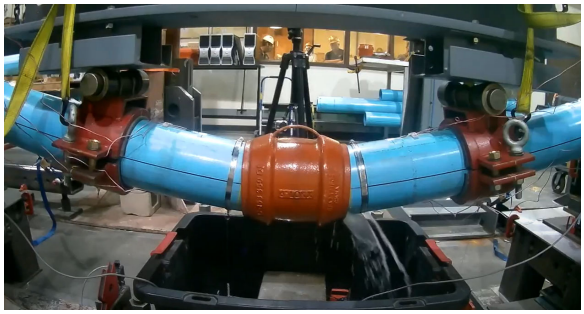

(d) 3rd Pause (Leaking at Coupling's East End)

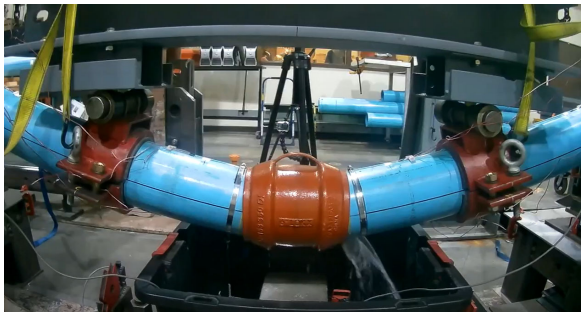

(e) 4th Pause (Leaking at Coupling's East End – Maximum Actuator Stroke)

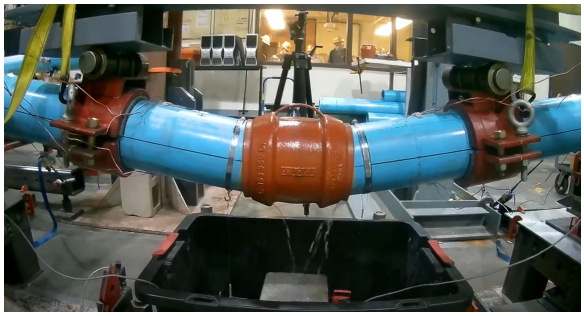

(f) 5th Pause (Leaking at Coupling's East and West Ends)

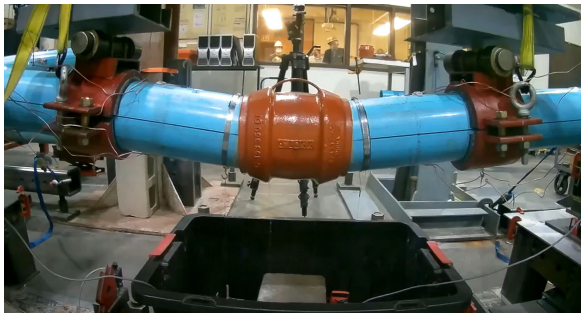

(g) 4.1 in. of Residual Deflection at the End of the Test

Figure 3.173. PB-14 Pictures during Test Progression

3.7.5 Bending Test PB15 Results – iPVC Hymax Grip Coupling

Pipe specimen PB15 consisted of an iPVC pipe with a bell and spigot connection equipped with an Hymax Grip coupling at the midpoint and was performed using Bending Test Setup 1. Pipe segments were inserted 4 in. (102 mm) into each end of the Hymax coupling. Restraint bolts, located at the top of the coupling were tightened to the minimum required torque specifications for 6 in. (152 mm) nominal diameter pipes [110 lb.-ft (149 N-m)]. During the test the specimen was pressurized to around 63 psi (434 kPa) with minor fluctuations. Transverse displacement was then applied to the system at the two interior loading saddles until the full stroke of the actuator was applied to the specimen. The applied force generated by the transverse loading was captured and recorded by the vertical actuator equipped with a 110-kip load cell.

Applied displacement is the average measurement of two string pots (VSP-20 and VSP+20) located directly under each loading saddle. Figure 3.174 presents the progression of pressure, applied displacement, and actuator force through the test.

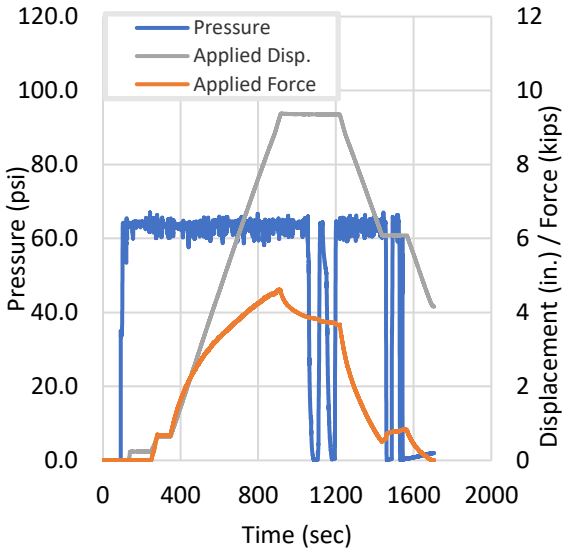

Figure 3.174. PB15-Progression of Pressure, Applied Displacement, and Force.

Force and applied displacement generated in the first 290 seconds can be attributed to the preloading of the specimen. A maximum force of 4.61 kips (20.5 kN) was recorded at the maximum stroke of the actuator, 9.37 in. (238 mm) of applied displacement. Load was applied to the specimen at a constant rate of 1 in (25.4 mm) per minute. After the maximum stroke of the actuator was reached, the test was paused, and two pressurization cycles were applied to the specimen. A gradual decrease in applied force was observed at the pause location as the system began to relax. The system was then unloaded, and another two pressurization cycles were applied to the specimen. A moment generated over the connection was calculated for the system by considering the pipe system as a continuous beam subjected to two equal concentrated loads. The moment generated over the connection as displacement is applied to the system is presented in Figure 3.175. Self-weight and the weight of water are included when calculating the moment of the system. Calculations for moment are provided in Appendix A.

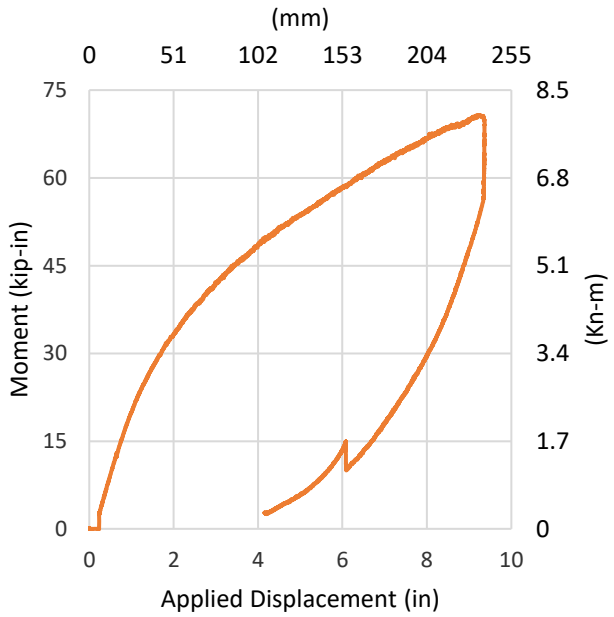

Figure 3.175. PB15-Moment vs. Applied Displacement

An initial moment of 2.65 kip-in (0.33 kN-m) and initial displacement of 0.23 in. (5.8 mm) was generated as the supporting jack was removed and self-weight was applied to the specimen. Once the restraint engages, moment in the system increases at a relatively constant rate. Initially, the system responds at a constant linear rate. However, at approximately 25 kip-in (2.82 kN-m) and 1.3 in. (33 mm) of applied displacement, the system's response begins to soften. A maximum moment of 70.7 kip-in (7.99 kN-m) was generated during the test at an applied displacement of 9.37 in. (238 mm).

Vertical displacements of the specimen were recorded at five locations, 40 in. (1016 mm) east, 20 in. (508 mm) east, 6 in. (152 mm) east, 6 in. (152 mm) west, and 20 in. (508 mm) west of centerline. Figure 3.176 presents vertical string pot measurements recorded throughout the test at corresponding applied displacements. String pot displacements show a relatively symmetric response in the system when subjected to lateral loading suggesting that the system is centered in the test frame throughout the test. At approximately 8.25 in. (210 mm) of applied displacement the string pot located at 6 in. (152 mm) east of centerline, detached from the invert of the specimen, and began to provide inaccurate displacement data. A maximum displacement of 13.1 in. (333 mm) was recorded by the string pot located 6 in. (152 mm) west of the centerline.

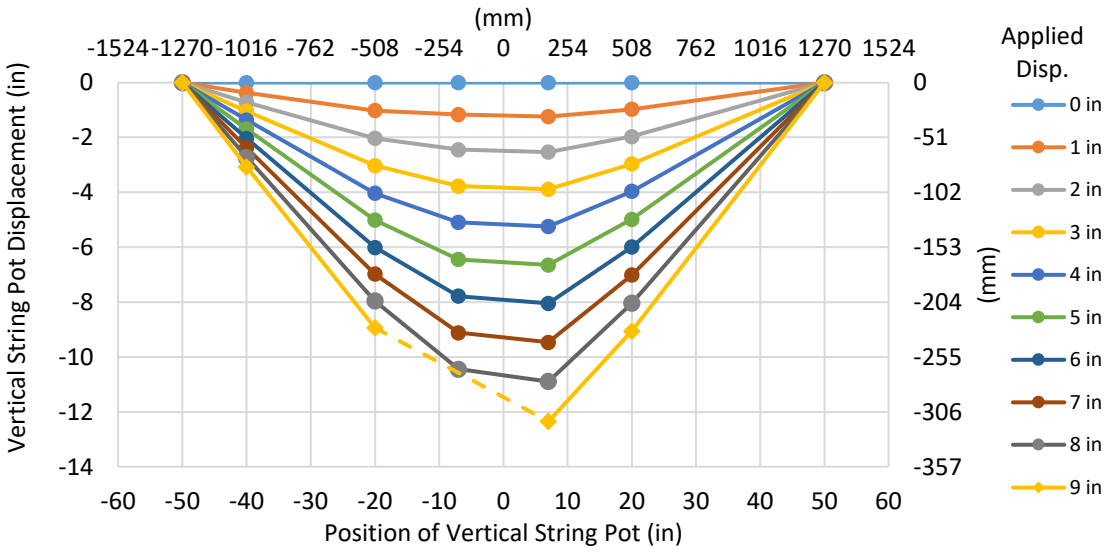

Figure 3.176. PB15 -Vertical String Pot Measurements

A radius of curvature was calculated using vertical string pot measurements along the invert of the specimen. A circumcenter for the system was able to be calculated using the location and vertical displacement of three string pots. Calculating the distance from the circumcenter to the location of the vertical string pots allowed a radius of curvature to be defined. By taking the inverse of this radius, a curvature of the system was able to be defined. Calculations for the radius of curvature and curvature are presented in Appendix B. To capture the maximum curvature experienced by the system, a local curvature was calculated using string pots located between the two load saddles (VSP-20, VSP+6, and VSP+20). Local curvature of the system versus applied displacement and moment versus curvature is shown in Figure 3.177 and Figure 3.178, respectively.

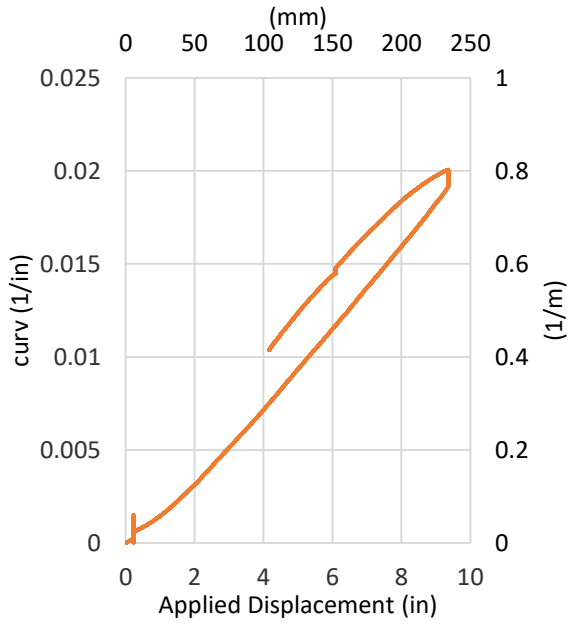

Figure 3.177. PB15 - Curvature vs. App. Disp.

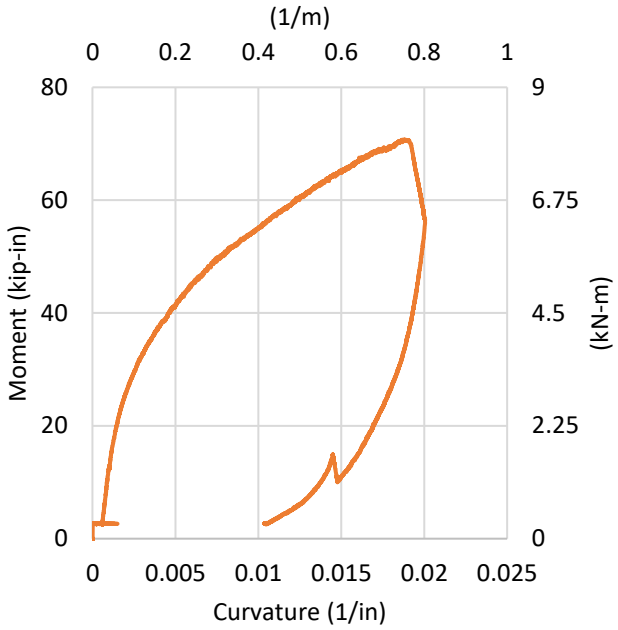

Figure 3.178. PB15 - Moment vs. Curvature

Curvature shows a linear response with respect to applied displacement throughout the test. Moment versus curvature increases at a constant rate until around 25 kip-in (2.82 kN-m) and a curvature of 0.0019 in^{-1} (0.075 m^{-1}) where the system response begins to become nonlinear. The system produced a minimum radius of curvature of 49.9 in (1267 mm) at the full stroke of the actuator, corresponding to a maximum curvature of 0.0201 in^{-1} (0.791 m^{-1}).

Axial and circumferential strains were recorded at the crown and invert of four locations along the specimen. Strain planes were located at 10 in. (254 mm) and 35 in. (889 mm) on either side of the centerline. Recorded strains were intended to provide a secondary measurement of force applied to the system. Figure 3.179 and Figure 3.180 present axial and circumferential strains with respect to applied displacement throughout the test.

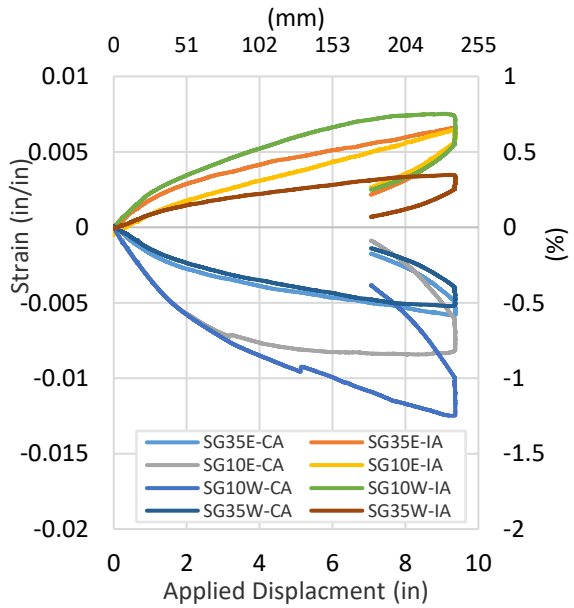

Figure 3.179. PB15 - Axial Strain vs. App. Disp.

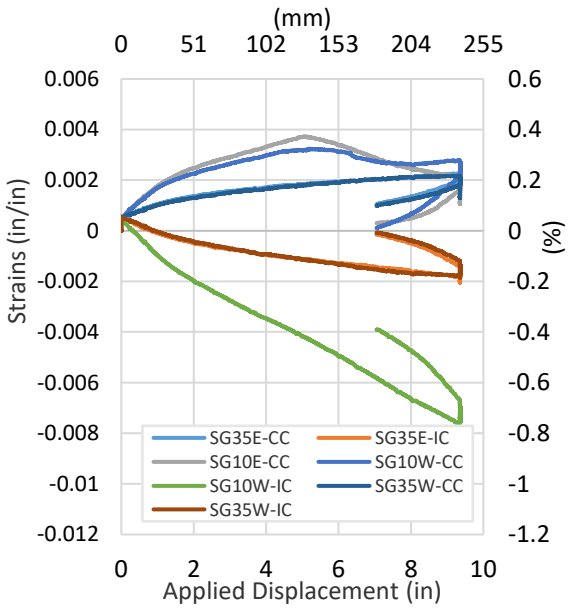

Figure 3.180. PB15 - Circumferential Strain vs. App. Disp.

The circumferential strain gauges located at the invert 10 in. east of the centerline recorded inaccurate data during the test sequence and are not presented in Figure 3.180. SG10E-CA recorded a maximum axial strain of -0.84% and a maximum circumferential strain of -0.76% was recorded by SG10W-IC at the maximum applied displacement during the test.

Figure 3.181 (a-c) presents pictures taken during significant moments during the test. During the test, there were no signs of leakage at the connection. After the test, there was 4.2 in. (107 mm) of residual deflection in the system at both loading saddle locations.

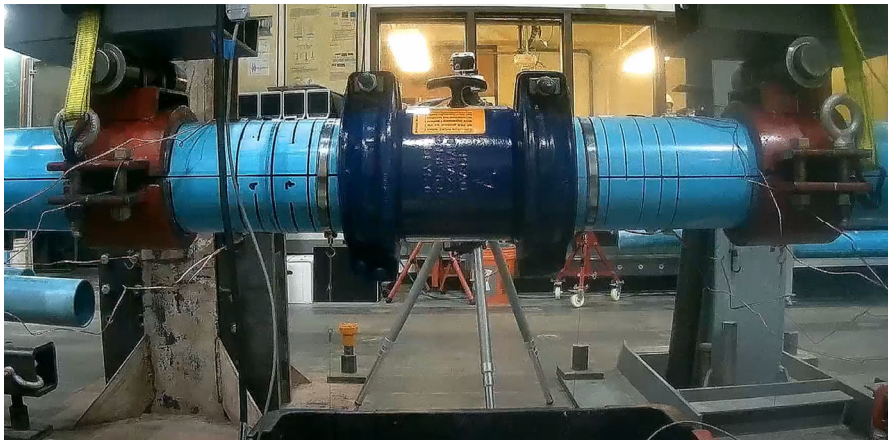

(a) Start of the Test

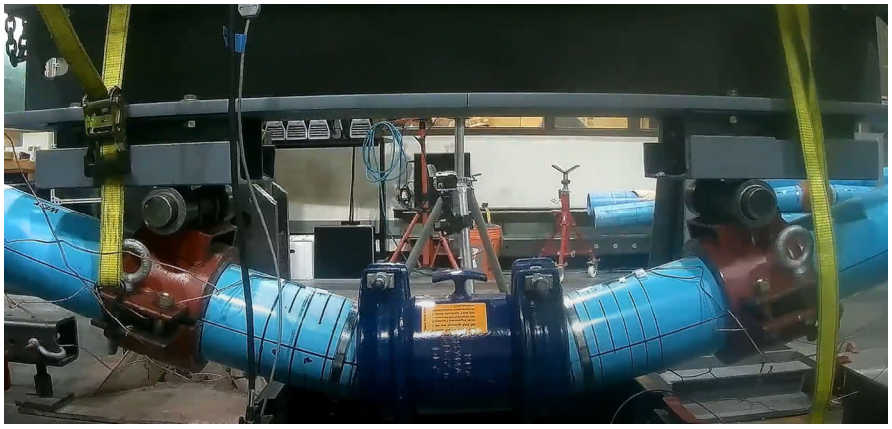

(b) Application of Full Actuator Stroke

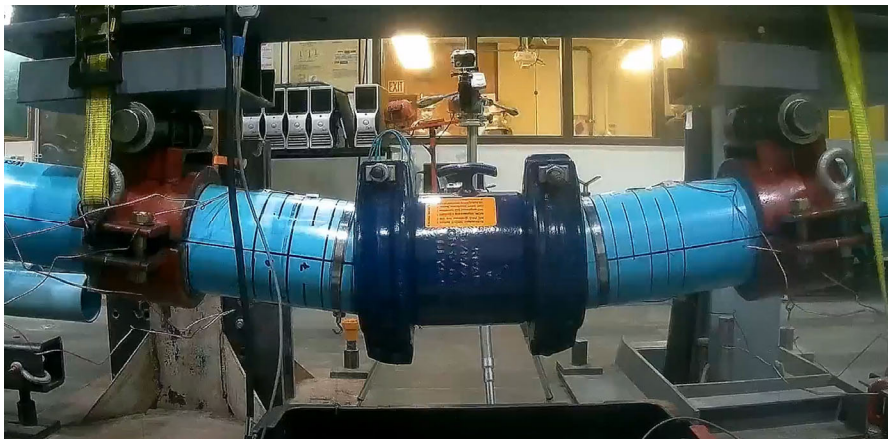

(c) 4.2 in. of Residual Deflection at the End of the Test

Figure 3.181. PB15- Pictures during Test Progression

Since pipe specimen PB15 performed well under monotonic loading, the specimen was subjected to modified cyclic loading protocols outlined in section 2.4.4. The Hymax connection allows for 8 degrees of rotation at the joint, exceeding the maximum category limits defined in Davis 2019. Therefore, the system was deformed to twice the Hymax's allowable rotation before the first set of cyclic loading was applied to the specimen. After cyclic loading was applied, the specimen was returned to a level position before unloading and the test was concluded. Instrumentation and measurements taken during the test were identical to PB12's monotonic test. The test begins at an initial applied displacement of 4.09 in. (104 mm) due to the residual deformation remaining from monotonic testing. The specimen was pressurized to an average pressure of 63 psi (434 kPa) throughout the test, experiencing moderate fluctuations at the locations of cyclic loading. The system was subjected to a pressurization sequence at approximately 790 and 1072 seconds into the data acquisition. No signs of leaking throughout cyclic loading. Figure 3.182 presents the progression of pressure, applied displacement, and actuator force through the test.

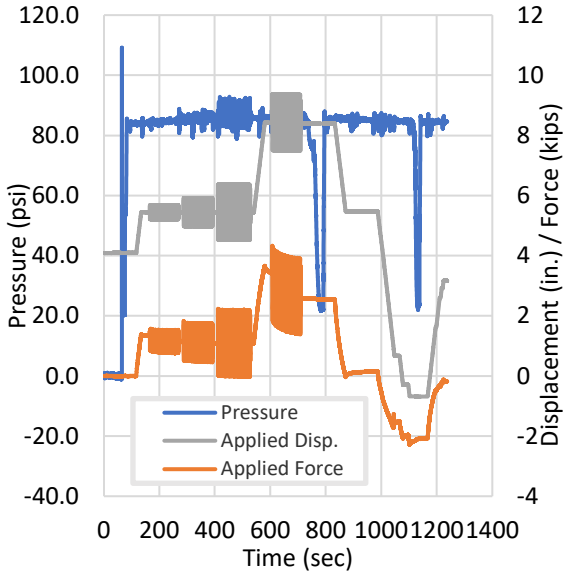

Figure 3.182. PB15-Cyclic - Progression of Pressure, Applied Displacement, and Force.

A maximum force of 4.33 kips (19.3 kN) was recorded at the maximum stroke of the actuator, 9.38 in. (41.7 mm) of applied displacement. Applied displacement locations at the start of each cycle and recorded applied force ranges are as follows for each cycle location:

- First Cycle:
  - Starting Applied Displacement: 5.45 in. (138 mm)
  - Applied Force Range: 0.74-1.57 kips (3.29-6.98 kN)
- Second Cycle:
  - Starting Applied Displacement: 5.45 in. (138 mm)
  - Applied Force Range: 0.45-1.83 kips (2.00-8.14 kN)
- Third Cycle:
  - Starting Applied Displacement: 5.45 in. (138 mm)
  - Applied Force Range: -0.03-2.23 kips (-0.13-9.92 kN)
- Final Cycle:
  - Starting Applied Displacement: 8.42 in. (214 mm)
  - Applied Force Range: 1.38-4.33 kips (6.14-19.3 kN)

A moment generated over the connection as well as curvature were calculated following the same procedure used in monotonic testing. The moment generated over the connection as displacement is applied to the system is presented in Figure 3.183. Moment generated over the connection versus local curvature is shown in Figure 3.184.

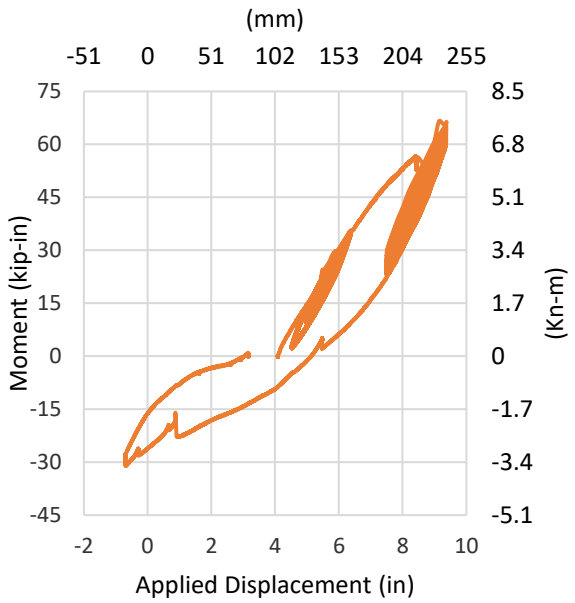

Figure 3.183. PB15-Cyclic - Moment vs. Applied Displacement

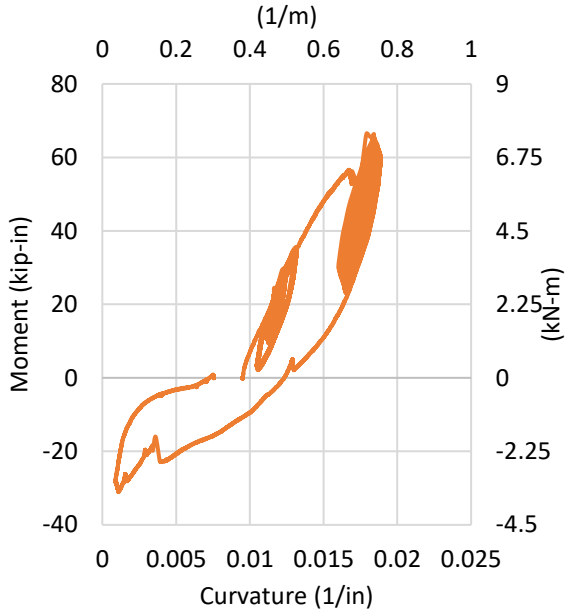

Figure 3.184. PB15-Cyclic - Moment vs. Curvature

A maximum moment of 66.5 kip-in. (7.51 kN-m) and a minimum radius of curvature of 52.9 in. (1.34 m), corresponding to a maximum curvature of 0.0189 in.$^{-1}$ (0.744 m^{-1}), was generated during the test. Ranges of generated moment and curvature produced during at each cycle location are as follows:

- First Cycle:
  - Moment Range: 13.6-25.9 kip-in. (1.54-2.93 kN-m)
  - Curvature Range: 0.0115-0.0120 in.$^{-1}$ (0.452-0.474 m^{-1})
- Second Cycle:
  - Moment Range: 9.33-29.6 kip-in. (1.05-3.34 kN-m)
  - Curvature Range: 0.0112-0.0124 in.$^{-1}$ (0.441-0.489 m^{-1})
- Third Cycle:
  - Moment Range: 2.15-35.6 kip-in. (0.24-4.02 kN-m)
  - Curvature Range: 0.0105-0.0132 in.$^{-1}$ (0.412-0.519 m^{-1})
- Final Cycle:
  - Moment Range: 23.1-66.5 kip-in. (2.61-7.51 kN-m)
  - Curvature Range: 0.0160-0.0189 in.$^{-1}$ (0.630-0.744 m^{-1})

Axial and circumferential strains were recorded at the crown and invert of four locations along the specimen. Figure 3.185 and Figure 3.186 present axial and circumferential strains with respect to applied

displacement throughout the test. SG10E-IC was damaged after monotonic testing and is not included in the circumferential strain data. SG10W-CA recorded a maximum axial strain of -1.5%. A maximum circumferential strain of -0.51% was recorded by SG10W-IC.

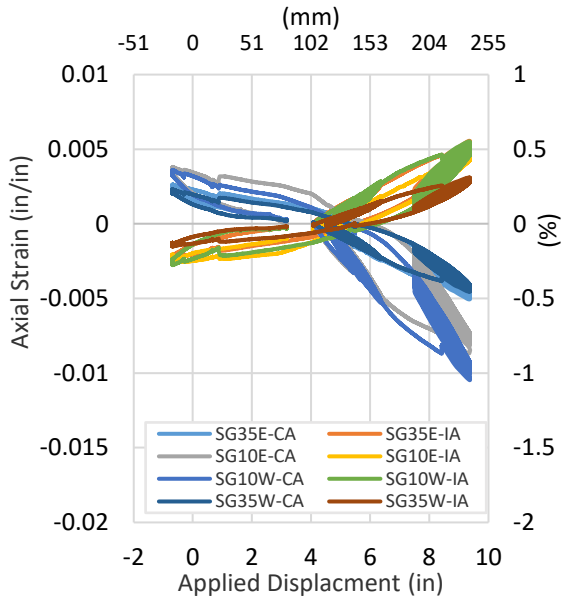

Figure 3.185. PB15-Cyclic - Axial Strain vs. App. Disp.

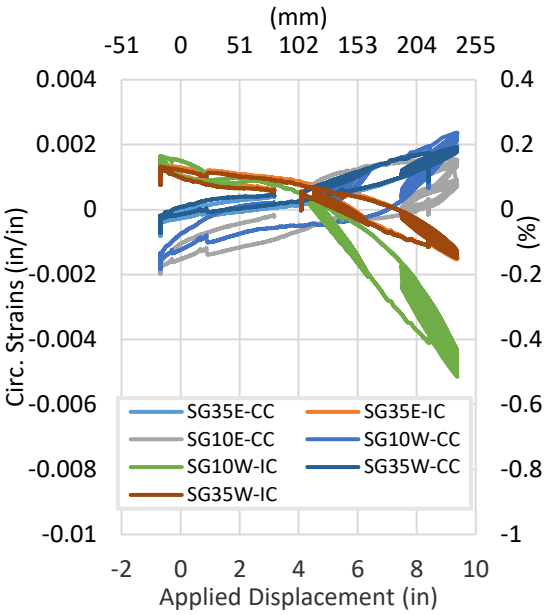

Figure 3.186. PB15-Cyclic - Circumferential Strain vs. App. Disp.

3.7.6 Bending Test PB02 Results – iPVC RCT Coupling

Pipe specimen PB02 consisted of an iPVC pipe with an RCT coupling connection at the midpoint and was performed using Bending Test Setup 2 (Section 2.3.2). During the test, the specimen was pressurized to around 55 psi (441 kPa) at the beginning of the test. Transverse displacement was then applied to the system at the two interior loading saddles by releasing the MTS system's crosshead locks, allowing the crosshead to displace at a consistent rate of 0.5 in./min (13 mm/min). At 2500 seconds into the data acquisition, the crosshead had reached its maximum allowable displacement. The crosshead locks were then re-engaged, and further displacement was applied to the system using the MTS system's actuator. The applied force generated by the transverse loading was captured and recorded by a 35-kip load cell attached to the crosshead of the loading frame. Applied displacement is the average measurement of two string pots (VSP-30 and VSP+30) located directly under each loading saddle. Figure 3.187 presents the progression of pressure, applied displacement, and actuator force through the test.

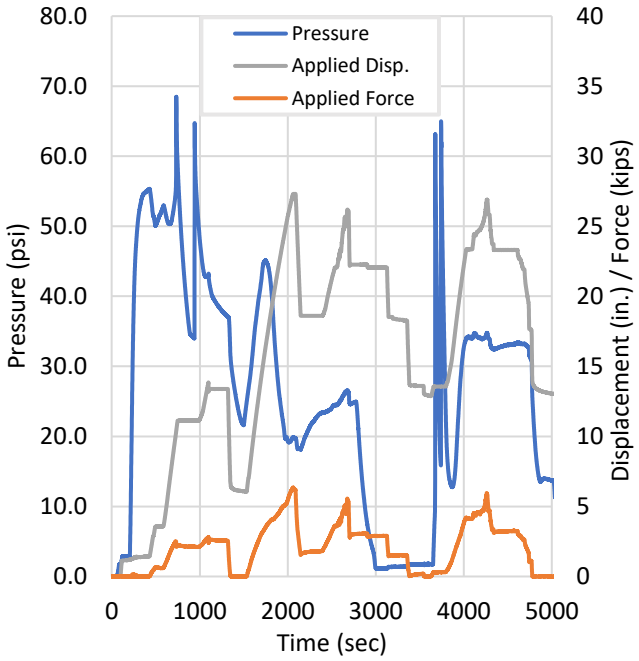

Figure 3.187. PB02-Progression of Pressure, Applied Displacement, and Force.

Force and applied displacement generated in the first 595 seconds can be attributed to the removal of the support jack and preloading of the specimen. Pressure was manually regulated throughout the test resulting in a large variation of internal pressure ranging from 1 - 68 psi (6.89 - 469 kPa). At 739 seconds into the data acquisition, leaking occurred at the west end of the RCT coupling. The test was temporarily paused and unloaded for inspection before the test sequence continued. Once the maximum allowable displacement

was applied to the system, the specimen was subjected to several cycles of transverse load ranging from 12.9 - 27.3 in. (328 – 693 mm) of applied displacement. A maximum force of 6.35 kips (28.2 kN) and maximum applied displacement of 27.3 in. (693 mm) was recorded during the test. Moment generated over the connection was calculated for the system by considering the pipe system as a continuous beam subjected to two equal concentrated loads. The moment generated over the connection as displacement is applied to the system is presented in Figure 3.188. Self-weight and the weight of water are included when calculating the moment of the system. Calculations for moment are provided in Appendix A.

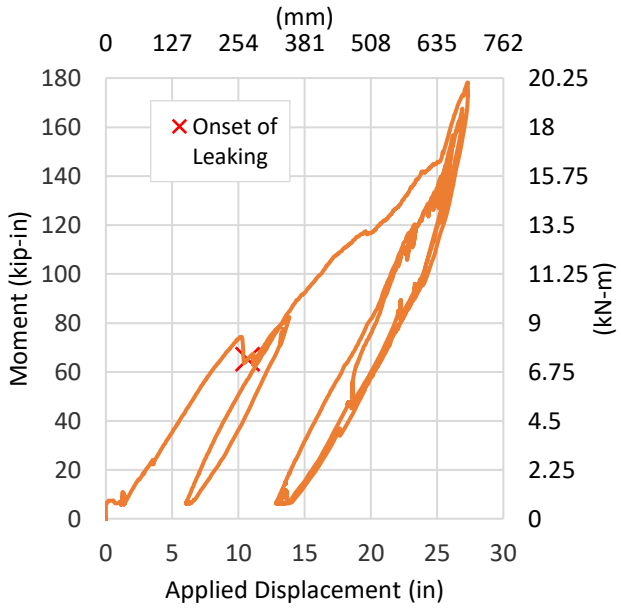

Figure 3.188. PB02-Moment vs. Applied Displacement

As the supporting jack was removed at the center of the specimen, an initial displacement of 1.14 in. (29 mm) was recorded at the loading saddles as the connection deflected under the self-weight of the system [5.18 kip-in (0.59 kN-m)]. At the onset of leaking, a moment of 65.2 kip-in. (7.37 kN-m) was generated at the connection at an applied displacement of 10.7 in. (272 mm). A maximum moment of 178 kip-in. (20.1 kN-m) was generated during the test, corresponding to the maximum applied displacement of 27.3 in. (693 mm).

Vertical displacements of the specimen were recorded at five locations, 70 in. (1178 mm) east and west of centerline, 33 in. (838 mm) east and west of centerline, and at the centerline of the specimen. Figure 3.189 presents vertical string pot measurements recorded throughout the test at corresponding applied displacements. String pot displacements show a relatively symmetric response in the system when subjected to lateral loading suggesting that the system is centered in the test frame throughout the test. A maximum vertical displacement of 45.1 in. (1146 mm) was recorded during the test by VSP-0.

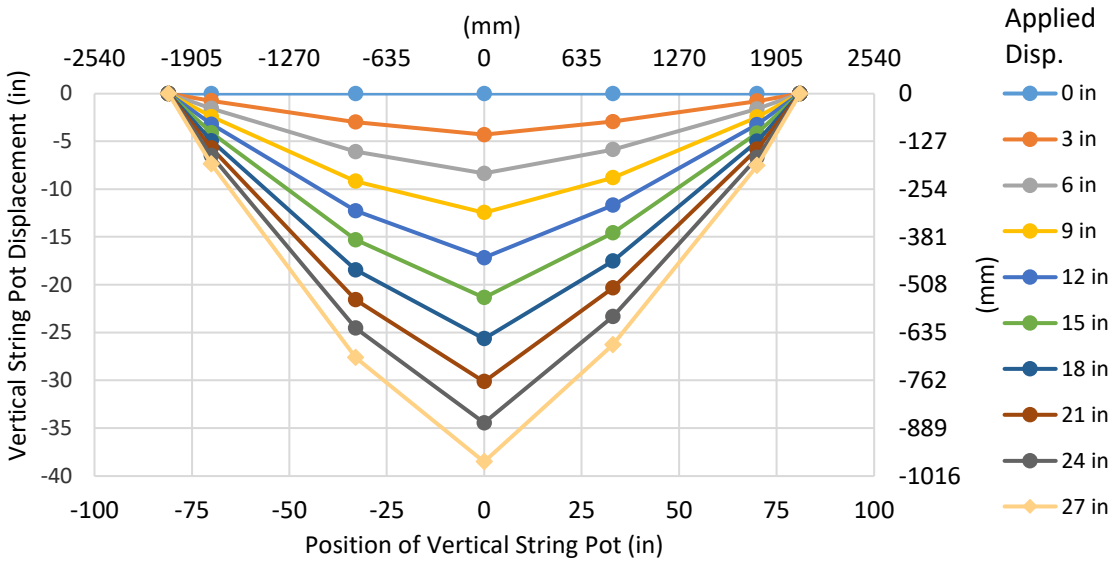

Figure 3.189. PB02 -Vertical String Pot Measurements

A radius of curvature was calculated using vertical string pot measurements along the invert of the specimen. A circumcenter for the system was able to be calculated using the location and vertical displacement of three string pots. Calculating the distance from the circumcenter to the location of the vertical string pots allowed a radius of curvature to be defined. By taking the inverse of this radius, a curvature of the system was able to be defined. Calculations for the radius of curvature and curvature are presented in Appendix B. To capture the maximum curvature experienced by the system, a local curvature was calculated using string pots located between the two load saddles (VSP-30, VSP-0, and VSP+30). Local curvature of the system versus applied displacement and moment versus curvature is shown in Figure 3.190 and Figure 3.191, respectively.

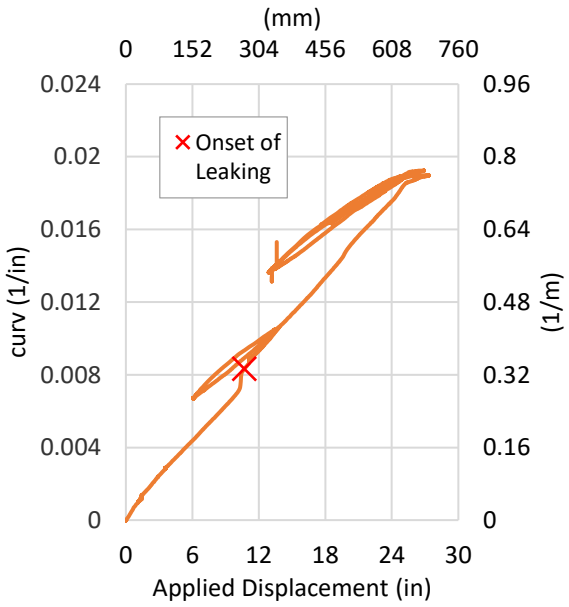

Figure 3.190. PB02 - Curvature vs. App. Disp.

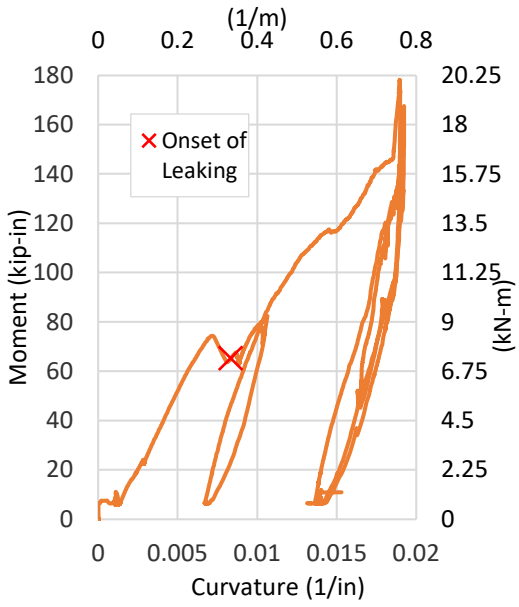

Figure 3.191. PB02 - Moment vs. Curvature

Curvature shows a linear response with respect to applied displacement throughout the test. The system reached a curvature of 0.0083 in^{-1} (0.327 m^{-1}) at the onset of leaking and a radius of curvature of 120 in. (3048 mm). A maximum curvature of 0.0192 in^{-1} (0.756 m^{-1}) was generated during the test, corresponding to the location of maximum applied displacement and a radius of curvature of 52.1 in. (1323 mm).

Axial and circumferential strains were recorded at the crown and invert of two locations along the specimen. Strain planes were located at 60 in. (1524 mm) on both sides of the centerline. Recorded strains were intended to provide a secondary measurement of force applied to the system. Figure 3.192 and Figure 3.193 present axial and circumferential strains with respect to applied displacement throughout the test. SG60W-IA recorded a maximum axial strain of 1.1% at the maximum applied displacement during the test. A maximum circumferential strain of -0.38% was recorded by SG60W-IC at the maximum applied displacement during the test. Figure 3.194 (a-d) presents pictures taken during significant moments during the test. After the test, there was 13 in. (330 mm) of residual deflection in the system at both loading saddle locations.

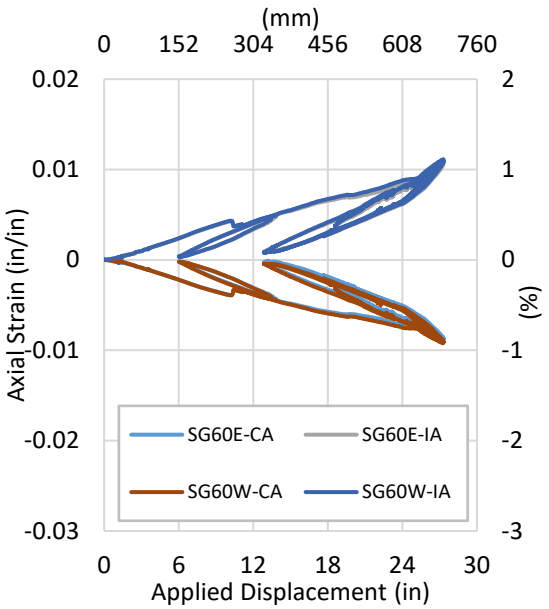

Figure 3.192. PB02 - Axial Strain vs. App. Disp.

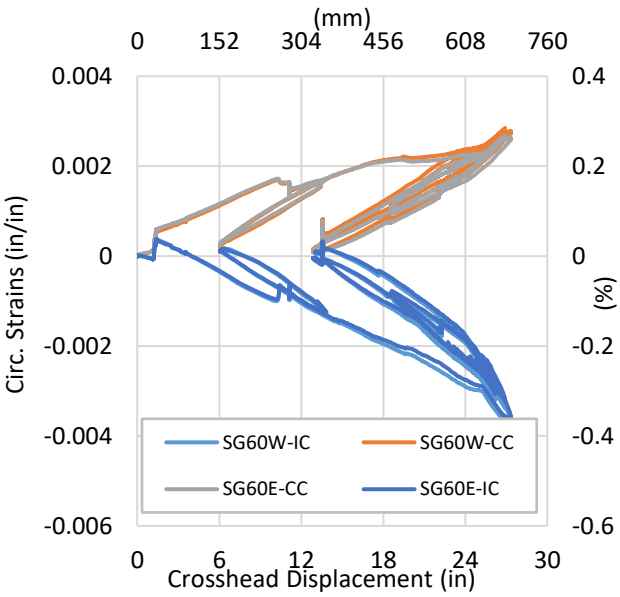

Figure 3.193. PB02 - Circumferential Strain vs. App. Disp.

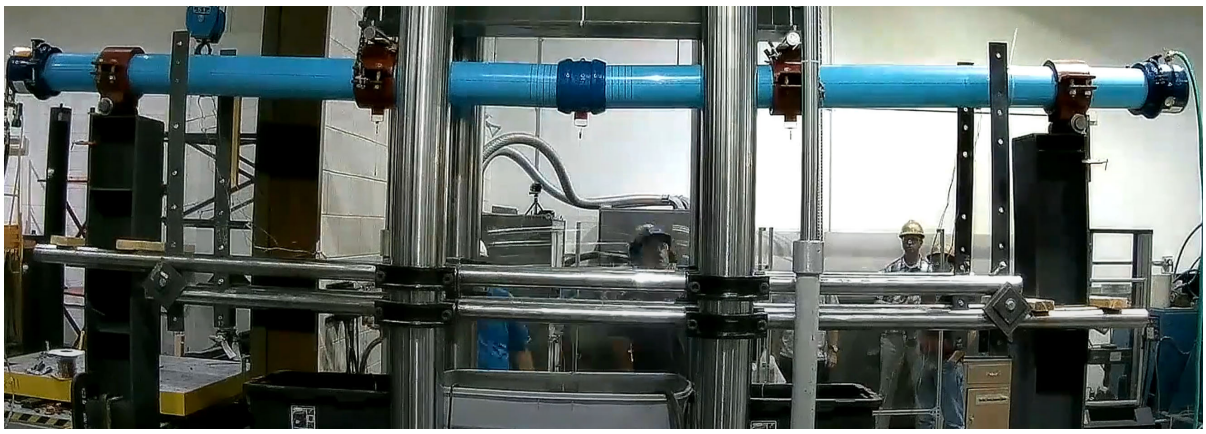

(a) Start of the Test

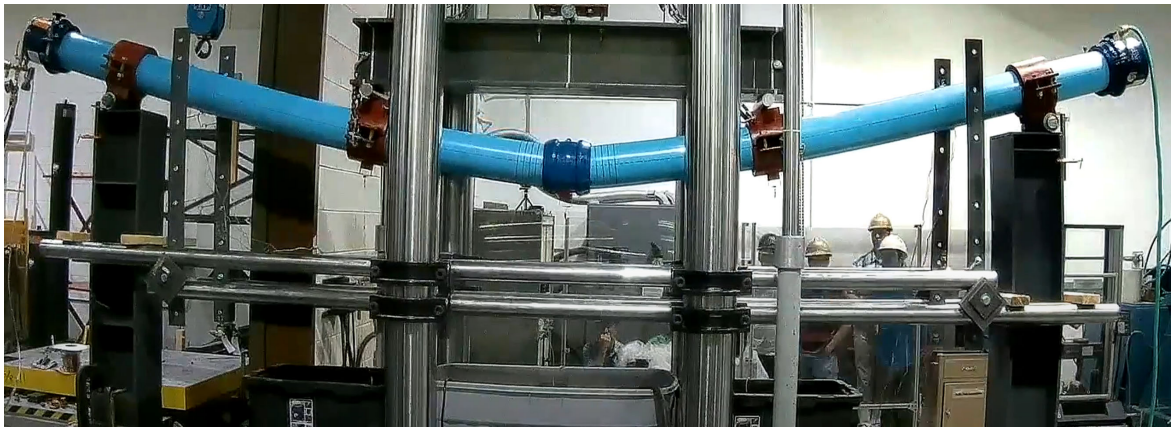

(b) Onset of Leaking at the RCT Coupling

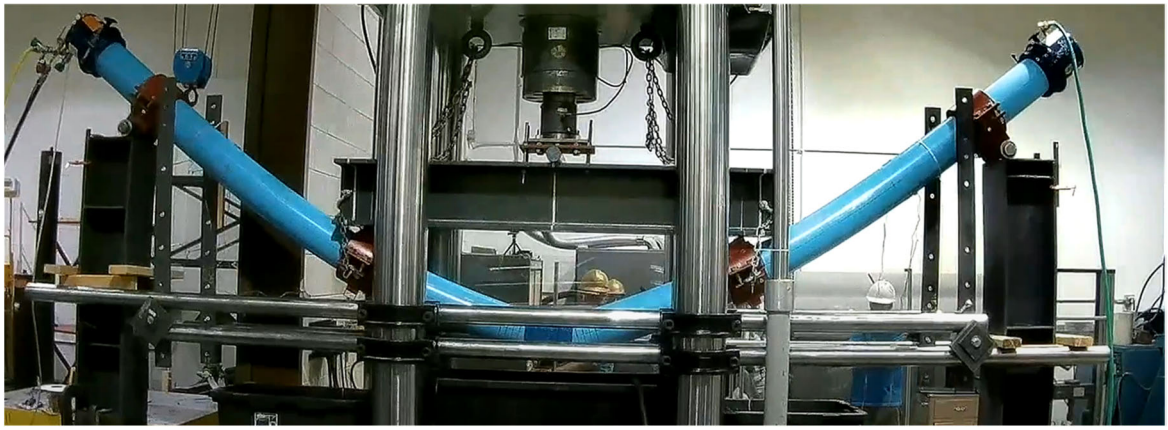

(c) Application of Full Setup Displacement

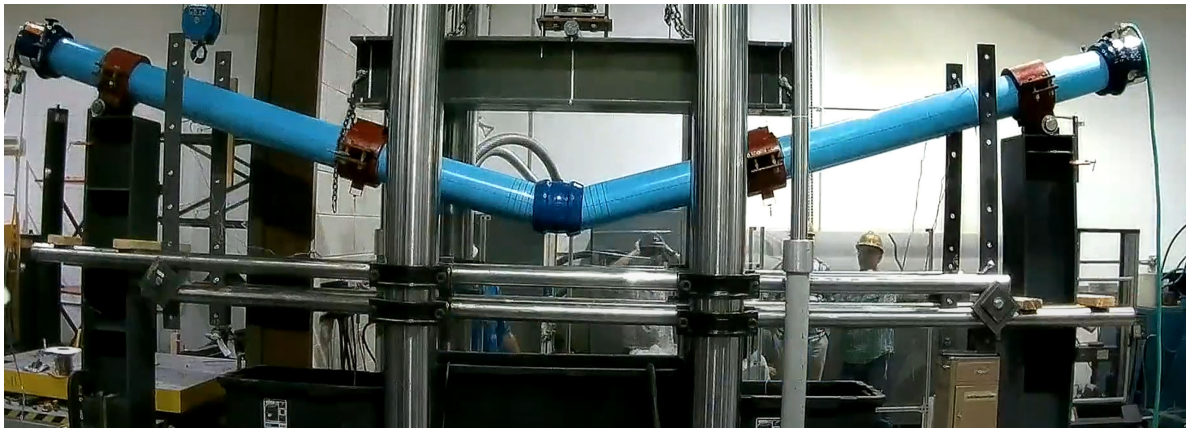

(d) 13 in. of Residual Deflection at the End of the Test

Figure 3.194. PB02 - Pictures during Test Progression

3.8 Four-Point Bending Summary and Comparison

This section provides a summary and comparison of the five four-point bending tests performed on iPVC pipe. Table 3.4 shows an overview of the tests and key factors recorded during testing. Figure 3.195 shows the moment versus displacement response for all iPVC bending tests. The EBAA C1900 (PB12) and the TurnerLok (PB11) show the stiffest response to applied displacement, allowing little rotation at the connection, and generating the highest moment of the four tests performed on the first bending test setup. The Hymax coupling (PB15) shows a similar response up to 30 kip-in. (3.4 kN-m) before rotation begins to occur at the coupling, softening the systems response under applied displacement. The Lokx coupling (PB14) allowed for an initial rotation under relatively little load before engaging with the pipe barrel and generating moment in the system. The RCT coupling (PB02) shows a much softer response than the other four connections tested due to the increased length of the pipe specimen used during the second test setup.

A comparison of the curvature response to applied displacement is provided in Figure 3.196. The curvature response to applied displacement follow a similar linear trend with little variation for the four tests performed on the first bending test setup. This response is expected for relatively stiff pipeline systems and shows that the bending test setup and procedures were consistent throughout testing. Test PB02 exhibits a much softer response, generating equivalent curvatures under higher displacements. This is expected and attributed to the longer pipe specimen and geometry used during the second pipe bending setup.

Table 3.4. Summary of Four-Point Bending Test Results

Test # (CIEST)	Pipe-Connection	Max Applied Disp.		Max Applied Force		Max. Moment		Min. Radius of Curvature		Max. Curvature	
		in	(mm)	kips	(kN)	kip-in	(kN-m)	in	(m)	in^{-1}	(m^{-1})
PB11	TurnerLok	9.30	(236)	7.61	(34)	115	(13.0)	59.1	(1.50)	0.0169	(0.665)
PB11 at Leak	TurnerLok	8.83	(224)	6.62	(29)	100	(11.3)	62.7	(1.59)	0.0159	(0.626)
PB12	EBAA C1900	9.50	(241)	7.60	(34)	115	(13.0)	64.5	(1.64)	0.0155	(0.610)
PB13	Continuous	9.60	(244)	9.01	(40)	135	(15.3)	80.2	(2.04)	0.0125	(0.491)
PB14	Lokx	9.35	(237)	6.25	(28)	94.8	(10.7)	53.9	(1.37)	0.0186	(0.732)
PB14 at Leak	Lokx	5.16	(131)	3.72	(17)	57.5	(6.50)	98.5	(2.50)	0.0102	(0.402)
PB15	Hymax Grip	9.37	(238)	4.61	(21)	70.7	(7.99)	49.9	(1.27)	0.0201	(0.791)
PB02	RCT	27.3	(693)	6.35	(28)	178	(20.1)	52.0	(1.32)	0.0192	(0.756)
PB02 at Leak	RCT	13.4	(340)	2.54	(11)	75.3	(8.51)	95.4	(2.42)	0.0105	(0.413)

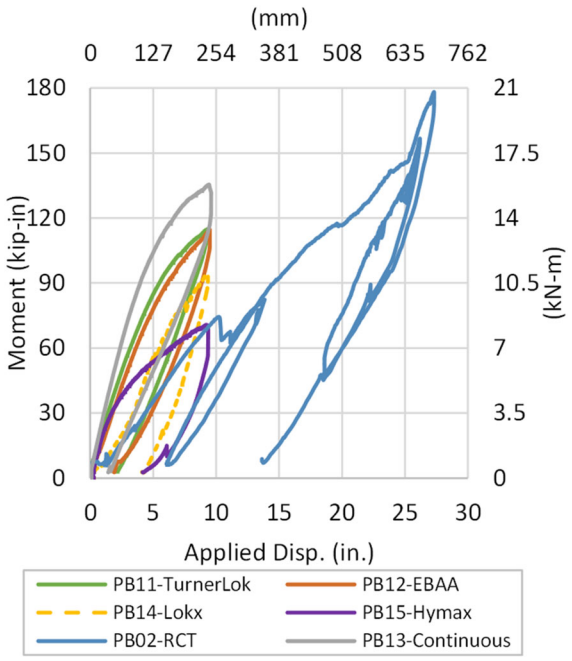

Figure 3.195. Four-Point Bending Comparison – Moment vs. App. Disp.

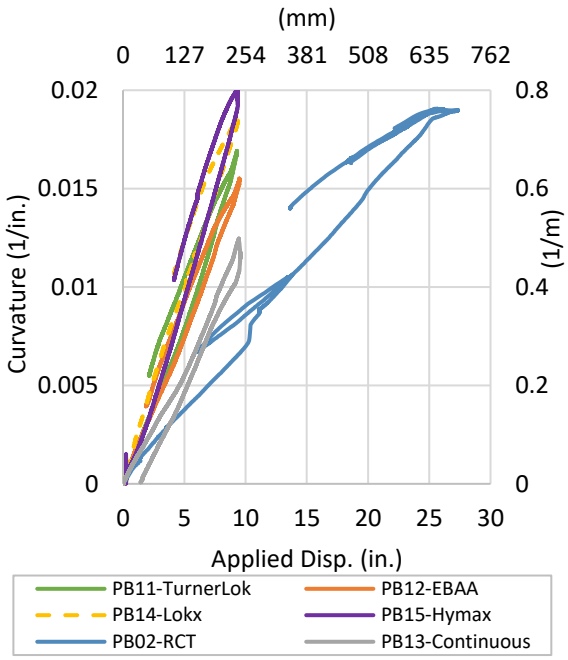

Figure 3.196. Four-Point Bending Comparison – Curvature vs. App. Disp.

The average axial strain recorded within the two loading points compared to the moment is plotted in Figure 3.197. Axial strains for PB02 were not recorded between the two loading points and are not presented. The strain response in each system follow similar trajectories as moment is applied to the system with the EBAA C1900 (PB12) and the TurnerLok (PB11) generating the highest moment and axial strain value, indicating that systems involving fully inserted bell and spigot connections allow for little rotation and the connection and will generate a relatively stiff response to transverse displacement. The Hymax connection (PB15) allowed for the greatest amount of rotation at the joint, transferring little load to the pipe barrels and generating the lowest strain in the system.

Figure 3.198 presents the moment versus curvature plot for all the systems tested. Since the curvature and moment relationship is not dependent on the geometry of the test setup, both the first and second bending test setup can accurately be compared. PB02, PB11, PB12, and PB15 show a similar linear response to moment for the first 30 kip-in. (3.4 kN-m), before the coupling begins to affect the system's response. The Lokx coupling (PB14) however, allows for an initial rotation at the coupling, developing a much softer initial response. As also visible in the strain response, the Hymax coupling generated the smallest moment throughout the test, allowing significant rotations at each end of the coupling, allowing greater displacements over the system and producing the greatest curvature values. Results from the bending test show that providing allowable joint rotation at connection points will improve the system's response when

subjected to transverse loading, allowing the system to generate less load in the pipe barrel of the system and accommodating larger applied curvatures.

While no failure was observed during the continuous pipe test (PB13), it is important to note that the continuous pipe generated higher moments and curvatures under less applied displacements than all the other tested systems. This response demonstrates how couplings with allowable rotation and joint deflection can minimize curvatures and associated bending stresses applied to pipe barrels throughout the system. This is clearly illustrated when comparing the Hymax connection, with an allowable rotation of 8 degrees, with the continuous pipe section. When compared to the continuous pipe test, the Hymax connection showed a 48% decrease in generated maximum moment and a 61% increase in maximum curvature.

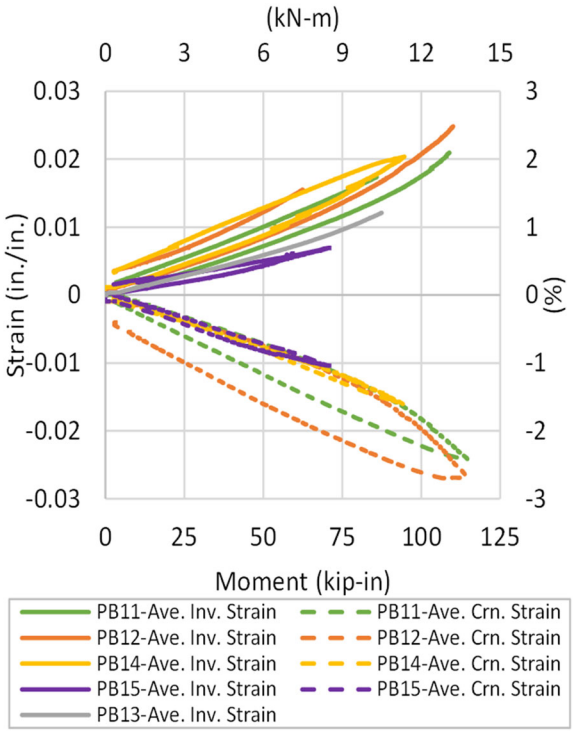

Figure 3.197. Four-Point Bending Comparison – Strain vs. Moment

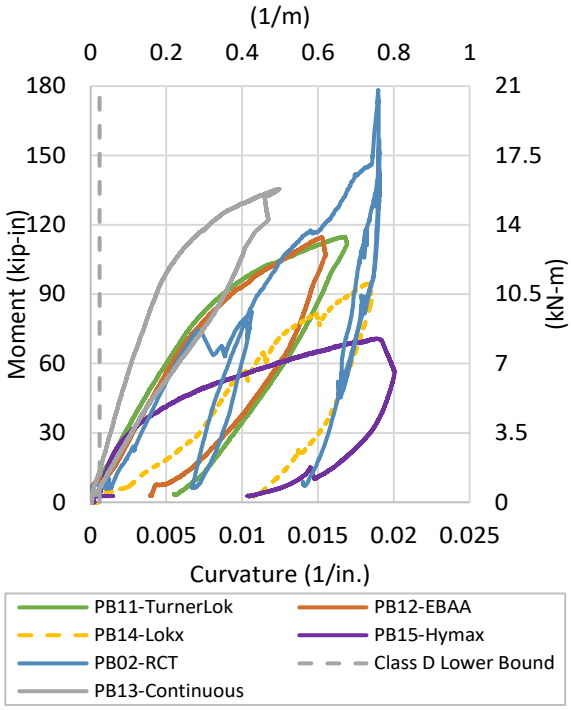

Figure 3.198. Four-Point Bending Comparison – Moment vs. Curvature

4. Seismic Performance Classification

The following section describes the procedures used to define seismic classes and ultimately classify each iPVC pipeline system's seismic response. Two methods were used to classify the systems' responses. The first method was introduced by Davis et al. (2019) and defines a pipeline system's seismic classification by assessing its ability to accommodate geological ground strain movements or strain demand along the pipeline. The second method was first proposed by Wham et al. (2019b). This method utilizes an analytical model to calculate axial force demand developed along pipeline systems and then categorizes them based upon survival rate when exposed to expected ground deformations defined in Barlett & Youd (1992).

4.1 Strain Demand

David et al. (2019) proposed four classes of seismically-induced ground movement demands, quantified by ground strains that a pipeline must be able to accommodate in either the axial or transverse direction. The proposed values are provided previously in Table 1.2 and, when compared against a pipeline system's capacity under laboratory test conditions, can be used to assess expected field performance.

To define a system's ability to accommodate ground strain along the axial direction, an overall system strain was defined for each pipe and coupling combination. System strain for each specimen was calculated using Equation 1, where ε_{pipe} is the maximum strain recorded in the pipe barrel during the test and ε_{joint} is the joint strain of the system. As shown in Equation 2, joint strain for the system was calculated by dividing the maximum joint displacement recorded throughout the test (ΔL_{joint}) by the typical field lay length (L_{lay}). A typical lay length of 20 ft. (6.1 m) was selected for all tests based on typical iPVC manufactured lay length. Pipe barrel strain over the joint was removed from joint strain calculations to provide an accurate representation of the mechanical movement of the joint. Joint length (L_{joint}) for each specimen was defined as the initial string pot span length at the start of the test. By comparing the system strain with seismic strain demand levels proposed by Davis et al. (2019), each system was categorized into a preliminary seismic strain demand class.

$$\varepsilon_{system} = \varepsilon_{pipe} + \varepsilon_{joint} \tag{1}$$

$$\varepsilon_{joint} = \frac{(\Delta L_{joint} - \varepsilon_{pipe} * L_{joint})}{L_{lay}} \tag{2}$$

System strain calculated for each pipeline system is provided in Table 4.1 along with values used in the system strain calculation. It is important to note that strains recorded during PT02 (RCT tension test) were determined to be inaccurate during analysis. Therefore, maximum tensile strains recorded during the

subsequent cyclic RCT test (PS12) were used to determine the upper bound system strain. It is also important to note that there was no compression test performed on iPVC with a Hymax Grip coupling. Therefore, the compressive system strain for the Hymax Grip coupling was defined using strain and joint displacements recorded at the maximum compressive cyclic during the Hymax Grip cyclic test (PS39). Table 4.2 presents the strain demand class for each tested system in both tension and compression. All the tests generated a system strain greater than the highest class threshold of 1% defined by Davis et al. (2019), placing each system in the highest seismic strain demand class of D. This suggests that the iPVC pipeline systems tested will perform well and maintain integrity in field conditions when subjected to axial ground movements.

Davis et al., (2019) defines strain demand due to transverse loading as a function of radius of curvature or rotation at the joint. Test results, providing a minimum radius of curvature produced by the system under transverse loading, allows for direct seismic classification of the systems bending response. Classification for the system relative to transverse loading is provided in Table 4.3. All iPVC systems tested far surpassed the minimum radius of curvature threshold of 1800 in. (45.7 m), suggesting that all the systems will perform well in the field and be able to accommodate some of the most severe ground deformations in the transverse direction.

Table 4.1. System Strain Values

Test # (CIEST)	Connection Type	Joint Length (L_{Joint})		Max. Recorded Joint Displacement		Max. Recorded Axial Stain		Joint Strain		System Stain	
		in.	(mm)	in.	(mm)	in./in.	%	in./in.	%	in./in.	%
PT02	RCT	4.4	(112)	0.93	(23.6)	0.0160	1.60	0.004	0.36	0.0196	1.96
PC37	RCT	19.1	(485)	1.23	(31.2)	0.0095	0.95	0.004	0.44	0.0139	1.39
PT27	TurnerLok	19.5	(495)	1.42	(36.1)	0.0078	0.78	0.005	0.53	0.0131	1.31
PC28	TurnerLok	31.2	(792)	8.38	(213)	0.0067	0.67	0.034	3.40	0.0407	4.07
PT30	EBAA 1900	23.3	(592)	4.36	(111)	0.0086	0.86	0.017	1.73	0.0259	2.59
PC31	EBAA 1900	26.8	(681)	6.52	(166)	0.0082	0.82	0.026	2.63	0.0345	3.45
PT33	Lokx	30.1	(765)	1.37	(34.8)	0.0169	1.69	0.004	0.36	0.0205	2.05
PC35 (Leak)	Lokx	17.6	(447)	1.05	(26.7)	0.0072	0.72	0.004	0.38	0.0110	1.10
PT38 (Leak)	Hymax	13.5	(343)	1.06	(26.9)	0.0063	0.63	0.004	0.41	0.0104	1.04
PS39 (Comp.)	Hymax	16.8	(427)	1.90	(48.3)	0.0035	0.35	0.008	0.77	0.0112	1.12

Note: Typical Lay Length, L_{Lay}, for each is assumed to be 240 in. (6.1m)

Table 4.2. Axial Strain Demand Classification

Test # (CIEST)	Pipe-Connection	Applied Force Direction	System Stain		Strain Demand Class*	Percent Exceeding Class D (%)
			in./in.	%		
PT02	RCT	Tension	0.0196	1.96	D	95.8
PC37	RCT	Compression	0.0139	1.39	D	38.7
PT27	TurnerLok	Tension	0.0131	1.31	D	30.9
PC28	TurnerLok	Compression	0.0407	4.07	D	307
PT30	EBAA C1900	Tension	0.0259	2.59	D	159
PC31	EBAA C1900	Compression	0.0345	3.45	D	245
PT33	Lokx	Tension	0.0205	2.05	D	105
PC35 (Leak)	Lokx	Compression	0.0110	1.10	D	10.5
PT38 (Leak)	Hymax Grip	Tension	0.0104	1.04	D	3.62
PS39 (Comp.)	Hymax Grip	Compression	0.0112	1.12	D	11.7

*Note: Axial Strain Demand Class D is 1.0% strain

Table 4.3. Bending Strain Demand Classification

Test # (CIEST)	Pipe - Connection	Min Radius of Curvature		Max Curvature		Strain Demand Class*	Percent Exceeding Class D
		in	(m)	in^{-1}	(m^{-1})		%
PB11 (Leak)	TurnerLok	62.7	(1.59)	0.0159	(0.626)	D	2762
PB12	EBAA C1900	64.5	(1.64)	0.0155	(0.610)	D	2690
PB13	Continuous	80.2	(2.04)	0.0125	(0.491)	D	2150
PB14 (Leak)	Lokx	98.5	(2.50)	0.0102	(0.402)	D	1736
PB15	Hymax Grip	49.9	(1.27)	0.0201	(0.791)	D	3518
PB02 (Leak)	RCT	95.4	(2.42)	0.0105	(0.413)	D	1790

*Note: Transverse Strain Demand Class D is a minimum radius of curvature of 1800 in. (45.7 m), equivalent to 3.8 deg. of rotation/deflection for a 10 ft. (3 m) pipe length

4.2 Connection Force Capacity (CFC)

The analytical model proposed by Wham & Davis (2019) was used to quantify the connection force capacity class limits of each iPVC pipeline system under investigation. The procedure quantifies the axial demand on a pipeline system, as a function of frictional resistance (f_r) along the system, by considering various geometric ground movements of block length (L_b) and ground displacement (δ), pipeline geometry, and various soil characteristics. Depending on the pipeline and ground movement geometries, connection force capacity can be calculated using the following two equations:

$$F_{CFC} = f_r l_s = \left[-\gamma_p + \sqrt{\gamma_p^2 + \frac{f_r \delta}{EA}}\right] EA \qquad \text{Condition I, } L_b \geq 2l_s \qquad (3)$$

$$F_{CFC} = \frac{f_r L_b}{2} \qquad \text{Condition II, } L_b \leq 2l_s \qquad (4)$$

where: A = cross sectional area of the pipe (in^2)

E = Modulus of Elasticity of the barrel (ksi)

γ_p= Average strain capacity at each joint (%)

f_r= friction generated across the pipe segment (kip/ft)

l_s = Length of friction being applied to the pipe due to ground movement (ft)

The model then defines connection force capacity for Earthquake Resilient Ductile Iron Pipe (ERDIP) systems that have historically performed well in past seismic events. The connection force capacity for the ERDIP system is defined using standard ISO 16134 specifications and is used to relate the performance of the systems being tested to current ISO standards. Initially arbitrary connection force capacity values are defined for the tested systems. Demands for the ERDIP and tested systems are then calculated for each ground movement scenarios, L_b and δ, from past earthquakes, defined by Bartlett & Youd (1992). A survival rate (SR) for each system is then calculated by comparing the number of surviving scenarios (F_{max}<CFC) to the total number of scenarios. Once survival ratios for each system are defined, they are compared for equivalence. If survival ratios for the systems are not equivalent, new CFC values are defined for the system of interest and the process is iterated until equivalent survival ratios are reached. K is defined as the ratio between CFC_{test} and CFC_{ERDIP}. The K factor is a multiplier used to define the system of interest's performance classes in relation to ISO standards ($3DK_C$,$1.5DK_B$, and $0.75DK_A$).

Geotechnical properties, presented in Table 4.4, used in the analysis consisted of baseline values defined by Rose et al. (2021) to represent typical field conditions. The same geotechnical parameters were used to evaluate all pipeline systems in the analysis.

Table 4.4. CFC Geotechnical Parameters

Parameter	Units		Value	
K_0	-		0.5	(0.5)
Soil Unit Weight, ɣ	pcf	(kPa)	115 (5.51)	(5.51)
Friction Angle, Φ	deg.	(rad)	36	(0.63)
Soil Cover, H	in.	(m)	45	(1.14)
Ground Movements, δ	in.	(m)	1.31-410	(0.03-10.4)
Block Length, L_b	ft	(m)	18 - 960	(0.46-24.4)

Pipeline characteristics for each system were defined based on a combination of information provided by pipeline manufacturers and experimental results. Table 4.6 presents a summary of the baseline characteristics defined for the ERDIP pipeline system, while Table 4.5 presents baseline characteristics used to define each of the iPVC pipeline systems. Pipeline characteristics for the ERDIP system were taken directly from manufacture catalogs listed by Kubota (2021). Outer diameter, thickness, bell diameter, and lay length for the iPVC pipeline system were provided by the manufacturer, PPI. An allowable joint displacement for the internal restraint connections was assumed to be 0 in., while an adjustable range of 0-2 in. (0-49 mm) was considered for the EBAA C1900 connection. A Young's Modulus for the iPVC system was selected based on tensile test experiments performed at Cornell University (Price et al., 2018). For external couplings an equivalent diameter calculated using the couplings cross sectional area was used to define the connection diameter (D_b).

Table 4.5. CFC Pipeline System Parameters – iPVC Systems

System Parameter	Units	RCT (iPVC)		TurnerLok (iPVC)		EBAA C1900 (iPVC)		Lokx (iPVC)		Hymax Grip (iPVC)	
Outer Diameter, D_o	in. (mm)	6.9	(175)	6.9	(175)	6.9	(175)	6.9	(175)	6.9	(175)
Thickness, t	in. (mm)	0.49	(12)	0.49	(12)	0.49	(12)	0.49	(12)	0.49	(12)
Connection Diameter, D_b	in. (mm)	8.73	(222)	8.0	(175)	9	(229)	8.75	(222)	11.3	(287)
Lay Length, L_p	ft. (m)	20	(6.1)	20	(6.1)	20	(6.1)	20	(6.1)	20	(6.1)
Allowable Joint Displacement, Δj	in. (mm)	0	(0)	0	(0)	0-2	(0-49)	0	(0)	0	(0)
Young's Modulus, E	ksi (GPa)	450	(3.1)	450	(3.10)	450	(3.10)	450	(3.10)	450	(3.10)
Allowable Joint Strain, γ_p	%	0	(0)	0	(0)	0 - 0.83	(0 - 0.83)	0	(0)	0	(0)
d_i/Φ	-	0.7	(0.7)	0.7	(0.7)	0.7	(0.7)	0.7	(0.7)	0.7	(0.7)

Table 4.6. CFC Pipeline System Parameters - ERDIP

System Parameter	Units	ERDIP	
Outer Diameter, D_o	in. (mm)	6.65	(169)
Thickness, t	in. (mm)	0.3	(7.6)
Connection Diameter, D_b	in. (mm)	9.53	(242)
Lay Length, L_p	ft. (m)	16.4	(5.0)
Allowable Joint Displacement, Δj	in. (mm)	2.36	(60)
Young's Modulus, E	ksi (GPa)	25400	(175)
Allowable Joint Strain, γ_p	%	1	(1)
d_i/Φ	-	0.9	(0.9)

Using experimental results, the controlling loading direction for each system was defined to assess the systems connection force capacity. The RCT, TurnerLok, EBAA C1900, and Hymax Grip connections performed exceptionally well when subjected to compressive loading, showing no signs of failure and reaching the limitations of the testing setup. Therefore, connection force capacity for these systems was defined as their ability to accommodate tensile loading. However, the Lokx connection experienced leaking at a lower compressive loading when compared to the monotonic tension test. Therefore, the primary failure loading direction for the Lokx connection was determined to be in compression and the load recorded at leaking was used as the system's maximum allowable load. A total of four analyses were run for each system, considering each frictional resistance solution defined by Wham et al. (2019a) and implemented by Rose et al. (2021). CFC and K values were then averaged over the four analyses to provide one set of seismic classes for the system. A summary of analysis results, in terms of category class limits, is presented in Table 4.7 and Table 4.8.

Table 4.7. CFC Performance Class Limits (RCT, TurnerLok, Lokx, and Hymax)

Performance Class	CFC Equation	RCT Coupling		TurnerLok Gasket		Lokx Coupling		Hymax Grip Coupling	
		K Values	Min. CFC (kips)	K Values	Min. CFC (kips)	K Values	Min. CFC (kips)	K Values	Min. CFC (kips)
Φ_A	Less than $4.3DK_A$	-	0	-	0	-	0	-	0
Φ_B	$4.3DK_A$ to $8.6DK_B$	$K_A = 0.75$	19.4	$K_A = 0.68$	17.5	$K_A = 0.75$	19.4	$K_A = 1.05$	27.2
Φ_C	$8.6DK_B$ to $17.1DK_C$	$K_B = 0.77$	39.7	$K_B = 0.70$	36.1	$K_B = 0.77$	39.7	$K_B = 1.06$	54.5
Φ_D	Greater than DK_C	$K_C = 0.75$	77.0	$K_C = 0.69$	70.8	$K_C = 0.75$	77.0	Kc= .95	97.7

Table 4.8. CFC Performance Class Limits (EBAA C1900)

Performance Class	CFC Equation	EBAA C1900 Restraint - 0 in.		EBAA C1900 Restraint - 1 in.		EBAA C1900 Restraint - 2 in.	
		K Values	Min. CFC (kips)	K Values	Min. CFC (kips)	K Values	Min. CFC (kips)
Φ_A	Less than $4.3DK_A$	-	0	-	0	-	0
Φ_B	$4.3DK_A$ to $8.6DK_B$	$K_A = 0.78$	20.1	$K_A = 0.73$	18.8	$K_A = 0 .72$	18.7
Φ_C	$8.6DK_B$ to $17.1DK_C$	$K_B = 0.80$	41.3	$K_B = 0.82$	42.1	$K_B = 0.71$	36.4
Φ_D	Greater than DK_C	$K_C = 0.78$	79.6	$K_C = 0.74$	75.7	$K_C = 0 .61$	62.6

Table 4.9 shows the connection force capacity class defined for each iPVC system tested. The RCT coupling generated the highest axial capacity placing it into the second highest seismic class of C. This suggests that the RCT coupling will be able to accommodate significant axial ground movements and around 47% of worst-case ground movements in the field. The other systems tested achieved a connection force capacity class of B. These systems will be able to accommodate moderate ground movements and are expected to survive around 22% of worst-case ground movements possible in the field. Interestingly, as shown in Figure 4.1, the EBAA C1900 restraint was able to achieve a higher classification (C) by allowing a joint displacement greater than 2 in. (51 mm). This response demonstrates that providing greater allowable joint displacement will improve the overall performance of a pipeline system when subjected to seismic loading.

Table 4.9. CFC Performance Classes

Pipe-Connection	Axial Capacity		Connection Force Capacity Class
	Kips	(kN)	
RCT Coupling	55.3	(246)	C
TurnerLok Gasket	34.6	(154)	B
EBAA C1900 Restraint	38.1	(169)	B-C
Lokx Coupling	-35.3	(-157)	B
Hymax Coupling	27.9	(124)	B

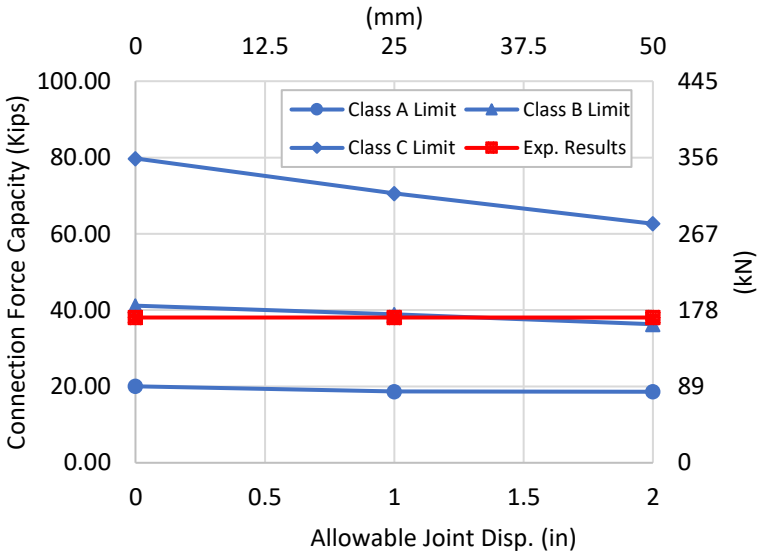

Figure 4.1. EBAA C1900 Restraint CFC vs. Allowable Joint Disp.

Based on results reported on in Price et al., (2018) and unrestrained pullout capacity from the EBAA C1900 tension test (PC30), connection force capacity analysis and classification were performed for an unrestrained bell and spigot connection. TurnerLok pipeline system parameters were used in the connection

force capacity analysis with an allowable joint displacement of 5.8 in. (147 mm) (Price et al., (2018)). Results produced an average minimum connection force capacity threshold over the four previously defined friction equations of 12.9 kips (57.4 kN) for class B. As shown in Figure 3.20, the tension capacity for an unrestrained bell and spigot connection is 200 lbs. (0.89 kN), placing typical unrestrained bell and spigot connections into the lowest CFC class (A). While the tested systems display a range of axial performance, all tested systems can be considered as improvements to standard unrestrained bell and spigot connections.

5. Summary and Conclusions

The intent of this study is to characterize and classify the seismic performance of a pipeline with various connection types for axial and transverse loading representative of worst-case permanent ground movements. The testing and analysis performed allow for a direct classification of each pipeline system relative to recently proposed seismic demand estimates. Testing and analysis was performed on 6-in nominal diameter, pressure class 305 psi (2103 kPa), C900, iPVC pipe with several different hazard resilient restraints and couplings.

Test results showed that the pipe connection has a significant impact on the pipeline system's ability to accommodate imposed ground strains and movements with maximum tensile and compressive forces ranging from 27.9 to 55.3 kips (124 to 246 kN) and -33.3 to -54.2 kips (-148 to -241 kN), respectively. Systems consisting of a reinforced bell and spigot connection performed exceptionally well under compressive loading, allowing the spigot to telescope through the bell. Cyclic loading was determined to have a minimal effect on the tested specimen's overall tensile capacity, suggesting that over insertion of the spigot during installation procedures should not significantly impact the overall performance of iPVC pipeline systems. Results from bending tests demonstrate that pipe systems with allowable rotations or deflections can significantly affect the system response to transverse loading, with tested couplings showing up to a 48% reduction in generated moments when compared to continuous pipe systems. This response suggests that systems with higher allowable joint rotation will be able to accommodate higher curvatures when compared to continuous pipe systems.

All iPVC systems showed a significant ability to accommodate ground strains in both axial and transverse directions, exceeding the final strain demand class threshold and were classified as "D" strain demand systems. The connection force capacity classes vary for each system. Despite the RCT connection's low allowable joint displacement, the connection was able to generate a significant axial load before failure, placing it into the second highest CFC category (C). The TurnerLok, Lokx, and Hymax Grip connections generated a slightly lower axial force during full-scale testing placing the system into the category (B) for CFC. The EBAA C1900 connection was able to achieve a performance class of (B) for 0 in. and 1 in. of allowable joint displacement and a performance class of (C) for 2 in. of allowable joint displacement. This result illustrates that the system's ability to accommodate ground movement is a function of joint displacement and that allowing greater displacement at a pipeline systems' connections will improve the overall performance of the system.

Based on results reported in Price et al., (2018) and pipe test PT30, a maximum joint displacement and tensile force capacity of 5.8 in. (147 mm) and 200 lbs (0.89 kN) were defined for a standard unrestrained

bell and spigot connection. The unrestrained connection produced a system strain of 2.4%, placing it into the highest axial strain demand class of D with the other tested systems. However, unrestrained bell and spigot connections only achieved the lowest connection force capacity class of A. While a wide range of seismic performances were produced by the tested systems, all systems with couplings provide an improved alternative when compared to unrestrained joint systems.

While this testing program provides valuable results for assessing earthquake performance, there are several limitations to note:

(1) This testing program only provides analysis and results concerning 6-in. (152 mm) nominal diameter iPVC pipe with a 305 psi (2103 kPa) pressure class and does not consider different pressure classes or diameters.
(2) Only a singular test in tension, compression, cyclic, and bending was performed for each pipeline system and does not consider potential variation in test results. To utilize upper-bound results, repeat tests are advisable to establish confidence in results and level of statistical variation.
(3) This study focuses on an upper bound classification of each system, using the ultimate capacity of the system without a safety factor, and does not consider a reduction in strength due to possible material deficiencies or potential aging of the pipeline system. Standard engineering design practice utilizes Safety Factors on the order of 1.5 or 2, which could be reduced through statistical assessment of repeat test runs.
(4) This study focuses on loading in one principal direction during each test (axial or transverse) and does not consider combined loading, which has the potential to decrease overall system capacity due to stress concentrations and combined loading effects.
(5) Connection force capacity limits were defined using assumed frictional resistant calculations, without a comparable system response to in-situ soil conditions.

Several subsequent testing programs are recommended to refine and expand on the assessment and classification of the pipeline systems reported on in this study:

(1) To assess how pipe diameter and pressure class affect the system response of iPVC pipeline systems, further testing at varying diameters and pressure classes are suggested.
(2) Repeat tests are suggested to identify variability in system response and determine allowable system safety factors.
(3) Combinational axial and transverse tests are recommended in future work to determine if combinational loading affects maximum capacity limits.

(4) Further research is recommended on how each system responds to multiple soil conditions through large scale or centrifugal testing, providing a better understanding of frictional forces developed along systems of different material and geometry.

Despite these limitations, this study provides a useful procedure for assessing seismic capacity of pipeline systems in the field based on laboratory testing and developing seismic design guidelines. The results define each system's response and maximum capacities for axial and transverse loading. Seismic strain demand and connection force capacities for each system were classified providing valuable feedback to design engineers on how the tested systems are expected to perform in the field. Overall, the findings suggest that each system will be able to accommodate significant ground motions expected in the field and are viable options when designing for pipeline systems in high seismic locations.

6. Acknowledgments

The authors wish to recognize the excellent effort of University of Colorado students and staff that made these experiments successful. Namely, the contributions of undergraduates Porter Hawkins, Ismail Hussein, and Johnathan Shaw are gratefully acknowledged. Great thanks are extended to CIEST staff members Kent Polkinghorne, and John Hindman for their constant support and expertise. Appreciation is extended to East Bay Municipal Utility Department and Denver Water for their continued support and financial contributions. The authors would also like to thank the following industry representatives for providing pipe material and connection restraints: PPI Pyungwha, S&B Technical Products, EBAA Iron, Georg Fischer, and Mueller-Hymax.

References

Applied Technology Council. (2007). FEMA 461: Interim Testing Protocols for Determining the Seismic Performance Characteristics of Structural and Nonstructural Components. Redwood, CA: FEMA.

AWWA. (2007). "AWWA C900-07 Polyvinyl Chloride (PVC) Pressure Pipe and Fabricated Fittings, 4 In. Through 12 In. (100 mm Through 300 mm), for Water Transmission and Distribution". *American Water Works Assoication*, 44. doi.org/http://dx.doi.org/10.12999/AWWA.C900.07

Davis, C.A., Rajah, S., Wham, B.P., & Heubach, W.F. (2019). "Strain Demands on Buried Pipelines from Earthquake-Induced Ground Movements". *Proceedings: Pipelines 2019* (pp. 357–367). Reston, VA: American Society of Civil Engineers. doi.org/10.1061/9780784482483.040

Hughes, D., Venkatesh, Lee A. H-J, Paradkar, A.B., Najafi, M. (2016) "Development, Evaluation, and Installation of New Improved PVC (iPVC) Pipe for Water Applications" *Proceedings,* 2016 ASCE Pipelines Conference, Kansas City, MO, ASCE, Reston, VA, July, pp 1046-1060.

Ihnotic, C.R. (2019). *Seismic Evaluation of Hazard-Resistant Lifelines: Thermoplastic Pipes and Connections*. M.S. Thesis, Boulder CO: University of Colorado Boulder.

Ihnotic, C.R., Anderson, D.K., Ramos, J.L., Balcells, D., & Wham, B.P. (2019). "Seismic Evaluation of Hazard-Resistant Lifelines: Fused PVC Pipe and Fittings". Boulder, CO: University of Colorado Boulder.

International Organization for Standardization (ISO). (2020). *ISO 16134:2006 Earthquake- and subsidence-resistant design of ductile iron pipelines*. Switzerland: ICS: 23.040.10, TC/SC: ISO/TC 5/SC 2. Retrieved from https://www.iso.org/standard/40651.html

Kubota Corporation. (2021). *Kubota Earthquake Resistant Ductile Iron Pipe (GENEX)*. Torrance, CA.

O'Rourke, T.D., Bonneau, A.L., Pease, J.W., Shi, P., & Wang, Y. (2006). "Liquefaction and Ground Failures in San Francisco". *Earthquake Spectra*, *22*(2_suppl), 91–112. doi.org/10.1193/1.2185686

O'Rourke, T.D., Jeon, S.-S., Toprak, S., Cubrinovski, M., Hughes, M., van Ballegooy, S., & Bouziou, D. (2014). "Earthquake Response of Underground Pipeline Networks in Christchurch, NZ". *Earthquake Spectra*, *30*(1), 183–204. doi.org/10.1193/030413EQS062M

Price, D., Berger, B.A., O'Rourke, T.D., Stewart, H.E., Wham, B.P., & Pariya-Ekkasut, C. (2018). *Performance Evaluation of iPVC Pipe under Earthquake-Induced Ground Deformation*. Ithaca, NY: Cornell University. Retrieved from https://lifelines.cee.cornell.edu/projects/

Rose, H.R., Wham, B.P., Dashti, S., & Liel, A.B. (2021). "Seismic-Resistant Pipeline Design: Parametric Study of Axial Connection Force Capacity". *Proceedings: Pipelines 2021*. Reston, VA: American Society of Civil Engineers.

Wham, B.P., Anderson D.K., & Ihnotic, C.R. (2020) "Experimental Assessment of Pipeline Connection Response to Transsverse Loading". *Proceedings,2020* ASCE Pipelines Conference Reston, VA: American Society of Civil Engineers.

Wham, B.P., & Davis, C.A. (2019). "Buried Continuous and Segmented Pipelines Subjected to Longitudinal Permanent Ground Deformation". *Journal of Pipeline Systems Engineering and Practice*, *10*(4), 04019036. doi.org/10.1061/(ASCE)PS.1949-1204.0000400

Wham, B.P., Berger, B.A., & Davis, C.A. (2019a). "Characterization of soil-structure interaction for seismic design of hazard-resistant pipeline systems". *Proceedings:* F. Silvestri & N. Moraci (Eds.), *7th International Conference on Earthquake Geotechnical Engineering*. Roma, Italy: CRC Press. doi.org/10.1201/9780429031274

Wham, B.P., Davis, C.A., & Rajah, S. (2019b). "Axial Connection Force Capacity Required for Buried Pipelines Subjected to Seismic Permanent Ground Displacement". *Proceedings: Pipelines 2019* (pp. 299–308). Reston, VA: American Society of Civil Engineers. doi.org/10.1061/9780784482483.034

Appendix A: Applied Moment Calculation

Moment generated over the connection of the specimen was calculated by considering point loads applied from the actuator and a distributed load generated from self-weight of the system. To calculate the moment generated from point loading the specimen was considered as a simply supported beam with two equal concentrated loads symmetrically placed along the specimen. The point load geometry and load path are provided in Figure A1. The equation used to calculate the moment generated by point loading is provided by Equation A1 where P is the load applied by the actuator and A is the distance from support to the loading saddle. The moment generated from self-weight of the system is provided in Equation A2 where W is the distributed load on the specimen and L is the simply supported length of the specimen. Self-weight not only includes the material weight of the pipe but also includes the weight of water. The total moment, provided in Equation A3, is calculated by summing the moment generated by point loads and the moment generated from self-weight.

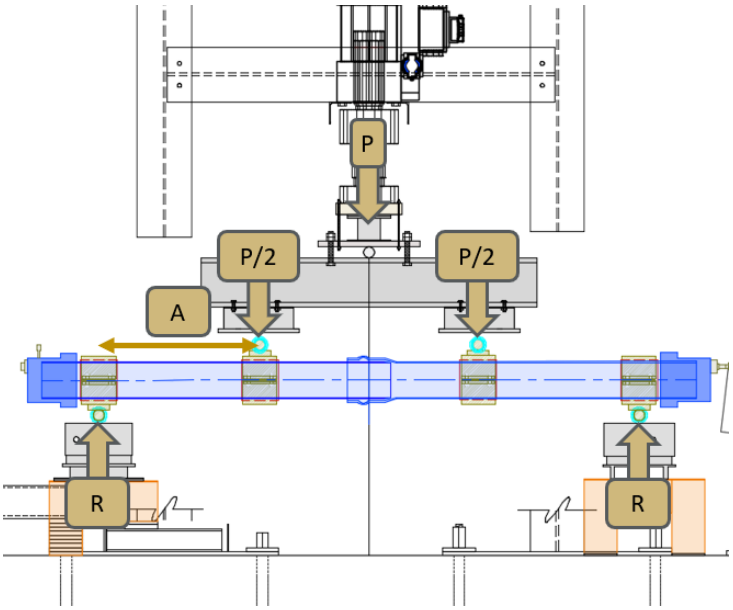

Figure A1. Load path of applied force, P

Point Load Moment: $$M_{point} = \frac{P * A}{2} \quad \text{(A1)}$$

Self-Weight Moment: $$M_{sw} = \frac{W * L^2}{8} \quad \text{(A2)}$$

Total Moment: $$M_{max} = M_{point} + M_{sw} \quad \text{(A3)}$$

Appendix B: Radius of Curvature (RoC) Calculations

Two major system curvatures were calculated to define the pipeline system's response to four-point bending load. The first curvature represented by the green curve shown in Figure B1 was defined as a local curvature of the system. The local curvature was calculated using string pots located within the constant moment region of the system. Since the moment within this constant moment region is the highest for the system, this local curvature is representative of the maximum curvature developed within the system. The second curvature used to represent the system's response was defined as the system's global curvature. The global curvature, represented by the red curve in Figure B1 was calculated using string pots located within and outside of the constant moment region of the test setup.

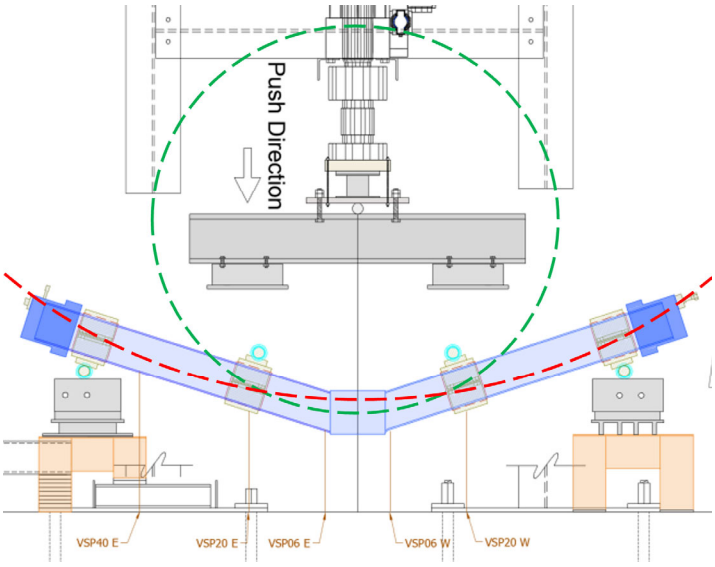

Figure B1. System Curvatures (Green: Local Curvature) (Red: Global Curvature)

For each curvature calculation, the location and deflection of three string pots were used to calculate a circumcenter of the system. All calculations assumed that there was limited horizontal movement in the system and that string pot locations were fixed at the start of the test. Once a circumcenter is located for the system, a radius of curvature can be defined by calculating the distance from the circumcenter to one of the string pot locations used in defining the circumcenter. Figure B2 presents an example of a potential local curvature calculated for the system where ρ is representative of the radius of curvature and Y_0 and X_0 are the coordinates defining the circumcenter location.

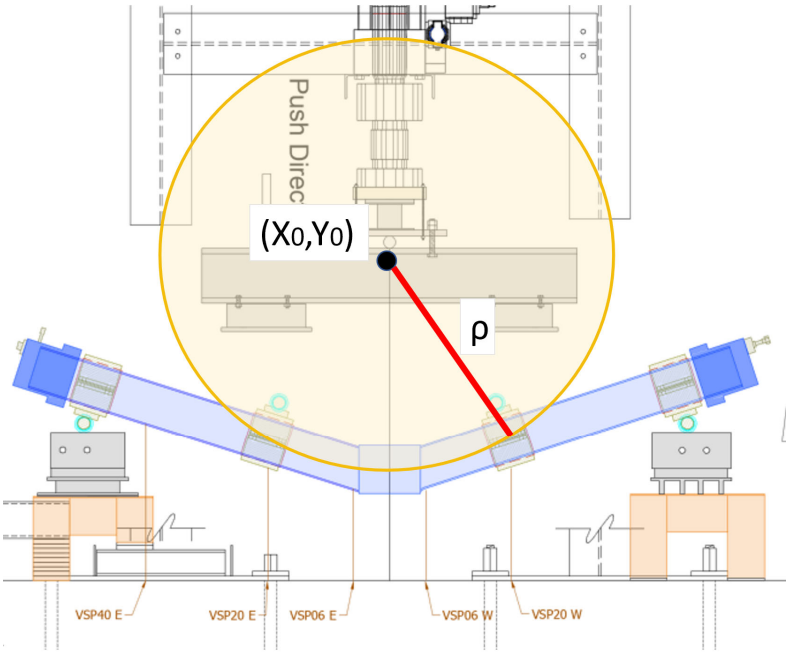

Figure B2. Circumcenter and Radius of Curvature Calculated using Local Coordinates

X and Y coordinates for the circumcenter can be calculated using Equation B1 and B2. Where A, B, and C are a system of matrices defining lateral string pot location (X_i) and vertical string pot displacement (Y_i). Matrices used for calculating circumcenter are provided in Equations B3-B6. Once coordinates are defined, a radius of curvature for the system can be calculated using Equation B7.

X-axis Circumcenter Coordinate:

$$x_0 = \frac{|B|}{2|A|} \tag{B1}$$

Y-axis Circumcenter Coordinate:

$$y_0 = \frac{|C|}{2|A|} \tag{B2}$$

Coordinate Matrix A:

$$A = \begin{bmatrix} x & y & 1 \\ x_1 & y_1 & 1 \\ x_2 & y_2 & 1 \\ x_3 & y_3 & 1 \end{bmatrix} \tag{B3}$$

Coordinate Matrix B:

$$B = \begin{bmatrix} x^2 + y^2 & x & 1 \\ x_1^2 + y_1^2 & x_1 & 1 \\ x_2^2 + y_2^2 & x_2 & 1 \\ x_3^2 + y_3^2 & x_3 & 1 \end{bmatrix} \tag{B4}$$

Coordinate Matrix C:

$$C = \begin{bmatrix} x^2 + y^2 & y & 1 \\ x_1^2 + y_1^2 & y_1 & 1 \\ x_2^2 + y_2^2 & y_2 & 1 \\ x_3^2 + y_3^2 & y_3 & 1 \end{bmatrix} \quad \text{(B5)}$$

Radius of Curvature:

$$R = \sqrt{(x_2 - x_0)^2 + (y_2 - y_0)^2} \quad \text{(B6)}$$

Once the radius of curvature has been determined, the curvature can be calculated for the system by taking the inverse of the radius of curvature as shown in Equation B7.

Curvature:

$$\varphi = 1/\rho \quad \text{(B7)}$$

Appendix C: Material Characterization

Material characteristics of PVC pipe, including iPVC, have been previously reported on in publications prepared by researchers at Cornell University. Wham et al. 2017 and Price et al. 2018 report on a series of series of tensile coupon tests performed on specimens extracted from factory produced pipe segment walls. Test setup and testing procedures are thoroughly described in Wham et al. 2017 and Price et al. 2018. Stress and strain data was obtained from the two studies to verify previously defined iPVC, PVC, and PVCO material properties.

Figure C1 and Figure C2 present stress-strain curves from tests performed on iPVC, PVCO, and PVC pipe material. Stress applied to the specimen was computed by dividing the measured force by the original cross-sectional area of the specimen. Strains up to 2-4% are direct measurements from attached strain gages. Due to strain gage debonding issues, supplemental measurements recorded from a clip-on extensometer were used to measure strains exceeding 2-4%. The linear response region for iPVC was defined to have an upper bound (proportional limit) of 0.6% strain, while the linear elastic range for PVC and PVCO was defined to have an upper bound of 0.8% strain. A modulus of elasticity was defined for each material using linear regression through the linear portion of response. An average modulus of elasticity of 450 ksi (3102 MPa) was calculated for iPVC, as presented in Figure C1 and Figure C2. PVC and PVCO achieved similar average modulus of elasticities of 456 ksi (3144 MPa) and 448 ksi (3089 MPa), respectively. Figure C3 presents the Poisson strain vs. axial strain response for each material. Poisson's ratio was calculated for each material using linear regression throughout the linear region of the material. As shown in Figure C3, an average Poisson's ratio of 0.38 was calculated for iPVC. PVC and PVCO produced a Poisson's ratio of 0.46 and 0.33, respectively.

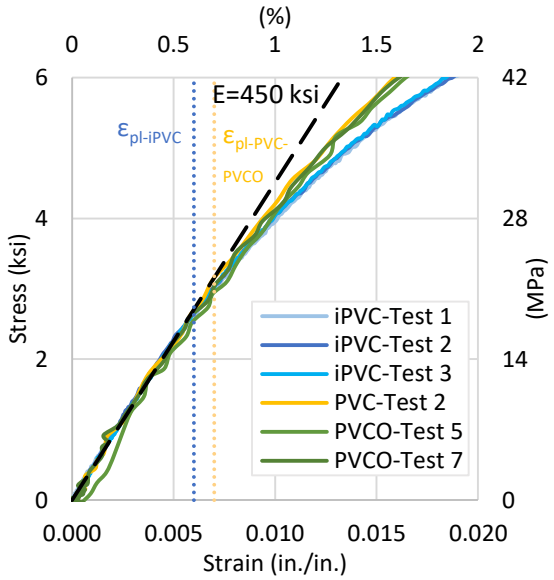

Figure C1. iPVC, PVC, and PVCO Tensile Stress-Strain Response (Linear Response)

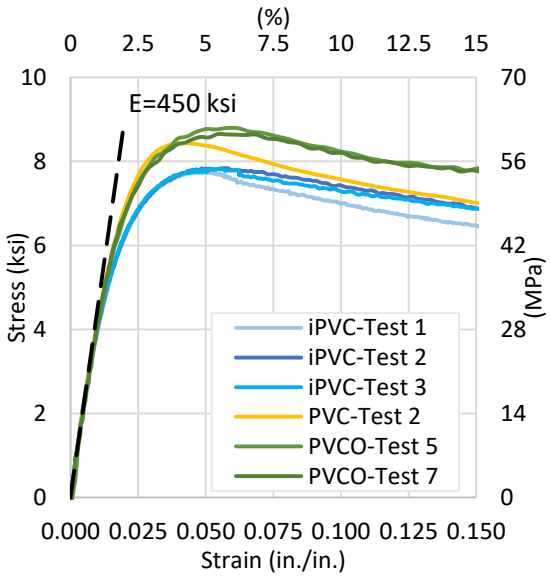

Figure C2. iPVC, PVC, and PVCO Tensile Stress-Strain Response

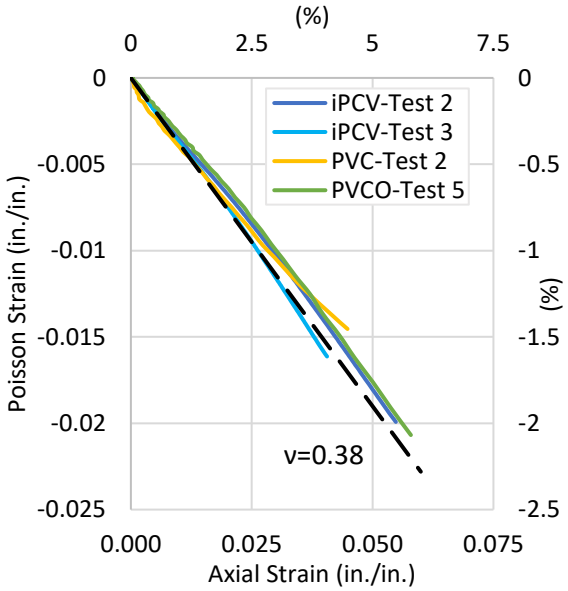

Figure C3. iPVC, PVC, and PVCO Poisson Strain vs. Axial Strain

Select results from the material characterization are summarized in Table C1. Results obtained during material characterization analysis agree with previously published reports. While iPVC, PVC, and PVCO have very similar moduli of elasticity and Poisson's ratio, there are some differences in the material responses. The proportional limit stresses of PVC and PVCO are 24-39% greater than the proportional limit stress of iPVC, suggesting that iPVC is more ductile. PVC and PVCO also produced maximum stresses 8-12% greater than those produced by iPVC.

Table C1. Material Characterization Results

		Modulus of Elasticity		Poisson's Ratio	Proportional Limit Stress		Maximum Stress		Strain at Maximum Stress	
		ksi	(MPa)		ksi	(MPa)	ksi	(MPa)	in./in.	%
iPVC	Test 1	447	(3082)	-	2.61	(18.0)	7.76	(53.5)	0.0468	4.68
	Test 2	456	(3144)	0.37	2.72	(18.7)	7.84	(54.1)	0.0485	4.85
	Test 3	448	(3089)	0.38	2.66	(18.3)	7.82	(53.9)	0.0564	5.64
	iPVC Average	450	(3105)	0.38	2.66	(18.3)	7.81	(53.8)	0.0506	5.06
PVC	Test 2	456	(3144)	0.46	3.69	(25.4)	8.43	(58.1)	0.0410	4.10
PVCO	Test 5	447	(3082)	0.33	3.35	(23.1)	8.79	(60.6)	0.0579	5.79
	Test 7	450	(3103)	-	3.27	(22.5)	8.65	(59.6)	0.0577	5.77
	PVCO Average	449	(3092)	0.33	3.31	(22.8)	8.72	(60.1)	0.0578	5.78

Note: Stress and strain data obtained from Wham et al. 2017 and Price et al. 2018

Appendix D: RCT Comparison

This appendix reports on a series of tension tests performed on an RCT coupling with various pipe materials and pressure classes.

D.1 - Tension Test PT40 – PVC RCT Coupling

Pipe specimen PT40 consisted of a PVC pipe with an RCT Flex-Tite coupling connection at the midpoint. The specimen was pulled in axial tension until failure occurred at the connection. Figure D.1 shows photos of the pre-test setup of specimen PT40 as well as the specimen just after failure at the connection.

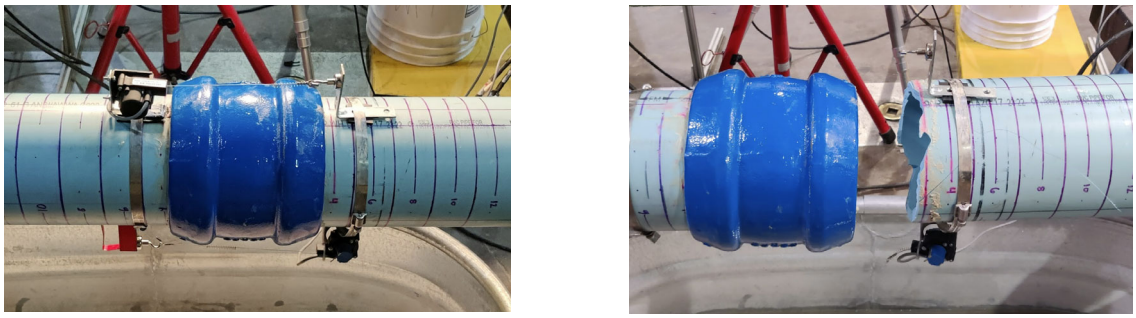

(a) Pre-Test Setup (b) Failure at Connection

Figure D.1. Specimen PT40 (a) Setup and (b) after Failure

The progression of pressure, actuator force, and actuator displacement is presented in Figure D.2. The specimen maintained an average pressure of 65 psi (448 kPa) with minor fluctuations until failure of the test occurred. Figure D.3 displays the actuator force versus displacement. Actuator displacement and actuator force are direct measurements of the actuator's hydraulic piston location and attached load cell, respectively. Throughout loading, actuator force and actuator displacement increase at a relatively consistent rate of around 16 kips/in. (2.8 kN/mm). Figure D.4 presents the actuator force versus joint displacement. Joint displacement was measured by two string pots at both the crown and invert of the specimen that spanned across the RCT connection. No signs of slipping at the joint were recorded during the test. A maximum average joint displacement of 0.75 in. (19.0 mm) was recorded at failure.

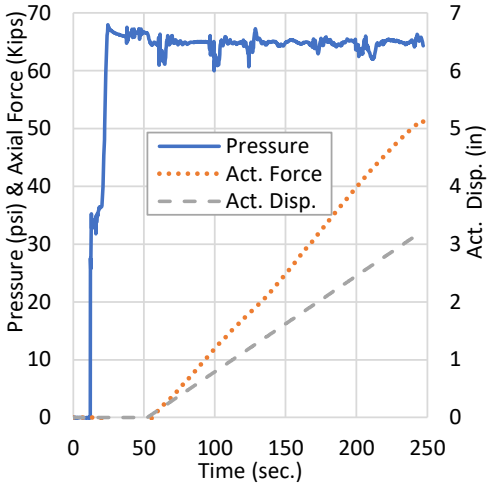

Figure D.2. PT40-Pressure and Act. Disp. vs. Time

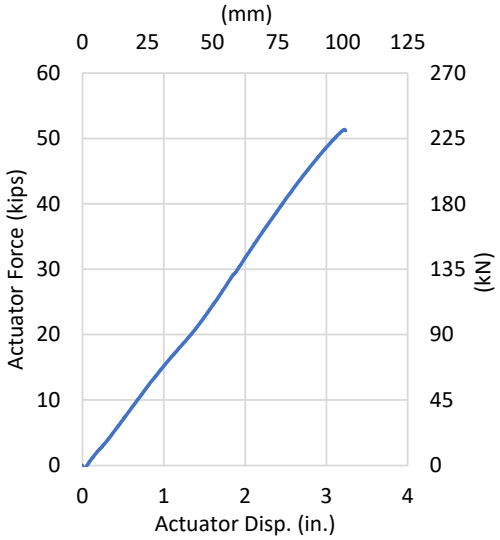

Figure D.3. PT40-Force vs. Act. Disp.

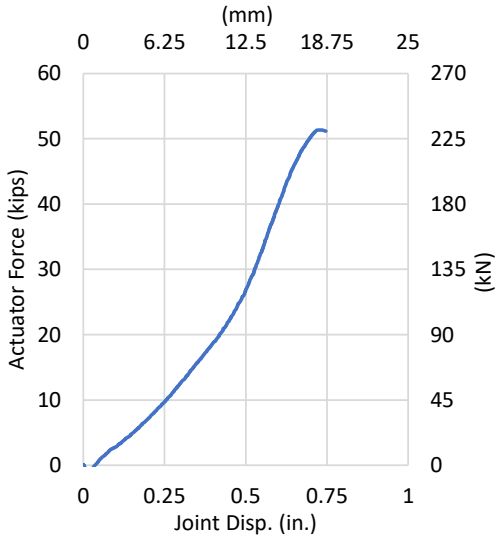

Figure D.4. PT40-Force vs. Average Joint Displacement

Axial and circumferential strains were recorded at the crown, invert, and both spring lines of the bell section. Strain versus time and strain versus actuator displacement can be viewed in Figure D.5 and Figure D.6, respectively. During pressurization at the start of the test, an increase in circumferential strain is observed, accompanied by a slight decrease in axial strain. This slight decrease in axial strain can be attributed to the Poisson's effect as the pipe barrel expands circumferentially due to the load applied from internal pressure. Once loading is applied to the system, a sharp increase in axial strain and a decrease in circumferential

strain is observed as the pipe barrel begins to elongate due to applied tensile force. The maximum axial strain peaked at 1.13 %, and the maximum circumferential strain peaked at -0.308%.

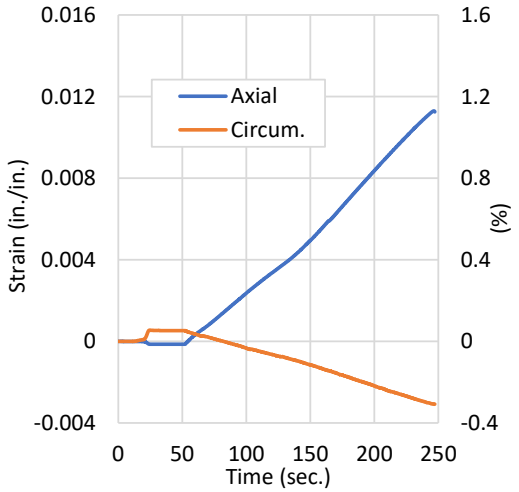

Figure D.5. PT40-Strain vs. Time

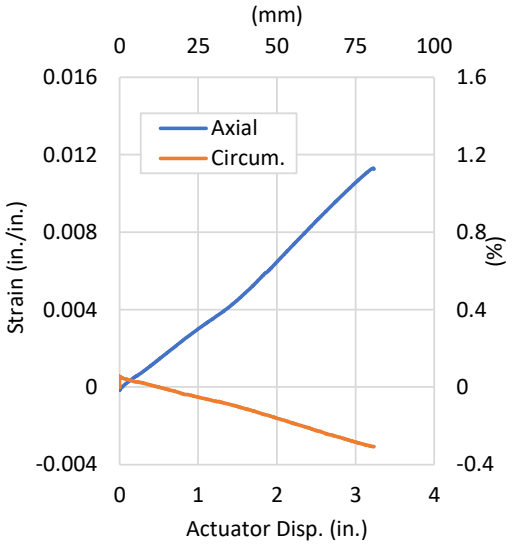

Figure D.6. PT40-Strain vs. Act. Disp.

The test concluded with circumferential fractures occurring at the east end of the RCT coupling. At fracture, a maximum axial force of 51.4 kips (229 kN) and a maximum actuator displacement of 3.24 in (82.3 mm) were recorded. The sudden fracture resulted in an abrupt loss of pressure in the system. Cracking propagated from the fracture location approximately 12 in. (305 mm) along the specimen barrel, as shown in Figure D.7. Prior to fracture, there were no signs of leakage.

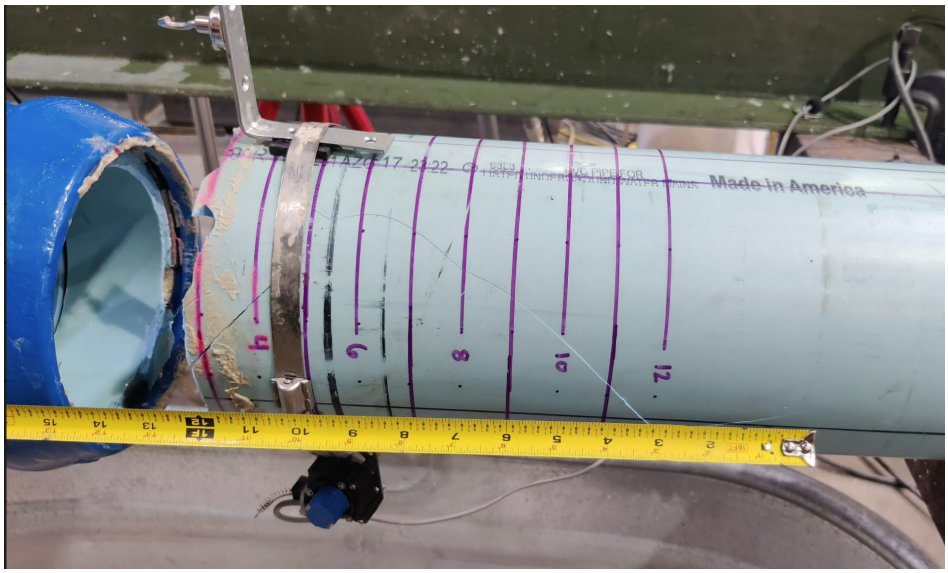

Figure D.7. Specimen PT40 Fracture at Connection

D.2 – RCT Tension Test Summary and Comparison

This section provides a summary and comparison of four compression tension tests performed on 6 in. (150mm)-diameter pipe with RCT couplings. Five axial tension tests were performed on iPVC, PVCO, and PVC pipe with 305 psi (2103 kPa) and 235 psi (1620 kPa) pressure classes. Table D.1 provides an overview of the five tests and key measures recorded during testing. In addition, a comparison of applied axial load versus actuator displacement is provided in Figure D.8, while Figure D.9 shows the comparison of applied axial load versus joint displacement response for all RCT tension tests performed in this study. Figure D.10 presents the tensile force versus strain and Figure D.11 shows the stress versus strain response for each of the RCT tests. It is important to note that inaccurate strain data was recorded for PT02. Strain data presented for iPVC-305 was recorded during cyclic test PS12 which failed at a similar maximum axial force to PT02.

Table D.1 Summary of RCT Tension Test Results

Test # (CIEST)	Pipe Material	Pressure Class		Max. Axial Force		Max Axial Strain		Max Act. Disp.		Joint Disp.	
		psi	(kPa)	Kips	(kN)	in/in	%	in	(mm)	in	(mm)
PT02	iPVC	305	(2103)	55.3	(246)	0.016	1.60	4.10	(104)	0.9	(24)
PT05	PVCO	305	(2103)	27.8	(124)	0.012	1.17	2.93	(74)	0.7	(18)
PT09	PVC	235	(1620)	32.8	(146)	0.010	1.02	2.43	(62)	0.6	(16)
PT22	PVCO	235	(1620)	10.1	(45)	0.005	0.53	2.25	(57)	1.9	(47)
PT40	PVC	305	(2103)	51.4	(229)	0.011	1.13	3.24	(82)	0.8	(19)

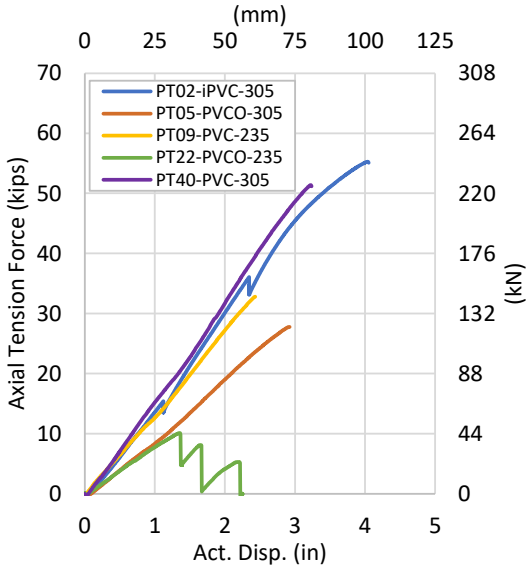

Figure D.8. RCT Tension Test Comparison – Axial Force vs. Act. Displacement

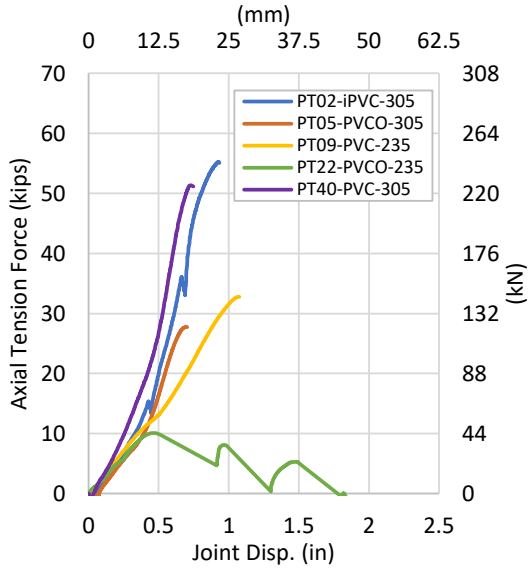

Figure D.9. RCT Tension Test Comparison – Axial Force vs. Joint Displacement

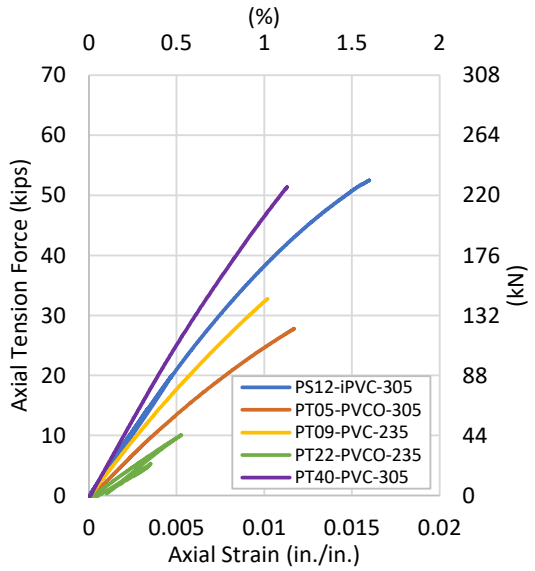

Figure D.10. RCT Tension Test Comparison – Axial Force vs. Axial Strain

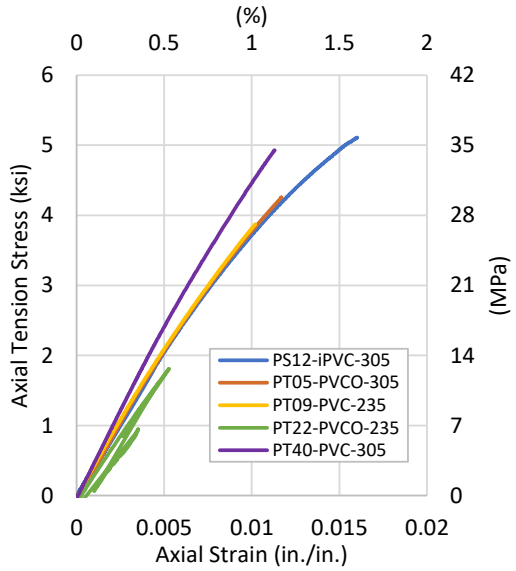

Figure D.11. RCT Tension Test Comparison – Axial Stress vs. Axial Strain

Pipe specimens with a 305-pressure class were able to generate higher forces and larger strains when compared to their 235-pressure class counterparts. PVC-305 produced a 57% increase in tensile capacity and an 11% increase in recorded strain at failure when compared to PVC-235. PVCO-305 produced a 175% increase in tensile capacity and a 121% increase in recorded strain at failure. Joint displacement between pressure classes was consistent with 235 pressure classes allowing for more joint displacement and joint slippage at failure. These results suggest that pipe specimens can significantly increase their axial capacities and ability to accommodate ground movements by increasing their pressure class.

iPVC generated the highest axial tension load before failure of the three tested 305-pressure class specimens showing an increase in axial tension capacity of 7.6% and 99% when compared to PVC and PVCO, respectively. iPVC also generated the highest axial strains during testing showing an increase of 42% and 37% when compared to PVC and PVCO, respectively. Despite PVCO producing the lowest force during testing, PVCO was able to generate more strain in the system resulting in failure at a higher actuator displacement when compared to traditional PVC pipe. Joint displacement for all three tested materials remained consistent ranging from 0.7 in. (18 mm) to 0.9 in. (23 mm). These results suggest that pipe material does significantly impact the pipe system's ability to accommodate ground movements, recording large variation in ultimate tensile load capacity as well as allowable axial strain at failure.